UNIVERSIDAD AUTÓNOMA DE MADRID

Doctorado en Biociencias Moleculares

TESIS DOCTORAL

“Protective role of SIRT1 activation against insulin resistance and defective thermogenesis associated to inflammation in brown adipose tissue”

CARMEN ESCALONA GARRIDO

Madrid, 2020

DEPARTAMENTO DE BIOQUÍMICA

FACULTAD DE MEDICINA

UNIVERSIDAD AUTÓNOMA DE MADRID

“Protective role of SIRT1 activation against insulin resistance and defective thermogenesis associated to inflammation in brown adipose tissue”

Memoria presentada por la graduada en Farmacia Carmen Escalona Garrido para optar al título con Mención Internacional de Doctor por la Universidad Auntónoma de Madrid

Tesis Doctoral dirigida por:

Ángela Mª Martínez Valverde

Patricia Vázquez Pérez

Instituto de Investigaciones Biomédicas “Alberto Sols” de Madrid, CSIC-UAM

Madrid, 2020

Ángela Mª Martínez Valverde, Investigadora Científica del Consejo Superior de Investigaciones Científicas en el Instituto de Investigaciones Biomédicas 'Alberto Sols' de Madrid (CSIC-UAM).

Patricia Vázquez Pérez, Investigadora Postdoctoral en el Instituto de Investigaciones Biomédicas 'Alberto Sols' de Madrid (CSIC-UAM).

CERTIFICAN: que Carmen Escalona Garrido, Graduada en Farmacia por la Universidad Complutense de Madrid, ha realizado bajo su dirección el trabajo de investigación titulado:

"PROTECTIVE ROLE OF SIRT1 ACTIVATION AGAINST INSULIN RESISTANCE AND DEFECTIVE THERMOGENESIS ASSOCIATED TO INFLAMMATION IN BROWN ADIPOSE TISSUE"

Las que suscriben consideran el trabajo realizado satisfactorio y apto para ser presentado como Tesis Doctoral en el Departamento de Bioquímica de la Universidad Autónoma de Madrid.

Y para que conste donde proceda, expiden el presente certificado.

Madrid, 24 de Febrero de 2020

Esta Tesis Doctoral ha sido realizada gracias a un contrato de Ayudas para la Formación de Profesorado Universitario (FPU), convocatoria 2015.
Beneficiario FPU15/00251

"Es mucho más hermoso iluminar que simplemente brillar; de la misma manera es más hermoso transmitir a los demás lo que se ha contemplado que sólo contemplar."

Santo Tomás de Aquino

“Cógelo, ve por él. Suéltate, inténtalo (…). Mírate, creételo. Sal de ahí, afróntalo. Ciérralo, déjalo ir. Di que sí o di que no. Tómalo, confía en ti (…) Cázalo, duro con él. Pruébate y pruébalo. Cámbialo, atrévete (…) Estarás cerca si en vez de mirar al suelo echas a caminar. Si puedes alcanzarlo, mira, lo tienes delante. Puedes dar un paso y otro y otro más. Casi lo tienes (…). No te deseo suerte, no hace falta. Porque sí que puedes, que nadie te diga que no porque sí que puedes”

Sí que puedes (El Kanka)

A Lolo

A mis padres y
a mi hermana

AGRADECIMIENTOS

No puedo más que agradecer a todas las personas que me han acompañado a lo largo de estos 4 años. ¡Lo he conseguido!

En primer lugar a mis directoras, las Doctoras Ángela M. Valverde y Patricia Vázquez. Ángela, muchas gracias por darme la oportunidad de formar parte de tu grupo y de iniciarme en el mundo de la investigación pese a que no sabía ni coger una pipeta. Admiro muchísimo tu capacidad de trabajo y dedicación. Gracias por tu compresión y por hacer de cada resultado inesperado, generalmente “dramático", el inicio de algo positivo. Nunca podré agradecerte lo suficiente lo que me has ayudado durante estos años. Patri, necesitaría también escribir otra Tesis para darte las gracias por todo. Gracias por tu innegable ayuda, siempre dispuesta a echar una mano. No se me ocurre una mejor profesora que tú. Espero que sientas esta Tesis casi tan tuya como mía.

Gracias a la Dra Mª Jesús Obregón, por acogerme en su laboratorio al principio y por iniciarme en el mundo del adiposo.

Um muito obrigado à Dra Carvalho por receber-me no seu laboratório no início da minha carreira no mundo da investigação. Não poderia ter começado a minha Tese num melhor sítio que o Porto. Uma palavra de apreço especial à Susana e ao João por me ensinarem tanto e tão bem. Vai ser sempre uma época que recordarei com um carinho especial. Y a mis amigos de Oporto por todo lo que hemos vivido en estos años.

Gracias a las Dras Herrero y Serra por acogerme en Barcelona. A Sebastián y Paula por los experis cuando las células iban bien y cuando no y a Mari Carmen, Kevin, Pia, Irene, Sergio y demás amigos de fuera del labo. Gracias a todos por hacer que sintiera Barcelona como si fuera mi casa y que haya sido un placer siempre volver.

Gracias a mis Valverdes. Sois geniales. Nuria, gracias por los inicios y todo lo que vino después, juntas de labo en labo. Te echaré de menos. Olé. Pili, siempre dispuesta a ayudarme. ¡Gracias por las clases de estadística! Tu predoc favorita es consciente de que te debe algún que otro ratito. Lauri, Irma y Rada, ha sido un placer trabajar con vosotras, os deseo lo mejor. Patri, eres rigor científico y sacrificio. Creo que no he podido tener un mejor ejemplo de cómo hay que trabajar. Gracias por ser mis brazos cuando no podía trabajar y mi cabeza cuando no podía pensar. Por las matanzas y sus datitos. Tiririririririri, ya sabes qué canción es. ¡Ay SIRT, que nos has dado 20 de cal y 1 de arena! Gracias por aguantarme y ser risas en los buenos momentos y un gran apoyo cuando no salía lo que esperábamos. Sin duda se me va a hacer muy raro dejar de trabajar contigo. No echaré de menos los eternos días de animalario pero sí las largas horas de confidencias. Me siento muy afortunada de haber aprendido de ti.

Y ¡quién te va a entender mejor que un predoc de tu labo! Diana, Rosa, Inés y Vitor, os voy a echar muCHísimo de menos. Gracias por haberme alegrado los días, por las tonterías y el apoyo constante. Vais a tener todos unas tesis geniales. ¡Os dejo en herencia mis post-its! Vitor, contigo todo son risas aseguradas. Gracias por solucionarme todos mis problemas tecnológicos y cuidarme siempre, por nuestras músicas y nuestras coñitas, imposible enumerar todas aquí. Inés, estoy escribiendo esto con la cabeza mirando hacia el teCHo, como en la foto más graciosa de la historia. ¡¡Vas a tener una gran Tesis!! Rosita, me gusta esta *involución*. Ya sabes que vas a poder seguir contando conmigo siempre. Te deseo lo mejor. Y sí Diana, te dejo para el final. Gracias por tu generosidad y por ser tan buena amiga. Siempre atenta y dispuesta a ayudarme. Es una gran suerte contar con alguien que sabes que siempre va a estar ahí para echarte un cable. Acho, reconojco que echaré de menos tu “bipolaridad” y meterme

contigo. Bueno y que te metas conmigo. Espero que antes de que te vayas tus post-its lleguen hasta el techo.

No me olvido de los estudiantes que han pasado por el labo, mención especial a Ángela, Dani, Ary y Ari, mi catalana preferida. Espero haberos ayudado y mil gracias también por vuestra ayuda.

A toda la gente del IIB, a mis amigos predocs que lo lograron y ya son Doctores. Yuri, mi viejoven favorito y Omar, te deseo que te vaya todo muy bien. Iara, no tengo ninguna duda de que nos seguiremos viendo allá por donde vayamos, eres genial. Mil gracias por ayudarme siempre. Y cómo no, Carla y Celia. No puedo imaginarme estos años sin vosotras a mi lado. Gracias por absolutamente todo. Si hablara la fuente del segundo piso… Carli desde que te fuiste el IIB no volvió a ser lo mismo. Me quedo con las miles de horas juntas en cultivos, nuestras comidas y nuestras conversaciones. Sigo alucinando con que te acuerdes de todas y cada una de mis historias, que no han sido pocas durante estos años. Celia, supe desde que nos cruzábamos por el pasillo que íbamos a ser muy amigas. Gracias por tus visitas, irradias felicidad. Gracias por sacarle el lado positivo a todo y estar ahí siempre. Y a los predocs de otros labos, Alberto, ¿con quién vas a comentar el lunes la última jornada? Que conste que aunque seas del barça me alegro mucho de haber coincidido contigo. Gracias por aguantarme tantas horas en cultivos. Elena, juntas desde la uni y ayudándome como siempre hasta hoy, Andrea, Adri, Carlos, Julia, Javi, Pilar os va a ir fenomenal seguro.

Gracias a todos mis amigos de fuera del labo. A mis guachis, Luis, Tito, Miki F, Miki B Carlos y a Joserra. Claudio gracias por el apoyo y por haber estado siempre pendiente ¡venga que no te queda nada a ti tampoco! Natalia, Marta, Andrea, Alber, Alberto, Coguis, Monti, etc si algo me llevo también de estos años son todos los planazos y viajes con vosotros. A mi pachoni y a las marinas por nuestros ratitos. A mis farmas, en especial Winki y Lu gracias por todo, benditos consejos. Eso eso.

Y a mis amigas, Isa, Sara y Marta. Gracias por los viajes, los festivales, los momentos buenos y los no tan buenos, por acompañarme y apoyarme. Isita, siempre dispuesta a apuntarse a cualquier plan, Sara, mi fiel compañera de viajes durante la Tesis ¡Viva la novia! y Marta, no olvidaré tus arcadas en el animalario, gracias por haber estado al pie del cañón durante estos 4 años. No puedo tener más suerte.

A mi familia, a mis orgullosas abuelas y a mis abuelos que seguro también lo están desde arriba. A todos mis tíos y mis primos, especialmente a mi tío Miguel Ángel y a mi primo Angelete por su constante interés.

A Nacho, por hacer del último año de Tesis que es el más duro, el más bonito. Gracias por sumar cuando todo resta, por apoyarme y cuidarme tanto y tan bien. Sacas lo mejor de mí. Gracias, gracias y gracias.

Y cómo no, a mis padres y a mi hermana. Por conseguir que se me olvidara todo lo malo al llegar a casa. Gracias por vuestros consejos y por ayudarme siempre. Mamá no puedo tener mejor ejemplo que el tuyo. No se me ocurre nadie que pueda entenderme tan bien como tú. Papá gracias por escucharme y ayudarme a relativizar todos mis problemas. Por tus tonterías con Isabel sobre los “pocitos” y los “western”. Isabel, gracias por aguantarme, por tu paciencia, por todos los viajes, los planes, y por ser la mejor hermana que se pueda tener. Si lo he conseguido ha sido gracias a vosotros. Os quiero muchísimo.

Carmen

RESUMEN

RESUMEN

Hoy en día, la incidencia de la obesidad está aumentando de manera alarmante, por lo que se ha convertido en la enfermedad metabólica más frecuente en el mundo. Esta patología está englobada por la Organización Mundial de la Salud dentro de las enfermedades crónicas junto a la diabetes mellitus tipo 2 (DMT2) y varios cánceres. El tejido adiposo tiene un papel importante en el estado inflamatorio crónico de bajo grado asociado a la obesidad debido a que el exceso de nutrientes altera la funcionalidad de los adipocitos e induce la secreción de citoquinas pro-inflamatorias y especies lipídicas reactivas que alteran las rutas metabólicas. El tejido adiposo marrón (BAT, del inglés brown adipose tissue) regula la homeostasis metabólica favoreciendo el gasto energético. Este depósito graso se postula como diana terapéutica frente a la obesidad debido a su capacidad de metabolizar grandes cantidades de lípidos y glucosa. Sin embargo, el impacto de la inflamación en el BAT no se ha estudiado en profundidad. En esta Tesis hemos analizado las respuestas insulínicas y β-adrenérgicas en el BAT en dos modelos de inflamación: ratones *db/db,* modelo genético de inflamación crónica asociada a obesidad y DMT2 y en ratones a los que se administró una dosis baja de lipopolisacárido bacteriano (LPS) para mimetizar la endotoxemia característica de los individuos obesos. Dado que la sirtuina 1 (SIRT1) se ha relacionado con la protección ante el daño metabólico en estados de obesidad, se ha estudiado el posible efecto beneficioso de dicha desacetilasa en condiciones pro-inflamatorias en la funcionalidad del BAT.

Nuestros resultados han evidenciado la susceptibilidad del BAT de los ratones *db/db* a la inflamación debido a la activación de cascadas de señalización y a la elevación de la expresión de genes pro-inflamatorios. Además, ambos modelos desarrollaron resistencia a la insulina en el BAT. En los ratones *db/db* esta alteración podría deberse, al menos en parte, a un cambio en el patrón de las isoformas del receptor de insulina (IR) poniendo de manifiesto la inmadurez metabólica del tejido. Además, los ratones que sobreexpresan SIRT1 (SIRT1^{Tg+}) estaban protegidos frente a la caída de la fosforilación de IR y AKT (proteína quinasa B) inducida por la insulina encontrada en los ratones de genotipo salvaje (WT, del inglés wild-type) inyectados con LPS. De acuerdo con estos resultados los adipocitos marrones diferenciados que sobreexpresan SIRT1 (BA-SIRT1^{Tg+}) y cultivados en condiciones pro-inflamatorias mantuvieron activada la vía de señalización de la insulina y la captación de glucosa. En relación a las respuestas adrenérgicas del BAT, los ratones *db/db* tratados con resveratrol, un activador de SIRT1, mostraron niveles más altos de proteína desacoplante 1 (UCP-1, del inglés uncoupling protein 1) en este tejido. Por otra parte, los ratones SIRT1^{Tg+} estaban protegidos contra el efecto nocivo del LPS en parámetros relacionados con la termogénesis y presentaron una caída menor de los niveles de T_3 en circulación y en el BAT después de la exposición al LPS y frío. Los experimentos en cultivo con adipocitos marrones de ambos genotipos revelaron que su diferenciación en presencia de altas concentraciones de T_3, rosiglitazona e insulina aumentaba la actividad de SIRT1 promoviendo la acumulación de lípidos en las gotas de grasa, la fisión mitocondrial y potenciando la respuesta lipolítica. Los adipocitos marrones de ambos genotipos mantuvieron la inducción de UCP-1 en la respuesta β-adrenérgica en condiciones pro-inflamatorias, siendo esta protección aún mayor en aquellos que sobreexpresan SIRT1. En conjunto, nuestros resultados proponen la activación de SIRT1 en el BAT como una posible herramienta terapéutica para combatir la inflamación crónica de bajo grado vinculada a la obesidad.

ABSTRACT

ABSTRACT

Nowadays, the global rate of obesity is increasing rapidly and has become the most frequent metabolic disease worldwide. This condition is considered by the Word Health Organization as a noncommunicable disease together with type 2 diabetes mellitus (T2DM) and several cancers. Numerous studies have clearly established that adipose tissue plays a relevant role in the chronic low grade inflammatory state associated to obesity since over-nutrition alters the functionality of adipocytes and induces the secretion of pro-inflammatory cytokines and reactive lipid species that negatively impact on whole body metabolism. Brown adipose tissue (BAT) plays a major role in the regulation of metabolic homeostasis by its ability to dissipate energy as heat. This fat depot is currently considered a therapeutic target against obesity due to its capacity of metabolize large amounts of lipids and glucose. In this Thesis we have analyzed insulin and β-adrenergic responses in BAT in two mouse models of inflammation: *db/db* mice as a genetic model of chronic inflammation linked to obesity and T2DM and in lean mice injected a low dose of bacterial lipopolysaccharide (LPS) to mimic endotoxemia. Since sirtuin1 (SIRT1) has been related to the protection from metabolic damage associated to obesity, we also studied the potential beneficial effect of targeting SIRT1 under pro-inflammatory conditions

Our results have provided evidences of the susceptibility of BAT from *db/db* mice to metabolic inflammation since activation of a pro-inflammatory signature of signaling cascades together with elevation of pro-inflammatory-related gene expression was found in this fat depot compared with the lean controls (*db*+). Furthermore, we demonstrated insulin resistance in BAT from *db/db* mice that might be due, at least in part, to alterations in the pattern of insulin receptor (IR) isoforms, revealing metabolic immaturity of the tissue. Moreover, mice with moderate overexpression of SIRT1 (SIRT1^{Tg+}) were protected against the drop in insulin-mediated IR and AKT (protein kinase B) phosphorylation detected in LPS-injected wild-type (WT) mice. In line with these findings, differentiated brown adipocytes overexpressing SIRT1 (BA-SIRT1^{Tg+}) upon stimulation with a pro-inflammatory medium showed similar protection as well as preserved insulin-mediated glucose uptake. Regarding the impact of inflammation in adrenergic responses in BAT, *db/db* mice treated with resveratrol, a SIRT1 activator, showed higher uncoupling protein 1 (UCP-1) levels in this tissue. Moreover, SIRT1^{Tg+} mice were protected against the deleterious effect of LPS in thermogenic-related parameters. Importantly, mice overexpressing SIRT1 attenuated the drop of T_3 levels both in circulation and BAT after the exposure to LPS and cold. Cellular experiments in brown adipocytes (BA) from the two genotypes revealed that differentiation in the presence of high concentrations of T_3, rosiglitazone and insulin increased SIRT1 activity favoring lipid accumulation in fat droplets, mitochondrial fission as well as potentiating the lipolytic response. In addition, BA from both genotypes maintained the induction of UCP-1 in response to norepinephrine (NE) under pro-inflammatory conditions, being this protection even higher in cells overexpressing SIRT1. Altogether, our results point to SIRT1 activation in BAT as a potential target against the low grade chronic inflammatory stage linked to obesity.

INDEX

INDEX

ABBREVIATIONS

^{18}FDG-PET: ^{18}Fluoro-labeled 2-deoxyglucose positron emission tomography

3,5,3'-T_3: Triiodothyronine

AC: Adenylyl cyclase

Acetyl-CoA: Acetyl coenzyme A

AKT: Protein kinase B

AMPK: AMP-activated protein kinase

ASPs: Acid-soluble products

ATF2: Activating transcription factor 2

ATM: Adipose tissue macrophages

ATP: Adenosine triphosphate

BA: Brown adipocytes

BAT: Brown adipose tissue

BMI: Body mass index

BSA: Bovine serum albumin

c/EBPβ: CCAAT-enhancer-binding protein β

cAMP: Cyclic adenosine monophosphate

CM: Conditions medium

CM-CTR: Conditioned media control

CM-LPS: Conditioned medium LPS

COXIV: Cytochrome c oxidase subunit 4

CPT1a: Carnitine palmitoyltransferase 1A

CR: Caloric restriction

CREB: cAMP response element-binding protein

CXCL14: Chemokine (C-X-C motif) Ligand 14

D1: Deiodinase iodothyronine, type 1 (enzyme)

D2: Deiodinase iodothyronine, type 2 (enzyme)

***Dbc1*:** inhibitor Deleted in breast cancer-1

DEPC: Diethylpirocarbonate

Dio1: Deiodinase iodothyronine, type 1 (gene)

Dio2: Deiodinase iodothyronine, type 2 (gene)

DMEM: Eagle's Minimal Essential Medium

DRP1: Dynamin-related protein-1

DTT: Dithiothreitol

EDTA: Ethylenediaminetetraacetic acid

ERK: Extracellular Mitogen-activated protein kinases

ETC: Electron transport chain

eWAT: Epididymal WAT

$FADH_2$: Flavin adenine dinucleotide, reduced form

FAO: Fatty acid oxidation

FBS: Fetal bovine serum

FFAs: Free fatty acids

FGF21: Fibroblast Growth Factor 21

FOXO1: Forkhead Box O1

GLUT-4: Glucose transporter type 4

GSV: GLUT4 storage vesicles

H&E: Hematoxylin and eosin

HbA1c: Glycated hemoglobin A1c

HFD: High-fat diet

HOMA-IR: Insulin resistance score (homeostatic model assessment)

HSL: Hormone-sensitive lipase

i.p.: Intraperitoneally

IBMX: Isobutylmethylxanthine

IFNγ : Interferon γ

IGF-I: Insulin-like growth factor I

IkB: Inhibitor of kB

IKK: IκB kinase

IL: Interleukin

iNOS: Inducible nitric oxide synthase

IR: Insulin receptor

IRAK: IL-1 receptor-associated kinase

IRS: Insulin receptor substrates

iWAT: Inguinal WAT

JAK: Janus kinase

JNK: c-JUN N-terminal kinase

KRB: Krebs-Ringer Modified Buffer

KRP: Krebs-Ringer-phosphate buffer

LPS: Bacterial lipopolysaccharide

MAPK: Mitogen-activated protein kinases

MFN1: Mitofusin 1

MFN2: Mitofusin 2

MKK: MAP kinase kinases

MnSOD: Manganese superoxide dismutase

mtDNA: Mitochondrial DNA

MTG: MitoTracker Green

mTORC2: Mechanistic target of rapamycin 2

NAD^+: Nicotinamide adenine dinucleotide

NADH: Nicotinamide adenine dinucleotide, reduced form

NCS: Newborn calf serum

NE: Norepinephrine

NEDA: N-(l-naphthyl) ethylenediamine

NF-kB: Nuclear factor-kappa B

NGS: Normal goat serum

NO: Nitric oxide

NOS-2: Nitric oxide synthase

NRF1: Nuclear respiratory factor 1

NRG4: Neuregulin-4

OCR: Oxygen consumption rate

O/N: Overnight

OPA1: Optic atrophy 1

OXPHOS: oxidative phosphorylation

PBS: phosphate buffered saline

PDK1: Phosphoinositide-dependent kinase-1

PFA: Paraformaldehyde

PGC-1α: Peroxisome proliferator-activated receptors-γ co-activator 1α

PI3K: Phosphatidylinositol 3-kinase

PINK1: PTEN-induced putative kinase 1

PIP2: Phosphatidylinositol-4,5-diphosphate

PIP3: Phosphatidylinositol-3,4,5-trisphosphate

PKA: Protein kinase A

PMSF: phenylmethanelsulfonyl fluoride

PMVECs: Pulmonary microvascular vein endothelial cells

PRDM16: PR domain zinc-finger protein 16

PRRs: Pattern recognition receptors

PTP1B: Protein tyrosine phosphatase 1B

RIA: Radioimmunoassay

RPMI: Roswell Park Memorial Institute

RT: Room temperature

SDS: sodium dodecyl sulphate

Ser: Serine

Sir2: silent information regulator 2

SirBACO: SirT1 Bacterial Artificial Chromosome Overexpressor

SIRT: Sirtuin

SNS: Sympathetic nervous system

SOCS: Suppressor of cytokine signaling

STACs: SIRT1 activating compounds

STAT-3: Signal transducer and activator of transcription 3

T2DM: Type 2 diabetes mellitus

T_4: Thyroxine

TBS: Tris-buffered saline

TCA: Tricarboxylic acid cycle

TG: Triglycerides

Thr: Threonine

THs: Thyroid hormones

TLR: Toll-like receptor

TNF-α: Tumor necrosis factor-α

TOM22: Translocase of the outer membrane of mitochondria

TR: Thyroid-hormone receptor

TRH: Thyroid releasing hormone

TSH: Thyroid stimulating hormone

Tyr: Tyrosine

UCP-1: Uncoupling protein 1

VEGF-A: Vascular Endothelial Growth Factor A

WAT: White adipose tissue

WT: Wild-type

β_3-AR: β_3-adrenergic receptor

INTRODUCTION

1. OBESITY AND TYPE 2 DIABETES MELLITUS.

Obesity is a multifactorial and polygenic disease that has become an alarming health issue since it is affecting both developed and developing countries [1-3]. Nowadays, obesity is the most frequent metabolic disease all over the world and its incidence is rising rapidly. According to the World Health Organization in 2016, 39% of adults over 18 years of age had overweight and, overall, about 13% of the world's adult population was obese. Worldwide the prevalence of obesity has tripled between 1975 and 2016 [4]. This obese population is at risk of developing several chronic non-communicable diseases. In this regard, cardiovascular diseases, non-alcoholic fatty liver disease, cancer and type 2 diabetes mellitus (T2DM) stand out among the major health concerns that are responsible for morbidity related to obesity [5].

In chronic over nutrition, the excess of nutrients and energy exceeds the storage capacity of metabolic tissues, mainly adipose tissues, thereby inducing metabolic stress and a low-grade chronic inflammation [6]. This pro-inflammatory state leads to lipid accumulation in adipocytes and is responsible for the decrease in insulin sensitivity, which makes obesity a major risk factor for insulin resistance and T2DM [7], the most prevalent disease in the world characterized by both defects in insulin action in peripheral tissues and insulin secretion. Despite the recent advances in molecular medicine, progression from obesity-related insulin resistance to T2DM and the initial triggers of low-grade inflammation remain unknown [8]. Many studies have clearly established that adipose tissues, liver, muscle and pancreas are key sites of inflammation in obesity and T2DM. In fact, adipose tissue seems to play a central role in the induction of inflammation since over-nutrition leads to substantial changes in adipocyte plasticity including the secretion of pro-inflammatory cytokines that impact on whole body metabolism. Thus, targeting adipose tissue inflammation is a potential therapeutic strategy in the prevention and treatment of obesity and related co-morbidities [9].

2. ADIPOSE TISSUES.

There are three types of adipose tissue: white, brown, and beige/brite that contain different types of adipocytes namely white, brown or beige adipocytes, respectively (Figure 1).

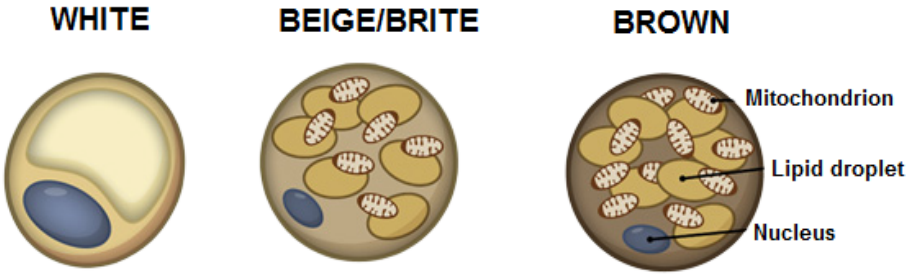

Figure 1. Types of adipose cells. As shown in the figure, adipose cells can be divided according to the number of mitochondria, type and number of lipid droplets and location of the nucleus.
NOTE: Adapted from [10]

The functional importance of these different adipose depots in energy metabolism mainly depends on their composition [11] (Table 1).

Characteristic property	White	Beige	Brown
Morphology			
(i) Shape	Spherical	Spherical	Ellipsoid/polygonal
(ii) Cell size	Variable, large (25–200 μm)	Variable, smaller than white	Small (15–60 μm)
(iii) Lipid droplet (LD)	Single large LD	Multiple LD with variable size	Multiple small LD
(iv) Mitochondria	+	++ (upon stimulation)	+++
Development	From $Myf5^-$ or $Myf5^+$ precursors	From $Myf5^-$ or $Myf5^+$ precursors	From $Myf5^+$ precursors
Location	Subcutaneous and visceral	Inguinal, neck (near carotid sheath and musculus longus colli), other locations?	Suprarenal, paravertebral, supraclavicular
Function	Energy storage	Adaptive thermogenesis	Heat production
Uncoupling protein	Nearly undetectable	++ (upon stimulation)	+++
Vascularization	Low	High upon stimulation	High
Impact on obesity	Positive	Negative	Negative

Table 1. Characteristics of white, beige and brown adipose tissue in rodents and humans.
NOTE: Adapted from [12].

2.1. WHITE ADIPOSE TISSUE (WAT).

WAT accounts for 5–50 % of the total body weight in humans and contains mature white adipocytes with a single lipid droplet (unilocular) in the cytoplasm and a peripherally-located nucleus. This tissue can store the excess of energy in the form of triglycerides that can be released as free fatty acids (FFAs) into the circulation upon activation of lipolysis [13]. WAT can be classified in subcutaneous/inguinal (iWAT) (underneath the skin) or visceral (within the abdominal cavity) according to its anatomical location [14, 15] and distinct metabolic functions. Various studies have described that expansion of visceral WAT is closely associated with inflammation, insulin resistance, and T2DM [16] whereas subcutaneous WAT, associated with improved insulin sensitivity [17], has been shown to be less inflammatory [18-21] and more susceptible to acquiring brown fat characteristics under certain conditions [22-27].

In obesity, WAT expands by a combination of an increase in both adipocyte size (hypertrophy) and number (hyperplasia). Notably, WAT is currently recognized not only as an inert energy storage depot, but also as a complex metabolically active organ with considerable impact on human health [28, 29] that protects other organs (liver and muscle) from lipid-associated toxicity (lipotoxicity) [30] and plays an important role in endocrine signaling [31, 32].

2.2. BROWN ADIPOSE TISSUE (BAT).

BAT is a highly vascularized and innervated adipose tissue [33] that differs morphologically from WAT since it contains multiple small (multilocular) lipid droplets in the cytoplasm, a central nucleus and a large number of mitochondria [34]. Moreover, this depot is much less abundant than WAT.

In BAT, mitochondria are distinct from those organelles present in other tissues in which their main function is the oxidative phosphorylation and adenosine triphosphate (ATP) production. BAT mitochondria represent an exception due to their ability to produce heat in addition to ATP by the process known as “non-shivering” thermogenesis [35]. To perform this specific function, BAT mitochondria express the uncoupling protein 1 (UCP-1) in their inner membrane which uncouples respiration from ATP synthesis and induces the generation of heat [34, 36-39].

Cold is the most potent stimulus for thermogenesis in brown adipocytes. Under cold-exposure, catecholamines are released from sympathetic nerve endings and bind to β-adrenergic receptors on the plasma membrane of brown adipose cells, mainly β_3-adrenergic receptors (β_3-AR). This binding enhances the interaction of these receptors with guanine nucleotide-binding proteins (G proteins) which, in turn, activates the enzyme adenylyl cyclase (AC) to increase intercellular cyclic adenosine monophosphate (cAMP) concentration [40]. The increase of cAMP levels triggers the activation of cAMP-dependent protein kinase A (PKA). In turn, PKA phosphorylates the hormone-sensitive lipase (HSL) leading to the hydrolysis of triglycerides from BAT lipid droplets. Afterwards, the released FFAs are β-oxidized to generate nicotinamide adenine dinucleotide (NADH), flavin adenine dinucleotide ($FADH_2$) and acetyl coenzyme A (acetyl-CoA). The latter metabolite enters the tricarboxylic acid cycle (TCA) where it produces additional electron carriers (NADH and $FADH_2$) that transfer electrons to the complexes of the electron transport chain (ETC) located in the inner mitochondrial membrane. The terminal electron acceptor is the molecular oxygen which is reduced to water. During this process protons are pumped through the mitochondrial respiratory chain complexes generating an electrochemical gradient. UCP-1 acts as a transmembrane protein allowing protons to re-enter the mitochondrial matrix, thereby dissipating the electrochemical gradient that drives ATP synthesis by the ATP synthase complex. This process results in the release of significant amounts of chemical energy in the form of heat [34, 41] as mentioned above and detailed in Figure 2.

The study of BAT has exponentially become more relevant since its re-discovery in adult humans in 2007 [42]. Clinical reports in oncology using ^{18}Fluoro-labeled 2-deoxyglucose positron emission tomography (^{18}FDG-PET) scanning in combination with computed tomography (CT) identified active BAT depots in adult humans mainly located in the supraclavicular region of the neck [43, 44]. Although BAT is present in relatively small amounts in the body, it has the potential to rapidly produce large amounts of heat that impact on both energy balance and glucose and lipid homeostasis [45], pointing BAT as a tissue capable of altering energy expenditure and fuel metabolism without increasing physical activity. This is exemplified by the rapid activation of brown fat around birth and the critical role of this process in the prevention of post-natal hypothermia [46].

The study of BAT in mice has also become increasingly important with the generation of transgenic mouse models [37]. Of note, the major BAT depots in mice are found in the interscapular, axillary, perirenal and periaortic regions [34].

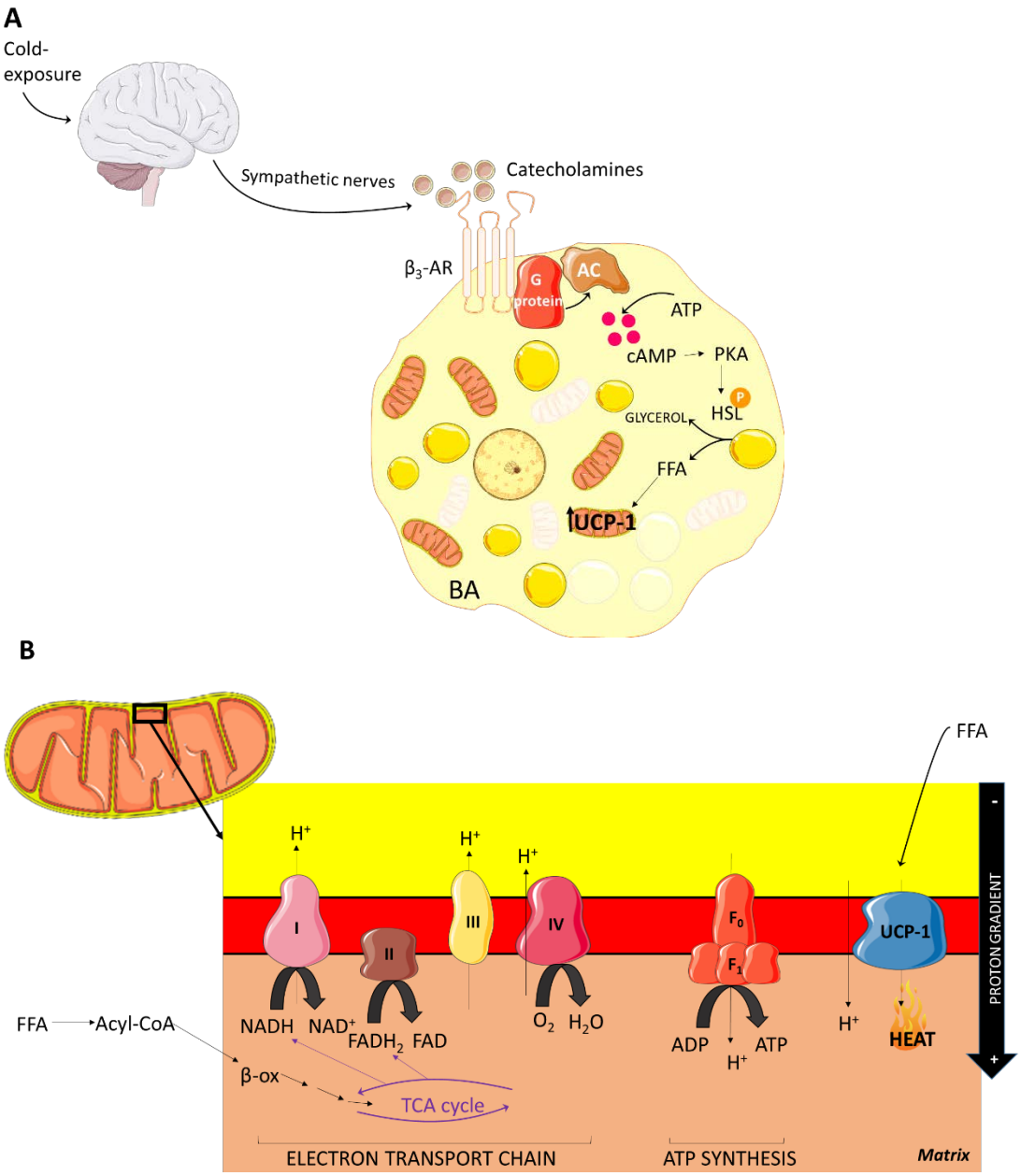

Figure 2. UCP-1 activation in BAT. (A) Activation of the sympathetic nervous system by cold-exposure results in the release of catecholamines that bind to the β_3-AR and elicit HSL-mediated lipolysis and further activation of UCP-1 in brown adipocytes (BA). **(B)** FFAs activated to acyl-CoAs by acyl-CoA synthetase (not represented in the figure) are imported into the mitochondria ensuring β-oxidation as well as the activity of the TCA. This leads to the formation of the reduced electron carriers $FADH_2$ and NADH, which are then oxidized by the electron transport chain. As a consequence, a pumping out of protons from the mitochondria and the creation of a proton-motive force that drives the protons back into the mitochondrial matrix through the UCP-1 leads to heat production.

2.2.1. ROLE OF BAT IN METABOLIC HOMEOSTASIS.

In addition to its thermogenic function, BAT plays an important role in the regulation of metabolic homeostasis affecting lipid and glucose metabolism. Regarding lipid metabolism, as mentioned above, activation of β_3-AR induces lipolysis and the released FFAs are used as substrates for mitochondrial respiration. Thus, BAT may be a major site of triglyceride clearance from the circulation. Regarding glucose metabolism, glucose uptake is essential for BAT function as glucose supports thermogenesis both

directly, as a fuel, and indirectly by replenishing TCA intermediates or supplying FFAs for thermogenesis via lipogenesis.

The insulin signaling pathway is critical for the maintenance of glucose homeostasis of the organism, and it also occurs in BAT. The insulin receptor (IR) has 2 extracellular α-subunits and 2 transmembrane β-subunits linked together by disulphide bonds. Binding of insulin to the α-subunits induces a conformational change resulting in the autophosphorylation of a number of tyrosine residues present in the β-subunits [47]. After insulin binding, the IR also phosphorylates the IR substrates (IRS proteins), mainly IRS1 and IRS2, in multiple tyrosine (Tyr) residues. Both IR and IRS1 are negatively regulated by the protein tyrosine phosphatase 1B (PTP1B) which dephosphorylates Tyr residues in the catalytic domain of the IR or in critical binding residues of IRS1 to downstream signaling mediators [48]. IRS proteins activate two major signaling pathways. The Ras/Raf/Extracellular Mitogen-activated protein kinases (ERK) pathway regulates the expression of genes related to cell growth and differentiation. The phosphatidylinositol 3-kinase (PI3K) pathway generates bioactive phosphoinositides that via phosphoinositide-dependent kinase-1 (PDK1) and mechanistic target of rapamycin 2 (mTORC2) activation leads to protein kinase B (AKT) phosphorylation in Threonine (Thr) 308 and Serine (Ser) 473, respectively, being responsible for the metabolic actions of insulin [49]. Likewise, AKT phosphorylation regulates the phosphorylation of various downstream signaling molecules. Among them, the Rab GTPase-activating protein AS160 is a substrate protein that stimulates the translocation of the glucose transporter type 4 (GLUT4), the main glucose transporter in brown adipocytes, from the cytoplasmic vesicles to the cell membrane surface. Non-phosphorylated AS160 binds to GLUT4 containing vesicles inhibiting its translocation. However, AKT phosphorylates and inactivates AS160 promoting GLUT4 translocation to the plasma membrane and increasing the insulin-dependent transport of glucose into the cell [50-52] (Figure 3).

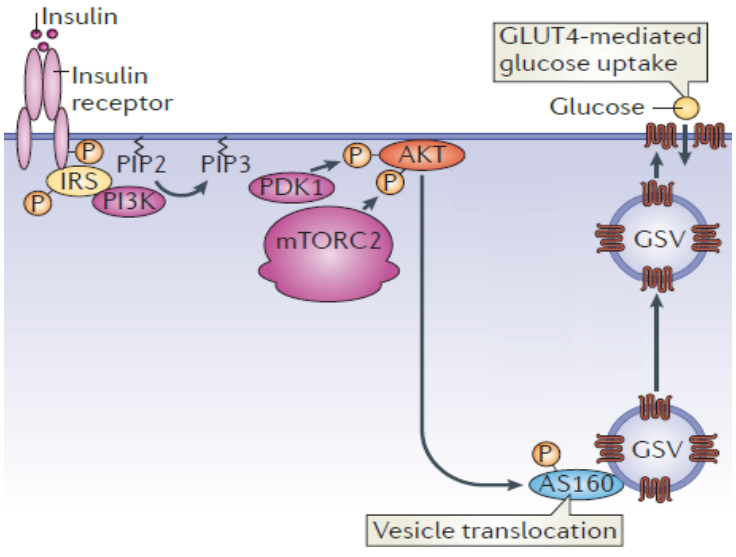

Figure 3. Insulin signaling pathway in adipose tissues. Binding of insulin to the IR activates the PI3K-dependent signaling cascade by phosphorylating IRS proteins, thus producing docking sites for the recruitment and activation of PI3K, which converts phosphatidylinositol-4,5-diphosphate (PIP2) to phosphatidylinositol-3,4,5-trisphosphate (PIP3). PIP3 recruits PDK1 and AKT, the latter is activated at the plasma membrane when is phosphorylated by PDK1 and mTORC2. AKT promotes the translocation of GLUT4 to the plasma membrane by phosphorylating and inactivating AS160. GSV: GLUT4 storage vesicles. NOTE: Adapted from [53].

2.2.2. BAT FUNCTION REGULATION.

The expression of the thermogenic program in BAT is regulated by a tightly transcriptional mechanism driven by several transcriptional regulators as shown in Figure 4 and detailed below.

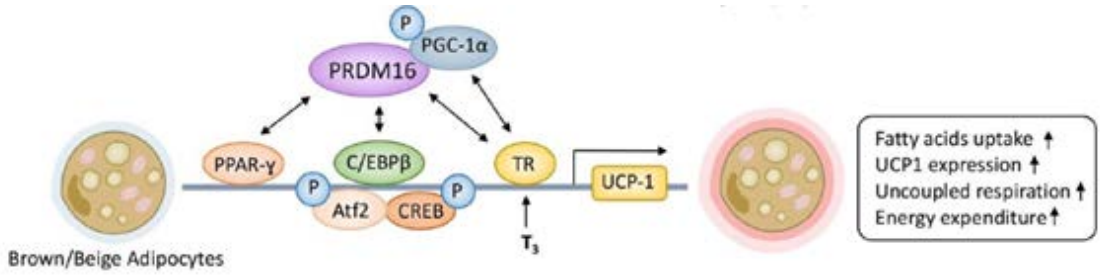

Figure 4. Molecular mechanisms governing thermogenesis. Double arrow indicates formation of transcription complex. ATF2: activating transcription factor 2; c/EBPβ: CCAAT-enhancer-binding protein β; CREB: cAMP response element-binding protein; PGC-1α: peroxisome proliferator-activated receptors-γ co-activator 1α; PPARγ: peroxisome proliferator-activated receptors-γ; PRDM16: PR domain zinc-finger protein 16; TR: thyroid hormone receptor.
NOTE: Adapted from [54].

- **PGC-1α–PPARγ complex.**

One of the first identified transcriptional regulators of adaptive thermogenesis was PGC-1α, a nuclear protein that is a strong activator of both mitochondrial function and biogenesis and is a master regulator of oxidative metabolism. In BAT, PGC-1α is a critical regulator of tissue activity in response to environmental stimuli as it is induced upon cold-exposure, exercise or fasting. PGC-1α exerts its function on thermogenesis mainly through binding to the nuclear receptor PPARγ, but also through the TR [55-57]. PGC-1α is indispensable for cold- or β-agonist- induced activation of brown adipocytes [58].

- **PRDM16.**

PR domain containing 16, also known as PRDM16, is a transcriptional co-regulator that controls the fate between muscle and brown fat cell development. During brown fat development, PRDM16 interacts with PPARα/PPARγ and C/EBPβ family leading to the induction of brown fat-related genes together with the repression of selective WAT markers. PRDM16 is also required for PPARγ agonist-mediated white-to-brown fat conversion, contributing to the browning of iWAT as it will be mentioned below. It has also been reported that rosiglitazone, a thiazolidinedione required for adipogenic differentiation in vitro, is a PPARγ agonist and exerts its thermogenic effects in adipocytes through increasing the half-life of PRDM16 [27, 59, 60].

- **3,5,3'-TRIIODOTHYRONINE (T_3).**

BAT is a target tissue of thyroid hormones (THs) that regulate crucial genes for its correct function related to lipogenesis, lipolysis, thermogenesis and mitochondrial function [61].

THs are synthesized by the thyroid gland. When hypothalamus senses low circulating THs levels it stimulates the synthesis and secretion of TRH (thyroid releasing hormone) which in turn stimulates the synthesis and secretion of TSH (thyroid stimulating hormone) by the pituitary gland. Then, circulating TSH activates THs production by the thyroid gland [62]. THs are present in two forms, thyroxine (T_4) and its active metabolite T_3. T_4 is the main synthesized hormone since most T_3 is produced by deiodination of T_4 in

peripheral tissues by the enzymes D1 and D2 (deiodinase iodothyronine, type 1 and 2, respectively) [63]. The genes involved in the expression of D1 and D2 are referred to as *Dio1* and *Dio2*. Deiodinases are a family of selenoproteins that regulate the bioavailability of active THs in a tissue specific manner. D1 is present in the thyroid gland, liver, kidney, and pituitary, its levels decrease in hypothyroidism and increase in hyperthyroidism, except for thyroid D1, which increases in hypothyroidism due to TSH stimulation. D2 is mainly present in the pituitary, brain and BAT and increases in hypothyroidism, producing T_3 for local needs. Both D1 and D2 contribute to the maintenance of adequate intracellular T_3 levels in the different tissues [64].

THs act in the brain to modulate energy balance since T_3 increases hypothalamic stimulation of the sympathetic nervous system to induce *Dio2* expression and increase local conversion from T_4 to T_3 [61] that can reach BAT. This fat tissue is enriched in TRs that are required to maintain the normal adrenergic responsiveness of brown adipocytes and also to mediate T_3-induced UCP-1 gene expression [65, 66]. Therefore, THs are essential to maintain the norepinephrine (NE)-mediated signaling in BAT as they can improve thermogenesis in brown adipocytes by promoting the expression of UCP-1 in mitochondria. Moreover, TRs interact with PGC-1α and bind to the UCP-1 enhancer region, resulting in increased UCP-1 expression in mitochondria [67] (Figure 5).

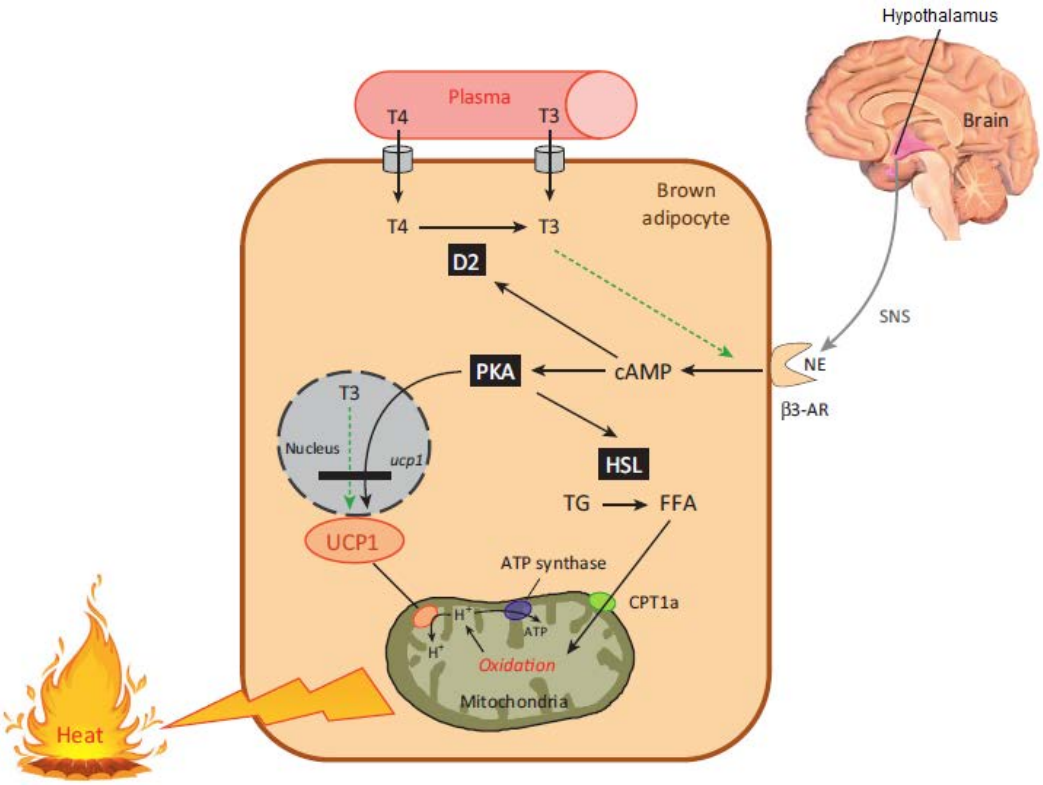

Figure 5. Modulation of uncoupling oxidative phosphorylation and heat production in BAT by thyroid hormones. Thyroid hormones (T_4 and T_3) act on the brown adipocytes by two different pathways: increasing the stimulatory action of NE on thermogenesis and enhancing the cAMP-mediated acute rise in UCP-1 gene expression by enhancing both gene transcription and mRNA half-life. SNS: sympathetic nervous system; TG: triglycerides; CPT1a: carnitine palmitoyltransferase 1A.
NOTE: Adapted from [68].

It has been extensively studied that in the absence of T_3 the thermogenic capacity of BAT is greatly reduced [69]. Clinically, these effects are manifested by the hyperthermia and hypothermia observed in patients with severe hyperthyroidism and hypothyroidism,

respectively [70]. Based on that, thyromimetics that specifically target BAT may be useful for pharmacological activation of this tissue [71].

Recent results reported by Yau et al. [70] have extended the knowledge on T_3 cell autonomous effects in BAT mitochondria. They showed that T_3 increases fatty acid oxidation, mitophagy, mitochondrial biogenesis and mitochondrial turnover in BAT and increases mitochondrial respiration in primary brown adipocytes. On the other hand, the work of Holtorf and co-workers [72] showed that chronic inflammation associated to obesity can alter THs-mediated signaling pathways and induce peripheral tissue resistance to THs action. For example, the increase in the release of pro-inflammatory cytokines in WAT can affect both local and systemic THs transport, alter DIO enzymatic activity and, therefore, T_4/T_3 activation as well as THs binding to TRs. In the same line, a recent study found that increased visceral adiposity may be responsible for changes in thyroid parameters associated with obesity including elevated TSH or free T_3/T_4 levels [73]. Some authors have studied the impact of inflammation in THs action by bacterial lipopolysaccharide (LPS) administration which results in decreased liver [74], heart [75] and skeletal muscle [76] TRs expression. Moreover, LPS also alters serum THs levels, an effect partly mediated via TRs and most likely due to either decreased THs secretion by the thyroid gland or increased THs clearance. The peripheral changes observed in *Dio* expression probably result in either decreased or increased local availability of T_3, which might lead to changes in metabolic activity [74]. Furthermore, T_3 suppresses interleukin (IL)-6 signaling in macrophages and hepatocarcinoma cells by inhibiting the signal transducer and activator of transcription 3 (STAT-3) activation in response to LPS [77].

A possible relationship between THs and glucose metabolism in diabetes has already been established since hyper and hypothyroidism causes dysglycemia. High circulating T_3 levels are associated with most features of insulin resistance and defects in glucose tolerance (reduced insulin-mediated glucose disposal and β-cell glucose sensitivity among others factors) [78]. Abnormalities in THs metabolism are also related to inflammation and disorders of glucose metabolism since TSH and free T_4 are correlated with inflammatory markers (IL-6 and Tumor necrosis factor-α, TNF-α), and free T_3 negatively correlates with IL-6 and markers of T2DM such as glycated hemoglobin A1c levels (HbA1c) and insulin resistance score (homeostatic model assessment, HOMA-IR) [79]. Further research is needed to study in more depth the exact mechanisms associated with inflammation-induced impairment of thyroid functionality in BAT.

- **BAT AS AN ENDOCRINE ORGAN: SECRETED PROTEINS BY BROWN ADIPOCYTES.**

In addition to its thermogenic capacity, BAT has also a secretory role that allows this tissue to communicate with the brain, liver, muscle, pancreas, and other organs in an endocrine manner. BAT can release a plethora of bioactive regulatory molecules (termed brown adipokines or batokines) that act in an endocrine, paracrine or autocrine manner [80]. These secretory factors enhance the thermogenic activity by regulating the hypertrophy and/or hyperplasia of brown adipocytes and also help to reach their maximum activity by regulating the innervation in response to prolonged cold environment. Among many other batokines, Fibroblast Growth Factor 21 (FGF21) Neuregulin-4 (NRG4), Vascular Endothelial Growth Factor A (VEGF-A), Chemokine (C-X-C motif) Ligand 14 (CXCL14) have been the most studied [80, 81].

As mentioned above, FGF21 is one of the best-known batokines. The liver is considered the main site of FGF21 production [82]. However, extrahepatic tissues, such as skeletal muscle, BAT and WAT also contribute to maintain FGF21 systemic levels. This molecule is a circulating peptide hormone that can be secreted by BAT and WAT under cold-

exposure and has a paracrine effect stimulating the expression of thermogenic genes and browning of iWAT involving PGC-1α-dependent mechanisms [83-87]. FGF21 is currently considered as a promising anti-obesity agent based on its beneficial effects on body weight, energy expenditure, lipid mobilization and peripheral insulin sensitivity [88].

- **BAT MITOCHONDRIA.**

As it has been already mentioned, BAT is highly enriched in mitochondria. Of note, mitochondrial dynamics, a process that controls the functionality of these organelles, is highly relevant in this fat depot (Figure 6).

Mitochondria are dynamic and go through continuous fusion and fission cycles depending on environmental signals such as the nutritional status. Fusion promotes elongated mitochondria, a response that is often observed under nutrient restriction. On the other hand, fission results in fragmented, separated mitochondria and is more common in a nutrient-rich environment [89, 90].

Fusion mitochondrial dynamics is controlled by GTPase enzymes such as mitofusins 1 and 2 (MFN1 and MFN2) that govern outer mitochondrial membrane fusion and optic atrophy 1 (OPA1) which controls inner mitochondrial membrane fusion. Conversely, mitochondrial fission is controlled mainly by the dynamin-related protein-1 (DRP1) [89]. MFN2 is critical for the thermogenic function of BAT [91] as its deletion in mice leads to impaired thermogenesis [92]. Furthermore, the absence of DRP1 impairs mitochondrial uncoupling respiration in beige adipocytes as described by Pisani and co-workers [93].

The maintenance of a healthy and functional mitochondrial network is critical during development as well as throughout life in the response to physiological adaptations and stress conditions. In this regard, quality control mechanisms are necessary to eliminate damaged mitochondrial proteins by mitophagy (a specialized type of autophagy) in order ensure a correct function of these organelles [94]. Several studies have reported that mitophagy mediated by PTEN-induced putative kinase 1 (PINK1) and Parkin may play a critical role in clearing the damaged mitochondria and maintaining the overall balance of intracellular mitochondria in quality and quantity [95, 96].

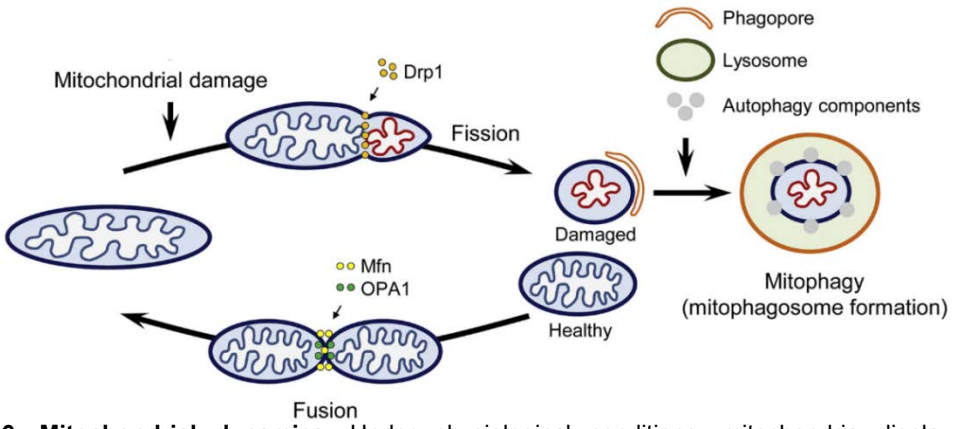

Figure 6. Mitochondrial dynamics. Under physiological conditions, mitochondria display tubular morphology. Different factors can change mitochondrial dynamics and shift this process towards either fission (mitochondrial fragmentation) or fusion (mitochondrial elongation). When mitochondria are damaged, mitochondrial fission facilitates the segregation of the healthy mitochondria from the damaged ones, which are subsequently removed by mitophagy.
NOTE: adapted from [97].

Obesity and insulin resistance alter mitochondrial number and/or function leading to "mitochondrial dysfunction" in adipocytes that may trigger cell death. In fact, pro-

inflammatory cytokines have been shown to regulate adipocyte mitochondrial metabolism and dynamics in 3T3-L1 adipocytes [98].

2.3. BEIGE / BRITE ADIPOSE TISSUE.

It has been previously described that brown adipocytes can also emerge in subcutaneous white adipose depots in response to various stimuli, including prolonged cold-exposure or β-adrenergic stimulation [26, 34, 83, 99-102], pharmacological treatment (Himms-Hagen, Melnyk et al. 2000), weight loss upon bariatric surgery (Neinast, Frank et al. 2015) or caloric restriction (CR) (Fabbiano, Suarez-Zamorano et al. 2016). Therefore, multiple genetic factors have recently been identified to regulate the browning of WAT. These adipocytes have been called “beige or brite” adipocytes and the process by which they transdifferentiate into brown fat-like cells is known as “browning”. The resultant beige or brite cells enhance energy expenditure by reducing lipids stored within WAT. The origin of beige adipocytes is not completely understood and several processes seem to be involved. Moreover, controversy on the impact of their contribution to whole body energy expenditure is under debate in the field.

3. OBESITY AND INFLAMMATION.

As stated above, obesity is associated with a low-grade chronic inflammation of WAT resulting from chronic activation of the innate immune system that can subsequently trigger insulin resistance, impaired glucose tolerance and even T2DM [103]. In obesity, adipose tissue macrophages (ATM) expressing the macrophage marker F4/80 are recruited and activated by an expanding adipose tissue mass [104-107]. Obese WAT is characterized by the increased production of many inflammatory molecules including TNF-α and IL-6, which have systemic effects on other metabolic organs. Moreover, ATM from obese mice secret higher levels of locally-produced pro-inflammatory cytokines [108] than ATMs isolated from lean mice [103, 109].

Macrophages are critical regulators of systemic metabolism that can undergo a dynamic switch in response to different microenvironment signals. Macrophages can be classified into two distinct subtypes: the ‘‘classically activated macrophages’’ phenotype, termed M1, and the ‘‘alternatively activated macrophages’’ phenotype, termed M2. M1 macrophages acquire this phenotype in response to pro-inflammatory signals, such as Toll-like receptor (TLR) ligands (LPS or interferon γ (IFNγ)) and they secrete pro-inflammatory cytokines such as IL-1β, IL-6 or TNF-α. Conversely, M2 macrophages are activated in the presence of anti-inflammatory cytokines such as IL-4 and IL-13, and produce anti-inflammatory cytokines such as IL-10 [110]. M1 macrophages express the enzyme inducible nitric oxide synthase (iNOS) which metabolizes arginine to nitric oxide (NO) that can be metabolized to reactive nitrogen species and also inhibits cell proliferation and kills pathogens. M2 macrophages are characterized by the expression of the enzyme arginase 1 that hydrolyzes arginine to ornithine and urea. The arginase pathway can further feed downstream pathways related to cellular proliferation and tissue repair [111]. Thus, iNOS and arginase 1 are thought to affect inflammatory responses in the opposite way. It is noteworthy to point that intermediate stages of macrophage polarization have also been identified [112].

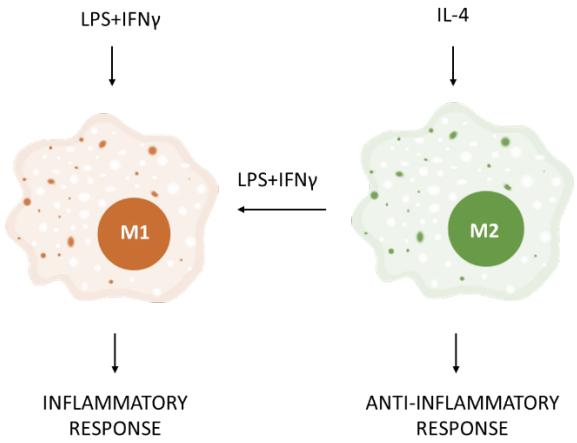

Figure 7. Representative scheme of macrophages polarization. Treatment of macrophages with LPS plus IFNγ generates NO, driving the pro-inflammatory phenotype of these cells. By contrast, IL-4/IL-13 promote an anti-inflammatory phenotype. The inflammatory M1 macrophage cannot be repolarized to M2. However, the anti-inflammatory M2 macrophage can be repolarized to M1.
NOTE: Adapted from [113].

In WAT from lean animals, ATM present an alternatively activated M2 phenotype, are less inflammatory than classically activated macrophages and are uniformly dispersed throughout the adipose tissue, whereas ATM of obese mice have a pro-inflammatory classical M1 phenotype and are primarily found in "crown-like" structures around the adipocytes [114, 115]. It has been reported in both mice and humans that during obesity infiltrating ATMs progressively polarize from the M2- to the M1-like state [116], correlating with the development of insulin resistance [114, 117].

Macrophages act in autocrine, paracrine and endocrine manner through the activation of the c-JUN N-terminal kinase (JNK), nuclear factor-kappa B (NF-kB) and Janus kinase (JAK)/STAT signaling pathways [118]. These pathways are activated in multiple tissues in obesity and T2DM and have a central role in promoting tissue inflammation as summarized in Figure 8.

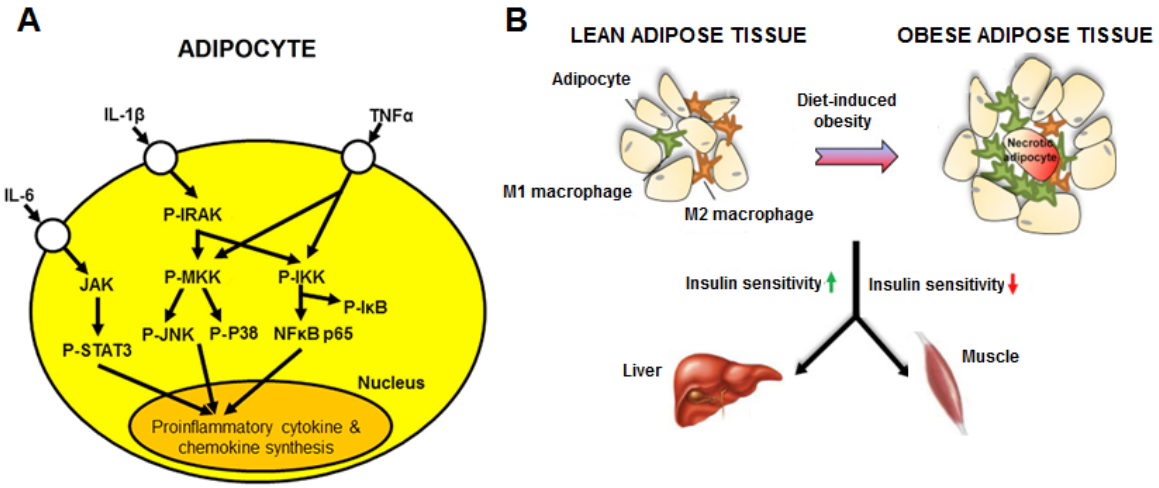

Figure 8. (A) Signaling cascades triggered by pro-inflammatory cytokines in the adipocyte. IRAK: interleukin-1 receptor-associated kinase; MKK: MAP kinase kinases; IkB: inhibitor of kB; IKK: IκB kinase
NOTE: Adapted from [119]. **(B) Impact of WAT inflammation in insulin target tissues (i.e. liver and skeletal muscle).** NOTE: Adapted from [120].

3.1. BAT AND INFLAMMATION.

Several studies have demonstrated that the inflammatory processes in BAT contribute to impair the thermogenic function and insulin sensitivity [34] and leads to obesity-associated metabolic disease. It is noteworthy to mention that in BAT the transcript levels of pro-inflammatory cytokines are lower than in WAT, which probably reflects the enhanced anti-inflammatory phenotype of the resident immune cells in BAT [21]. However, increased expression levels of some pro-inflammatory cytokines such as TNF-α or IL-1β [121, 122], as well as insulin resistance [122] and a reduction of energy expenditure and impaired cold-induced thermogenesis [123] have been reported in BAT from rodents under obesogenic conditions. According to these studies, *ob/ob* mice, a preclinical animal model of obesity, showed marked reductions in UCP-1 and other markers of thermogenesis such as β_3-AR or PGC-1α in BAT in parallel with concomitant increases in the expression of inflammatory markers (TNF-α, IL-1, IL-6) in this tissue [124].

The ability of pro-inflammatory signaling to regulate in a negative manner the thermogenic activity of BAT may reflect that this fat depot expresses many cytokine receptors and TLRs, all of them playing important roles in mediating inflammatory signaling by sensing metabolic signals [125]. For example, TLR4 activation by LPS represses β_3-adrenergic-mediated browning of iWAT, whereas TLR4 deletion protects thermogenic activation [126]. Moreover, the induction of low-grade chronic inflammation in mice by continuous infusion with low amounts of LPS reduces UCP-1 expression in BAT [127].

Activation of BAT, even in humans in which the size of this tissue is small, is associated with a healthy systemic metabolic profile. In addition to its intrinsic capacity to oxidate glucose and lipids, the secretory role of BAT and its modulation according to its thermogenic activity may be related to this association. The identification and characterization of brown adipokines is expected to provide potential tools and targets that might be useful in future intervention strategies for complex metabolic diseases such as obesity or T2DM [128]. BAT transplantation might be also a strategy to take advantage of the beneficial effects of brown adipocytes in modulating energy balance [80]. In this regard, it has been shown that subcutaneous BAT transplants normalized glucose levels and reversed diabetes symptoms in rodent models of type 1 diabetes [129]. The authors proposed that BAT-released insulin-like growth factor I (IGF-I) acts as an endocrine factor resembling the actions of insulin in ameliorating diabetes. Stanford et al. [130] also reported that BAT transplantation to mice improved glucose tolerance, enhanced insulin sensitivity, decreased fat mass, and reversed high-fat diet (HFD)-induced insulin resistance. BAT transplantation was associated with higher levels of circulating FGF21 levels, consistent with the idea that FGF21 could be the endocrine factor that mediates the systemic effects of BAT transplantation. BAT-derived IL-6 was also found to be required for the effects of BAT transplantation, as transplantation of BAT from IL-6-deficient mice did not improve the metabolic status of mice and neither increased FGF21 levels. BAT transplantation had also beneficial effects in *ob/ob* mice by reducing body weight and increasing energy expenditure and adiponectin levels [131]. As suggested by Villarroya and co-workers, the identification of endocrine factors released by BAT would be of high relevance to be used in future clinical applications focused in improving metabolic health in highly relevant diseases such as obesity, diabetes, and dyslipidemia [132].

4. SIRTUIN 1 (SIRT1) AS A MODULATOR OF ENERGY BALANCE IN OBESITY.

Sirtuins, a family of highly conserved protein modifying enzymes founded by the yeast silent information regulator 2 (Sir2) protein, are NAD^+-dependent protein deacetylases. Mammals express 7 sirtuins that are found in different subcellular locations including the nucleus (SIRT1, SIRT6, and SIRT7), cytosol (SIRT2), and mitochondria (SIRT3, SIRT4, and SIRT5). Among them, SIRT1, the ortholog of the yeast Sir2 protein, is a metabolic sensor that directly couples the cellular metabolic state, via NAD^+, to the chromatin structure and regulates gene expression through deacetylation of histones, transcription factors and co-factors [133].

4.1. SIRT1 AND ENERGY METABOLISM.

Studies in mice have demonstrated that SIRT1 is involved in energy metabolism, inflammation, adipose tissue function and systemic insulin sensitivity. In fact, there are plenty of studies that highlight the essential role of this sirtuin in obesity-associated metabolic disorders [133-136]. As a protein deacetylase, SIRT1 has a very wide range of protein substrates and shuttles between the nucleus and cytosol in response to specific environmental signals. A low-energy status that increases cellular levels of NAD^+ such as fasting, CR, and exercise, stimulates SIRT1 activity. Conversely, a high-energy status that decreases cellular NAD^+ levels such as HFD feeding and acute inflammatory responses, reduces SIRT1 activity. Moreover, SIRT1 is negatively regulated by ATP, which binds to its C-terminal domain, impairing its ability to bind to the deacetylase domain as well as its ability to function as the substrate recruitment site [137].

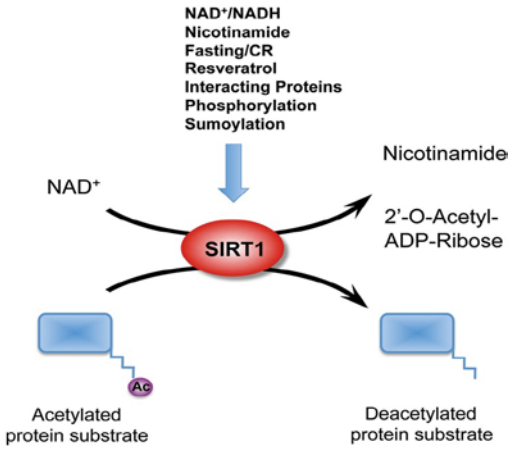

Figure 9. Schematic representation of SIRT1 functions. SIRT1 converts NAD^+ into nicotinamide and ADP-ribose, and then transfers the acetyl group from the protein substrate to the 2'-OH group of the ribose ring in the ADP-ribose molecule. Nutritional, hormonal, and environmental signals can modulate the deacetylase activity of SIRT1.
NOTE: Adapted from [133].

Due to its ability to modify and control many transcription factors and co-factors involved in systemic metabolic homeostasis, SIRT1 is increasingly referred to as a master metabolic regulator that can directly adapt the nuclear transcriptional networks to the cellular metabolic state.

4.2. ROLE OF SIRT1 IN INFLAMMATION OF ADIPOSE TISSUES.

SIRT1 has been identified as an important repressor of inflammation in multiple tissues and cells. Some studies indicate that the beneficial effects of SIRT1 in metabolic disorders are partly due to its ability to deacetylate the RelA/p65 subunit of NFκB that inhibit its activity, thereby reducing the expression of pro-inflammatory cytokines [138]. In line with this notion, constitutive moderate overexpression of SIRT1 in mice leads to suppression of the inflammatory responses and reduces NF-κB activity in liver [139], while knock-down of SIRT1 in the mouse macrophage cell line RAW 264.7 and intraperitoneal macrophages increases LPS-stimulated TNF-α secretion [140]. Moreover, whole-body deficiency of SIRT1 induces systemic inflammation upon HFD challenge [139, 141]. Therefore, SIRT1 and inflammatory signals mutually interact at various levels and this interactome is an essential molecular link between inflammation and metabolic dysfunction.

SIRT1 has been shown play an important function in WAT since it regulates adipogenesis [142] and lipolysis [143] in this tissue. Picard et al. described that SIRT1 represses PPARγ activity attenuating adipogenesis and triggering lipolysis and loss of fat mass [144]. A recent study shows that specific SIRT1 deficiency in WAT leads to impaired lipid metabolism and promotes interactions between exosomes, recently identified as mediators of intercellular signaling, and PPARγ, which in turn promotes lipid accumulation, increases fat mass and eventually results in obesity [145].

It is noteworthy to mention that SIRT1 plays an important role in facilitating browning of WAT via PRDM16 and activating the thermogenic program in beige adipocytes. SIRT1-mediated deacetylation of PPARγ leads to the recruitment of PRDM16 and subsequently induces the clearance of the nuclear co-repressor 1 from the PPARγ complex, therefore activating thermogenic genes and repressing white adipose-related genes. Moreover, SIRT1 promotes browning of white adipocytes in response to cold-exposure, but not under basal conditions, in different models of increased SIRT1 activity such as the transgenic mice model that overexpress SIRT1, SirBACO (SirT1 Bacterial Artificial Chromosome Overexpressor) or as a result of genetic deletion of the SIRT1 endogenous inhibitor Deleted in breast cancer-1 (*Dbc1*$^{-/-}$) [146].

SIRT1 also plays a key role in BAT function. The first generated model of moderate overexpression of SIRT1 in mice revealed a phenotype mimicking calorie restriction as manifested by higher energy expenditure and inhibition of diet-induced accumulation of fat [147]. Moreover, SIRT1 activation has been associated with an increase in the expression and/or activity of PGC-1α and oxidative phosphorylation (OXPHOS) genes in BAT that is not accompanied by a higher mitochondrial content [148-151]. However, constitutive SIRT1 overexpression increases BAT thermogenesis and improves systemic glucose tolerance in mice [139, 147-150, 152].

Boutant et al. [150] described that the expression of just one additional copy of SIRT1 is sufficient to enhance BAT activity. They detected higher SIRT1 activity, as indicated by reduced acetylation of NFkB and forkhead box O1 (FoxO1), and higher *Dio2* expression in BAT from SIRT1 overexpressing mice, supporting a higher catabolic rate. Furthermore, Banks and colleagues [153] showed that mice with moderate overexpression of SIRT1 exhibited normal insulin sensitivity but a decrease in food intake and locomotor activity. They concluded that SIRT1 overexpression primes the organism for metabolic adaptation to insulin resistance increasing hepatic insulin sensitivity and decreasing whole-body energy requirements. In another study, Pfluger and co-workers [139] reported the protective potential of SIRT1 overexpression against the metabolic consequences of chronic exposure to HFD. In this regard, mice with moderate overexpression of SIRT1 exhibited fat mass gain similar to wild-type (WT) controls when

exposed to HFD. However, they showed higher energy expenditure that was compensated by an increase in food intake. In addition, lower lipid-induced inflammation and a better glucose tolerance was observed in transgenic SIRT1 mice under HFD. These beneficial effects are due to the induction of antioxidant proteins such as manganese superoxide dismutase and nuclear respiratory factor 1 (MnSOD and NRF1 respectively) and lower activation of pro-inflammatory cytokines, such as TNFα and IL-6, by down-regulation of NFκB activity in liver.

In line with these notions, SIRT1-deficient mice have the opposite effect and displayed an exacerbated BAT degeneration phenotype with more accumulation of lipid droplets, lower thermogenic activity and aggravated mitochondrial dysfunction (less mitochondrial content and respiratory chain complex subunits abundance) under HFD. These mice also showed a diminished cold tolerance and exacerbated glucose intolerance and insulin resistance in response to HFD [154]. Moreover, the specific deletion of SIRT1 in both WAT and BAT increases adiposity, thereby increasing the weight of both tissues [155].

SIRT1 is also involved in the insulin downstream signaling pathway by repressing the expression of PTP1B, a negative regulator of insulin signaling, thereby improving insulin sensitivity, particularly under insulin-resistant conditions [156]. Therefore, SIRT1 could be an important therapeutic target for insulin-resistance-associated metabolic syndrome.

4.3. PHARMACOLOGYCAL MODULATION OF SIRT1 ACTIVITY.

Recent studies indicate that both natural and synthetic SIRT1 activating compounds (STACs) stimulate sirtuin activity and confer many health benefits in rodents and possibly in humans. Small molecule SIRT1 activators include: first generation molecules such as resveratrol and related polyphenols, second generation STACs such as the imidazothiazols and third generation STACs such as benzimidazols and urea-based scaffolds [157].

Since SIRT1 is an essential regulator of systemic energy homeostasis, its pharmacological modulation could be of interest to control diseases associated with obesity. Consistent with this notion, resveratrol, a natural polyphenol present in grapes, red wine, peanuts and some berries, has shown promise as a therapeutic agent for the treatment of metabolic diseases [158]. In rodents, resveratrol can exert positive effects on glucose tolerance suppressing the effects of metabolic dysfunction, including diabetes and obesity [149]. In this regard, previous studies of our laboratory showed improvement in hepatic insulin sensitivity in diabetic IRS-2-deficient mice treated with resveratrol [159, 160].

Wang and co-workers [161] and Mendez and co-workers [162] showed that dietary supplementation of resveratrol exerts anti-obesity effects and reduces body weight and adipocyte size in obese people. These anti-obesity properties of resveratrol may be derived from its effects in inhibiting adipogenesis or lipogenesis [163] and promoting lipolysis [164, 165]. This dietary intervention also induces browning of iWAT and up-regulates UCP-1 in this fat depot in mice [166] and also in BAT of rats fed an obesogenic diet [167]. These results are consistent with the study of Andrade et al. [168] showing that resveratrol promotes BAT thermogenic gene expression and energy metabolism in mice fed a standard diet. In line with these studies, administration of high doses of resveratrol induces weight loss in HFD-fed mice in parallel with decreased weight of visceral fat pads and smaller adipocytes in epididymal WAT (eWAT) [149]. Another recent in vitro study has revealed that resveratrol enhances brown adipocyte formation and function as it promotes the expression of PRDM16, UCP-1, PGC-1α, cytochrome C

and pyruvate dehydrogenase in differentiated brown adipocytes [169]. Together, these findings support that resveratrol supplementation plays a significant role in the management of weight gain and related complications. However, it is still not clear if resveratrol can influence energy expenditure or body composition in humans [170].

Taking into account all these studies, moderate overexpression of SIRT1, as well as its activation by resveratrol, might be beneficial for the treatment of diseases linked to chronic inflammation including obesity.

OBJECTIVES

OBJETIVES

Activation of BAT is a promising approach to combat obesity or type 2 diabetes mellitus (T2DM), conditions associated with chronic low-grade systemic inflammation, a critical underlying factor in the development of insulin resistance and impaired thermogenesis. Since inflammation has only recently been recognized as a disruptor of BAT functionality, the general goal of this Thesis is the study of the impact of inflammation in this tissue and how to tackle it. As sirtuin 1 (SIRT1) has been recognized to protect against the metabolic damage during obesity, we hypothesized that its activation might be of benefit in BAT to combat chronic inflammation and metabolic dysfunction. To achieve these issues, we propose the following concise objectives:

1. To characterize the inflammatory signature and insulin signaling in BAT from *db/db* mice, an *in vivo* model of obesity and T2DM.

2. To evaluate the efficacy of pharmacological SIRT1 activation with resveratrol in *db/db* mice regarding thermogenic activation.

3. To analyze the effect of inflammation and SIRT1 overexpression in insulin and thermogenic responses in BAT from mice upon bacterial lipopolysaccharide challenge as a trigger of inflammation.

4. To explore cell autonomous effects in brown adipocytes exposed to an inflammatory medium in both insulin signaling and adrenergic responses and the potential beneficial effect of SIRT1 overexpression.

5. To establish a protocol of brown preadipocytes differentiation towards a mature phenotype resistant to inflammation.

MATERIALS AND METHODS

1. *IN VIVO* ANIMAL STUDIES.

1.1. ANIMAL HOUSING.

All animal procedures were approved by the Ethics Committees of Consejo Superior de Investigaciones Científicas and Comunidad de Madrid (Spain) in accordance with the European Union guidelines.

Db+ and *db/db* male mice both in the C57BL/KsJ genetic background were purchased from Charles Rivers (Harlan Laboratories).

SIRT1^{Tg+} mice (C57Bl/6J) were provided by Dr. Manuel Serrano (CNIO, Madrid).

Mice were housed at the animal facilities of the Alberto Sols Biomedical Research Institute (CSIC/UAM, Madrid) under controlled conditions on 12 h:12 h light-dark cycles and at 22°C temperature and 45-55 % humidity and allowed free access to standard rodent chow diet (A04, U8220G10R, SAFE) and water. All the studies were performed using groups of adult (2-4 months) male littermates.

1.2. SIRT1 GENOTYPING.

A piece of a mouse ear was mixed with 300 µL of 25 mM NaOH and incubated at 95ºC for 10 min. After vortex, samples were neutralized with 50 µL of 1 M Tris/HCl buffer pH 8.0 and centrifuged at 13200 x g for 10 min at 4ºC. For preparing the PCR mixture, reagents were mixed as follows:

10 µL H_2O
4 µL Taq DNA Polymerase (TAQL-RO, 11647679001, Sigma)
2 µL 10 µM T7 Tg oligonucleotide (Sigma) 5'-AGCTTCTTGCACACCACAT-3`
2 µL 10 µM T7 Bac oligonucleotide (Sigma) 5'-TAATACGACTCACTATAGGG-3`

18 µL of mix/sample were prepared and 2 µL of DNA were added (final volume of 20 µL). H_2O was used as negative control and a DNA from a SIRT1^{Tg+} mouse was the positive control. PCR was conducted with the following cycles:

1) 94ºC 00:01:00
2) 94ºC 00:00:30
3) 55ºC 00:00:30
4) 72ºC 00:00:30
5) Repeat 2) to 4) 34 times
6) 72ºC 00:10:00
7) Hold on 4ºC

PCR products were loaded on 2.5 % agarose gels with an intercalating agent that allows visualizing DNA bands under UV light (SYBR Safe, S33102, Thermofisher). The electrophoresis was run in TAE buffer (0.04 M Tris-acetate, 1 mM EDTA pH 8.0) at 100-120 V. Transgenic mice were identified by the presence of a 450-bp band (Figure 10).

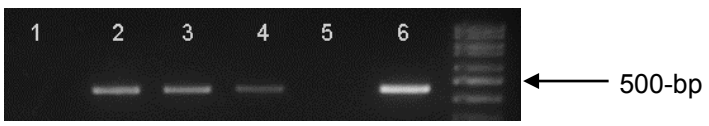

Figure 10. Gel photograph showing PCR products for genotyping SIRT1^{Tg+} mice. The presence of a 450-bp band corresponds to SIRT1^{Tg+} mice whereas absence of this band corresponds to WT mice. Lane 1: WT mouse, lanes 2-4: SIRT1^{Tg+} mice, lane 5: negative control, lane 6: positive control. Last lane represents a 100-bp DNA ladder marker (MWD100, Nippon Genetics).

1.3. ANALYSIS OF INSULIN AND THERMOGENIC RESPONSE IN *db*+ AND *db/db* MICE.

To perform insulin response experiments, *db*+ and *db/db* mice were fasted 4 h and then intraperitoneally (i.p.) injected 0.75 U/kg of human recombinant human insulin (Actrapid, Novo Nordisk) and sacrificed 20 min later.

Db+ and *db/db* mice were treated with resveratrol (R5010, Sigma) for 8 weeks. Resveratrol was dissolved in the drinking water to a concentration of 50 mg/L and protected from the light as previously described [159]. The dose of resveratrol is equivalent to approximately 2.5 mg/kg/day. During our study, we confirmed that mice were consuming the amount of water necessary to reach the desired pharmacological dose of resveratrol [156]. Body weight and glycaemia were monitored weekly (data not shown). After this period, mice were sacrificed to perform the analysis of BAT.

After being weighed, tissues (BAT, iWAT, eWAT, liver and brain) were collected in dry ice and stored at -80ºC until use. Blood was collected by beheading in tubes with 12 µL of 0.5 M ethylenediaminetetraacetic acid (EDTA).

1.4. ANALYSIS OF INSULIN AND THERMOGENIC RESPONSE UNDER PRO-INFLAMMATORY CONDITIONS IN WT AND SIRT1^{Tg+} MICE.

After 5 h fast, WT and SIRT1^{Tg+} mice were i.p. administered 2 mg/kg LPS (LPS, tlrl-eblps-InvivoGen, Invitrogen) or saline (vehicle) for different time-periods ranging from 30 min to 1 h to check the activation of the pro-inflammatory signaling cascades (Figure 11A). In order to analyze the effect of SIRT1 overexpression in BAT response to insulin stimulation under pro-inflammatory conditions, adult mice were randomly divided into 4 experimental groups (injected or not with insulin in the presence or absence of LPS) and fasted for the last 4 h as shown in Figure 11B.

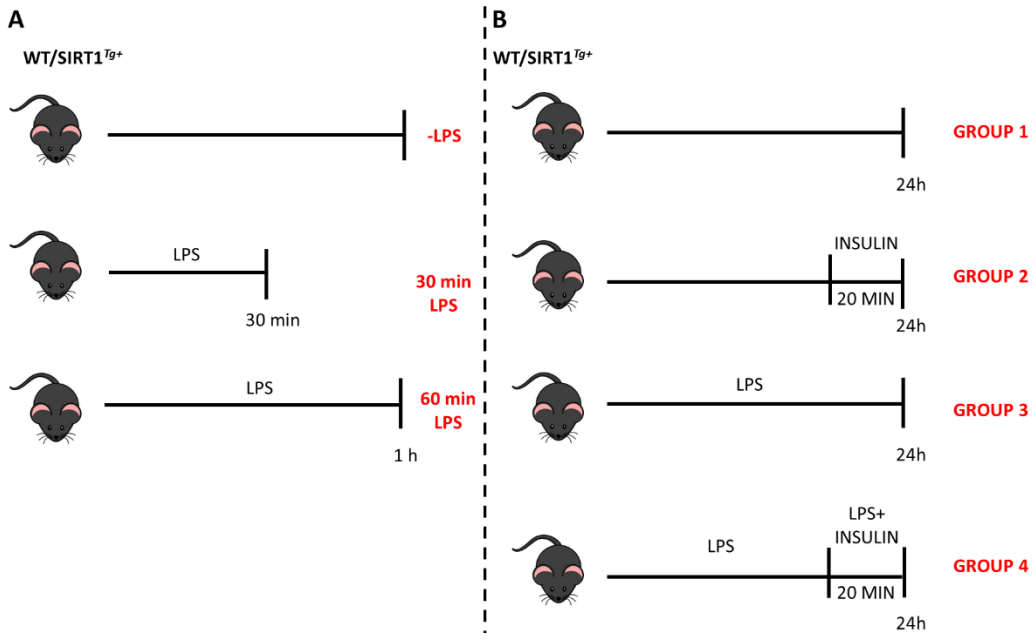

Figure 11. Experimental groups and time-flow for studying the impact of LPS-induced inflammation in BAT. (A) One group (Group 1) was maintained under control conditions (22ºC) without receiving LPS (-LPS). The other 2 groups were injected 2 mg/kg LPS (i.p.) and sacrificed after 30 min (30 min LPS) or 60 min (60 min LPS). Prior to the sacrifice, all groups of mice were fasted for 5 h. **(B)** All groups of mice were fasted for the last 4 h. Group 1 was maintained under control conditions (22ºC). Group 2 was injected 0.75 U/g insulin (i.p.) and sacrificed after 20 min. Groups 3 and 4 were treated with 2 mg/kg LPS (i.p.). Half of the mice (Groups 1, 3) were sacrificed at 24 h. The other half (Groups 2, 4) received an insulin injection and were sacrificed after 20 min.

To address a possible impact of SIRT1 overexpression in the thermogenic response of mice to cold exposure, adult mice from both genotypes were housed at 28°C for one week. After that, mice were randomly divided into 4 experimental groups represented in Figure 12.

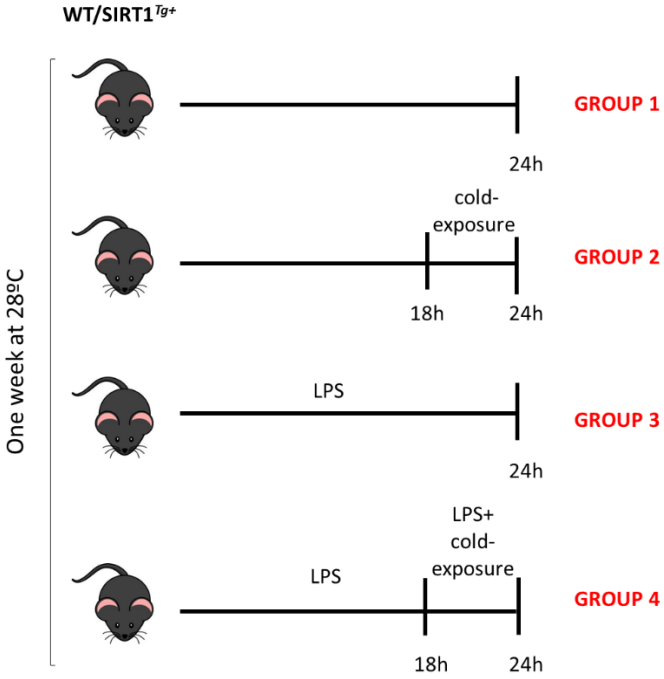

Figure 12. Experimental groups and time-flow for the study of the cold response under pro-inflammatory conditions in BAT from WT and SIRT1^{Tg+} mice. All experimental groups were housed at least one week at 28ºC. Group 1 was maintained at thermoneutral conditions (28°C). Group 2 was subjected to cold challenge (4°C) for 6 h. Groups 3 and 4 were treated with 2 mg/kg LPS (i.p.) for 24 h, one of which (Group 4) was subjected to the cold challenge (4°C) for the last 6 h.

1.5. MEASUREMENT OF RECTAL AND SKIN TEMPERATURE SURROUNDING BAT IN WT AND SIRT1^{Tg+} MICE.

Rectal temperature was measured with a rectal probe (RTC-1, Cibertec). The skin temperature surrounding BAT was recorded with an infrared camera (B335: Compact-Infrared-Thermal-Imaging-Camera; FLIR; West Malling, Kent, UK) and analyzed with a specific software package (FLIR-Tools-Software, FLIR). Pictures were captured and temperature measured at thermoneutrality or immediately after the cold exposure (6 h). In mice injected with LPS (i.p.), the measurements were recorded 24 h after LPS injection.

1.6. ANALISIS OF FGF21 PLASMA LEVELS.

FGF21 plasma levels were quantified by ELISA (catalog no. RD291108200R, BioVendor) following the manufacturer's instructions and using a 1/10 dilution of the plasma. Samples were collected from *db+* and *db/db* mice treated or not with resveratrol for 8 weeks and after 4 h of fasting.

1.7. HISTOLOGICAL ANALYSIS.

Hematoxylin and eosin (H&E) staining was performed in paraffin sections of BAT from WT and SIRT1^{Tg+} mice for histopathological analysis. A piece of BAT was fixed in 4 %

paraformaldehyde (PFA) for 24 h, then washed twice with PBS 1X and kept in 70 % ethanol. Samples were processed in the histological service of the National Centre for Biotechnology (CNB, CSIC) following the protocol detailed below.

First, samples were placed in an automatic tissue processor in a 22-hour cycle consisting of 2 h in 70 % ethanol, 2 h in 80 % ethanol, 2 cycles of 2 h in 96 % ethanol, 2 cycles of 2 h in 100 % ethanol, 2 h in a mix of ethanol + xylol (50:50), 2 cycles of 2 h in xylol and 2 cycles of 2 h in liquid paraffin. The paraffin block was formed when liquid paraffin solidified at -5ºC and was cut in a microtome (5 microns sections), stretching of the cuts in a water bath at 40ºC. The slides were collected and dried overnight (o/n) in a dry oven at 37- 40ºC. After that, the slides were stained following the H&E protocol: 2 cycles of 10 min in xylol, 2 cycles of 10 min in 100 % ethanol, 5 min in 96 % ethanol and 5 min in 70 % ethanol. After 5 min in running water, samples were dyed with 100 % Mayer's hematoxylin for 15-20 min. After washing 3 min with running water, eosin (70 % ethanol + 1 % stock eosin + glacial acetic acid) was added for 10-15 sec. Slides were put again into running water for 3 min and then in 96 % ethanol a few sec to remove the excess of eosin. Finally, after 2 cycles of 5 min in 100 % ethanol and 2 cycles of 10 min in xylol, slides were assembled in embedding medium for covering the coverslips and dried o/n.

Then we collected images with an Axiophot light microscope (Zeiss) with a 40x objective. To estimate the cell density, the nuclei were counted in 3 fields of different BAT sections of each animal using ImageJ software (The National Institutes of Health; https://imagej.nih.gov/ij/). Around 200 total nuclei per section were counted.

1.8. *EX VIVO* MEASUREMENT OF CELLULAR BIOENERGETICS PROFILE IN BAT EXPLANTS.

Seahorse technique in BAT explants and differentiated brown adipocytes was performed in collaboration with Dr. Laura Herrero and Dr. Dolors Serra of Faculty of Pharmacy (University of Barcelona) and CIBERobn.

Oxygen consumption rate (OCR) was measured in BAT explants from WT and SIRT1^{Tg+} male. Mice were treated with an i.p. injection of vehicle (saline) or 2 mg/kg LPS for 24 h before the OCR analyses. BAT was excised and cut using a scalpel into 9 mg pieces and then placed into a tube containing wash media (Eagle's Minimal Essential Medium (DMEM) (L0102-500, Biowest) supplemented with 25 mM glucose and 25 mM HEPES). Tissues were kept in wash media until the respiration assay measurement.

The capture screens (Seahorse Bioscience, North Billerica, MA) were pre-wet in wash media in a small petri dish to remove air bubbles. A pair of sterile forceps was used to position the screens (ring facing up) in a new empty small petri dish, and a total of 9 mg of BAT was placed on the screen with forceps. Then, the capture screen insert tool (Seahorse Bioscience, North Billerica, MA) was used to pick up the tissue-containing screens from the petri dish and to place them in an XF24 Islet Capture Microplate (Seahorse Bioscience, North Billerica, MA). Once in position, 450 µL of Assay media ((DMEM) (L0102-500, Biowest) supplemented with 25 mM glucose)) was added to all the samples.

- **OXYGEN CONSUMPTION RATE MEASUREMENT.**

The Seahorse XF24 (Seahorse Bioscience, North Billerica, MA) was used to measure the OCR in real time as previously described [171]. This system measures changes in oxygen concentration in a small amount of media that is placed above the tissue. For a typical bioenergetic profile, a set of inhibitors (all from Sigma-Aldrich) of key components

of cellular respiration was added: 24 µg/mL oligomycin A, which blocks ATP synthase; 0.8 µM of the uncoupler FCCP; and a mix of 5 µM rotenone and 15 µM antimycin A to inhibit complexes I and III in the electron transport chain, respectively. Before the measurement, the microplate containing the tissues in assay media was incubated at 37°C without CO_2 for 45 min. The protocol was conducted as follows:

1. Equilibration (Auto)
2. 6 cycles of mix (3 min), wait (2 min) and measure (3 min)
3. Inject port A (Oligomycin A)
4. 4 cycles of mix (3 min), wait (2 min) and measure (3 min)
5. Inject port B (FCCP)
6. 4 cycles of mix (3 min), wait (2 min) and measure (3 min)
7. Inject port C (FCCP)
8. 4 cycles of mix (3 min), wait (2 min) and measure (3 min)
9. Inject port D (Rotenone + Antimycin A)
10. 4 cycles of mix (3 min), wait (2 min) and measure (3 min)

OCR was calculated by plotting the O_2 tension of media as a function of time (pmol/min) and data were normalized by the protein concentration measured in each individual well. Calculations were performed as previously described [171] using the Agilent Seahorse Wave Desktop software.

1.9. RADIOIMMUNOASSAYS OF T_3 AND T_4 IN PLASMA AND BAT OF WT AND SIRT1^{Tg+} MICE.

T_3 and T_4 determinations were performed in collaboration with Dr. Ana Guadaño Ferraz at Instituto de Investigaciones Biomédicas “Alberto Sols” in Madrid.

Individual 80 µL aliquots of plasma as well as total BAT of individual mice were extracted for radioimmunoassay (RIA) determinations. Extraction of T_3 and T_4 from the plasma and tissue, as well as T_3 and T_4 determinations in plasma and tissues, were performed as previously described [172].

For the extraction and purification of THs from plasma, T_3 and T_4 were labelled with ^{125}I from (3,5)-T2 and 3,5,3’-triodo-L-thyronine (T_3) respectively with a high specific activity (3000 µCi/µg) as internal tracers and extracted with methanol chloroform (1:2) in 0.05 % Cl_2Ca. THs purification of the extracts obtained was carried out by ion exchange chromatography on Dowex 50W-X2 resin columns (Bio-Rad) and subsequent elution with 70 % acetic acid. The radioactivity of the resulting fraction was quantified with a gamma counter to calculate the individual recovery of each hormone in each sample tested. The resulting fraction was then subjected to evaporation and resuspended in RIA buffer) (0.04 M phosphate buffer pH 8 with 0.2 % Bovine serum albumin (BSA) and 0.6 mM merthiolate)). Extract were kept frozen until further analysis by RIA according to Weeke and Orskov [173] and Obregon et al. [174]

For the extraction and purification of THs from BAT, frozen tissue samples (70–100 mg) were homogenized in methanol with the amount of radioactive tracer described for plasma samples. The iodothyronines were extracted using chloroform–methanol (2:1), back-extracted into an aqueous phase, and purified through Bio-Rad AG 1X2 resin columns (Bio-Rad Laboratories S.A.) using a pH gradient. The acetic extracts were then evaporated to dryness and dissolved in RIA buffer. Each extract was counted to determine the recovery of [^{131}I]-T_4 and [^{125}I]-T_3 in each sample. The samples were submitted to highly sensitive RIA for the determination of T_3 and T_4. Concentrations are calculated using the amounts of T_3 and T_4 found in the RIAs, the individual recovery of

the [^{131}I]-T_4 and [^{125}I]-T_3 added to each sample, and the weight of the tissue sample extracted.

1.10. ANALYSIS BY PCR OF IRA/IRB ISOFORMS.

Total RNA from *db+ or db/db* BAT was treated with DNAse. For preparing the DNAse mixture, reagents were mixed as follows:

2.5 µg of isolated total RNA
1 µL DNAse I (79254, Qiagen)
0.5 µL RNAse OUT (10777019, Thermofisher)
0.5 µL 0.1 M Dithiothreitol (DTT, 707265ML, Thermofisher)
Diethylpirocarbonate (DEPC) H_20 to a final volume of 11 µL

Samples were incubated first at 37ºC for 30 min and then at 95ºC for 5 min to inactivate DNAse I. Retrotranscription was carried out using the iScript™ cDNA Synthesis Kit (1708890, BioRad) and reagents were mixed as follows:

8 µL reaction mix 5X
19 µL DEPC H_20
2 µL Reverse Transcriptase

After cDNA synthesis, reagents were mixed as follows for carrying out PCR:

IRA/IRB

25.75 µL DEPC H_20 (462224, Invitrogen)
5 µL 10X Standard Reaction Buffer (10012-4103, Biotools)
1 µL 40 mM dNTPs (110001, Bioron)
2.5 µL 10 µM Oligonucleotide Forward IR (Sigma):
5'ATCAGAGTGAGTATGACGACTCGG3'
2.5 µL 10 µM Oligonucleotide Reverse IR (Sigma):
5'TCCTGACTTGTGGGCACAATGGTA3'
1.25 µL Taq DNA Polymerase (10012-4103, Biotools)
2 µL 50 mM $MgCl_2$ (10012-4103, Biotools)
10 µL cDNA

β-ACTIN

34.75 µL DEPC H_20
5 µL 10X Standard Reaction Buffer
1 µL 40 mM dNTPs
1 µL 10 µM Oligonucleotide Forward (Sigma):
5'CTCTGGCTCCTAGCACCATGAAGA3'
1 µL 10 µM Oligonucleotide Reverse (Sigma):
5'GTAAAACGCAGCTCAGTAACAGTCCG3'
1.25 µL Taq DNA Polymerase
2 µL 50 mM $MgCl_2$
4 µL cDNA

PCR was conducted with the following cycles:

1) 94ºC 00:05:00
2) 94ºC 00:00:30
3) 60ºC 00:00:45
4) 72ºC 00:01:00
5) Repeat 2) to 4) 30 times
6) 72ºC 00:07:00
7) Hold on 4ºC

PCR products were loaded on 2.5 % agarose gels with an intercalating agent that allows visualizing DNA bands under UV light. The electrophoresis was run in 1X TAE at 100-120 V. 2 fragments could be visualized: a long fragment of 258 pb containing exon 11 (IRB) and a short fragment of 222 pb not containing it (IRA).

2. CELLULAR STUDIES.

2.1. CELL LINES AND CULTURE CONDITIONS.

2.1.1. GENERATION OF AN IMMORTALIZED BROWN PREADIPOCYTE CELL LINES FROM WT AND SIRT1^{Tg+} MICE.

Primary brown preadipocytes were isolated from interscapular BAT of WT and SIRT1^{Tg+} lactating mice and immortalized as described by Garcia-Casarrubios in 2016 [175] (Figure 13).

Once the BAT was removed, tissue was chopped with scissors on a sterile petri dish with a drop of 0.2 % (w/v) collagenase solution (C-0130 SIGMA) prepared in DMEM supplemented with 100 U/mL penicillin, 100 µg/mL streptomycin (15140 122, Gibco), 2 mM glutamine, 10 mM Hepes and 1.5 % BSA . The homogenized tissue was then placed in a sterile tube with collagenase solution and incubated at 37ºC for 30 min in a stirring bath, being shaked in a vortex for 10 sec every 5 min. The homogenized tissue was filtered through a 250 µm silk filter using a sterile funnel. The filtrate was collected in a sterile tube and incubated at room temperature (RT) for 20-30 min, so mature brown adipocytes were allowed to float and then discarded. The infranatant was removed with a pipette from below the floating fat layer and poured through a 25 µm silk filter. Then, it was collected in a sterile tube and centrifuged at 720 x g for 10 min. The pellet, containing the precursor cells, was washed twice with culture medium (DMEM supplemented with 100 U/mL penicillin, 100 µg/mL streptomycin (15140 122, Gibco), 2 mM glutamine, 10 mM Hepes,10 % newborn calf serum (NCS, N4637, Sigma), 3 nM insulin) and resuspended in this medium. Finally, brown preadipocytes were seeded in 6-multiwell plate, so precursor cells could proliferate actively under these conditions. The day after plating, the wells washed with medium to remove the excess of blood cells and then maintained in 20 % fetal bovine serum (FBS, 10270-106, Gibco)-supplemented medium. Once brown preadipocytes reached 70-80 % confluence, we proceeded to the infection with retroviral particles encoding SV40 Large T antigen in 20 % FBS medium and polybrene (8 µg/mL) (Sequabrene, Sigma, S2667) for 48 h. Retroviral particles were obtained as previously described (Garcia-Casarrubios, 2016). Then, selection with

puromycin (P9620, Sigma) (1 µg/mL) was performed in 10 % FBS supplemented medium.

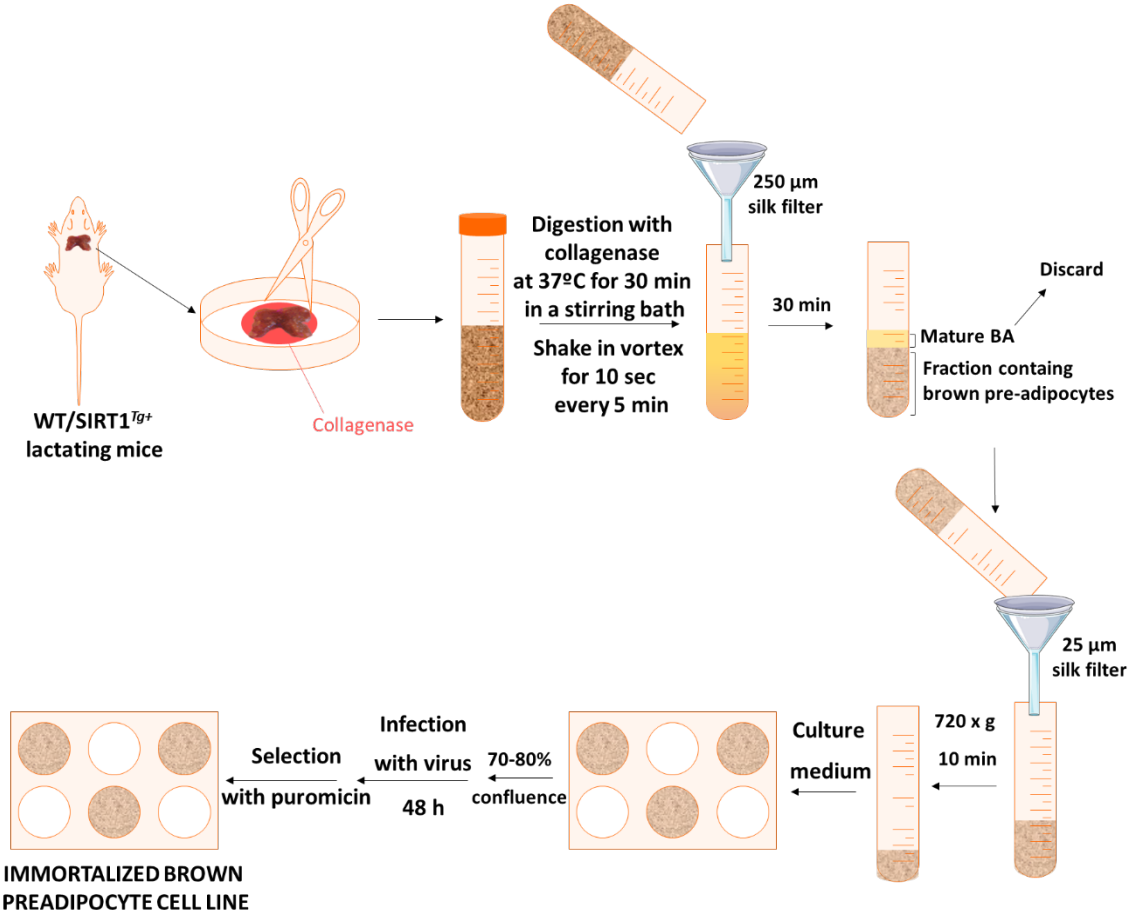

Figure 13. Generation of immortalized brown preadipocyte cell lines from WT and SIRT1^{Tg+} mice.

2.1.2. MAINTENANCE AND DIFFERENTIATION OF BROWN ADIPOCYTES.

Preadipocytes immortalized were maintained in DMEM supplemented with 100 U/mL penicillin, 100 µg/mL streptomycin, 10 mM HEPES and 10 % FBS. Before plating, cells were incubated with trypsin (0.05 % Trypsin-EDTA, 25200-072 Gibco) for 1 min at 37°C and after neutralizing, 215000 cells were plated in 6-well multiwell plates or 42000 cells/cm^2 (for WT) and 36000 cells/cm^2 (for SIRT1^{Tg+}) were plated in 12-multiwell plates in medium containing DMEM supplemented with 10 % FBS, 1 nM T_3 (T6397, Sigma) and 20 nM insulin (I0516, Sigma). This medium was referred as medium 1.

For differentiation, cells were grown until 90 % confluence and then we followed two differentiation protocols as described below and represented in Figure 14.

- **Protocol 1**: cells were stimulated during 36 h with "differentiation medium 1" containing medium 1 supplemented with 0.5 µM dexamethasone, 1 µM rosiglitazone, 0.5 mM isobutylmethylxanthine (IBMX) and 0.125 µM indomethacin. After that, cells were cultured back in medium 1 for a further 3 days.

- **Protocol 2**: cells were stimulated during 36 h with "differentiation medium 2" containing medium 1 supplemented with, 35 nM dexamethasone, 10 μM rosiglitazone, 2.99 μM T_3 and 830 nM insulin. After that, cells were maintained in medium 1 supplemented with 10 μM rosiglitazone, 2.99 μM T_3 and 830 nM insulin for 3 days (referred as medium 2).

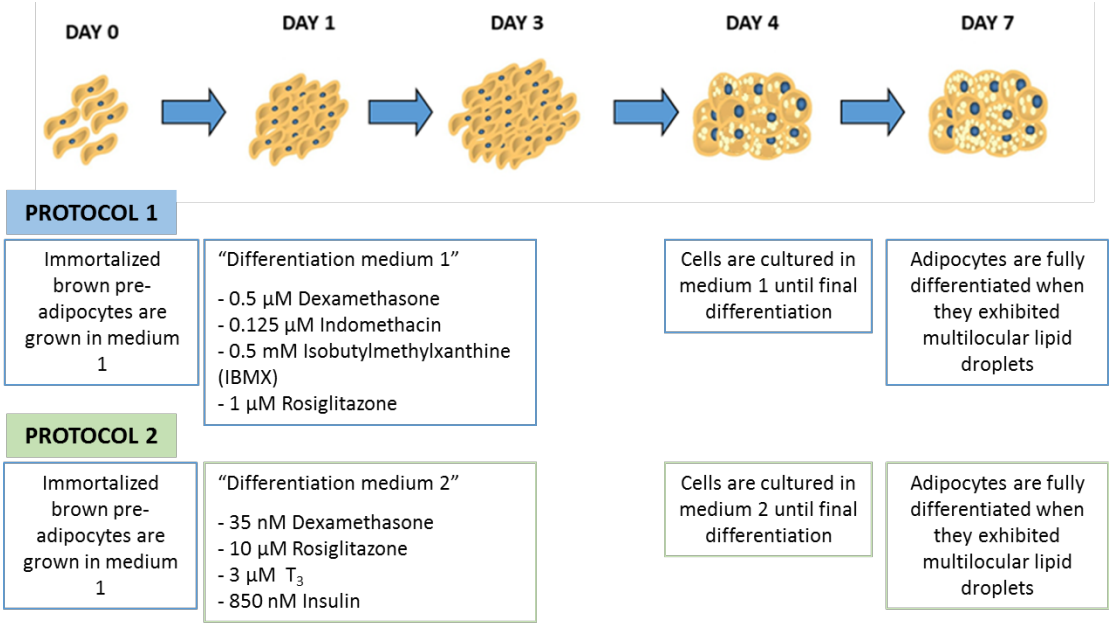

Figure 14. Representative scheme of the two different protocols used to differentiate brown preadipocytes immortalized into mature brown adipocytes.

2.1.3. PRODUCTION OF PRO-INFLAMMATORY CONDITIONED MEDIUM FROM MACROPHAGES.

The murine macrophage cell line Raw 267.4 was used to obtain a pro-inflammatory conditioned medium (CM) in order to check the effect of inflammation in brown adipocytes. This process is depicted in Figure 15.

Raw 264.7 cells were maintained in 10 cm culture dishes with Roswell Park Memorial Institute (RPMI) medium supplemented with 100 U/mL penicillin, 100 μg/mL streptomycin, 10 mM HEPES, 2 mM L-glutamine (25030-024, Gibco) and 10 % FBS. Macrophages were grown until 95-100 % of confluence. Then, the medium was changed to RPMI-2 % FBS for 1 h and macrophages were then treated or not with 100 ng/mL of LPS for 5 h. Then, culture medium was removed and after a wash with phosphate buffered saline (PBS) 1X the macrophages were maintained with RPMI-2 % FBS medium which allowed them to secret cytokines for a further 17 h (referred as conditioned medium LPS (CM-LPS) or conditioned media control (CM-CTR), respectively). Both CM were filtered and supplemented with FBS (final 5 %) before the addition to brown adipocytes (BA).

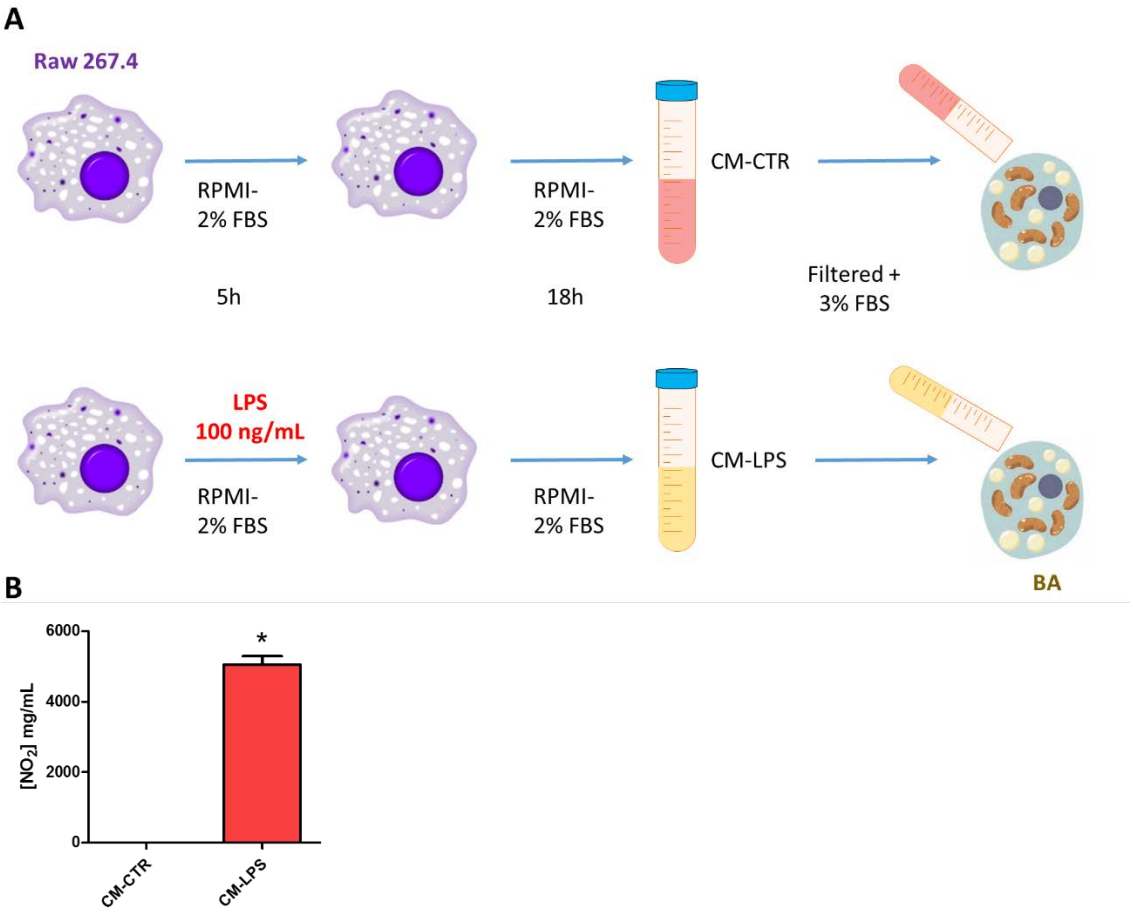

Figure 15. Representative scheme for the generation of CM from Raw 267.4 macrophages (A) and measurement of nitrites concentration (B).

2.1.4. NITRITES DETERMINATION.

A spectrophotometric determination of nitrite production was performed to assess the pro-inflammatory potency of the CM. Macrophages were stimulated as described in figure 15A and 200 µL supernatant of CM-CTR or CM-LPS were collected and mixed with 20 µL of 10 mM sulphanidic acid and 20 µL of 10 mM N-(l-naphthyl) ethylenediamine (NEDA). Nitrite production was measured spectrophotometrically at 548 nM (Figure 15B). The concentration was determined by a standard curve of known concentrations of NO_2.

2.2. PROTEIN ANALYSIS BY WESTERN BLOTTING.

2.2.1. PREPARATION OF PROTEIN EXTRACTS.

Tissue samples: a piece of BAT was lysed in lysis buffer (50 mM HEPES pH 7.5, 1 % Triton X-100 (T8787, Sigma), 50 mM sodium pyrophosphate tetrabasic (P8010, Sigma), 0.1 M sodium fluoride (NaF, S7920, Sigma) 10 mM EDTA, 10 mM o-sodium vanadate (S6508, Sigma), 1 mM phenylmethanelsulfonyl fluoride (PMSF, p7626, Sigma) and 10 µg/mL of protease inhibitors (P-8340, Sigma)) pH 7.4-7.6, using a tissue homogenizer (0003737000, IKA). After centrifugation at 98560 x g for 40 min at 4°C, the supernatant was centrifuged at 16000 x g for 1h at 4ºC and the supernatant resulted was collected. Protein levels were determined using the BCA dye method (23225, Thermo Scientific).

Cell samples: brown adipocytes were lysed in lysis buffer (10 mM Tris pH 7.5, 5 mM EDTA, 50 mM HCl, 30 μM sodium pyrophosphate, 50 mM NaF, 100 mM o-vanadate sodium, % Triton X-100, 1 mM PMSF and 10 μg/mL of protease inhibitors pH 7.4-7.6). Then, cells were centrifuged twice at 11200 x g for 7 min at 4°C and the supernatant was collected. Protein levels were determined using the BCA dye method (23225, Thermo Scientific).

2.2.2. WESTERN BLOT.

Protein extracts (15-30 μg) were boiled at 95ºC for 5 min in loading buffer (100 mM Tris pH 6.8, 10 % glycerol, 4 % sodium dodecyl sulphate (SDS), 0.2 % bromophenol blue and 2 mM β-mercaptoethanol), and subjected to 8-15 % SDS polyacrylamide gel electrophoresis (SDS-PAGE) in electrophoresis buffer (25 mM Tris pH 8.3, 250 mM Glycine, 0.1 % (p/v) SDS).

Electrophoresis was carried out at 120 V during 1.5 h. Proteins were separated by molecular weight and then transferred to PVDF membranes (immobilon-P IPVH00010, Merck). Membranes were activated for 5 min in methanol and then washed twice with distilled water. Wet transfer was performed using an electrotransferred system (Bio-Rad) during 2 h at 100 V in transfer buffer (66 mM Tris pH 8.5, 383 mM Glycine, 20 % (v/v) Methanol, 0.1 % (p/v) SDS). Then, a Ponceau solution (0.1 % Ponceau (P_3SO_4, Sigma) and 5 % acetic acid in water) was added to the membranes to visualize protein loading. After washing with TBS-T buffer (10 % Tris-buffered saline (TBS) 10X and 0.05 % Tween-20 (T1379)), membranes were blocked with 5 % skimmed milk powder in TBS-T buffer for 2 h at RT. Membranes were then washed with TBS-T buffer and incubated with primary antibodies used at the dilutions indicated in Table 2 at 4°C waving o/n. After 3 washes with TBS 1X, membranes were incubated with the corresponding secondary antibody for 1 h waving at RT (Table 3). Membranes were washed again with TBS-T buffer and developed with chemiluminescent substrate (Clarity Western ECL Substrate, 170-5060 BioRad) and different exposure times were performed for each primary antibody, with radiographic films in a radiology cassette (Medical X-ray film blue, EWPJH AGFA). Blots were normalized using antibodies against vinculin or tubulin. Values of densitometry were determined using Image J.

Table 3. List of primary antibodies used.

PRIMARY ANTIBODIES					
ANTIBODY	MW(kDA)	REFERENCE	SPECIE	DILUTION	COMMERCIAL
Ac-p65	65	ab19870	Rabbit	1:1000	Abcam
AKT-T	60	sc-8312	Rabbit	1:2000	Santa Cruz
FAS	265	610962	Mouse	1:1000	BD
GAPDH	36	ab8245	Mouse	1:5000	Abcam
GLUT4	50-63	2213	Mouse	1:1000	Cell signaling
IR-T	95	sc-711	Rabbit	1:2000	Santa Cruz
IκBα	35-41	sc-371	Rabbit	1:2000	Santa Cruz
JNK-T	46-54	sc-571	Rabbit	1:2000	Santa Cruz
MFN2	86	ab56889	Mouse	1:2000	Abcam
p38-T	38	9212	Rabbit	1:2000	Cell signaling
p-AKT (Ser 473)	60	9271	Rabbit	1:2000	Cell signaling
p-AKT (Thr 308)	60	4056	Rabbit	1:3000	Cell signaling
p-DRP1	78-82	3455	Rabbit	1:1000	Cell signaling
p-IKK α/IKK β	85-87	2682	Rabbit	1:1000	Cell signaling
p-IGF1R/p-IR	95	3024	Rabbit	1:1000	Cell signaling
p-JNK	46-54	9251	Rabbit	1:2000	Cell signaling
p-p38	38	9211	Rabbit	1:2000	Cell signaling
p-STAT3	79	9131	Rabbit	1:2000	Cell signaling
PTP1B	50	ABS40	Mouse	1:2000	Millipore
SIRT1	110	07-131	Rabbit	1:2000	Milipore
TUBULIN	50	T5168	Mouse	1:10000	Sigma
UCP-1	32	ab10983	Rabbit	1:10000	Abcam
VINCULIN	117	sc-73614	Mouse	1:10000	Santa Cruz

Table 3. List of secondary antibodies used.

SECONDARY ANTIBODIES				
ANTIBODY	SPECIE	REFERENCE	DILUTION	COMMERCIAL
Anti-rabbit	Goat	A120-108P	1:25000	BETHYL
Anti-mouse	Goat	sc-2005	1:10000	Santa Cruz

2.3 QUANTITATIVE REAL TIME PCR (QRT-PCR).

Tissue samples: RNA was extracted by adding 1 mL of TRIzol Reagent (15596026, Invitrogen/Thermo Fisher) to a piece of BAT (25 µg approximately) placed in a 2 mL sterile tube and homogenized with a polytron homogenizer (0003737000, IKA). The liquid was passed several times through a 1 mL syringe, first with a green needle (21 G) and then with an orange one (25 G). The homogenate was centrifuged for 10 min at 13300 x g at 4ºC and the supernatant was collected in another sterile eppendorf tube.

Cell samples: RNA was extracted with 500 µL of TRIzol Reagent in a well of 12-multiwell plate and incubated for 5 min to allow complete dissociation of the nucleoproteins complex. After scraping, the lysate was transferred to an eppendorf tube.

After adding 200 µL of chloroform/mL TRIzol, the tube was shacked vigorously for a minimum of 20 times. The samples were then centrifuged for 15 min at 13300 x g at 4°C.

The mixture separates into a lower red phenol-chloroform, and interphase, and a colourless upper aqueous phase containing the RNA, which was transferred to a new tube and immediately mixed with 500 µL/mL TRIzol of isopropanol by inverting carefully the tube 5 times. After centrifugation at 13300 x g for 10 min at 4°C, total RNA precipitates in a white gel-like pellet at the bottom of the tube. The pellet was washed twice in 1 mL of 70-80 % ethanol/mL TRIzol and the tubes were centrifuged for 5 min at 13300 x g at 4°C. The supernatant was discarded and the RNA pellet was dried for at least 1 h and finally resuspended in 0.1 % DEPC H_2O by pipetting up and down.

The resuspended pellet was incubated in a heat block set at 55–60°C for 10 min and the RNA concentration was determined using Nanodrop ® (Nanodrop ND-1000).

Reverse transcription was performed using the High-Capacity cDNA Reverse Transcription Kit using random primers and Superscript III enzyme 18080093 according to the manufacturer's instructions 4368813, Thermofisher). Quantitative real-time PCR was performed in a 7900 HT-Fast real-time PCR (Life Technologies) with TaqMan Universal PCR Master Mix. qRT-PCR was carried out at the Genomics Service of the CSIC-UAM using 5 ng of cDNA. Samples were amplified in duplicate according to the following schedule: 50ºC for 2 min, 95ºC for 10 min; 40 cycles of 15 sec at 95ºC and 1 minute at 60ºC. The following probes and primers are listed in Table 4. The relative change in gene expression was calculated using the $2^{-\Delta\Delta Ct}$ (cycle threshold) quantification method, normalizing to expression levels of the *Tbp* (TATA-binding protein) gene.

Table 4. Reagents used to perform qRT-PCR. The TaqMan probes used are also detailed.

REAGENT	VOLUME (µL)
TaqMan Universal Master Mix	5
Probe (20x)	0.5
DEPC Water	2.5
Total volume	8

GEN	TaqMan Probe	Commercial House
Pgc1α	Mm01208835_m1	Applied Biosystems
Dio2	Mm00515664_m1	
Ucp1	Mm01244861_m1	
Prdm16	Mm00712556_m1	
Fgf21	Mm00438930_m1	
Il6	Mm00446190_m1	
Tlr4	Mm00445273_m1	
Nos2	Mm00440502_m1	
Tbp	Mm00446973_m1	

2.4 ANALYSIS OF UCP-1 EXPRESSION IN BROWN ADIPOCYTES.

For analysis of UCP-1 expression, differentiated BA either with protocol 1 or 2 were cultured in DMEM supplemented with 5 % FBS for 1 h and then stimulated or not with 5 µM norepinephrine (NE, A'9512, Sigma) for 17 h.

For studying the impact of a pro-inflammatory environment in the thermogenic response, BA were cultured with CM-CTR or CM-LPS in the absence or presence of 5 µM NE for 17 h.

At the end of the treatments, cells were lysed and processed by Western blot.

2.5 ANALYSIS OF INSULIN SIGNALING IN BROWN ADIPOCYTES.

For insulin signalling analysis, BA were differentiated with either protocol 1 or 2 and then cells were cultured for 1 h with serum-free DMEM. After that, cells were stimulated with 10 nM insulin for 15 min.

For assessing the insulin response in a pro-inflammatory environment, BA were stimulated with CM-CTR or CM-LPS for 17 h and after a 1 h incubation with serum-free DMEM, 10 nM insulin was added for 15 min.

At the end of the treatments, cells were lysed and processed by Western blot.

2.6 MEASUREMENT OF GLUCOSE UPTAKE.

In order to study the uptake of glucose, differentiated BA from both genotypes differentiated with medium 1 or 2 were serum-deprived for 1 h. Then, cells were washed twice with Krebs-Ringer-phosphate buffer (KRP) (135 mM NaCl, 5.4 mM KCl, 1.4 mM $CaCl_2$, 1.4 mM $MgSO_4$, 10 mM sodium pyrophosphate, pH 7.4) and incubated with KRP buffer for 15-30 min at 37°C. After stimulation with 10 nM insulin for 10 min, 2-Deoxy-D [$^{1\text{-}3}$H] glucose (500 nCi/mL) was added to this solution, and the incubation was continued for 5 min at 37°C. Control cells were maintained in the absence of insulin stimulation. The cells were then washed twice with KRP buffer and solubilized with a syringe in 1 % (p/v) SDS. After 2 h incubation at 37°C, radioactivity was measured by liquid scintillation counting. Total protein was determined by BCA method and results were normalized to protein amount.

2.7 FATTY ACID OXIDATION (FAO).

The measurement of FAO in differentiated brown adipocytes with medium 1 or 2 was performed in collaboration with Dr. Laura Herrero and Dr. Dolors Serra of Faculty of Pharmacy (University of Barcelona) and CIBERobn.

Palmitate oxidation to CO_2 and acid-soluble products (ASPs), essentially acyl-carnitine, Krebs cycle intermediates, and acetyl-CoA, was measured in WT and SIRT1^{Tg+} brown adipocytes grown and differentiated in 24-well plates. The day of the assay, cells were washed in Krebs-Ringer bicarbonate HEPES buffer (KRBH buffer: 135 mM NaCl, 3.6 mM KCl, 0.5 mM NaH_2PO_4, 0.5 mM $MgSO_4$, 1.5 mM $CaCl_2$, 2 mM $NaHCO_3$, and 10 mM HEPES, pH 7.4) and 0.1 % BSA, preincubated at 37°C for 30 min in KRBH-1 % BSA and washed again in KRBH-0.1 % BSA. Cells were then incubated for 3 h at 37°C with fresh KRBH containing 25 mM glucose and 8 mM carnitine plus 2.5 mM palmitate and 1 µCi/mL [1-14C] palmitate bound to BSA. Oxidation measurements were performed as described [176] with minor modifications by trapping the radioactive CO_2 in a 1 cm^2 whatman paper soaked with 100 µL 0.1 N KOH using parafilm-sealed system. The reaction was stopped by the addition of 40 % perchloric acid through a syringe that pierced the parafilm.

The following day, the system was opened and the papers were left to dry out, before transferring them into tubes with 5 mL scintillation liquid (Perkin Elmer, ref. 6013159). Then, 300 µL of the reaction mix with perchloric acid was removed and centrifuged at maximum speed for 10 min. 150 µL of the supernatant, which contained the ASPs, were transferred into a tube with 5 mL scintillation liquid. After 2 h of stabilization, samples are analyzed and data for CO_2 are expressed as: nmol palmitate mg-1 prot h-1 = (cpmsample – cpmblanc) * 80 / (total cpm * mg prot * h).

The results for ASPs are expressed as: nmol palmitate mg-1 prot h-1 = (cpm sample – cpm blanc) * 80 * (352/150) / (total cpm * mg prot * h) as described in [176].

2.8. MEASUREMENT OF OXYGEN CONSUMPTION.

The Seahorse XFe24 (Seahorse Bioscience, www.seahorsebio.com) was used to measure OCR in mature BA as described [171]. For a typical bioenergetic profile we used 2 μM oligomycin to block ATP synthase; then 2 μM of the uncoupler FCCP to measure maximal respiratory capacity followed by a mix of 10 μM rotenone and 10 μM antimycin-A to totally inhibit mitochondrial respiration (all from Sigma-Aldrich). Cells were differentiated with medium 1 or 2 in customized Seahorse 24-well plates and stimulated with CM-CTR and CM-LPS for 18 h. Before any measurement, cells were incubated for 1 hour with XF Assay Medium (Seahorse Bioscience) plus 5 mM glucose. We followed the protocol and injection strategies of the Mito Stress Assay (Seahorse Bioscience). OCR was calculated by plotting the O_2 tension of media as a function of time (pmol/min), and data were normalized by the protein concentration measured in each individual well by Bradford method by. Calculations were performed using the Agilent Seahorse Wave Desktop software.

2.9. IMMUNOFLUORESCENCE OF MITOCHONDRIAL MARKERS.

Brown adipocytes were plated on the sterile round glass coverslips and differentiated with medium 1 or 2 following the procedures described above.

2.9.1. TRANSLOCASE OF THE OUTER MEMBRANE OF MITOCHONDRIA (TOM) 22 AND CYTOCHROME C OXIDASE SUBUNIT 4 (COXIV) IMMUNOFLUORESCENCE.

Cells were fixed with 4 % PFA pH 7.5 for 20 min at RT and, after washing with PBS 1X, cells were permeabilized with 0.1 % sodium citrate pH 6, 0.1 % Triton X-100 for 5 min at RT. After washing with Washing Buffer (0.25 % BSA and 0.1 % Tween-20 in PBS 1X) for 10 min and blocking in Blocking Buffer (2.4 % BSA in Washing Solution) for 30 min at RT, cells were incubated with primary antibody ((Tom 22, (T6319, SIGMA), COXIV (1D6EIA9, Thermofisher)) (1:200 in blocking solution) o/n at 4°C and incubation was continued in the following day for 30 min at RT. Then, cells were washed with Washing Solution for 10 min at RT and incubated with fluorocrome-conjugated secondary antibody (goat anti-rabbit Alexa 488 (A11034, Thermofisher) for TOM22 and goat anti-mouse Alexa 488 (A11029, Thermofisher) for COXIV), 1:250 in blocking buffer for 1 h at RT followed by incubation with DAPI (1:5000 in blocking buffer) for 5 min at RT in the dark. Coverslips were adhered with antifade mounting medium (00-4958-02, Thermofisher) and samples were dried o/n and maintained at 4ºC until the analysis by confocal microscopy.

2.9.2. MFN2 AND p-DRP1 IMMUNOSTAINING.

Cells were fixed with 4 % PFA pH 7.5 for 20 min at RT and after washing with PBS 1X, cells were permeabilized with 0.1 % Triton X-100 in PBS 1X for 5 min at RT. After washing with Washing Buffer (0.25 % BSA and 0.1 % Tween-20 in PBS 1X) for 10 min and blocking in PBS 1X with 5 % Normal Goat Serum (NGS, ab7481, Abcam) and 5 % BSA for 30 min at RT, cells were incubated with primary antibodies (p-DRP1, 3455, Cell Signaling; MFN2, ab56889, Abcam) (1:150 in PBS 1X with 1 % NGS and 1 % BSA) o/n at 4°C and incubated the day after 30 min at RT. After washing twice with PBS 1X, cells were incubated with fluorocrome-conjugated secondary antibody ((goat anti-mouse Alexa 488 (A11029, Thermofisher) for MFN2 and goat anti-rabbit Alexa 647 (A21245, Thermofisher) for p-DRP1)), both 1:250 in blocking buffer for 1 h at RT and incubated with DAPI (1:5000 in blocking buffer) for 5 min at RT in the dark. Coverslips were adhered

with antifade mounting medium and keep them drying o/n and then transferred to 4ºC until the analysis by confocal microscopy.

2.10. ANALYSIS OF MITOCHONDRIAL CONTENT BY FLOW CYTOMETRY USING MITOTRACKER.

BA from both genotypes were differentiated with medium 1 or 2 and stimulated with 100 nM MitoTracker Green (MTG, M7514, ThermoFisher) in medium 1 or 2 during 30 min at 37ºC. After washing with PBS 1X, BA were trypsinized, neutralized and after centrifuged at 238 x g. The pellet was resuspended in PBS 1X and the relative fluorescence of MTG was determined by flow cytometry.

2.11. STAINING OF LIPID-DROPLETS BY BODIPY DYE.

BA from both genotypes were differentiated with medium 1 or 2 and incubated with 1-5 µg/mL Bodipy dye (D3835, Thermofisher) (1:1000 in medium 1 or 2) for 30 min at 37 ºC. Cells were then washed twice with PBS 1X, fixed with 4 % PFA pH 7.5 for 20 min at RT and then incubated with DAPI (1:5000) for 5 min at RT in the dark. Coverslips were adhered with antifade mounting medium and keep them drying o/n and then transferred to 4ºC until the analysis by confocal microscopy.

2.12. LIPOLYSIS ASSAY.

Cells were stimulated 18 h with DMEM-5 % FBS and after that incubated with Krebs-Ringer Modified Buffer (KRB) (118.5 mM NaCl, 4.75 mM KCl, 1.92 mM $CaCl_2$, 1.19 mM KH_4PO_4, 1.19 mM $MgSO_4(H_2O)_7$, 25 mM $NaHCO_3$, 10 mM HEPES, 6 mM D-Glucose, 4 % BSA pH 7.4) and 5 µM NE for the last 4 h. After that, supernatants were collected and the amount of glycerol was quantified spectrophotometrically at 540 nm with the Free Glycerol Reagent colorimetric kit (12812, BioSystems). The amount of glycerol was determined from a commercial standard solution and normalized to protein amount.

2.13. ATP PRODUCTION.

To detect ATP levels, cells were lysed in cold milliQ water, heated to 80ºC for 5 min and centrifuged at 134 x g for 5 min. ATP levels were detected using a bioluminescent kit (ATP determination kit, PRO (LBR-PO10)) following the manufacturer's instructions (Biaffin GMbH& co KG). This assay uses firefly luciferase to convert ATP and luciferin to oxyluciferin and light. The light emitted in this reaction is directly proportional to the concentration of ATP present based on the following reaction:

$$\text{luciferin} + \text{ATP} + O_2 \xrightarrow[\text{luciferase}]{Mg^{2+}} \text{oxyluciferin} + \text{AMP} + \text{pyrophosphate} + CO_2 + \text{light}$$

Chemiluminescence generated was detected at 560 nm wavelength in a luminometer. A curve with increasing concentrations of ATP was performed in order to calculate the amount of ATP present in each sample.

2.14. STATISTICAL ANALYSIS.

Statistical analysis was performed using GraphPad Prism software version 5 and version 8 (Graph software, Inc, San Diego, CA). D'Agostino and Pears onomnibus normality test was run to determine if the samples showed a parametric or non-parametric distribution. Mann-Whitney U test was used to do pairwise comparisons in non-parametric distributions. Two-way ANOVA with post hoc Bonferroni was employed to compare two different categorical independent variables. When another statistical analysis, different from the above described, was used it is indicated in the description of the corresponding result. The data are presented as the mean ± SEM (standard error of the mean). Statistical significance was set at $^{*,\#}p<0.05$, $^{**,\#\#}p<0.01$, $^{***,\#\#\#}p<0.001$.

RESULTS

1. *IN VIVO* ANIMALS STUDIES.

1.1. STUDIES IN TWO MICE MODELS TO ADDRESS THE IMPACT OF INFLAMMATION IN BAT.

The use of preclinical animal models of obesity-related insulin resistance and/or inflammation is relevant for understanding the specific pathways contributing to alterations in BAT function. Therefore, we have conducted studies in two different mouse models of inflammation, *db/db* mice, representing a genetic model displaying key features of obesity and T2DM, and a systemic model of inflammation by administration of an i.p. injection of LPS in WT and SIRT1^{Tg+} mice.

1.1.1 *db/db* MICE AS A MODEL OF INFLAMMATION LINKED TO OBESITY.

First, we studied and characterized the inflammatory signature of BAT from *db/db* mice compared to their *db*+ lean counterparts. As it has been reported [177-180], *db/db* mice showed higher levels of blood glucose and increased total body weight (Figure 16A and 16B) that concurred with lower UCP-1 protein expression in BAT (Figure 16C). In agreement with hyperplasia and/or hypertrophy of adipose cells during obesity, we observed an increase in the weight of different fat depots (BAT, iWAT and eWAT) in *db/db* mice (Figure 16D).

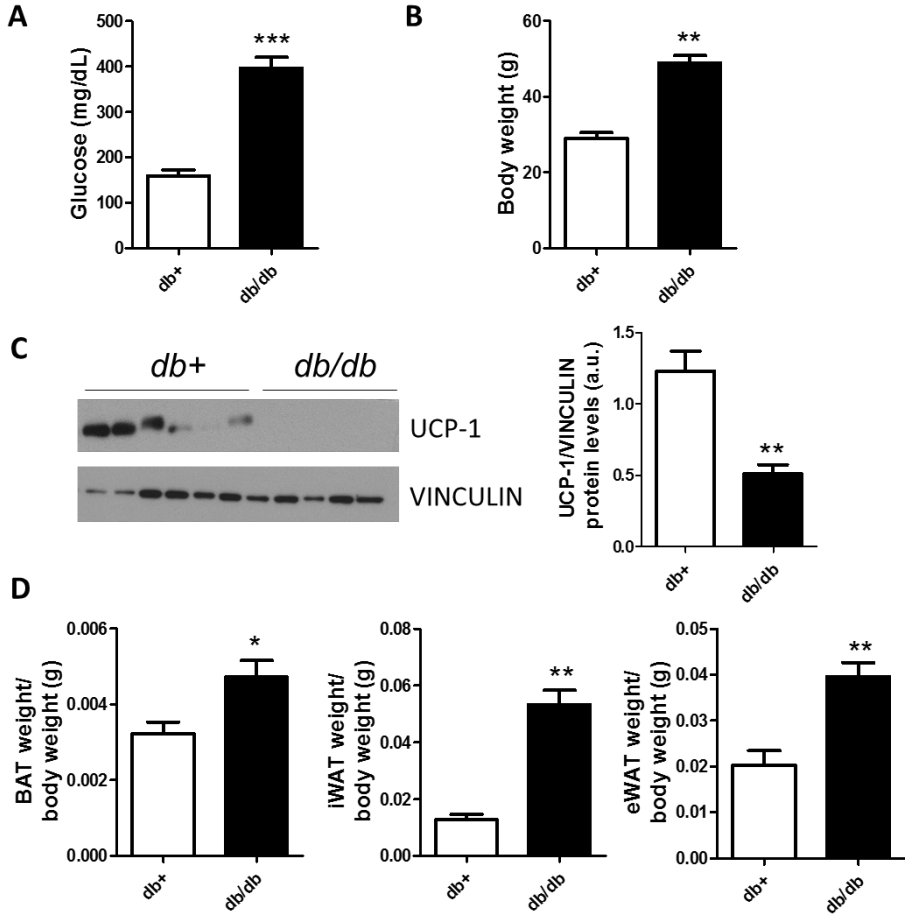

Figure 16. *Db/db* mice showed higher body weight and circulating glucose levels concomitant with lower UCP-1 protein levels in BAT and higher weight of adipose depots. (A, B) Glucose levels and body weight in *db/db* and *db*+ mice at 12 weeks of age (n= 6-13 mice/group). **(C)** UCP-1 protein levels in BAT analyzed by Western blot (left panel). The right panel represents the quantification of data from 5-7 mice/group. **(D)** BAT, iWAT and eWAT weight relative to total body weight (n=7-13 mice/group). The bars represent mean ± SEM. Statistical analysis was performed with Mann-Whitney U test. *p<0.05, **p<0.01, ***p<0.001.

Accumulation of adipose tissue depots plays a role in the development of a systemic inflammatory state that contributes to obesity-associated metabolic disorders. TLR4 signaling pathway is acknowledged as one of the main triggers of obesity-induced inflammatory responses. TLR4 is responsible for the transcriptional activation of pro-inflammatory genes such as those encoding for the cytokine IL-6 or iNOS [181]. As shown in Figure 17A, we detected increases in *Il6*, *Nos2* and *Tlr4* mRNA expression levels in BAT from *db/db* mice compared to *db+* lean controls. We next studied the activation of pro-inflammatory signaling cascades in BAT from both genotypes of mice. As expected, the increase in pro-inflammatory-related gene expression in BAT from *db/db* mice was accompanied by a pro-inflammatory signaling signature. As shown in Figure 17B, phosphorylation levels of JAK-STAT3, IKKα/β, JNK and p38 MAPK were significantly elevated in BAT extracts from *db/db* mice compared with the lean counterparts.

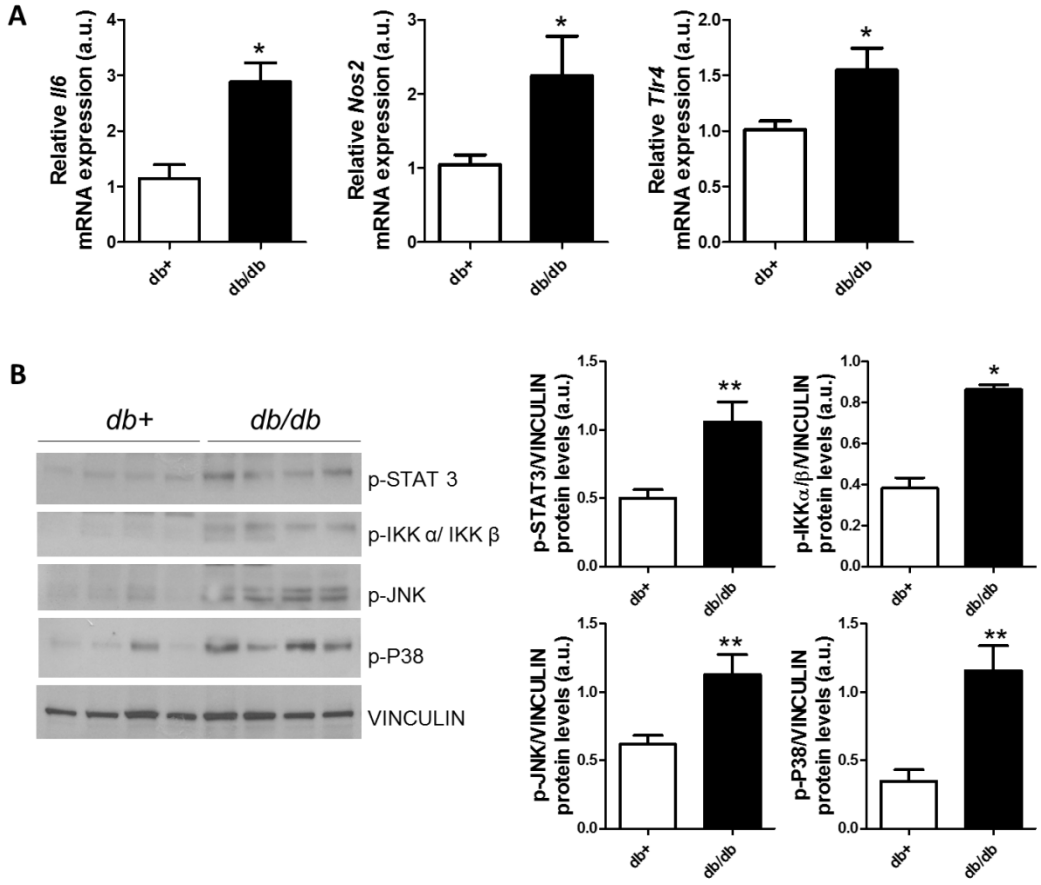

Figure 17. *db/db* mice showed an increase of pro-inflammatory-related gene expression and activation of pro-inflammatory signaling cascades in BAT. (A) *Il6, Nos2* and *Tlr4* mRNA expression levels in BAT from *db/db* mice compared to *db+* lean controls (n=3-7 mice/group). **(B)** Activation of pro-inflammatory signaling cascades mediated by phosphorylation of JAK-STAT3, IKKα/β, JNK and p38 MAPK in BAT from *db/db* mice compared to *db+* lean controls analyzed by Western blot. Vinculin was used as a loading control. The bars represent mean ± SEM (n=4-9 mice/group). Statistical analysis was performed with Mann-Whitney U test. *p<0.05, **p<0.01.

Once we characterized the inflammatory state of BAT from *db/db* mice we aimed to study whether the insulin signaling pathway was impaired in this fat depot. As observed in Figure 18A, *db/db* mice were insulin resistant in BAT due to the attenuated phosphorylation levels of IR and AKT in both Serine 473 (Ser 473) and Threonine 308 (Thr 308) residues.

IR is expressed in cells in two different two isoforms containing or not the exon 11 (IRB and IRA, respectively). Both isoforms have similar affinity for insulin, but IRA, an immature form of the receptor, exhibits a higher affinity for IGFs [182]. Although we observed the two IR isoforms in both groups, a robust presence of IRA was detected in BAT from *db/db* mice (Figure 18B) that could account, at least in part, for the attenuated insulin signaling.

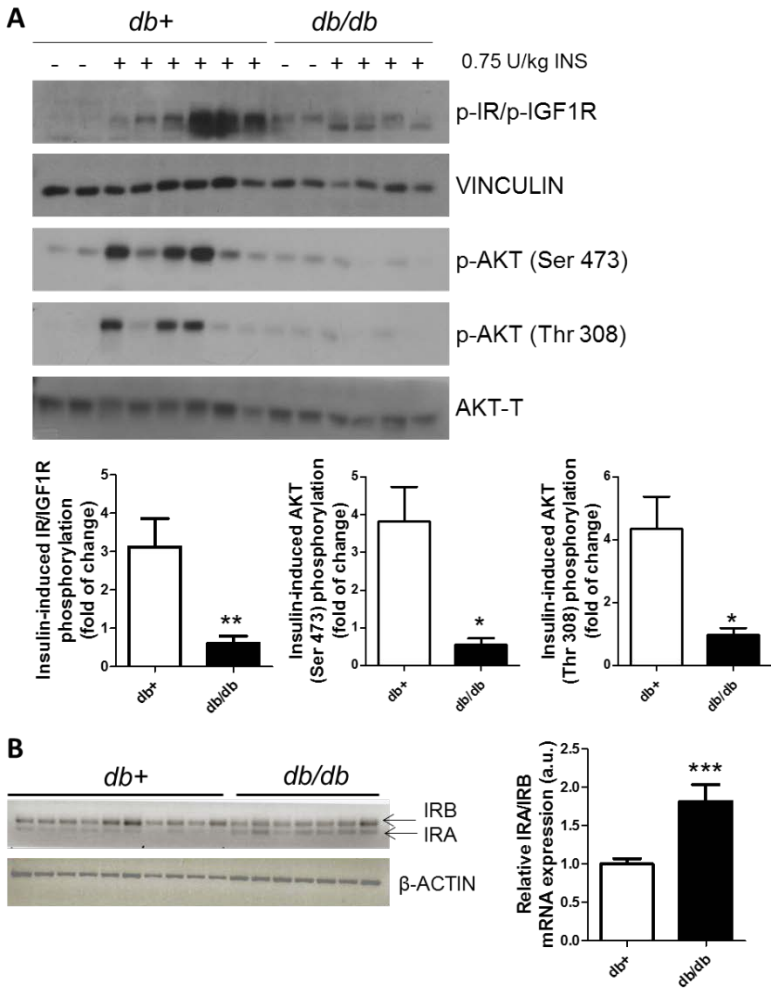

Figure 18. BAT from *db/db* mice showed decreased IR/IGF-IR-mediated signaling in BAT. (A) Four h fasted mice were injected (i.p.) 0.75 U/kg human recombinant insulin and sacrificed after 20 min. Phosphorylation of IR/IGF1R and AKT in BAT was analyzed by Western blot (n=2 controls and 4-6 insulin-injected mice/group). **(B)** Pattern of IR isoforms showing a robust presence of IRA in BAT from *db/db* mice analyzed by semi-quantitative PCR. The bars represent mean ± SEM (n=7-10 mice/group). Statistical analysis was performed with Mann-Whitney U test. *p<0.05, **p<0.01, ***p<0.001.

1.1.2. SYSTEMIC MODEL OF LPS-MEDIATED INFLAMMATION IN WT AND SIRT1^{Tg+} MICE.

1.1.2.1 EFFECT OF AN ACUTE LPS TREATMENT IN WT AND SIRT1^{Tg+} MICE IN THE ACTIVATION OF PRO-INFLAMMATORY SIGNALING CASCADES IN BAT.

In order to induce a mild systemic inflammation in an obesity-independent manner, we administered a low dose (2 mg/kg) of LPS via i.p. injection for several time-periods up to 24 h in WT and SIRT1^{Tg+} mice.

For studying if the pro-inflammatory signaling cascades mediated by JAK-STAT3, JNK and p38 MAPK were activated in BAT from these mice, we first performed a short-term time-course experiment by injecting LPS for 30 min and 1 h and, as depicted in Figure 19, mice overexpressing SIRT1 showed a lower activation of STAT3 after LPS challenge.

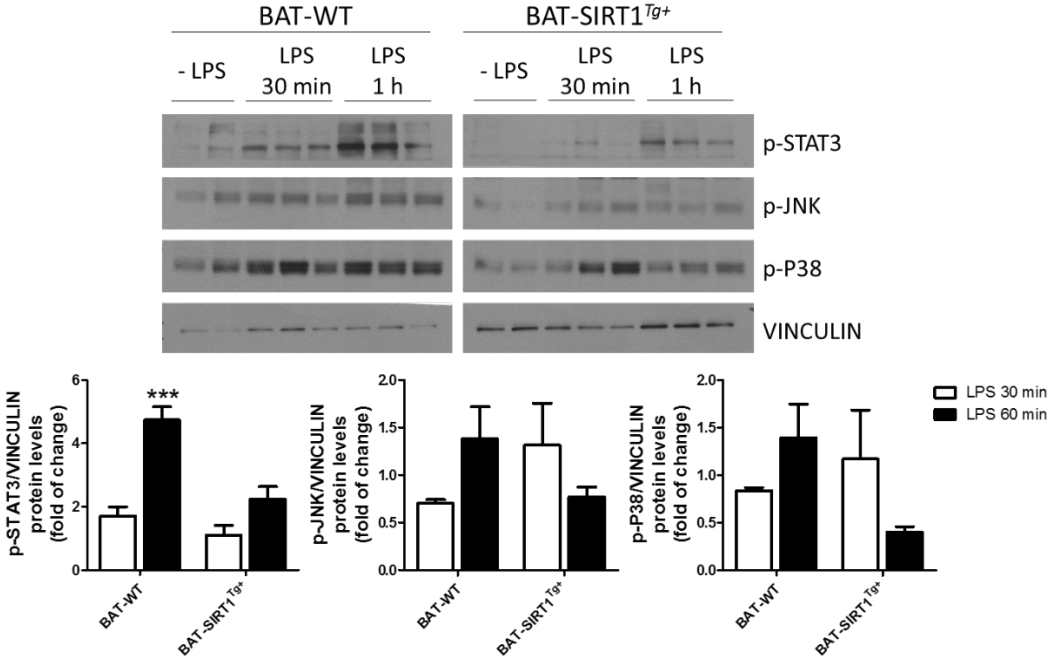

Figure 19. Activation of pro-inflammatory signaling cascades in BAT by short-term treatment of WT and SIRT1^{Tg+} mice with LPS. Activation of pro-inflammatory signaling cascades mediated by JAK-STAT, JNK and p38 MAPK in BAT analyzed by Western blot after stimulation or not with LPS at different time-periods (30, 60 min). The graphs show the fold increase *vs*. control condition (–LPS) in WT and SIRT1^{Tg+} mice (n= 3 mice/group). Vinculin was used as a loading control. Bars represent mean ± SEM. Statistical analysis was performed with a Two-way ANOVA. ***p<0.001 compared to -LPS.

1.1.2.2 IMPACT OF LPS IN THE INSULIN SIGNALING PATHWAY IN BAT FROM WT AND SIRT1^{Tg+} MICE.

We next ascertained the impact of SIRT1 overexpression and LPS-mediated inflammation in insulin signaling in BAT. For this goal, we injected WT and SIRT1^{Tg+} mice LPS and, after 24 h, mice received an injection of insulin and they were sacrificed at 20 min post-insulin injection (see materials and methods, Figure 11B). Although LPS induced insulin resistance in BAT from both genotypes, monitored by the analysis of IR and AKT phosphorylation, moderate SIRT1 overexpression protected from the drop of insulin signaling induced by LPS (Figure 20).

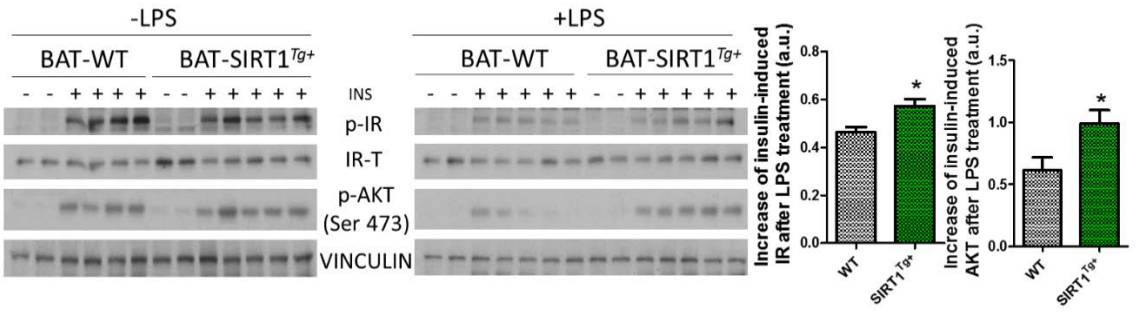

Figure 20. Moderate overexpression of SIRT1 protected from LPS-induced insulin resistance in BAT. Representative Western blots of IR and AKT (Ser 473) phosphorylation in BAT. The graphs show the relative increase in p-IR and p-AKT (Ser 473) signal after LPS treatment *vs.* p-IR and p-AKT (Ser 473) detected in the control condition (-LPS). IR-T and vinculin were used as loading controls. Bars represent mean ± SEM. (n=5-6 mice/group). Statistical analysis was performed with Mann-Whitney U test. **p<0.01.

1.1.2.3 IMPACT OF LPS IN THE THERMOGENIC RESPONSE OF BAT IN WT AND SIRT1^{Tg+} MICE.

In order to study the effect of LPS-mediated inflammation in the thermogenic response of BAT, adult mice from both genotypes were housed at 28°C for one week. After that, one group was maintained at thermoneutral conditions (28°C) and the other was treated with 2 mg/kg LPS and both groups of mice were sacrificed after 24 h (see materials and methods, Figure 12)

As shown in Figure 21A, LPS treatment induced a slight decrease in *Ucp1* mRNA levels, a significant decrease in rectal temperature (Figure 21B), as well as a tendency to a decrease of the temperature in the skin surrounding BAT (Figure 21C) in WT mice, but these effects were not observed in SIRT1^{Tg+} mice.

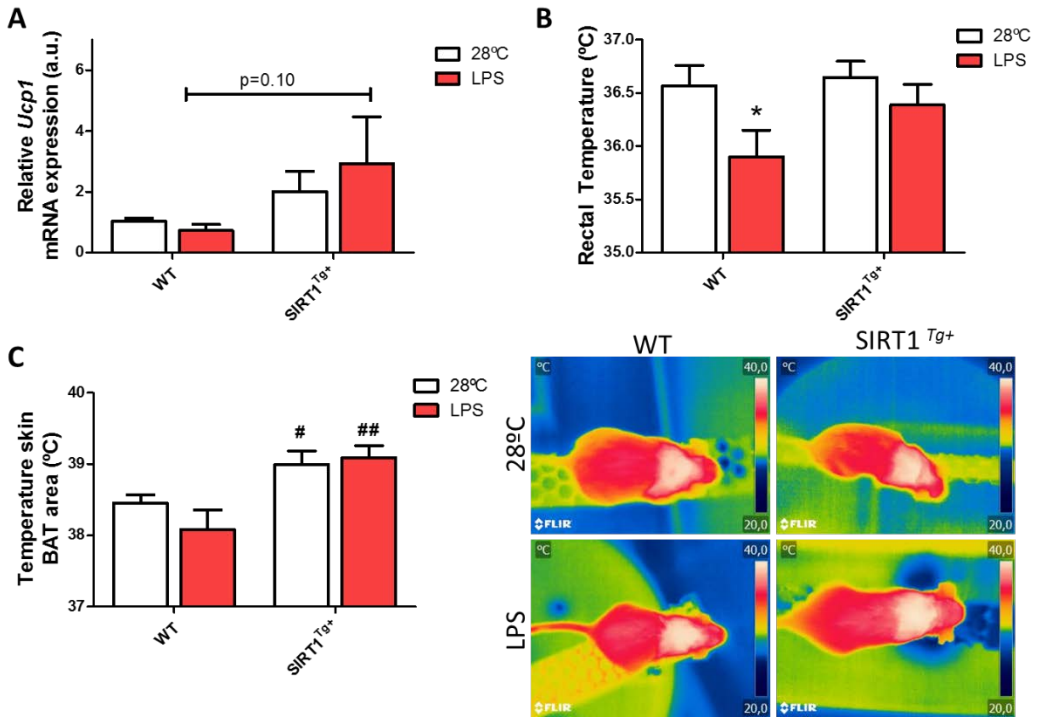

Figure 21. Impact of LPS treatment in *Ucp1* mRNA levels and temperature of WT and SIRT1^{Tg+} mice. **(A)** *Ucp1* mRNA levels in BAT of WT and SIRT1^{Tg+} mice (n= 4-6 mice/group). **(B)** Rectal temperature was measured with a rectal probe in mice at 28ºC with or without LPS treatment (24 h) (n= 15-20 mice/group).

(C) Skin temperature surrounding BAT recorded with an infrared camera. Pictures were captured at 28ºC with or without LPS treatment (24 h) (n= 10-16 mice/group). The bars represent mean ± SEM. Statistical analysis was performed with a Two-way ANOVA. *Comparison between mice treated or not with LPS in the same genotype. #Comparison between genotypes with the same treatment. *,#p< 0.05, ##p< 0.01.

Next, we analyzed the bioenergetic profile of BAT explants to address a possible effect of inflammation and SIRT1 overexpression in BAT respiration. Seahorse analysis was performed in BAT explants after treating or not mice from the two genotypes with LPS and, as shown in Figure 22, higher basal and a tendency to increase maximal respiration in SIRT1^{Tg+} mice was found. Moreover, both parameters decreased in BAT explants of both genotypes after LPS injection.

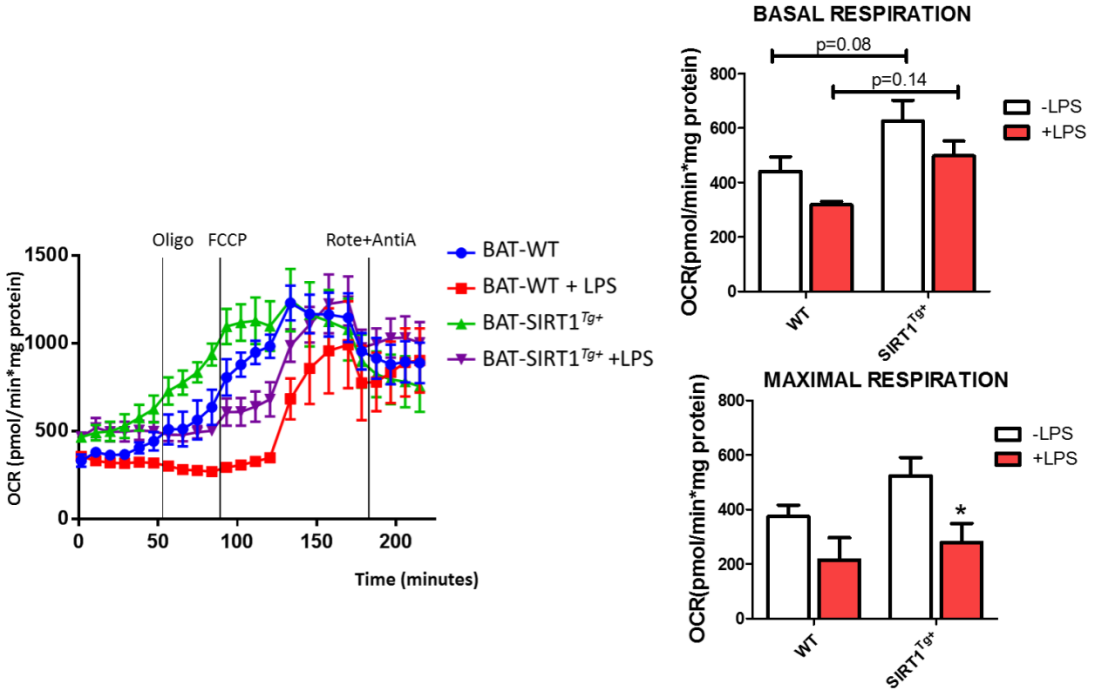

Figure 22. Bioenergetic profile of interscapular BAT explants from WT and SIRT1^{Tg+} mice. OCR in BAT explants from WT and SIRT1^{Tg+} mice treated or not with LPS. The left panel shows the Seahorse profile and the right panel shows basal and maximal respiration measured in BAT explants (n=3-4 mice/group). Bars represent mean ± SEM. Statistical analysis was performed with a Two-way ANOVA. *p< 0.05 compared with non-injected mice.

To check whether SIRT1 overexpression affects the cellular density of BAT we analyzed BAT slides. Although a slight increase in cell density was found in BAT from SIRT1^{Tg+} mice at thermoneutrality, H&E staining revealed similar BAT histology in WT and SIRT1^{Tg+} mice treated with LPS compared with their corresponding controls (Figure 23).

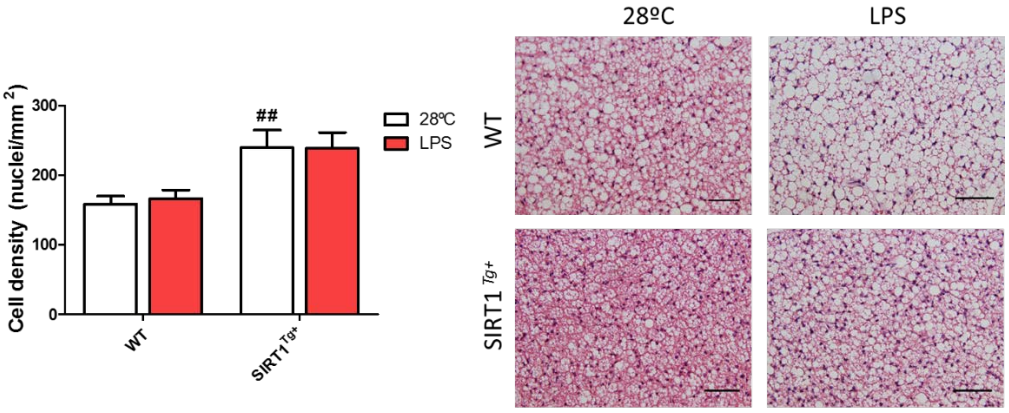

Figure 23. BAT histology of WT and SIRT1^{Tg+} mice. To estimate the cell density the nuclei were counted after H&E staining in at least 3 fields of different BAT sections of each animal (n=3-4 mice /group). Around 200 total nuclei per section were counted. Scale bars represent 50 µm. The bars represent mean ± SEM. Statistical analysis was performed with a Two-way ANOVA. $^{\#\#}p< 0.01$ compared with non-injected WT mice.

1.1.2.4 STUDY OF COLD RESPONSES UNDER PRO-INFLAMMATORY CONDITIONS IN BAT.

To further evaluate the impact of LPS-mediated inflammation and SIRT1 overexpression in BAT, we subjected WT and SIRT1^{Tg+} mice to cold-exposure under pro-inflammatory conditions (24 h of LPS injection). For this goal, WT and SIRT1^{Tg+} mice were housed at 28°C for at least one week. Then, mice were randomly divided into 2 experimental groups as schematized in Figure 24. One group was subjected to cold challenge (4°C) for 6 h and the other group was treated with 2 mg/kg LPS for 24 h and then exposed to the cold challenge (4°C) for the last 6 hours

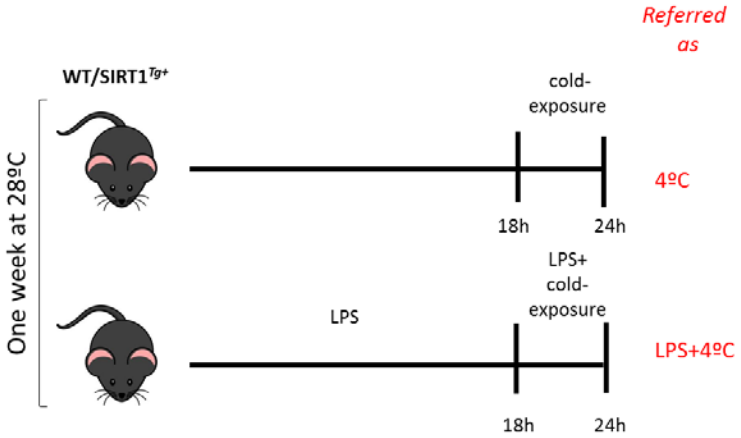

Figure 24. Experimental groups of mice and time-flow for the study of the thermogenic response of mice under LPS-induced pro-inflammatory environment.

We analyzed UCP-1 protein and mRNA levels of some thermogenic markers in both genotypes. As shown in Figure 25A, UCP-1 protein levels decreased in WT mice injected LPS and exposed to the cold, being these effects ameliorated in SIRT1^{Tg+} mice. At the mRNA level, *Ucp1, Dio2, Prdm16* and *Pgc1a* expression decreased after LPS and cold-exposure when compared to the cold-exposure without LPS injection condition in both genotypes. However, this decrease was attenuated in SIRT1 over-expressing mice (Figure 25B).

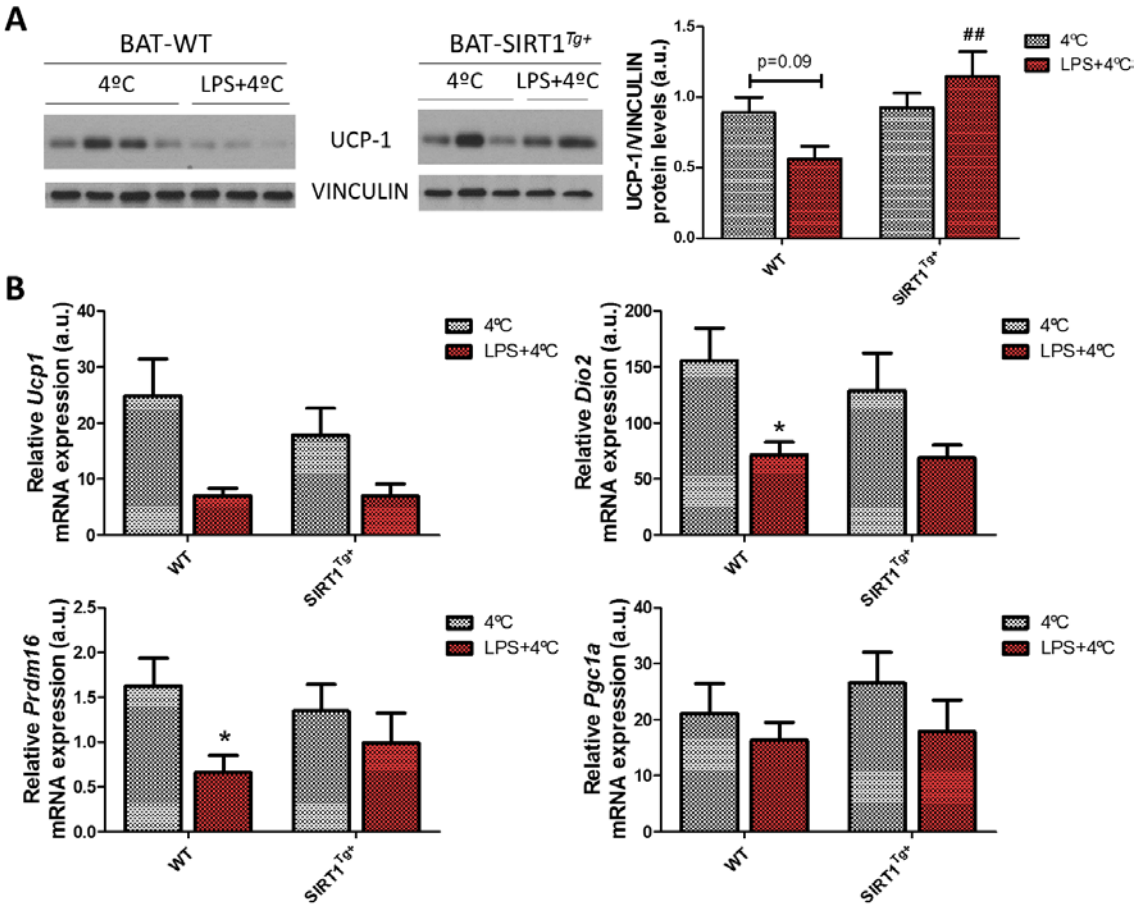

Figure 25. Analysis of thermogenic markers after cold-exposure under pro-inflammatory conditions in BAT. (A) Representative Western blots of UCP-1 protein expression in BAT. The right panel represents the quantification of n=7-10 mice/group. **(B)** The graphs represent *Ucp1, Dio2, Prdm16* and *Pgc1a* mRNA levels in BAT after 4ºC or LPS+4ºC. The bars represent mean ± SEM (n=5-10 mice/group). Statistical analysis was performed with a Two-way ANOVA. *Comparison between mice treated or not with LPS of the same genotype. #Comparison between genotypes with the same treatment. *p< 0.05, ##p< 0.01.

In order to study more in-depth the thermogenic response, we analyzed different parameters such as the temperature of the skin surrounding BAT (Figure 26A), which significantly decreased in WT animals after cold-exposure under pro-inflammatory conditions compared to SIRT1^{Tg+} mice. On the other hand, SIRT1^{Tg+} mice maintained rectal temperature under these conditions (Figure 26B). Both BAT and iWAT weight was lower in SIRT1^{Tg+} animals after LPS and cold-exposure conditions (Figure 26C). When analyzing BAT samples, a lower number of nuclei/field were counted in WT mice subjected to LPS and 4ºC rather than in SIRT1 overexpressing mice (Figure 26D).

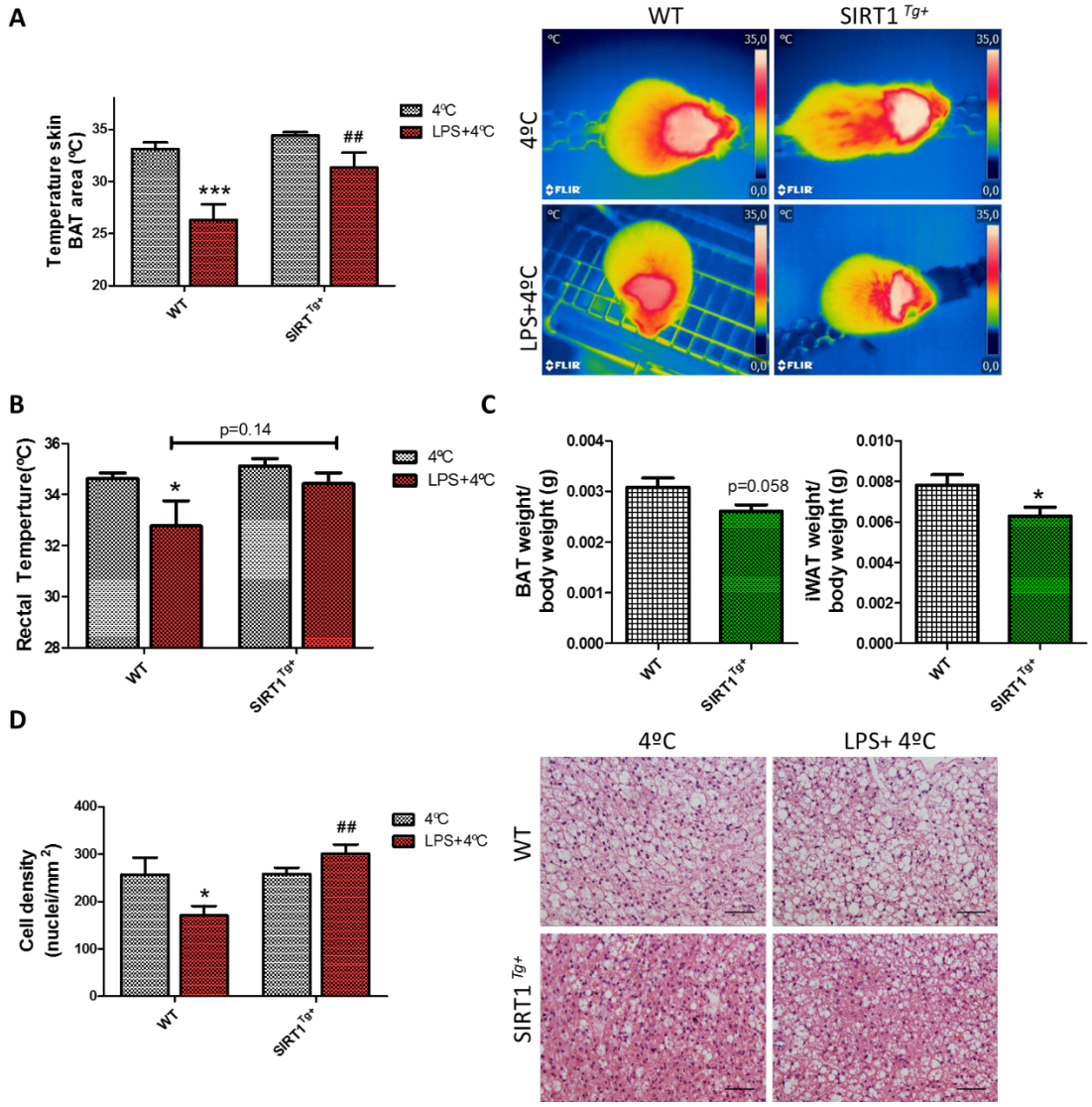

Figure 26. Analysis of the temperature of the skin surrounding BAT, rectal temperature, BAT and iWAT weight and histological analysis of BAT samples after cold-exposure under pro-inflammatory challenge in mice. (A) Skin temperature surrounding BAT recorded with an infrared camera. Pictures were captured immediately after cold exposure (6 h) (n= 7-12 mice/group). **(B)** Rectal temperature was measured with a rectal probe immediately after the cold exposure (6 h) (n=8-14 mice/group). **(C)** BAT and iWAT weight relative total body weight after LPS and cold exposure (n= 20 mice/group). **(D)** To estimate the cell density, the nuclei were counted in at least 3 fields of different BAT sections of each animal (n=3-4 mice/group). Around 200 total nuclei per section were counted. Scale bars represent 50 µm. **(A,B,D)** The bars represent mean ± SEM. Statistical analysis was performed with a Two-way ANOVA.*Comparison between mice treated or not with LPS in the same genotype. #Comparison between genotypes with the same treatment.*p< 0.05, ## p< 0.01, ***p< 0.001. **(C)** The bars represent mean ± SEM. Statistical analysis was performed with Mann-Whitney U test. *p<0.05.

2. CELLULAR STUDIES.

2.1 GENERATION OF AN IN VITRO MODEL OF BROWN ADIPOCYTES FROM WT AND SIRT1^{Tg+} MICE: CHARACTERIZATION OF INSULIN AND NORADRENERGIC RESPONSES.

To identify the molecular mechanisms implicated in the enhancement of the insulin and thermogenic responses found in SIRT1^{Tg+} mice, we isolated and immortalized brown preadipocytes from the interscapular BAT of WT and SIRT1^{Tg+} mice (see materials and methods, Figure 13).

In order to monitor the differentiation from brown preadipocytes to mature brown adipocytes, we analyzed the expression of some markers that define the maturity of brown adipocytes along the differentiation process. First, as shown in Figure 27A both WT and SIRT1^{Tg+} brown preadipocyte cell lines differentiated correctly and showed the typical phenotype of mature brown adipocytes at day 7 of differentiation. We analyzed the levels of proteins that are involved in adipogenesis and thermogenesis such as fatty acid synthase (FAS) and UCP-1, respectively, as well as key proteins of the insulin signaling pathway as IR and GLUT-4 (Figure 27B,C). Although we did not observe significant changes in FAS, GLUT4 or IR protein levels between the two genotypes of mature adipocytes, SIRT1^{Tg+} brown adipocytes showed significant lower protein levels of UCP-1 at the final stage of differentiation as depicted in Figure 27B and C in agreement with a previous study [150]. These differences in UCP-1 protein expression were also found at the mRNA level.

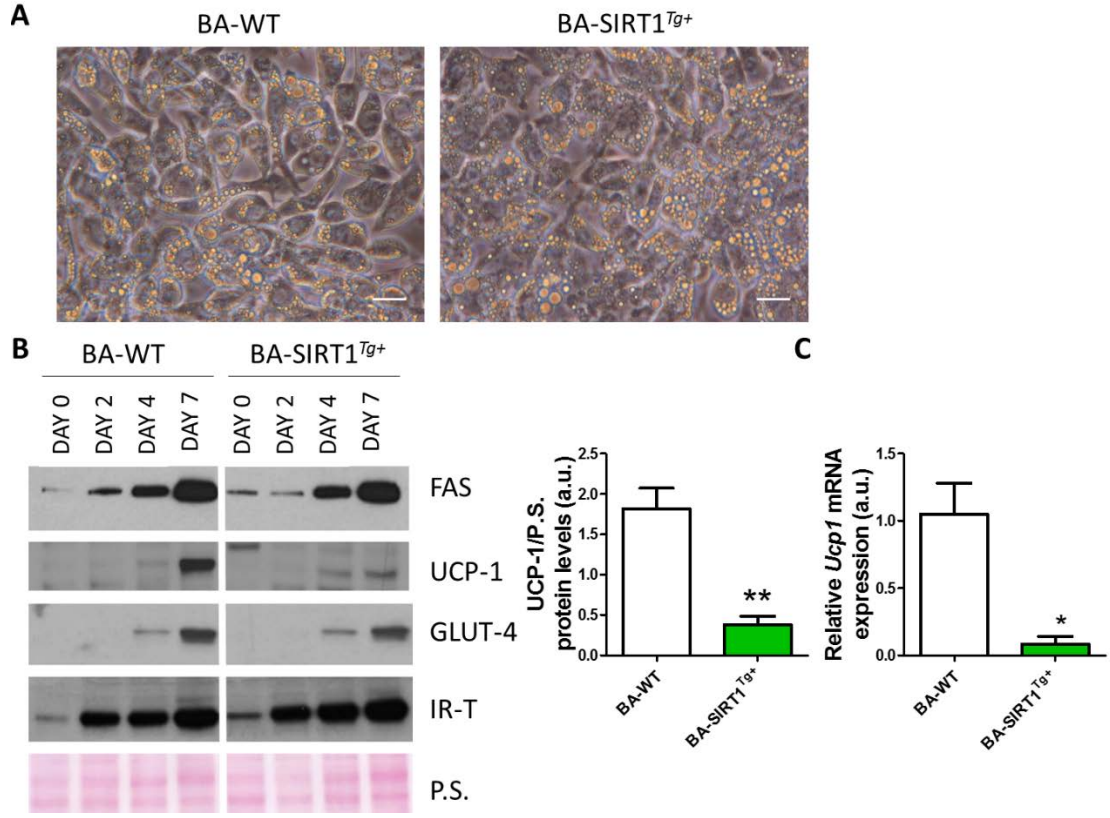

Figure 27. Characterization of relevant markers of differentiated brown adipocytes in WT and SIRT1^{Tg+} cell lines. (A) Microscopic characterization of BA-WT and BA-SIRT1^{Tg+} differentiation process. Both genotypes showed the typical multilocular and small lipid droplets. Microscopy images were captured

with the 40X objective at day 7 of differentiation. Scale bars represent 20 µm. **(B**) Protein levels of FAS, UCP-1, GLUT-4 and IR were determined along differentiation from the preadipocyte stage (day 0) until the mature adipocytes stage (day 7) was reached. The graph shows the relative increase in UCP-1 protein levels at day 7 of differentiation. Ponceau staining was used to visualize gel loading. Bars represent mean ± SEM (n=5 independent experiments). Statistical analysis was performed with Mann-Whitney U test. **p<0.01. **(C)** *Ucp1* mRNA levels at day 7 analyzed by qRT-PCR. The bars represent mean ± SEM (n=3 independent experiments). Statistical analysis was performed with Mann-Whitney U test. *p<0.05.

In order to study the effect of SIRT1^{Tg+} overexpression in insulin signaling, differentiated BA from the two genotypes were stimulated with 10 nM insulin during 15 min. The results shown in Figure 28A revealed higher phosphorylation levels of IR and AKT (Ser 473) in BA overexpressing SIRT1. Moreover, BA-SIRT1^{Tg+} showed higher basal levels of AKT phosphorylation in the absence of insulin. When we analyzed the basal levels of PTP1B, we found significant constitutive lower protein levels in BA-SIRT1^{Tg+} compared with BA-WT (Figure 28B).

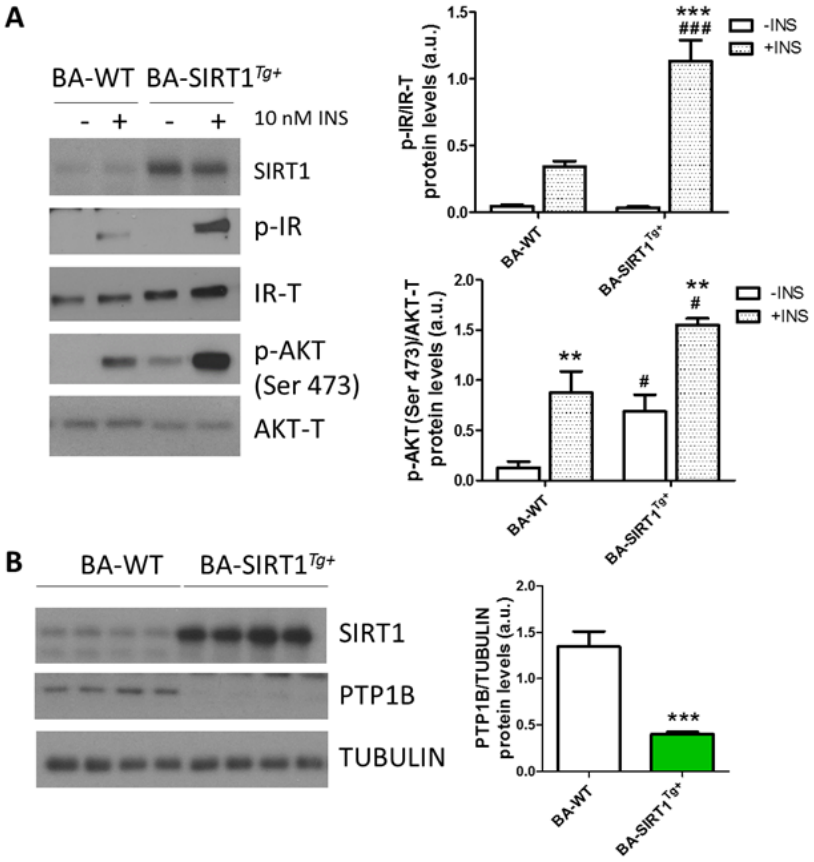

Figure 28. Analysis of the insulin signaling pathway in WT and SIRT1^{Tg+} differentiated brown adipocytes. (A) Insulin signaling in differentiated BA stimulated or not with 10 nM insulin for 15 min and analyzed by Western blot. The graphs show IR and AKT phosphorylation levels. IR-T and AKT-T were used as loading controls (n=4 independent experiments). Bars represent mean ± SEM. Statistical analysis was performed with a Two way ANOVA. *Comparisons between insulin-treated and untreated BA of the same genotype. #Comparisons between genotypes with the same treatment. #p< 0.05, **p< 0.01, ***,###p< 0.001. **(B)** PTP1B protein levels in BA-WT and BA-SIRT1^{Tg+} analyzed by Western blot. Tubulin was used as a loading control (n=8 independent experiments). Bars represent mean ± SEM. Statistical analysis was performed with Mann-Whitney U test. ***p<0.001.

As indicated in the introduction, brown adipocytes have the ability to induce UCP-1 after adrenergic stimulation. In order to analyze the impact of SIRT1 overexpression in the two genotypes, cells were stimulated with 5 µM NE during 17 h. As shown in Figure 29A, higher levels of UCP-1 after NE stimulation were found in BA-SIRT1^{Tg+} compared with BA-WT. These differences were also observed at the mRNA level (Figure 29B).

Moreover, NE-induced lipolysis was enhanced in BA overexpressing SIRT1 (Figure 29C).

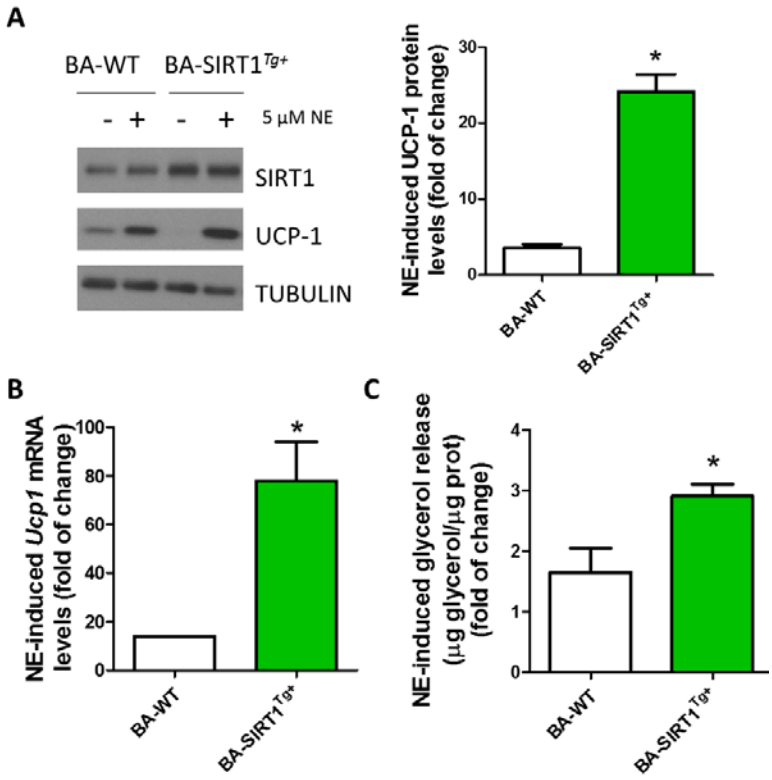

Figure 29. NE-mediated UCP-1 induction and glycerol release were enhanced in brown adipocytes overexpressing SIRT1. (A) UCP-1 levels in differentiated BA stimulated or not with 5 µM NE for 17 h analyzed by Western blot. The graph shows the fold increase of UCP-1 induction after NE stimulation in BA-WT and BA-SIRT1^{Tg+}. Tubulin was used as a loading control (n=4 independent experiments). Bars represent mean ± SEM. Statistical analysis was performed with Mann-Whitney U test. *p<0.05 compared to BA-WT. **(B)** *Ucp1* mRNA levels in the experimental conditions described in **A** analyzed by qRT-PCR (n=3 independent experiments). The bars represent mean ± SEM. Statistical analysis was performed with a Student t-test. *p<0.05. **(C)** Glycerol released by BA-WT and BA-SIRT1^{Tg+} after NE stimulation (n=3 independent experiments). The bars represent mean ± SEM. Statistical analysis was performed with Mann-Whitney U test. *p<0.05.

2.2. EFFECT OF SIRT1 OVEREXPRESSION IN BROWN ADIPOCYTES UNDER PRO-INFLAMMATORY CONDITIONS.

It is already known that obesity induces local proliferation of resident macrophages in adipose tissues that contributes to obesity-associated adipose tissue inflammation. To analyze the cross-talk between macrophages and BA, conditioned medium was generated from Raw 267.4 macrophages stimulated or not with LPS (CM-LPS and CM-CTR, respectively) and spectrophotometric determination of nitrite production was performed to assess the pro-inflammatory potency of the CM-LPS (see Material and Methods, Figure 15).

2.2.1. ANALYSIS OF THE PRO-INFLAMMATORY SIGNALING CASCADES.

We treated differentiated BA with CM-CTR and CM-LPS for several time-periods ranging from 15 to 120 min to analyze the effect of the pro-inflammatory environment in the activation of pro-inflammatory signaling cascades. As expected, CM-LPS triggered an

early activation of the signaling pathways mediated by STAT3, IKKα/β, JNK, and p38 MAPK, together with the degradation of IκBα. Interestingly, BA overexpressing SIRT1 showed a decrease in STAT3 phosphorylation at all time-periods analyzed compared with the response of BA-WT (Figure 30).

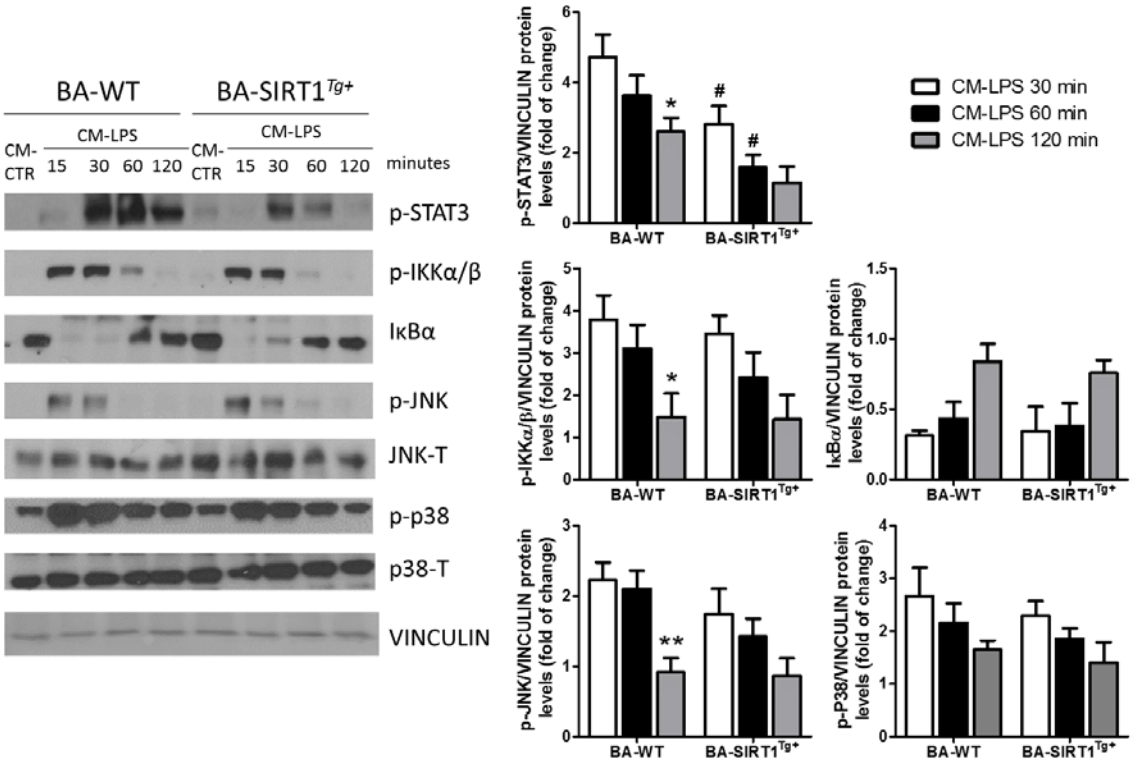

Figure 30. Analysis of the pro-inflammatory signaling cascades upon short-term stimulation of WT and SIRT1^{Tg+} BA with CM-LPS. Activation of the pro-inflammatory signaling cascades mediated by JAK-STAT, IKKα/β, IκBα, JNK and p38 MAPK analyzed by Western blot in both genotypes of BA treated with CM-LPS at different time-periods (15, 30, 60,120 min). The graphs show the fold increase *vs.* CM-CTR in BA-WT and BA-SIRT1^{Tg+}. Vinculin was used as a loading control (n=5 independent experiments). Bars represent mean ± SEM. Statistical analysis was performed with a Two-way ANOVA. *Comparison with CM-LPS 30 min in the same genotype. #Comparison between genotypes with the same treatment. *,#p<0.05, **p<0.01.

2.2.2 ANALYSIS OF THE MITOCHONDRIAL FUNCTIONALITY OF BA-WT AND BA-SIRT1^{Tg+} UNDER PRO-INFLAMMATORY CONDITIONS.

We used the Seahorse technique to study more in-depth the mitochondrial respiration capacity and we also measured FAO to evaluate the oxidative capacity of BA-WT and BA-SIRT1^{Tg+} under pro-inflammatory conditions.

The Seahorse profile analyzed in differentiated BA revealed the absence of differences in the impact of the pro-inflammatory environment in the complexes of the ETC (see red and blue lines in Figure 31A). The effect of the oligomycin, which inhibits the ATP synthase; FCCP, that uncouples oxygen consumption from ATP production, and rotenone and antimycin A that are inhibitors of complexes I and III, respectively, was similar between genotypes of BA (green and blue lines in Figure 31A).

We next studied FAO by detection of CO_2 and acid-soluble products (ASPs) released from oxidation of C^{14} labelled palmitate. As shown in Figure 31B, BA overexpressing

SIRT1 showed higher basal FAO that further decreased after the treatment with CM-LPS but, even though, levels remained higher than those of the BA-WT (Figure 31B).

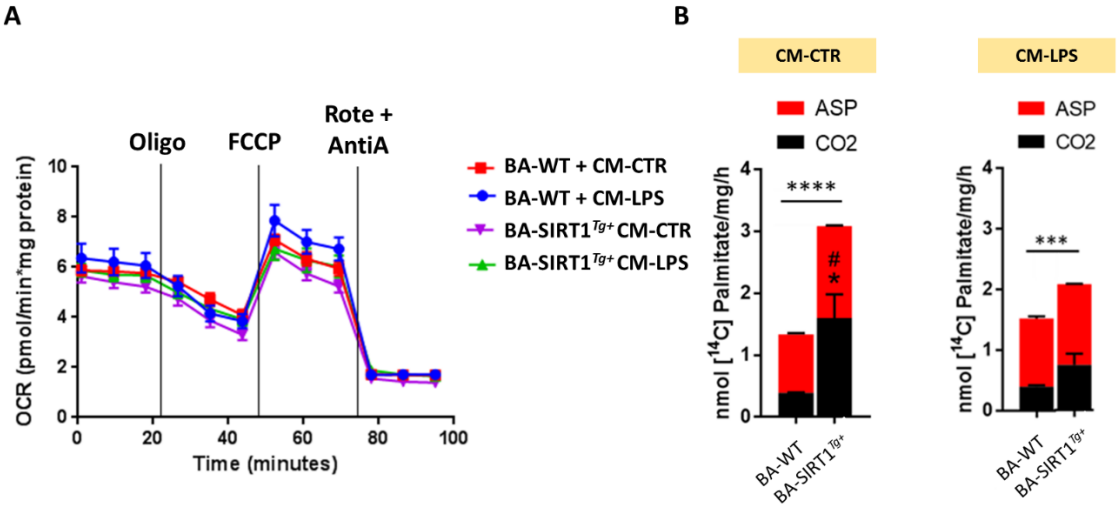

Figure 31. Seahorse profile and analysis of β-oxidation in WT and SIRT1^{Tg+} BA treated with pro-inflammatory CM. (A) Representative Seahorse profile performed in differentiated BA treated with CM-CTR or CM-LPS for 18 h (n=3 experiments performed in triplicate). **(B)** Representative FAO assay performed in differentiated BA treated with CM-CTR or CM-LPS for 18 h (n=3 experiments performed in triplicate). The bars represent mean ± SEM. Statistical analysis was performed with Mann-Whitney U test. *Comparison of ASP between genotypes. #Comparison of CO_2 between genotypes. *,#p<0.05, ***p<0.001, ****p<0.0001.

2.2.3. IMPACT OF SIRT1 OVEREXPRESSION IN THE INSULIN SIGNALING PATHWAY IN BA UNDER PRO-INFLAMMATORY CONDITIONS.

Regarding insulin signaling, the results in the *in vivo* model showed that SIRT1 overexpression protected mice against the drop in the insulin signaling pathway induced by LPS administration (see Figure 20). On that basis, we aimed to corroborate these results in differentiated BA. We found that the treatment of BA with CM-LPS before insulin stimulation decreased the response of the hormone in inducing IR and AKT phosphorylation in BA-WT compared with the response of the cells in the presence of CM-CTR. By contrast, insulin-mediated signaling was preserved in BA-SIRT1^{Tg+} (Figure 32).

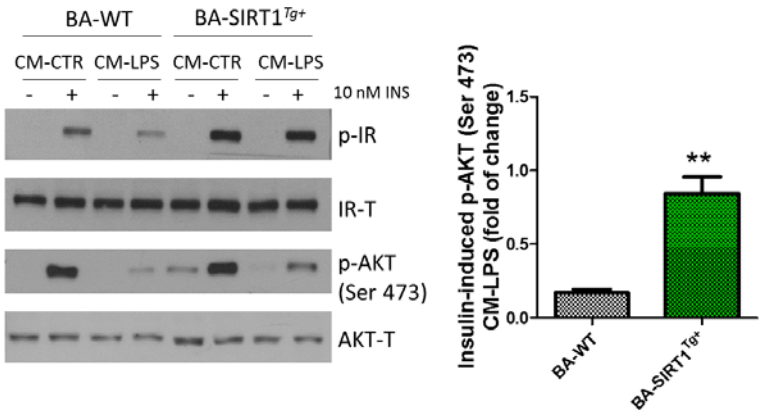

Figure 32. SIRT1 overexpression ameliorated the drop in insulin signaling induced by the pro-inflammatory CM-LPS. WT and SIRT1^{Tg+} BA were treated with CM-CTR or CM-LPS for 18 h and then stimulated with 10 nM insulin for 15 min. Insulin-mediated IR and AKT phosphorylation were analyzed by Western blot. The graphs show the fold increase of IR and AKT phosphorylation after insulin stimulation.

IR-T and AKT-T were used as loading controls, respectively (n=6 independent experiments). Bars represent mean ± SEM. Statistical analysis was performed with Mann-Whitney U test. The bars represent mean ± SEM. **p<0.01.

In addition to its thermogenic function, BAT constitutes an important glucose-clearing organ [183]. We next studied the effect of the pro-inflammatory environment in glucose uptake of brown adipocytes and, as shown in Figure 33A, we observed an increase in basal (insulin-independent) glucose uptake in BA-WT after the treatment with CM-LPS that was absent in BA overexpressing SIRT1. Notably, BA-SIRT1^{Tg+} showed higher levels of glucose uptake under non-pro-inflammatory conditions (CM-CTR) that were maintained in the presence of CM-LPS. The analysis of the insulin response (Figure 33B) revealed a marked reduction in glucose uptake in BA-WT pre-treated with CM-LPS that did not occur in BA-SIRT1^{Tg+}.

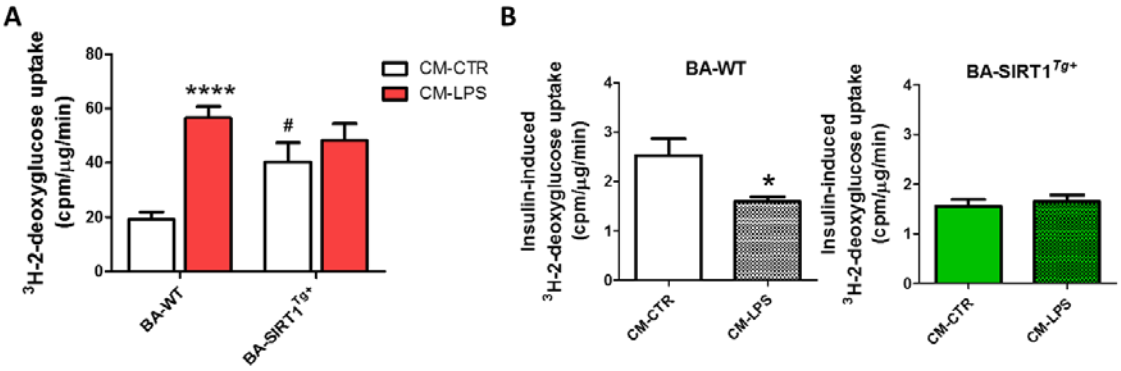

Figure 33. SIRT1 overexpression ameliorated the drop in glucose uptake induced by the pro-inflammatory CM-LPS. (A) Measurement of ^{3}H-2-deoxyglucose uptake in WT and SIRT1^{Tg+} BA treated with CM-CTR or CM-LPS for 18 h (n=4 independent experiments). Bars represent mean ± SEM. Statistical analysis was performed with a Two-way ANOVA. *Comparisons between CM-LPS and CM-CTR in the same genotype of BA. $^{\#}$Comparisons between genotypes with the same treatment. $^{\#}$p< 0.05, ****p< 0.001. **(B)** The graphs represent fold increase in insulin-induced glucose uptake in BA from both genotypes treated as described in **A** and then stimulated with 10 nM insulin for 15 min (n=4 independent experiments). The bars represent mean ± SEM. Statistical analysis was performed with Mann-Whitney U test. *p<0.05.

2.2.4. ANALYSIS OF THE NORADRENERGIC RESPONSE OF BA-WT AND BA-SIRT1^{Tg+} UNDER PRO-INFLAMMATORY CONDITIONS.

We next analyzed the response of the two genotypes of BA to NE in the presence of CM-LPS. As shown in Figure 34, the pro-inflammatory environment decreased NE-mediated UCP-1 induction in BA-WT but, unexpectedly, SIRT1 overexpression not only failed to protect from this drop, but also showed a more profound decrease in UCP-1 induction under pro-inflammatory conditions.

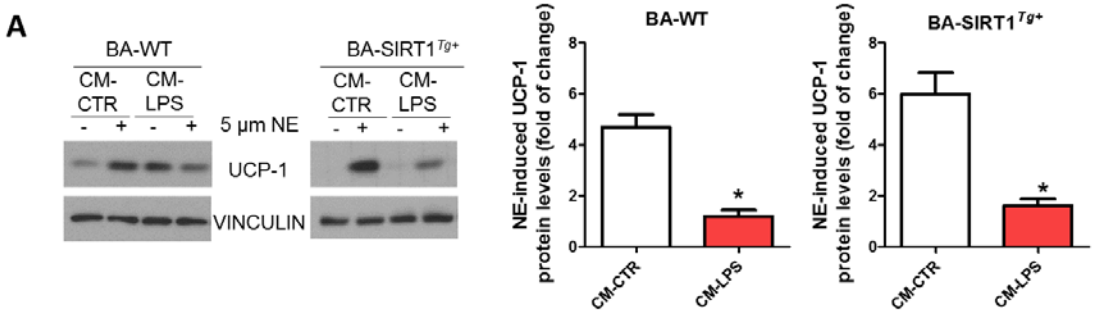

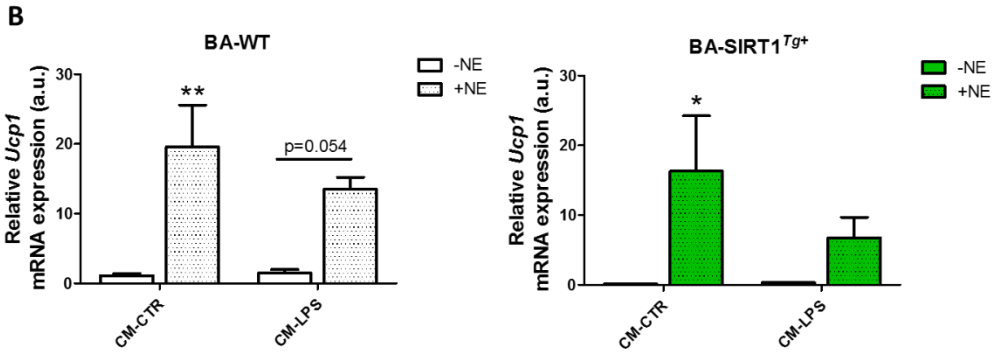

Figure 34. Reduced response to NA in the induction of UCP-1 in BA-WT and BA overexpressing SIRT1 in in a pro-inflammatory environment. (A) WT and SIRT1^{Tg+} brown adipocytes were treated with CM-CTR or CM-LPS for 18 h in the absence or presence of 5 μM NE. UCP-1 protein levels were analyzed by Western blot. The graph shows fold increase of UCP-1 induction after NE stimulation in WT and SIRT1^{Tg+} BA. Vinculin was used as a loading control (n=5 independent experiments). Bars represent mean ± SEM. Statistical analysis was performed with a Two-way ANOVA. *Comparisons between CM-LPS-treated and CM-CTR in the same genotype. ***p< 0.001, ****p< 0.0001. **(B)** *Ucp1* mRNA levels in same conditions as described in **A** (n=3 independent experiments). The bars represent mean ± SEM. Statistical analysis was performed with a Two-way ANOVA. *Comparisons between NE-treated and its control. *p< 0.05 , **p< 0.01.

2.3. CHARACTERIZATION OF AN ALTERNATIVE PROTOCOL OF DIFFERENTIATING BA.

In order to reverse the failure of NE to increase UCP-1 expression in BA under pro-inflammatory conditions, we differentiated WT or SIRT1 overexpressing brown preadipocytes with a protocol previously described by others [184] to differentiate inguinal white adipocytes into beige adipocytes. Of relevance, this differentiation medium contains higher T_3, rosiglitazone and insulin concentrations (see Material and Methods, Figure 14).

As shown in Figure 35A, the differentiation of the two genotypes of brown preadipocytes with this medium (hereafter referred to as medium 2) was comparable to the differentiation with medium 1 (Figure 27A). However, the staining of lipid droplets with Bodipy showed higher lipid accumulation in both genotypes upon differentiation with medium 2 (Figure 35B).

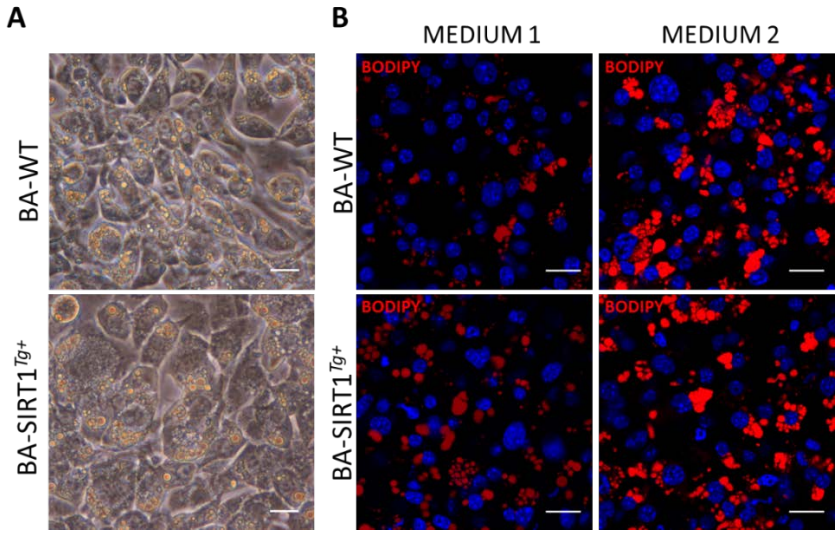

Figure 35. Characterization of BA-WT and BA-SIRT1^{Tg+} differentiated with medium 2. (A) Microscopic characterization of BA-WT and BA-SIRT1^{Tg+} differentiation process with medium 2. Both genotypes showed

the typical multilocular and small lipid droplets phenotype. Microscopy images were captured with the 40X objective at day 7 of differentiation. Scale bars represent 20 µm. **(B)** Immunofluorescence of Bodipy (red) in BA-WT and BA-SIRT1^{Tg+} differentiated with medium 1 or medium 2 (day 7). Nuclei staining with DAPI (blue). Scale bars represent 20 µm.

When we analyzed relevant genes for the process of BA differentiation we observed a marked down-regulation of *Dio2* mRNA levels in BA-WT and BA-SIRT1^{Tg+} differentiated in medium 2. However, both genotypes presented similar high levels of *Prdm16* and *Ucp1* while the levels of *Pgc1a* were not modified (Figure 36A). When we analyzed UCP-1 protein levels we found that medium 2 increased UCP-1 protein levels at final stage of differentiation in both genotypes of BA (Figure 36B).

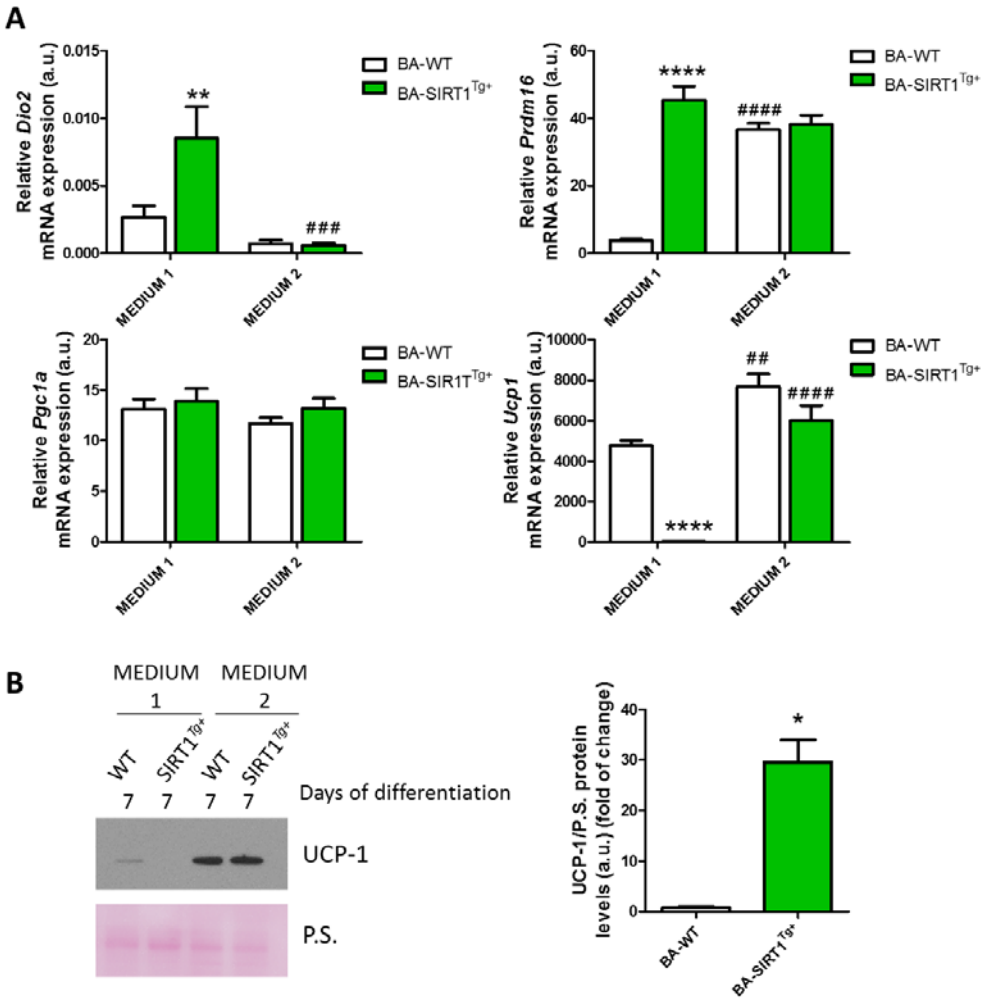

Figure 36. Differentiation of BA with medium 2 modulates the expression of brown-related genes and generates mature BA with higher UCP-1 levels. (A) *Dio2, Prdm16, Pgc1a* and *Ucp1* mRNA levels in BA from both genotypes at 7 of differentiation with the two media analyzed by qRT-PCR relative to levels of day 0 (n=3 independent experiments). Bars represent mean ± SEM. Statistical analysis was performed with a Two-way ANOVA. *Comparisons between different genotypes and same medium. #Comparisons between the two media and same genotype. **,##p< 0.01, ###p< 0.001, ****,####p< 0.0001. **(B)** Western blot of UCP-1 protein levels in BA from both genotypes at days 0 and 7 of differentiation with medium 1 or medium 2. Ponceau staining was used to visualize loading. The graph represents fold of change of UCP-1 protein levels in BA from both genotypes differentiated with medium 2 relative to values in medium 1 (n=4 independent experiments). The bars represent mean ± SEM. Statistical analysis was performed with Mann-Whitney U test. *p<0.05.

To study the capacity of BA-SIRT1^{Tg+} and BA-WT to respond to NE upon differentiation with medium 2 we analyzed UCP-1 protein and *Ucp1* mRNA levels after treatment with 5 µM NE for 17 h. As shown in Figure 37A, medium 2 promoted higher NE-induced *Ucp1* mRNA levels compared to medium 1 in both genotypes of brown adipocytes. Regarding UCP-1 protein levels, a higher induction in response to NA was detected in BA differentiated with medium 2 (Figure 37B). Moreover, BA-SIRT1^{Tg+} showed higher NE-induced lipolytic rate when compared to BA-WT (Figure 37C).

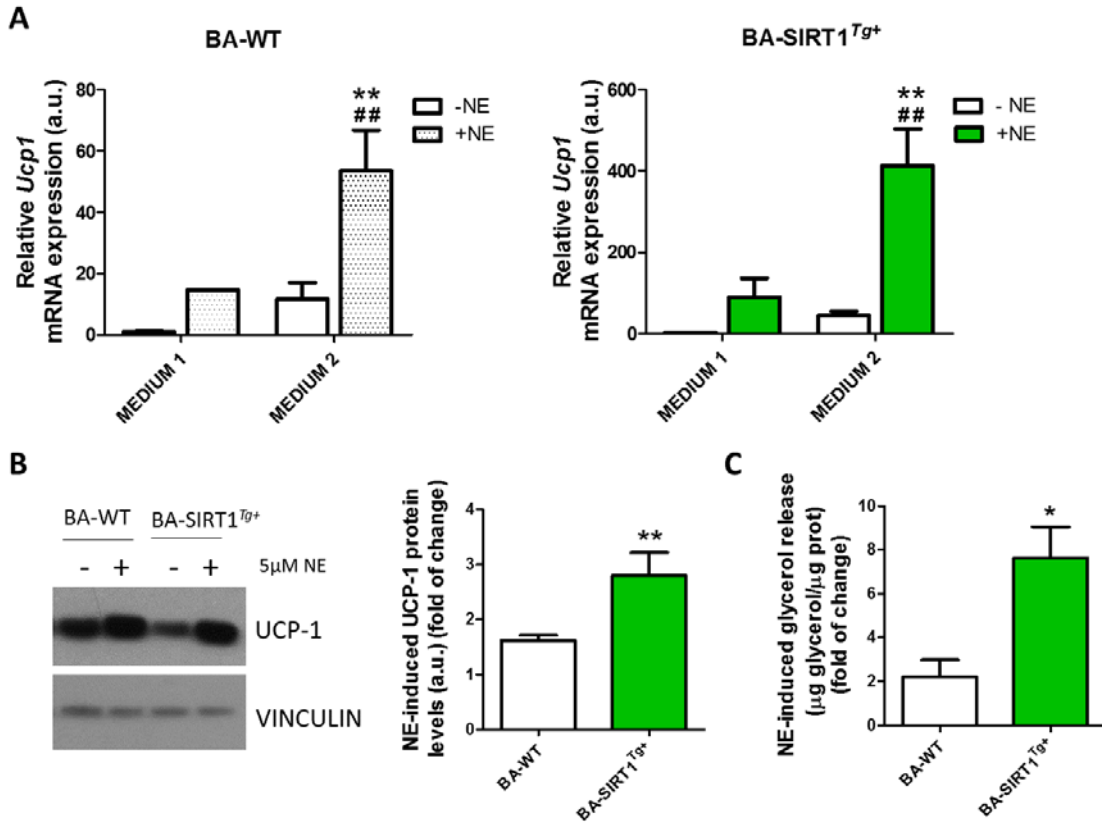

Figure 37. Differentiation with medium 2 generates mature BA with higher NE-induced UCP-1 levels and lipolytic rate. (A) *Ucp1* mRNA levels after stimulation of WT and SIRT1^{Tg+} BA with 5 µM NE for 17 h upon differentiation with medium 1 or medium 2 (n=3 independent experiments). Bars represent mean ± SEM. Statistical analysis was performed with a Two-way ANOVA. *Comparisons between NE-treated and untreated in the same medium. $^{\#}$Comparisons between same treatment and different media. **,## p< 0.01. **(B)** Western blot of UCP-1 protein levels after stimulation of WT and SIRT1^{Tg+} BA with 5 µM NE for 17 h with medium 2. Vinculin was used as a loading control (n=5 independent experiments). Bars represent mean ± SEM. Statistical analysis was performed with Mann-Whitney U test. **p<0.01 compared to BA-WT. **(C)** Glycerol released by BA-WT and BA-SIRT1^{Tg+} differentiated with medium 2 (n=3 independent experiments). Bars represent mean ± SEM. Statistical analysis was performed with Mann-Whitney U test. *p<0.05 compared to BA-WT.

Next, we addressed a possible effect of medium 2 in the amount of mitochondria by performing TOM22 (Figure 38A) and COX IV (Figure 38B) immunofluorescence. We detected a higher signal of both markers in BA overexpressing SIRT1. Mitochondrial mass was also measured using MitoTracker green, a green-fluorescent mitochondrial stain, and flow cytometry (Figure 38C). Altough BA-SIRT1^{Tg+} showed significant higher mitochondrial mass upon differentiation with medium 1, the signal decreased when BA were differentiated with medium 2 in both genotypes of BA.

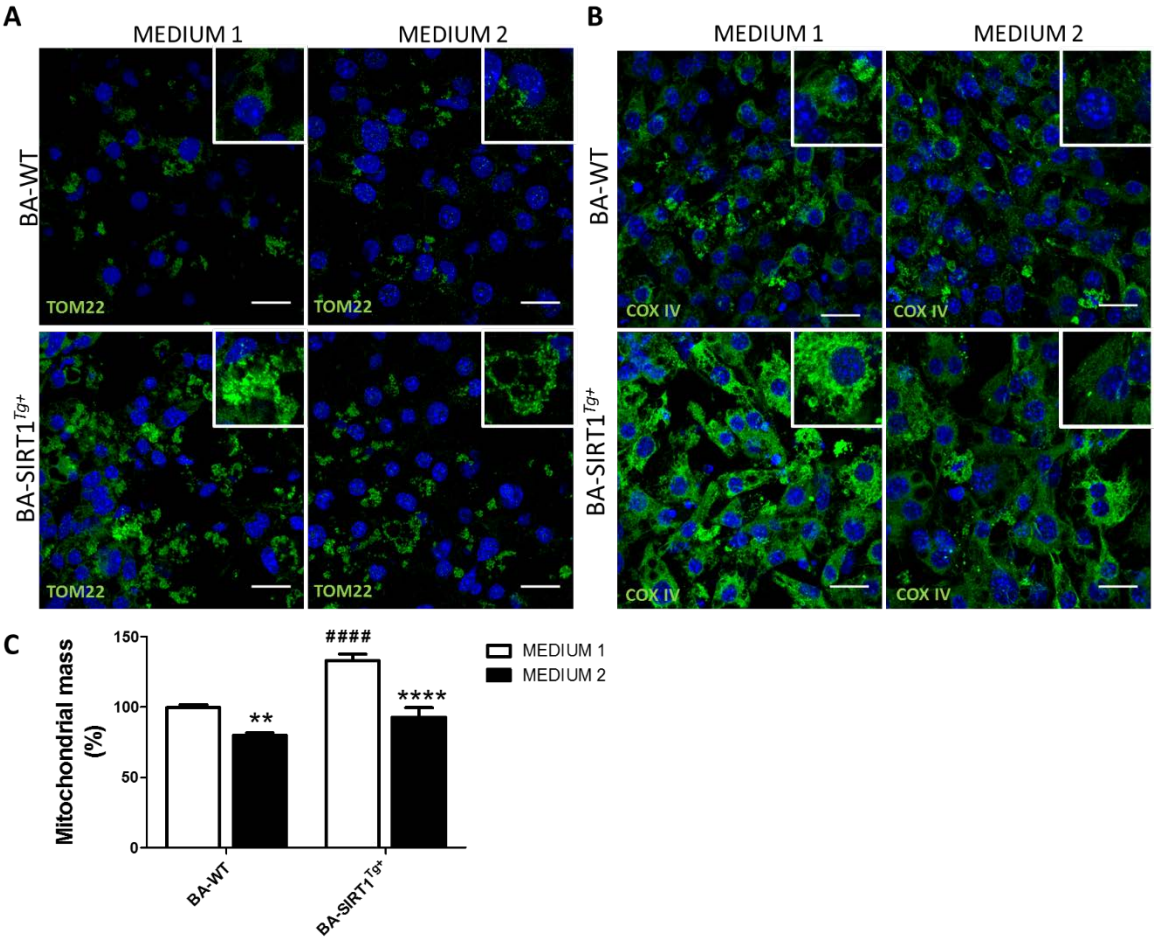

Figure 38. Immunofluorescence analysis of mitochondria in BA-WT and BA-SIRT1^{Tg+} differentiated with medium 1 and medium 2. TOM22 immunofluorescence (green) **(A)** and COX IV immunofluorescence (green) **(B)** in BA-WT and BA-SIRT1^{Tg+} differentiated with medium 1 or medium 2 (day 7). Nuclei staining with DAPI (blue). Scale bar is 20 μM. The inset shows a magnifcation of the signal. **(C)** Analysis of mitochondrial mass using MitoTracker Green and flow cytometry (n=3 independent experiments). Bars represent mean ± SEM. Statistical analysis was performed with a Two-way ANOVA. *Comparisons between same genotype and different media. #Comparisons between genotypes differentiated with the same media. **p< 0.01, ****,#### p< 0.0001.

We next studied markers of mitochondrial dynamics. We analyzed p-DRP1 and MFN2 (Figure 39) by immunofluorescence and Western blot at day 7 of differentiation of BA from the 2 genotypes with each differentiation medium. The expression of p-DRP1 (marker of fission) was higher in both genotypes differentiated with medium 2 while MFN2 (marker of fussion) was decreased. These results suggest a switch in the mitochondrial dynamics of BA differentiated with medium 2.

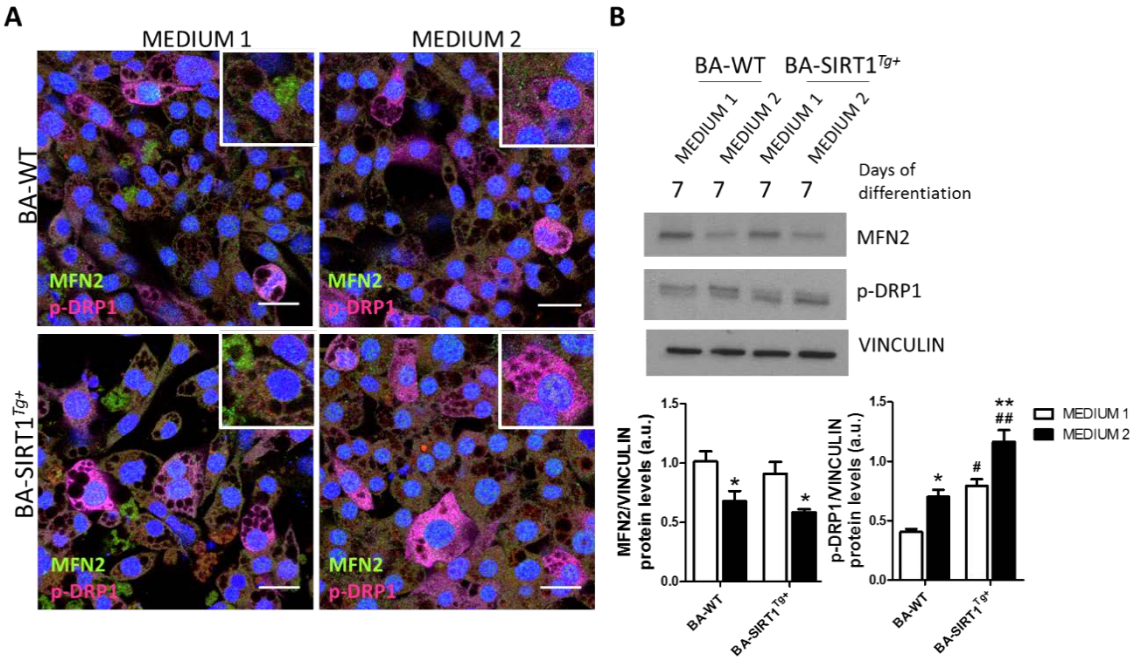

Figure 39. Analysis of markers of mitochondria dynamics in BA-WT and BA-SIRT1^{Tg+} differentiated with medium 1 or medium 2. (A) p-DRP1 (pink) and MFN2 (green) immunofluorescence in BA-WT and BA-SIRT1^{Tg+} differentiated with medium 1 or medium 2 (day 7). Nuclei were stained with DAPI (blue). Scale bar is 20 µm. The inset shows magnifcation of the signal. **(B)** MFN2 and p-DRP1 protein levels at day 7 of differentiation analyzed by Western blot. Vinculin was used as a loading control (n=4 independent experiments). Bars represent mean ± SEM. Statistical analysis was performed with a Two-way ANOVA. *Comparisons between different media in the same genotype. #Comparisons between genotypes differentiated with the same media. *,#p< 0.05 , **,## p< 0.01.

Taking into account the results reported by Yau and co-workers [70] regarding a direct relationship between T_3 and SIRT1 activity, we hypothesized that medium 2 would modulate SIRT1 enzimatic activity. The analysis of the acetylation state of the p65 subunit of NFκB, a downstream target of SIRT1, revealed a decrease in BA-WT adipocytes differentiated with medium 2. As expected, SIRT1 overexpression led to a decreased acetylation of p65-NFκB in BA differentiated with either medium 1 or 2 (Figure 40A). We also measured ATP and, as shown in Figure 40B, lower levels were detected in both genotypes after differentiation with medium 2. This decrease in ATP levels could be indicative of higher SIRT1 activity as described by Kang and co-workers [137]. In fact, BA-SIRT1^{Tg+} BA showed lower levels compared to BA-WT regardless of the differentiation medium used.

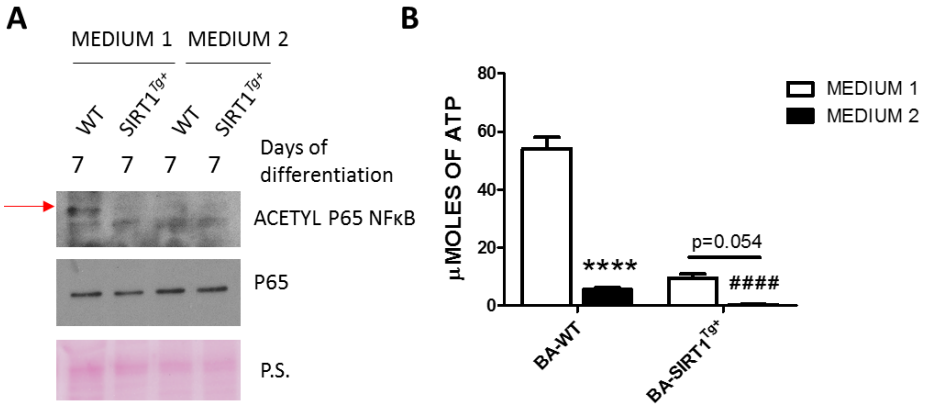

Figure 40. Differentiation with medium 2 generates mature brown adipocytes with higher SIRT1 activity. (A) SIRT1 activity was measured indirectly analyzing p65-NFκB acetylation levels by Western blot. Ponceau staining was used to visualize loading. **(B)** ATP levels were detected in BA at day 7 of differentiation using a bioluminescent kit. Bars represent mean ± SEM (n=3 independent experiments). Statistical analysis was performed with a Two-way ANOVA. *Comparisons between different medium and same genotype. #Comparisons between same medium and different genotype. ****, #### p< 0.0001.

2.3.1. IMPACT OF THE PRO-INFLAMMATORY ENVIRONMENT IN BA-WT AND BA-SIRT1^{Tg+} DIFFERENTIATED WITH MEDIUM 2.

Since substantial differences were found in ATP levels in BA differentiated with medium 1 or medium 2, we next studied whether inflammation could modulate ATP levels under these conditions. For this purpose, BA from both genotypes were stimulated with CM-CTR or CM-LPS and ATP levels were measured. As shown in Figure 41, treatment with CM-LPS decreased ATP levels in BA-WT differentiated with either medium 1 or medium 2. By contrast, ATP levels did not decrease in BA-SIRT1^{Tg+} with medium 2.

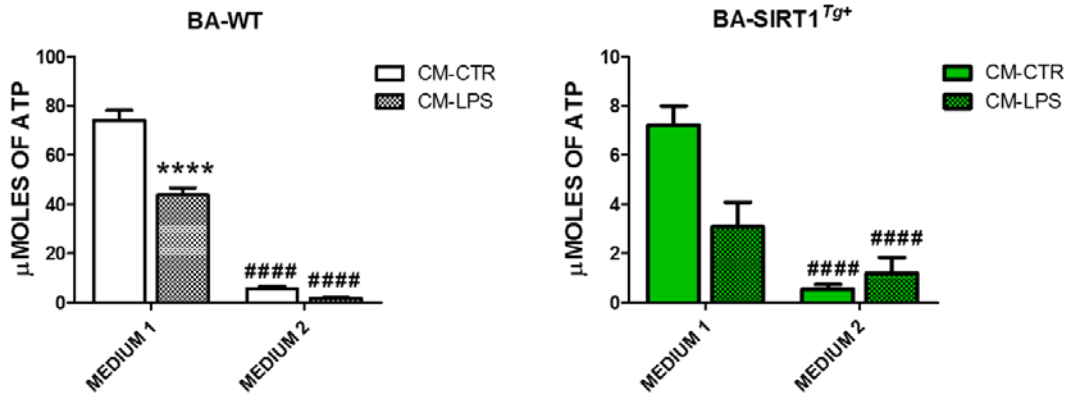

Figure 41. SIRT1 overexpression and medium 2 induce changes in ATP levels under pro-inflammatory conditions. ATP levels were detected in differentiated BA after being stimulated with CM-CTR or CM-LPS using a bioluminescent kit (n=4 independent experiments). The bars represent mean ± SEM. Statistical analysis was performed with a Two-way ANOVA. *Comparisons between LPS-treated and CM-CTR in the same medium. #Comparisons between same treatment and different media. ****, ####p< 0.0001. **Note the different scales of the panels.**

We next studied the mitochondrial respiration capacity using the Seahorse technique and the oxidative capacity by measuring FAO in BA-WT and BA-SIRT1^{Tg+} differentiated with medium 2 and challenged with pro-inflammatory conditions.

The Seahorse profile revealed an increase in OCR in BA-WT after CM-LPS treatment (see blue lines in Figure 42A). However, we did not find differences in the impact of the

pro-inflammatory environment in OCR levels in BA-SIRT1^{Tg+} (see purple and pink lines in Figure 42A).

As shown in Figure 42B, FAO analysis revealed an increase in CO_2 and ASPs released from palmitate oxidation in BA overexpressing SIRT1 after CM-CTR or CM-LPS treatment. Moreover, pro-inflammatory CM-LPS did not induce changes in β-oxidation in either genotype differentiated in medium 2 (note the similar scale in the two graphs in Figure 42B).

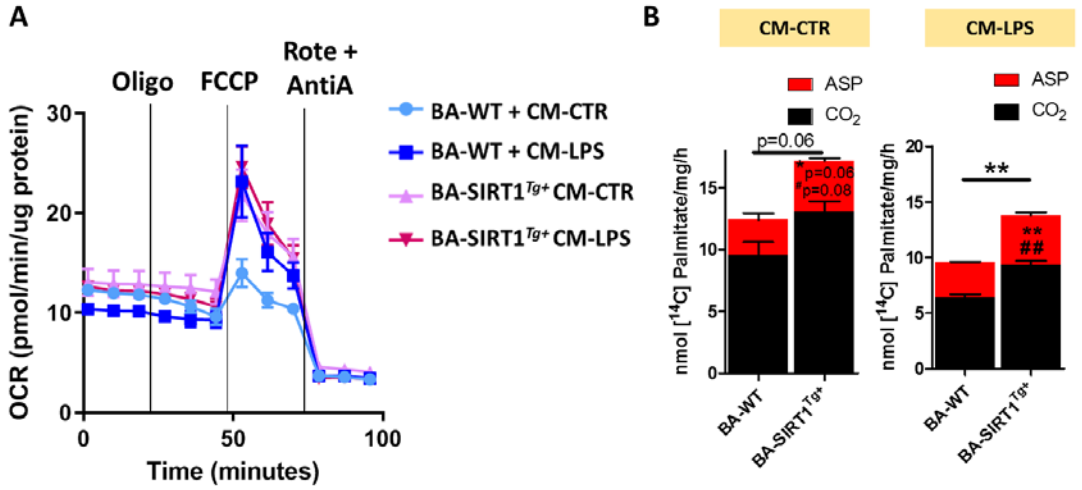

Figure 42. Seahorse profile and analysis of β-oxidation in WT and SIRT1^{Tg+} BA differentiated with medium 2 and treated with pro-inflammatory CM. (A) Representative Seahorse profile performed in differentiated BA differentiated with medium 2 and treated with CM-CTR or CM-LPS for 18 h (one experiment performed in quintupled). **(B)** Representative FAO assay performed in differentiated BA differentiated with medium 2 and treated with CM-CTR or CM-LPS for 18 h (n=3 experiments performed in triplicate). The bars represent mean ± SEM. Statistical analysis was performed with Mann-Whitney U test. *Comparison of ASP between genotypes. #Comparison of CO_2 levels between genotypes. **,##p<0.01.

We next wondered if medium 2 would play a protective role against the activation of the pro-inflammatory signaling cascades induced by CM-LPS. We ascertained the activation of the pro-inflammatory pathways mediated by JAK-STAT3, IKKα/β, JNK and p38 MAPK and found lower activation of STAT3 in BA-WT differentiated with medium 2 and less activation of these cascades in BA overexpressing SIRT1 (Figure 43).

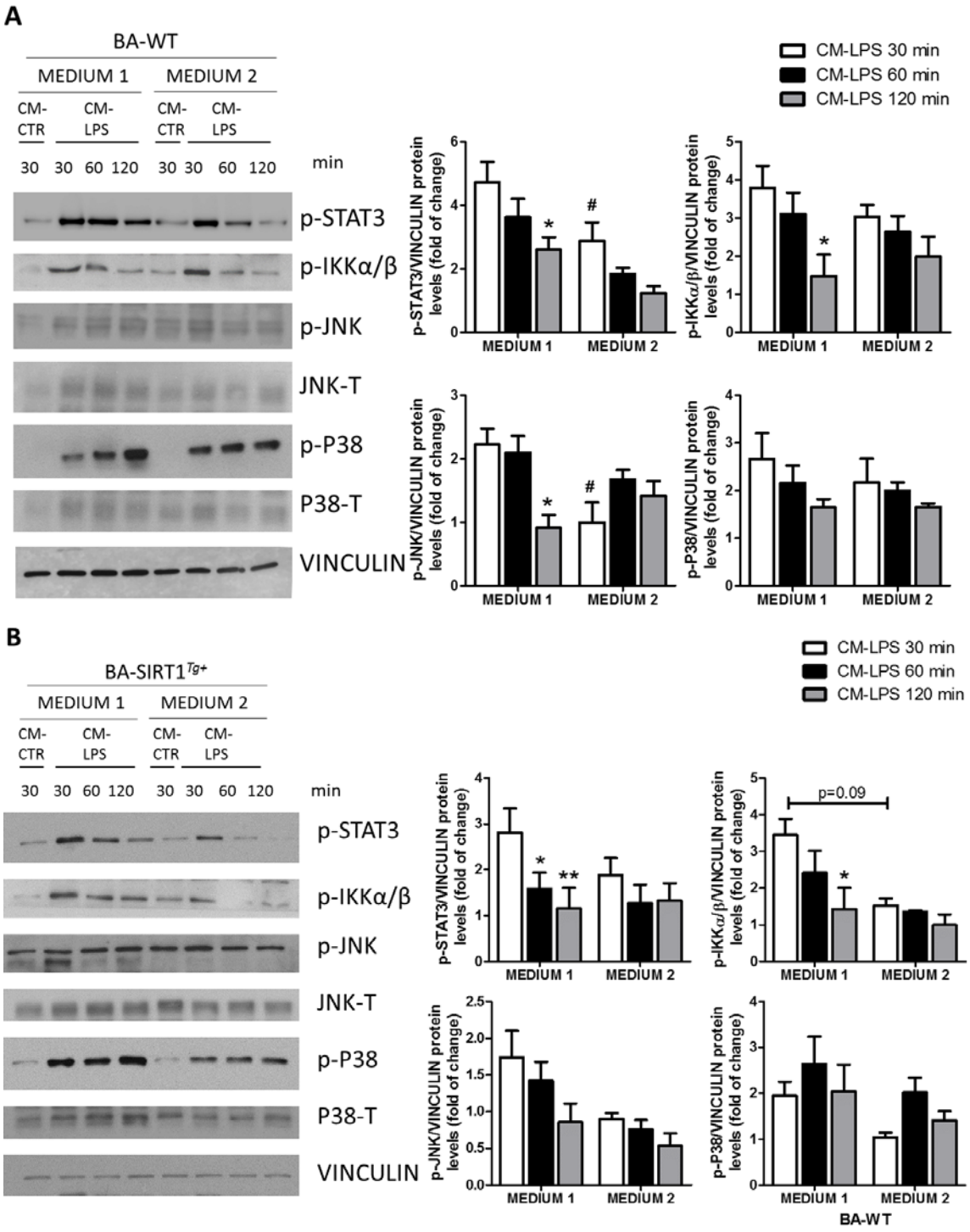

Figure 43. Analysis of the early activation of pro-inflammatory signaling cascades by CM-LPS in BA differentiated with medium 1 or medium 2. Representative Western blots of the activation of pro-inflammatory signaling cascades mediated by JAK-STAT3, IKKα/β, JNK and p38 MAPK in BA-WT **(A)** and BA-SIRT1^{Tg+} **(B)** differentiated with the two media and stimulated with CM-LPS at different time-periods (15, 30, 60,120 min). The graphs show the fold increase *vs.* CM-CTR. Vinculin was used as a loading control (n=3-6 independent experiments). Bars represent mean ± SEM. Statistical analysis was performed with a Two-way ANOVA. *Comparisons between CM-LPS 60 or 120 min and CM-LPS 30 min in the same genotype. $^{\#}$Comparisons between medium 1 or 2 in each genotype. $^{*,\#}p< 0.05$, $^{**}p< 0.01$.

2.3.2. EFFECT OF THE TREATMENT WITH CM-LPS IN THE INSULIN SIGNALING PATHWAY IN BOTH GENOTYPES OF BROWN ADIPOCYTES DIFFERENTIATED WITH MEDIUM 2.

To analyze the insulin signaling and insulin-mediated glucose uptake, we differentiated BA-WT and BA overexpressing SIRT1 with medium 2 and we observed the same effect as in medium 1 (depicted in Figures 32 and 33). SIRT1 overexpression protected against the drop of insulin-mediated AKT phosphorylation and glucose uptake induced by the pro-inflammatory CM (Figure 44A and 44B), this effect being absent in BA-WT. Moreover, CM-LPS induced an increase in insulin-independent glucose uptake in BA-WT that was not observed in BA overexpressing SIRT1 (Figure 44C).

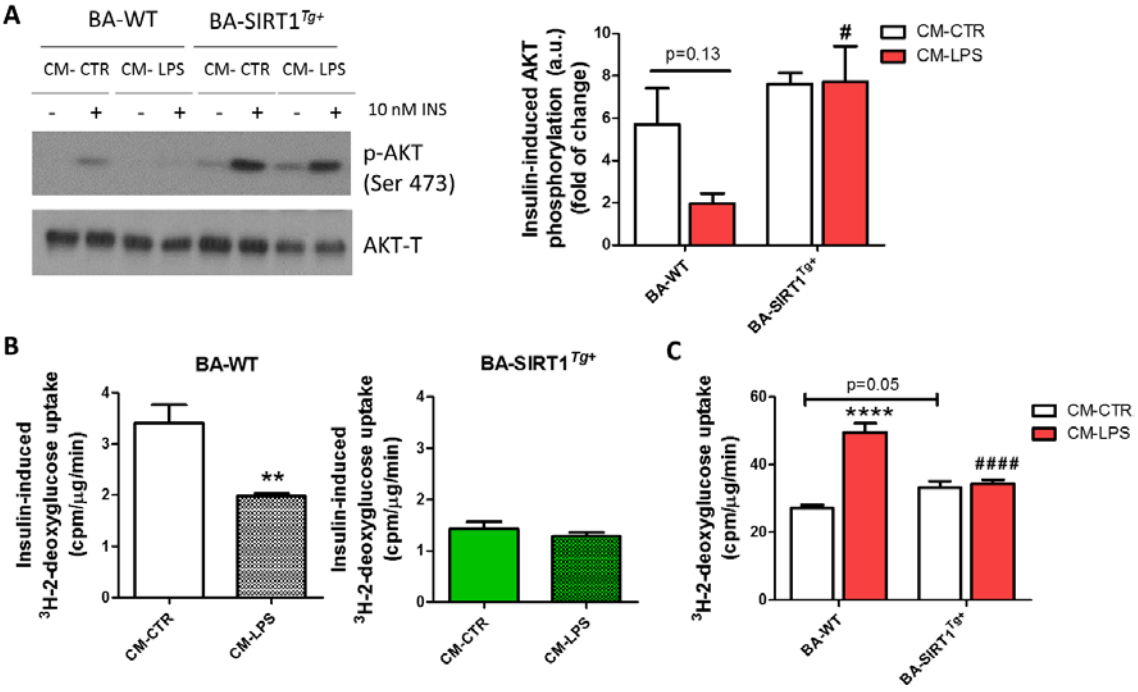

Figure 44. Insulin-induced AKT phosphorylation and glucose uptake under pro-inflammatory conditions in BA differentiated in medium 2. (A) WT and SIRT1^{Tg+} BA differentiated with medium 2 were treated with CM-CTR or CM-LPS for 17 h and then stimulated with 10 nM insulin for 15 min. AKT phosphorylation was analyzed by Western blot (n=3 experiments). The graph shows fold increase of AKT phosphorylation after insulin stimulation. AKT-T was used as a loading control. Bars represent mean ± SEM. Statistical analysis was performed with a Two-way ANOVA. $^{\#}$Comparisons between same treatment and different genotype. $^{\#}$p<0.05. **(B)** The graphs represent fold increase in insulin-induced glucose uptake in BA from both genotypes treated with CM-CTR or CM-LPS for 17 h and then stimulated with 10 nM insulin for 15 min (n=3 experiments). The bars represent mean ± SEM. Statistical analysis was performed with Mann-Whitney U test. **p<0.01. **(C)** Measurement of ^{3}H-2-deoxyglucose uptake in WT and SIRT1^{Tg+} BA differentiated with medium 2 treated with CM-CTR or CM-LPS for 17 h (n=3 experiments). Bars represent mean ± SEM. Statistical analysis was performed with a Two-way ANOVA. *Comparisons between CM-LPS and CM-CTR in the same genotype. $^{\#}$Comparisons between genotypes with the same treatment. ****, $^{\#\#\#\#}$p< 0.001.

2.3.3. EFFECT OF THE PRO-INFLAMMATORY CM IN THE NORADREGENERGIC RESPONSE IN BA-WT AND BA-SIRT1^{Tg+} DIFFERENTIATED WITH MEDIUM 2.

We finally assessed if differentiation of BA with medium 2 could prevent the drop in NE-induced UCP-1 activation under pro-inflammatory conditions found upon differentiation of the cells with medium 1. For this purpose, we treated BA-WT and BA-SIRT1^{Tg+} differentiated with either medium 1 or 2 with CM-CTR or CM-LPS in the absence or presence of NE for 17 h and we observed that BA differentiated in medium 2 were able to induce UCP-1, being this effect higher in BA overexpressing SIRT1 at both protein and mRNA level (Figure 45).

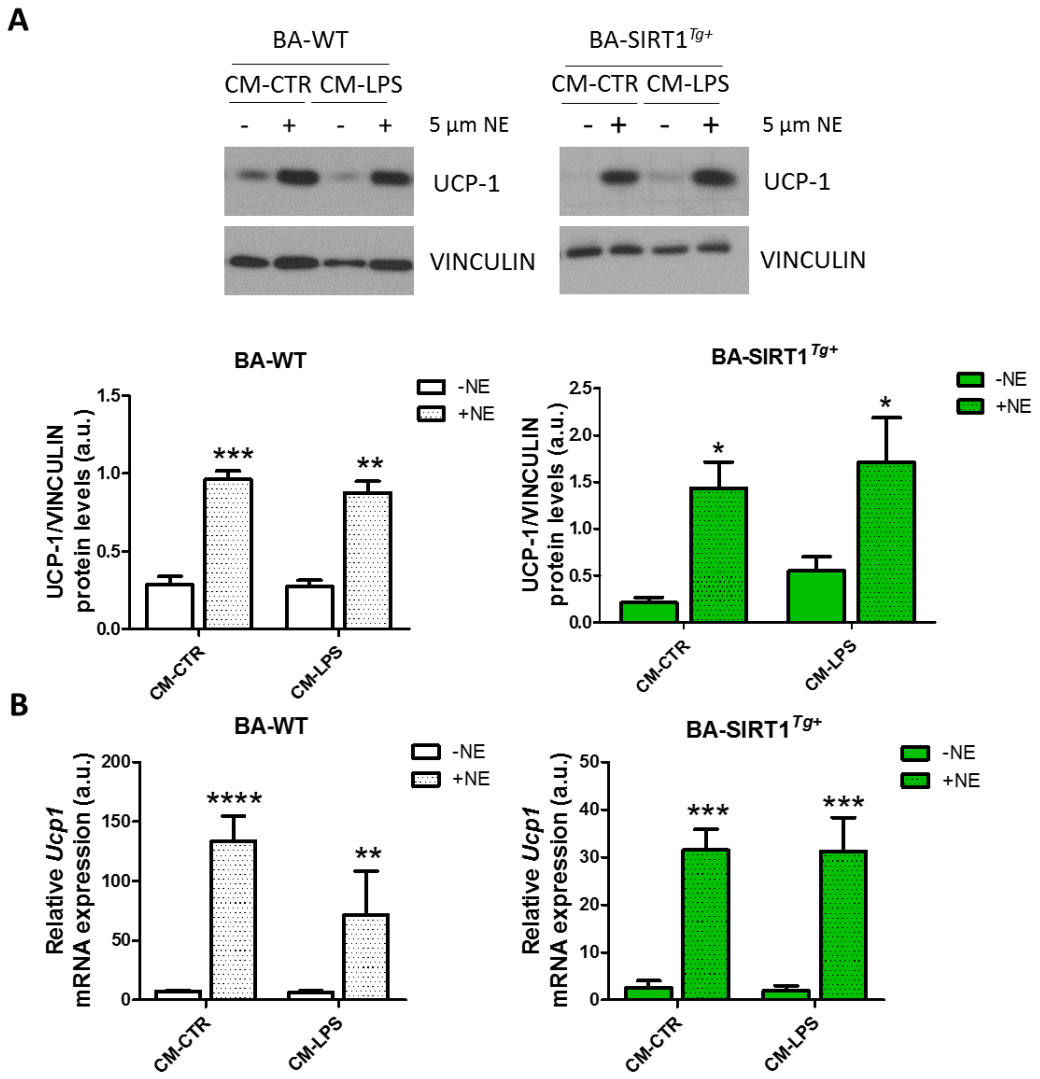

Figure 45. NE-induced UCP-1 expression was higher under pro-inflammatory conditions in BA differetiated in medium 2. (A) UCP-1 protein levels analyzed by Western blot after differentiation of BA from both genotypes with medium 1 or medium 2 and treatment with CM-CTR or CM-LPS in the absence or presence of 5 µM NE for 17 h (n= 5 independent experiments). **(B)** *Ucp1* mRNA levels in the same conditions described in **A** (n=3 independent experiments). The bars represent mean ± SEM. Statistical analysis was performed with a Two-way ANOVA. *Comparisons between NE-treated and its untreated control. #Comparisons between same treatment and different media. *p< 0.05 , **p< 0.01, ***p< 0.001, ****p< 0.0001.

2.4 ANALYSIS OF T_3 AND T_4 IN PLASMA AND BAT OF WT AND SIRT1^{Tg+} MICE.

Since the *in vitro* data have established a direct relationship between the differentiation of BA in the presence of high levels of T_3 and UCP-1 expression under normal and pro-inflammatory conditions, we analyzed T_3 and T_4 levels in WT and SIRT1^{Tg+} mice exposed to both pro-inflammatory and thermogenic conditions. As shown in Figure 46A, both WT and SIRT1^{Tg+} mice showed increased circulating T_3, but not T_4, levels upon cold exposure. However, after the pro-inflammatory challenge mice overexpressing SIRT1 exhibited a trend (non-significant) less decrease in T_3 plasma levels when compared to WT mice (Figure 46B). Of relevance, the analysis of T_3 and T_4 in BAT tissue (intra-BAT) revealed, on the one hand, more abundance of T_3 in SIRT1^{Tg+} mice challenged with cold (Figure 46C) and, on the other, a protection against the drop of T_3 in mice injected with LPS followed by cold exposure (Figure 46D). Interestingly, the combination of LPS injection and cold exposure did not affect intra-BAT content of T_4 in WT mice although SIRT1^{Tg+} mice reached higher levels.

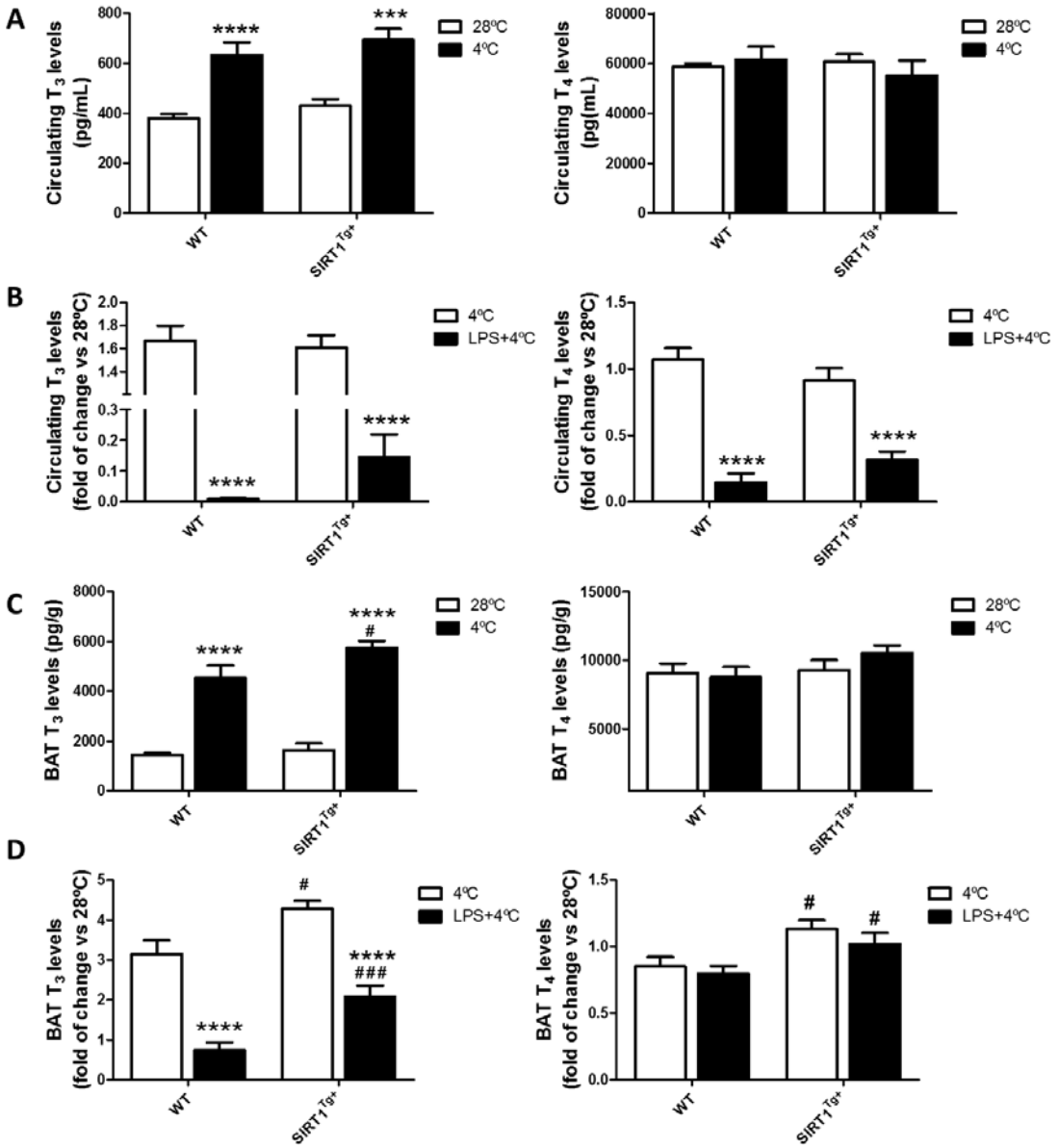

Figure 46. Circulating and BAT THs levels in WT and SIRT1^{Tg+} mice. Circulating T_3 and T_4 levels measured by RIAs in plasma of WT and SIRT1^{Tg+} mice after being exposed to termoneutrality for one week or after 6 h of cold-exposure (4ºC) **(A)** or after treatment with LPS for 18 h and then challenged to cold-

exposure for a further 6 h (LPS+4ºC) **(B). (C)** T_3 and T_4 levels in BAT from both genotypes in the same conditions detailed in **A** were determined by RIAs in purified BAT extracts. **(D)** T_3 and T_4 levels in BAT from both genotypes in the same conditions described in **B** were determined by RIAs in purified BAT extracts. The bars represent mean ± SEM (n=9-13 mice/group). All data are referred to the thermoneutrality (28ºC) WT group. Statistical analysis was performed with a Two-way ANOVA. **A** and **C** *Comparisons between 28ºC and 4ºC. #Comparisons between same condition and different genotype. **B** and **D** *Comparisons between LPS-treated or non-treated mice. #Comparisons between same condition and different genotype. #p< 0.05 , ***,###p< 0.001, ****p< 0.0001.

2.5 RESVERATROL TREATMENT INCREASED UCP-1 LEVELS IN BAT OF *db/db* MICE.

Finally, in an attempt to enhance UCP-1 protein in BAT from *db/db* mice by a pharmacologycal approach targeting SIRT1 we treated these animals with resveratrol, a well-known SIRT1 activator as mentioned in the introduction. Figure 47A and 47B shows increased UCP-1 expression at both protein and mRNA levels after 8 weeks of treatment. In line with this result, *Dio2* and *Fgf21* mRNAs were elevated in BAT from resveratrol-treated *db/db* mice. Moreover, FGF21 plasma levels also increased in mice receiving resveratrol.

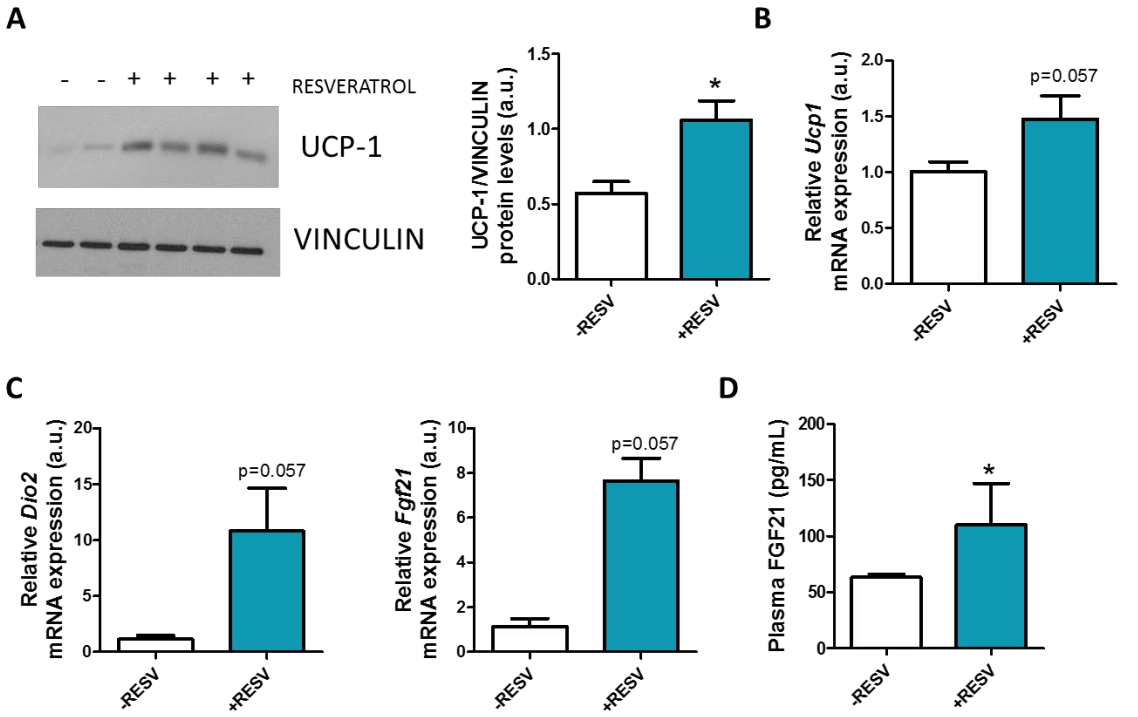

Figure 47. Analysis of thermogenic markers in BAT or plasma from *db/db* mice treated or not with resveratrol. (A) UCP-1 protein expression in BAT analyzed by Western blot. Vinculin was used as a loading control. The graph shows UCP-1 protein levels in *db/db* mice receiving 2.5 mg/kg per day of resveratrol in the drinking water for 8 weeks. Control animals remained untreated. *Ucp1* **(B)** *Dio* and *Fgf21* **(C)** mRNA levels in BAT. **(D)** FGF21 plasma levels analyzed by ELISA. Bars represent mean± SEM. (n=4-5 mice/group). Statistical analysis was performed with Mann-Whitney U test *p<0.05.

DISCUSSION

IMPACT OF INFLAMMATION IN INSULIN SIGNALING IN BAT: PROTECTIVE ROLE OF SIRT1 OVEREXPRESSION.

Since obesity represents a worldwide epidemic that has increased the incidence of metabolic diseases [185], the research focused in deciphering the underlying mechanisms responsible of the low-grade chronic inflammation associated to this pathological condition is highly needed.

The initial trigger of obesity-related inflammation is a sustained positive energy balance and an overall hyper-anabolic state, particularly in white adipocytes. This dysfunction, in turn, leads to the expansion of adipocytes in size and number in order to accommodate the storage of lipid overload. However, when the expandability of adipocytes is overwhelmed these cells become stressed and initiate a pro-inflammatory program [186]. As a result, adipocytes release FFA/adipokines and monocytes are recruited to the adipose tissue that, together with ATMs, are polarized to an M1 pro-inflammatory stage characterized by the secretion of pro-inflammatory cytokines, thereby boosting adipose tissue dysfunction [116, 187-189]. M1 macrophages proliferate in crown-like structures surrounding the adipocytes and contribute to the typical histological signature of adipose tissue in obesity [190]. These alterations are observed in the adipose tissue of experimental preclinical murine models of obesity and, more importantly, in obese people [191, 192]. Under these conditions, adipose tissue becomes an endocrine organ that, as mentioned above, secretes a plethora of pro-inflammatory molecules including FFA, lipotoxic species and the aforementioned adipo/cytokines and this is the main reason by which obesity and overweight are often accompanied by a low-grade chronic inflammatory state [193] linked to insulin resistance and other metabolic disturbances. More recently, obesity is thought to increase intestinal permeability and the leakage of gut-derived bacterial products including endotoxins (i.e. LPS) produced by intestinal Gram-negative bacterial species [194]. Gut-derived LPS initiates pro-inflammatory signaling cascades by activating pattern recognition receptors (PRRs), such as TLR4, particularly in the adipocytes located in the visceral fat [195] among other cells. In line with this notion, obese individuals have elevated levels of circulating LPS [196]. Notably, this recent research has completely changed the scenario of the field, opening new therapeutic windows to tackle obesity and co-morbidities.

The study of BAT has increasingly gained interest after its re-discovery in adult humans in 2007 [42-44]. Since then, BAT activation has acquired much more metabolic significance in normal human physiology and is currently considered as a therapeutic target against obesity due to its capacity to metabolize large amounts of glucose and fatty acids to be used as fuels for thermogenesis in order to dissipate energy as heat [45]. In fact, a negative relationship between body mass index (BMI) percentile and skin temperature overlying BAT depots has been reported [197]. However, pro-inflammatory signals have only recently been recognized as potential negative modulators of BAT functionality, an issue that deserves further investigation. For this reason, the study of the impact of inflammation in BAT and how to tackle have been the main topics of this Thesis.

We have conducted *in vivo* studies in two different mouse models of inflammation. On the one hand, we used *db/db* mice as a genetic model of chronic inflammation linked to obesity and T2DM and, on the other, we administered a low dose (non-lethal) of LPS to lean mice to mimic the impact of endotoxemia by itself [198].

A number of studies have characterized the systemic inflammatory state of *db/db* mice. For instance, we and others found elevations in inflammatory cytokines such as TNF-α and IL-1β in serum [198-200] together with the activation of a pro-inflammatory signature of signaling cascades (i.e NF-κB/p65, JNK, p38 MAPK, JAK/STAT) and gene expression

in different tissues of these mice [105, 199-207]. Our results herein have demonstrated for the first time that BAT from *db/db* mice is susceptible to inflammation since the aforementioned signaling pathways and pro-inflammatory-related gene expression (*Tlr4, Il6, Nos2*) were elevated in this fat depot compared with levels found in their lean counterparts (*db+).*

Several reports have suggested that inflammation-mediated changes in adipose tissue [208-211], as well as the hyperinsulinemia and hyperglycemia found in *db/db* mice contribute to the development of insulin resistance [212]. In this regard, a severe impairment of insulin sensitivity [207, 213] and decreased insulin-stimulated AKT-phosphorylation (Ser473) was found in skeletal muscle and adipose tissue adjacent to the urinary bladder [214]. Concomitant with systemic metabolic alterations, our results in the present study have provided evidence of insulin resistance in BAT from *db/db* mice.

It has been described that insulin resistance and related pathologies such as diabetes, obesity, atherosclerosis and cancer concur with an altered ratio in the expression of the isoforms of the IR. Briefly, in mammals alternative splicing of the IR gives rise to two isoforms containing or not exon 11 (IRB and IRA, respectively) with different affinities for insulin or IGFs [215, 216]. IRA is predominantly expressed during fetal development and enhances the effects of proinsulin and IGF-II [217]. By contrast, IRB is abundant in the adult state in tissues such as liver, skeletal muscle, adipose tissue, and kidney and exerts mainly the metabolic actions of insulin [182, 218]. Of relevance, an increase in IRA/IRB ratio has been reported in muscle or liver in insulin resistant states [219, 220]. However, the pattern of IR isoforms has not been previously analyzed in adipose tissues in the context of obesity-linked insulin resistance. In this regard, we found altered IRA/IRB ratio in BAT from *db/db* mice characterized by a robust presence of IRA that could explain, at least in part, the impairment in the insulin signaling pathway, an effect probably due to a metabolic immaturity of the tissue. Whether or not this altered IRA/IRB ratio in BAT from *db/db* mice is a direct consequence of systemic and/or local inflammation deserves future research.

Seeking for an inflammatory factor causative of the onset of insulin resistance we explored a non-obese model of inflammation using LPS, a triggering factor of inflammation during dysbiosis. Based on previous studies [221] we used a non-septic dose of LPS in WT mice and found a pro-inflammatory signaling signature in BAT similar to that found in *db/db* mice related to activation of JAK-STAT3, JNK, p38 MAPK and NFκB. Of note, these pathways have been extensively reported to be negative modulators of insulin signaling mainly at the level of serine phosphorylation of IRS proteins [222-224] and are likely responsible of the decrease in AKT phosphorylation found in BAT from LPS-treated mice that received an insulin injection. Moreover, we observed a decrease in insulin-mediated IR phosphorylation in LPS-injected mice that can be a consequence of the activation of the IKKβ/NFκB pathway, which increases the expression of PTP1B, a critical node of the insulin response due to its ability to dephosphorylate and inactivate the IR, thereby inhibiting the insulin signaling pathway [225].

As mentioned in the introduction, SIRT1 has been involved in the protection from the metabolic damage associated to obesity. Mice lacking SIRT1 in adipose tissue developed inflammation in this fat depot [226]. Conversely, transgenic mice with moderate overexpression of SIRT1 (SIRT1^{Tg+}) fed a HFD exhibited similar body weight, fat mass and weight gain than mice fed a chow diet and also presented improved glucose tolerance [139, 153], although specific effects of SIRT1 in BAT insulin sensitivity were not reported in these studies. Moreover, SIRT1 alleviates LPS-induced metabolic dysfunction in the lung [227], keratinocytes [228], endothelial cells [229] and periodontal ligament fibroblasts [230]. Taking into account these previous studies, we decided to

explore the potential benefit of SIRT1 overexpression in BAT inflammation by challenging both WT and SIRT1^{Tg+} mice with LPS and study the activation of inflammatory pathways as well as insulin signaling. Our data provided evidences of a protection against the drop of IR and AKT phosphorylation in BAT from LPS-injected SIRT1^{Tg+}mice in line with the improvement of fatty liver by SIRT1 activation recently reported [231].

We also performed *in vitro* studies by using differentiated BA overexpressing SIRT1 that presented increased IR and AKT phosphorylation in response to insulin in parallel with reduced expression of PTP1B protein levels. Our results agree with the work of Sun et al. that reported improved insulin sensitivity in hepatocytes and myotubes by enhancing SIRT1 expression/activity under normal or insulin-resistant conditions through the repression of PTP1B [156]. Of note, no changes in IRA/IRB ratio were found in differentiated BA from both genotypes (results not shown) excluding this effect as a causative of insulin resistance in these adipose cells.

To verify the protective effect of SIRT1 overexpression in BA in the context of inflammation, we performed cell-based experiments mimicking the cross-talk (interactome) between macrophages and BA. For this purpose, we used Raw 267.4 murine macrophages to obtain a pro-inflammatory conditioned medium (CM-LPS), since these cells secrete a plethora of pro-inflammatory cytokines after LPS stimulation [232]. In a second step, BA from both genotypes were treated with the pro-inflammatory CM-LPS and the activation of the pro-inflammatory signaling cascades mentioned above was verified. Importantly, we found a decrease only in STAT3 phosphorylation in BA overexpressing SIRT1, suggesting a specific modulation of JAK-STAT pathway by SIRT1 in these adipocytes [233].

Regarding the study of the insulin signaling pathway, we observed that BA-SIRT1^{Tg+} were protected from the drop in insulin-mediated AKT-phosphorylation under pro-inflammatory conditions compared to the response of BA-WT and this effect might be a consequence of the synergy of lower PTP1B expression and less STAT3 phosphorylation. Phosphorylated STAT3 dimerizes with other STAT family members, and the activated STAT3 complex translocates into the nucleus where activates the transcription of suppressor of cytokine signaling (SOCS) 3. This, in turn, inhibits insulin signaling by different mechanisms such as disruption of the interaction of IR and IRSs and subsequent degradation of IRSs by the proteasome [224, 234]. Regarding studies in 3T3-L1 adipocytes, it has been shown that SOCS3 regulates insulin signaling [235] since its inhibition along with the JAK2/STAT3 pathway counteracts inflammation [236] and enhances insulin sensitivity [237].

It is noteworthy to mention that the inflammatory CM-LPS upregulated basal (insulin-independent) glucose uptake in BA-WT ameliorating the effect of insulin as occurred in myotubes and white adipocytes treated with TNFα, IL-1β or IL-6 [98, 238, 239], an effect likely mediated by up-regulation of GLUT1 [240]. Moreover, the pro-inflammatory CM-LPS led to a decrease in insulin-induced glucose uptake as found in other insulin sensitive cells such as myotubes [239, 241], adipose stromal cells [242] or white adipocytes [243]. Since insulin induces glucose uptake in BA in a PI 3-kinase/AKT-dependent manner [244], the reduced response in the presence of CM-LPS is probably due to the decrease in AKT phosphorylation. By contrast, the CM-LPS did not increase insulin-independent glucose uptake in BA-SIRT1^{Tg+}. Furthermore, we did not observe the drop of insulin-induced glucose uptake in BA overexpressing SIRT1 maintained under pro-inflammatory conditions and this effect concurred with preserved threshold levels of AKT phosphorylation. Our results agree with the work of Yoshizaki and co-workers in which treatment with SIRT1 activators led to an increase in glucose uptake and insulin signaling in white adipocytes and also rescued from TNF-α-induced

insulin resistance [245]. Likewise, Chen et al. described that SIRT1 activation by resveratrol increases glucose uptake in insulin-resistant 3T3-L1 adipocytes through the AMP-activated protein kinase (AMPK) α/AKT signaling pathway [246].

Recent years widened our understanding of the role of BAT that, in addition to its thermogenic function, also contributes to regulate whole body energy homeostasis and glucose metabolism. Altogether, the results of this part of the Thesis making use of *in vivo* and *in vitro* models of SIRT1 overexpression have unraveled a new potential target for increasing insulin sensitivity and ameliorate the defects in the insulin signaling pathway induced by inflammation in BAT.

IMPACT OF INFLAMMATION IN THE THERMOGENIC RESPONSE OF BAT: PROTECTIVE ROLE OF SIRT1 OVEREXPRESSION/ACTIVATION AND T_3.

Despite of the significant contribution of BAT to whole-body glucose homeostasis its main physiological function is the maintenance of core temperature after birth to avoid hypothermia by activation of "non-shivering" thermogenesis [34, 247]. Under a pathological situation such as obesity, β-adrenergic signaling is reduced, resulting in impaired thermogenesis in BAT [98, 248, 249]. On the other hand, evidences of the involvement of SIRT1 in energy expenditure have been reported [139, 150, 153]. On that basis, we investigated the impact of SIRT1 overexpression/activation in BAT thermogenesis under the pro-inflammatory context associated to obesity, a less explored issue in the field.

SIRT1 partly mimics calorie restriction, favoring a state of increased energy efficiency [153]. Regarding pharmacological approaches targeting SIRT1 in metabolic diseases, several animal studies have demonstrated the beneficial effects of resveratrol, a well-known SIRT1 activator, in managing diabetes and associated complications in preclinical models [250, 251]. In the context of inflammation, a study in rats fed an obesogenic diet and treated with resveratrol reported an increase in UCP-1 protein levels in BAT [167]. Another work showed a partial protection by resveratrol against the drop of UCP-1 mediated by IL-1β [127]. Our results in obese and type 2 diabetic *db/db* mice have confirmed those of Masaki and co-workers that found diminished *Ucp1* levels in BAT compared to those of lean *db*+ littermates [252]. More importantly, we demonstrated that resveratrol-treated *db/db* mice presented higher UCP-1 levels pointing to a potential therapeutic efficacy of SIRT1 activation in this tissue. This effect might be related to elevations of FGF21 detected in both plasma and BAT and the increased expression of *Dio2* isoform in this tissue. FGF21, a critical factor regulating multiple metabolic pathways that plays a role in BAT-induced thermogenesis, has been also described to up-regulate *Dio2* and *Ucp1* gene expression in this fat depot [253].

Moderate SIRT1 overexpression has been linked to higher energy expenditure and enhanced transcriptional responses to β-adrenergic stimulation in BAT [139, 147, 150, 254, 255]. In agreement with these studies we found higher temperature in the skin surrounding BAT and higher basal respiration in BAT explants from SIRT1^{Tg+} mice in parallel with higher UCP-1 protein and mRNA levels. Interestingly, histological evaluation revealed lipid-depleted BAT sections in mice overexpressing SIRT1, a feature of tissue activation. BAT morphology in SIRT1^{Tg+} mice likely results from increased basal lipolytic rate as previously described [150]. However, upon exposure of mice to thermoneutrality followed by a cold challenge we did not detect differences in the induction of thermogenic-related genes among mice with or without SIRT1 overexpression. These data differ from those reported by Gerhart-Hines and colleagues that found increased basal and cold-induced *Ucp1* mRNA levels in BAT from SirBACO mice [254]. A potential

explanation for such differences can be different mice strains and experimental procedures such as absence of thermoneutrality in their study [254] that might predispose the mice to rapid response to the cold challenge.

Taking into account these results we next explored the impact of SIRT1 overexpression in mice with LPS-induced inflammation since, as mentioned above, other authors have used this bacterial endotoxin as a disruptor of the functionality of adipose tissues [125, 256]. For instance, Nohr and co-workers described how an infusion of LPS (600 µg/kg/day for 28 days) decreased *Ucp1* in BAT without affecting *Prdm16* and *Dio2* expression [127]. In the same line, Okla and co-workers described that chronic administration of LPS (7.5 µg/mouse for 2 weeks) followed by acute cold exposure lowered *Ucp1, Pgc1a,* and *Prdm16* expression in subcutaneous WAT. It also decreased UCP-1 protein content in BAT together with core body temperature and heat release [257]. Likewise, IL-1β decreased *Ucp1* expression after cold exposure in both WAT and BAT in mice, revealing the deleterious effect of inflammation in thermogenesis [258]. In this regard, it was shown that TLR4-mediated signaling represses the transcriptional activation of brown and beige-specific genes [125, 126]. Thus, stimulation of TLR4 by LPS is likely responsible for the decrease in *Ucp1* expression found in WT mice injected LPS. In addition, the protection of SIRT1^{Tg+} mice against the effects of LPS in BAT agrees with the beneficial effect of overexpressing SIRT1 in the context of low grade chronic inflammation associated to obesity [139].

Of relevance, our analysis of BAT from mice upon LPS-induced inflammation and cold exposure showed that SIRT1 overexpression conferred protection against the drop in rectal temperature and temperature of the skin surrounding BAT. Remarkably, UCP-1 protein levels decreased in LPS-injected WT mice exposed to the cold compared to their counterparts that did not receive the endotoxin and this effect was ameliorated in SIRT1^{Tg+} mice that maintained UCP-1 protein levels under these conditions. In addition, BAT histology showed a further decrease of the lipid content in SIRT1^{Tg+} sections suggesting utilization of lipids stored in BAT lipid droplets as a fuel to maintain body temperature. It is noteworthy to mention the work of Qiang and colleagues demonstrating that SIRT1 enhances browning of subcutaneous WAT upon cold exposure [146]. In this regard, our results revealed lower iWAT/body weight ratio in mice overexpressing SIRT1 upon LPS injection and cold exposure pointing to an additional contribution of the browning process in SIRT1^{Tg+} mice to maintain the thermogenic response under pro-inflammatory conditions. Recent data from our laboratory have evidenced higher UCP-1 protein levels in subcutaneous white adipocytes from SIRT1^{Tg+} mice (results not shown).

Taking altogether these results in mice have provided previously unknown evidences of a mechanism conferring protection against the drop of the thermogenic response induced by systemic inflammation, proposing SIRT1 activation as a potential therapeutic strategy against the low grade chronic inflammatory state linked to obesity.

To get more insights of the cell autonomous effects of SIRT1 overexpression in brown adipose cells we studied the response of differentiated BA-WT and BA-SIRT1^{Tg+} to NE. Previous results in collaboration with Carles Cantó's lab revealed that terminally differentiated BA overexpressing SIRT1 showed lower UCP-1 expression under basal conditions [150] in line with the role of SIRT1 as a metabolic sensor triggering adaptations in order to optimize energy production [133]. By contrast, upon β-adrenergic stimulation, SIRT1 overexpressing BA showed higher *Ucp1* mRNA and protein levels (Figure 29 and [150]) pointing to a better responsiveness upon a thermogenic stimulus. A step further, we studied the response of BA exposed to CM-LPS and NE as pro-inflammatory and β-adrenergic stimulus, respectively. As expected, we observed a decrease in NE-induced *Ucp1* mRNA and protein expression in BA-WT. However, an unexpected response was found in BA overexpressing SIRT1 in which the pro-inflammatory milieu totally impaired their response to NE in inducing UCP-1.

In agreement with our data, CM from LPS-stimulated RAW 264.7 macrophages led to the suppression of isoproterenol-induced *Ucp1* activation in 10T1/2 adipocytes derived from a mouse mesenchymal stem cells, an effect mimicked by IL-1β [258]. The authors of this study attributed these responses to PPARγ inactivation in an IL-1β-mediated ERK-dependent manner that likely contributes to the suppression of UCP-1 levels. Likewise, Nohr and co-workers found that IL-1β, but not direct LPS stimulation, reduced *Ucp1, Prdm16* and *Pgc1a* mRNA levels in BA [127]. However, they observed reduced expression of brown-related genes in mice chronically treated with a low-dose LPS. These authors hypothesized that, although BA might be capable of sensing LPS, the reduced *Ucp1* expression *in vivo* is likely mediated by the effect of LPS targeting BAT resident macrophages and switching their polarization towards an M1 phenotype characterized by down-regulation of tyrosine hydroxylase, the rate-limiting enzyme of catecholamines synthesis, and promoting the release of pro-inflammatory cytokines including IL-1β [21]. Of interest, it is important to highlight that other authors did not find a relationship between macrophages inflammation and tyrosine hydroxylase levels [259].

The expression or activity of SIRT1 have been found attenuated in response to LPS in mouse pulmonary microvascular vein endothelial cells (PMVECs) [229], rat Kupffer cells [260] and RAW 264.7 macrophages [260-262]. Thus, the lack of protection of SIRT1 overexpression against the drop of UCP-1 upon pro-inflammatory stimuli might be due to a decrease in SIRT1 activity in BA. Current experiments are being performed to corroborate this possibility.

In an attempt to find an alternative protocol to differentiate brown preadipocytes to mature adipocytes resistant to the deleterious effects of CM-LPS we adapted a method previously used for induction of "browning" of inguinal white adipocytes [184]. The main differences in this new differentiating procedure (referred to as medium 2) in comparison with medium 1 are the higher concentrations of insulin, rosiglitazone and T_3, all of them major triggers of BAT adipogenic and thermogenic programs [34, 263, 264].

It has been reported that T_3 increases intracellular NAD^+/NADH and activates SIRT1 in both hepatocytes and BA [70, 265] and also it increases SIRT1 expression and activity in livers of rats treated with rosiglitazone [266]. Herein we have demonstrated higher SIRT1 activation, monitored by reduced p65-NFκB acetylation levels, in BA from both genotypes differentiated with medium 2. However, we cannot distinguish whether BA-SIRT1^{Tg+} differentiated in medium 2 display higher SIRT1 enzymatic activity compared with either BA-WT differentiated in the same medium or BA-SIRT1^{Tg+} differentiated in medium 1. Since the commercially tools available to measure SIRT1 enzymatic activity have limited range of sensitivity, we addressed this issue indirectly by measuring ATP levels based on the study of Kang and co-workers describing ATP-mediated suppression of SIRT1 activity [137]. Our results confirmed this modulation in BA from both genotypes differentiated with medium 2 that presented a substantial decrease in ATP levels; this effect being more pronounced in those overexpressing SIRT1.

Mitochondria play a key role in maintaining energy homeostasis in metabolic tissues, including adipose tissues and, since SIRT1 has been considered a master regulator of mitochondrial biogenesis in a PGC-1α-dependent manner [267-269], we studied more-in depth the mitochondria after differentiating BA with medium 2. In this regard, it is known that an optimal mitochondrial function is ensured by a quality-control system coupled to mitochondrial fusion and fission. In fact, the imbalance of mitochondrial dynamics, as well as mitochondrial dysfunction, results in deleterious effects on differentiation, lipid metabolism, insulin sensitivity, oxidative capacity and thermogenesis in adipose cells [270]. The analysis of key markers of mitochondrial fusion (MFN2) and fission (p-DRP1) revealed higher fusion in BA from both genotypes differentiated with medium 1 in parallel with higher ATP levels as reported by Lee and co-workers [270]. Our results also showed that fission, a process associated with diminished OXPHOS and mitochondrial DNA (mtDNA) depletion in the same study, was enhanced in BA

differentiated with medium 2 concomitantly with less COXIV, TOM22 and MTG staining. The differences in BA differentiated with medium 1 or 2 regarding mitochondrial dynamics might have an impact in their responses as will be discussed below, although the pattern of mitochondrial dynamics in BA was found to be dependent on the differentiation medium rather than the genotype. In fact, the role of SIRT1 in mitochondrial dynamics is ambiguous and contradictory depending on the cell type or experimental conditions as reviewed by Lin and co-workers [271].

It has been demonstrated that knockdown of *Mfn2* gene in adipose tissue results in an obese phenotype characterized by thermogenic dysfunction and impaired lipolytic and mitochondrial function [91, 272]. However, Wikstrom and colleagues knocked down *Mfn2* gene in primary BA and did not find alterations in the ability of NE to stimulate energy expenditure, suggesting that forced mitochondrial fragmentation does not alter mitochondrial function nor lipolysis or FFA-mediated activation of UCP-1 [273]. Likewise, an increase of DRP1 phosphorylation was found in activated BAT, whereas the blockade of mitochondrial fission reduced uncoupled respiration in BA [93, 273]. These results are in agreement with the higher UCP-1 levels found in both basal and NE-stimulated BA differentiated with medium 2 in which MFN2 protein levels are markedly reduced and p-DRP1 is increased. These data reinforce that mitochondrial fission may be considered as a physiological adaptation instead of a deleterious mechanism, suggesting that induction of mitochondrial fragmentation could be used as a mechanism to enhance thermogenesis in unfavorable conditions such as inflammation. It is noteworthy to mention that an increase in DRP1 phosphorylation has been reported in beige adipocytes treated with rosiglitazone [93]. Of note, BA differentiated with medium 2 are exposed to a higher concentration (10X) of rosiglitazone compared to medium 1 and this can also contribute to the fission/fusion rate in addition to the well-known effect of this TZD in inducing *Ucp1* gene expression in a p38 MAPK-dependent manner [274]. Interestingly, differentiation of white adipocytes in the presence of rosiglitazone resulted in more lipid accumulation and UCP-1 expression even in the absence of NE stimulation [275] and in our study BA differentiated in a “browning-like” medium 2 showed similar effects.

Of interest is the increase in *Prdm16* mRNA levels in BA differentiated with medium 2. Ohno et al. suggested that the “browning” effect of PPAR ligands, including rosiglitazone, is due to stabilization of PRDM16 protein [60], leading to the induction of *Pgc1α*, *Ucp1* and *Dio2* expression, and also by increasing uncoupled respiration in white adipocytes and BA [276]. Taking these studies into account, rosiglitazone *per se* and its effects mediated by the stabilization of PRDM16 might contribute to the UCP-1 expression levels observed in BA differentiated with medium 2.

Medium 2 also contains high levels of insulin, the main regulator of energy homeostasis in its metabolic target tissues, primarily liver, muscle and adipose tissue. Insulin action in adipocytes induces two major metabolic effects: stimulation of glucose transport for glycerol synthesis and inhibition of lipolysis [277-279]. Regarding glucose uptake, basal levels were higher in BA-SIRT1^{Tg+} regardless of the differentiating medium used. As it is known, insulin favors fatty acid storage as triacylglycerol species in lipid droplets, an effect exacerbated in BA differentiated with medium 2 regardless of the genotype.

The third main component of medium 2 is T_3, classically considered a stabilizer of *Ucp1* mRNA levels [69], an effect manifested by increases in *Ucp1* mRNA and UCP-1 protein levels upon differentiation of BA from the two genotypes with this medium. This effect was not associated to changes in *Pgc1a* and was markedly enhanced in BA-SIRT1^{Tg+} that presented very low UCP-1 protein levels in medium 1 as discussed above.

Once characterized the differentiation of BA with T_3, insulin and rosiglitazone-enriched medium, we analyzed their responses to insulin and NE in a pro-inflammatory context. Regarding insulin signaling and glucose uptake, we did not observe any difference when

compared with medium 1. However, BA from both genotypes differentiated with medium 2 preserved their response to NE in the induction of UCP-1 under pro-inflammatory conditions, being this protection even higher in BA overexpressing SIRT1. In order to find an explanation for such effect, previous studies have suggested that the effects of thyroid hormones in BAT are primarily mediated via hypothalamic stimulation of sympathetic innervation, revealing a central role for T_3 in the hypothalamus-BAT axis by inducing lipolysis and mitochondrial uncoupling [280]. In agreement with this study, we observed higher lipolysis in BA differentiated with medium 2 and in BA overexpressing SIRT1 when compared to BA-WT. In line with this notion, BAT from SIRT1 overexpressing mice showed higher lipid-depleted BAT sections. During cold exposure, sympathetic stimulation of BAT increases *Dio2* expression and raises intracellular T_3 content which, in turn, stimulates thermogenesis by increasing *Ucp1* transcription/mRNA stabilization and lipid metabolism in BA [69]. The additive effect of thyroid hormones and cold-exposure in BAT activity could be also attributed to the up-regulation of β-adrenergic receptors [281]. In this regard, we detected higher circulating T_3 levels in WT and SIRT1^{Tg+} mice after cold exposure. Although LPS impairs thyroid function decreasing serum T_3, T_4 and TSH [282-285], SIRT1 has been described on one hand to activate TH receptor β1 in the liver [286] and, on the other, to mediate a positive regulation of TSH secretion [287]. Although we found a drop of T_3 and T_4 levels after exposing mice from both genotypes to LPS and cold, this effect was attenuated in SIRT1^{Tg+} mice that showed higher T_3 and T_4 levels in circulation and intra-BAT and this might be responsible, at least in part, of the beneficial effects observed in SIRT1^{Tg+} mice in the thermogenic-related parameters studied and previously discussed. Altogether, the *in vivo* data point to the relevance of T_3 in SIRT1^{Tg+} mice since those mice showed similar circulating insulinemia than their WT counterparts [150, 153].

Taking into account all these results, we can postulate that moderate overexpression of SIRT1 or its activation by resveratrol can be of benefit in diseases linked to chronic inflammation including obesity. At the cellular level, our data have provided evidences of the contribution of both SIRT1 overexpression and T_3 in switching the cell fate of brown preadipocytes towards differentiation to more responsive BA even under a deleterious pro-inflammatory macrophage-mediated interactome.

Finally, we would like to highlight that the results of this Thesis might have a translational impact. Actually, hypothyroid patients showed decreased adaptive thermogenesis during cold exposure that was corrected by thyroid hormone replacement [288]. Therefore, combinatorial therapies of thyromimetics that specifically target BAT with SIRT1 activators may be useful to activate thermogenesis in this fat depot and could be considered as a therapeutic tool for the treatment of obesity and other metabolic diseases with potential fewer side effects than THs [70, 288, 289].

Figure 48 shows a graphical abstract of the processes described in this Thesis regarding the importance of SIRT1 in BAT inflammation.

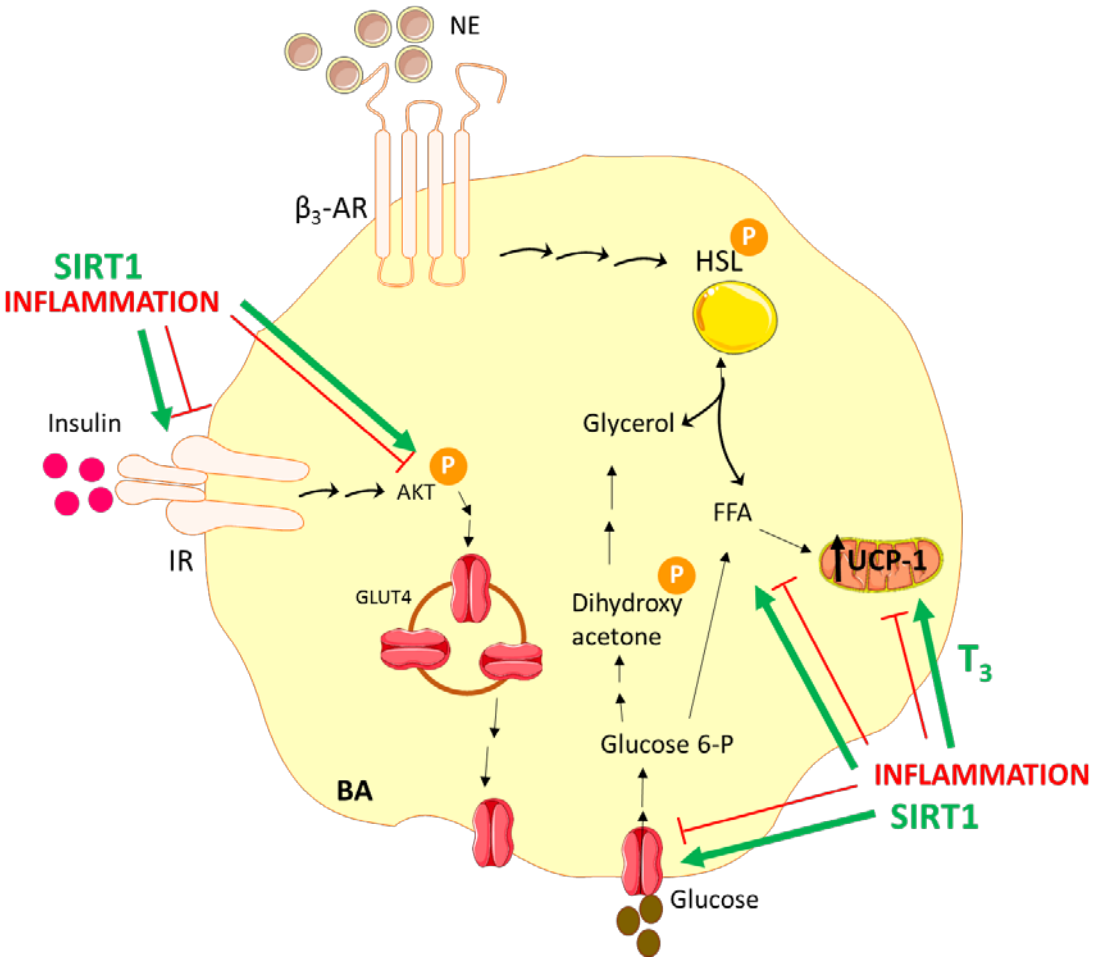

Figure 48. Proposed model of insulin and NE signaling pathways and effects in brown adipocytes after the challenge of inflammation and the protective role of SIRT1 and T_3 in these processes. Inflammation impairs both insulin and noradrenergic responses of BA. SIRT1 activation/overexpression induces signaling and gene-expression changes aimed to counteract inflammation and maintain BAT functionality.

CONCLUSIONS

The conclusions of the present Doctoral Thesis are as follows:

1. BAT from obese and type 2 diabetic *db/db* mice is susceptible to inflammation due to the activation of pro-inflammatory signaling cascades and elevation of pro-inflammatory-related gene expression.

2. BAT from *db/db* mice showed impaired insulin signaling and altered ratio of the insulin receptor isoforms (IRA/IRB) characterized by higher presence of IRA.

3. Treatment of *db/db* mice with resveratrol increased UCP-1 levels in BAT.

4. Mice overexpressing SIRT1 treated with lipopolysaccharide (LPS) before insulin injection showed a protection against the drop in IR and AKT phosphorylation detected in wild-type mice.

5. Mice overexpressing SIRT1, but not wild-type mice, were protected against alterations in thermogenic-related responses when challenged with LPS as pro-inflammatory stimulus and cold as a thermogenic inducer. Moreover, these mice showed elevated T_3 in circulation and BAT.

6. Differentiated brown adipocytes overexpressing SIRT1 were protected against the drop of insulin signaling and glucose uptake under pro-inflammatory conditions in parallel with preserved threshold levels of AKT phosphorylation. However, SIRT1 overexpression did not protect against the drop in UCP-1.

7. Differentiation of brown preadipocytes in the presence of high concentrations of T_3, insulin and rosiglitazone generates mature brown adipocytes protected from inflammation; this effect being more evident in those overexpressing SIRT1.

Final conclusion: Altogether, the results of this preclinical study using animal and cellular models of SIRT1 overexpression have unraveled a new potential target for preventing the attenuation of insulin signaling and thermogenic-related expression in BAT in the context of chronic inflammation linked to obesity.

CONCLUSIONES

Las conclusiones de la presente Tesis Doctoral son las siguientes:

1. El BAT de los ratones *db/db* que desarrollan obesidad y diabetes mellitus tipo 2 es susceptible a la inflamación debido a la activación de cascadas de señalización pro-inflamatorias y a la elevación de la expresión genes pro-inflamatorios.

2. El BAT de los ratones *db/db* mostró alteraciones en la vía de señalización de la insulina, así como una alteración del ratio de las isoformas del receptor de insulina (IRA/IRB) mostrando por una mayor abundancia de IRA.

3. El tratamiento de los ratones *db/db* con resveratrol aumentó los niveles de UCP-1 en el BAT.

4. Los ratones que sobreexpesan SIRT1 y que fueron tratados con lipopolisacárido (LPS) previamente a la inyección de insulina mostraron una protección frente a la caída de la fosforilación del IR y AKT en el BAT detectada en los ratones de genotipo salvaje.

5. Los ratones con sobreexpresión de SIRT1, pero no los ratones de genotipo salvaje, estaban protegidos de las alteraciones en marcadores termogénicos cuando se les trataba con LPS como estímulo pro-inflamatorio y con el frío como inductor termogénico. Además, estos ratones mostraban niveles mayores de T_3 en circulación y en el BAT.

6. Los adipocitos marrones diferenciados que sobreexpresan SIRT1 y sometidos a condiciones pro-inflamatorias están protegidos contra las alteraciones en la ruta de señalización de la insulina tanto en la captación de glucosa como manteniendo fosforilación de AKT. Sin embargo, la sobreexpresión de SIRT1 no protegió de la disminución de UCP-1.

7. La diferenciación de preadipocitos marrones en presencia de altas concentraciones de T_3, insulina y rosiglitazona genera adipocitos marrones maduros protegidos frente la inflamación, siendo este efecto más evidente en aquellos que sobreexpresan SIRT1.

Conclusión final: En conjunto, los resultados de este estudio preclínico utilizando modelos experimentales animales y celulares propone a SIRT1 como una diana terapéutica para proteger frente a las alteraciones en el BAT tanto en la vía de señalización de la insulina como en la termogénesis en el contexto de la inflamación asociada a la obesidad.

BIBLIOGRAPHY

1. Kopelman, P.G., *Obesity as a medical problem.* Nature, 2000. **404**(6778): p. 635-43.
2. Yach, D., D. Stuckler, and K.D. Brownell, *Epidemiologic and economic consequences of the global epidemics of obesity and diabetes.* Nat Med, 2006. **12**(1): p. 62-6.
3. Ogden, C.L., et al., *Prevalence of obesity and trends in body mass index among US children and adolescents, 1999-2010.* JAMA, 2012. **307**(5): p. 483-90.
4. World Health Organisation. *Obesity and overweight*. 2018 [cited 2019 27 Nov]; Available from: https://www.who.int/news-room/fact-sheets/detail/obesity-and-overweight.
5. Abdelaal, M., C.W. le Roux, and N.G. Docherty, *Morbidity and mortality associated with obesity.* Ann Transl Med, 2017. **5**(7): p. 161.
6. Catrysse, L. and G. van Loo, *Inflammation and the Metabolic Syndrome: The Tissue-Specific Functions of NF-kappaB.* Trends Cell Biol, 2017. **27**(6): p. 417-429.
7. Chen, L., et al., *Mechanisms Linking Inflammation to Insulin Resistance.* Int J Endocrinol, 2015. **2015**: p. 508409.
8. Esser, N., et al., *Inflammation as a link between obesity, metabolic syndrome and type 2 diabetes.* Diabetes Res Clin Pract, 2014. **105**(2): p. 141-50.
9. Villarroya, F., et al., *Inflammation of brown/beige adipose tissues in obesity and metabolic disease.* J Intern Med, 2018. **284**(5): p. 492-504.
10. Brestoff, J.R. and D. Artis, *Immune regulation of metabolic homeostasis in health and disease.* Cell, 2015. **161**(1): p. 146-160.
11. Fenzl, A. and F.W. Kiefer, *Brown adipose tissue and thermogenesis.* Horm Mol Biol Clin Investig, 2014. **19**(1): p. 25-37.
12. Cedikova, M., et al., *Mitochondria in White, Brown, and Beige Adipocytes.* Stem Cells International, 2016. **2016**: p. 1-11.
13. Attie, A.D. and P.E. Scherer, *Adipocyte metabolism and obesity.* J Lipid Res, 2009. **50 Suppl**: p. S395-9.
14. Smith, S.R., et al., *Contributions of total body fat, abdominal subcutaneous adipose tissue compartments, and visceral adipose tissue to the metabolic complications of obesity.* Metabolism, 2001. **50**(4): p. 425-35.
15. Gesta, S., Y.H. Tseng, and C.R. Kahn, *Developmental origin of fat: tracking obesity to its source.* Cell, 2007. **131**(2): p. 242-56.
16. Trayhurn, P., *Adipocyte biology.* Obes Rev, 2007. **8 Suppl 1**: p. 41-4.
17. Oh, Y.H., et al., *Visceral-to-subcutaneous fat ratio as a predictor of the multiple metabolic risk factors for subjects with normal waist circumference in Korea.* Diabetes Metab Syndr Obes, 2017. **10**: p. 505-511.
18. Rao, R.R., et al., *Meteorin-like is a hormone that regulates immune-adipose interactions to increase beige fat thermogenesis.* Cell, 2014. **157**(6): p. 1279-91.
19. Ye, L., et al., *TRPV4 is a regulator of adipose oxidative metabolism, inflammation, and energy homeostasis.* Cell, 2012. **151**(1): p. 96-110.
20. Ghoshal, S., et al., *Cyclooxygenase-2 deficiency attenuates adipose tissue differentiation and inflammation in mice.* J Biol Chem, 2011. **286**(1): p. 889-98.
21. Nguyen, K.D., et al., *Alternatively activated macrophages produce catecholamines to sustain adaptive thermogenesis.* Nature, 2011. **480**(7375): p. 104-8.
22. Wu, J., P. Cohen, and B.M. Spiegelman, *Adaptive thermogenesis in adipocytes: is beige the new brown?* Genes Dev, 2013. **27**(3): p. 234-50.
23. Vitali, A., et al., *The adipose organ of obesity-prone C57BL/6J mice is composed of mixed white and brown adipocytes.* J Lipid Res, 2012. **53**(4): p. 619-29.
24. Wu, J., et al., *Beige adipocytes are a distinct type of thermogenic fat cell in mouse and human.* Cell, 2012. **150**(2): p. 366-76.
25. Auffret, J., et al., *Beige differentiation of adipose depots in mice lacking prolactin receptor protects against high-fat-diet-induced obesity.* Faseb j, 2012. **26**(9): p. 3728-37.

26. Cousin, B., et al., *Occurrence of brown adipocytes in rat white adipose tissue: molecular and morphological characterization.* J Cell Sci, 1992. **103 (Pt 4)**: p. 931-42.
27. Seale, P., et al., *Prdm16 determines the thermogenic program of subcutaneous white adipose tissue in mice.* J Clin Invest, 2011. **121**(1): p. 96-105.
28. Kucera, J., et al., *Human White Adipose Tissue Metabolome: Current Perspective.* Obesity (Silver Spring), 2018. **26**(12): p. 1870-1878.
29. Longo, M., et al., *Adipose Tissue Dysfunction as Determinant of Obesity-Associated Metabolic Complications.* Int J Mol Sci, 2019. **20**(9).
30. Tan, C.Y. and A. Vidal-Puig, *Adipose tissue expandability: the metabolic problems of obesity may arise from the inability to become more obese.* Biochem Soc Trans, 2008. **36**(Pt 5): p. 935-40.
31. Kajimura, S., *Adipose tissue in 2016: Advances in the understanding of adipose tissue biology.* Nat Rev Endocrinol, 2017. **13**(2): p. 69-70.
32. Choe, S.S., et al., *Adipose Tissue Remodeling: Its Role in Energy Metabolism and Metabolic Disorders.* Front Endocrinol (Lausanne), 2016. **7**: p. 30.
33. Bartness, T.J., C.H. Vaughan, and C.K. Song, *Sympathetic and sensory innervation of brown adipose tissue.* Int J Obes (Lond), 2010. **34 Suppl 1**: p. S36-42.
34. Cannon, B. and J. Nedergaard, *Brown adipose tissue: function and physiological significance.* Physiol Rev, 2004. **84**(1): p. 277-359.
35. Porter, C., *Quantification of UCP1 function in human brown adipose tissue.* Adipocyte, 2017. **6**(2): p. 167-174.
36. Klingenberg, M., *Uncoupling protein--a useful energy dissipator.* J Bioenerg Biomembr, 1999. **31**(5): p. 419-30.
37. Feldmann, H.M., et al., *UCP1 ablation induces obesity and abolishes diet-induced thermogenesis in mice exempt from thermal stress by living at thermoneutrality.* Cell Metab, 2009. **9**(2): p. 203-9.
38. Aherne, W. and D. Hull, *Brown adipose tissue and heat production in the newborn infant.* J Pathol Bacteriol, 1966. **91**(1): p. 223-34.
39. Fedorenko, A., P.V. Lishko, and Y. Kirichok, *Mechanism of fatty-acid-dependent UCP1 uncoupling in brown fat mitochondria.* Cell, 2012. **151**(2): p. 400-13.
40. Inagaki, T., J. Sakai, and S. Kajimura, *Transcriptional and epigenetic control of brown and beige adipose cell fate and function.* Nat Rev Mol Cell Biol, 2017. **18**(8): p. 527.
41. Klingenberg, M. and S.G. Huang, *Structure and function of the uncoupling protein from brown adipose tissue.* Biochim Biophys Acta, 1999. **1415**(2): p. 271-96.
42. Nedergaard, J., T. Bengtsson, and B. Cannon, *Unexpected evidence for active brown adipose tissue in adult humans.* Am J Physiol Endocrinol Metab, 2007. **293**(2): p. E444-52.
43. Virtanen, K.A., et al., *Functional brown adipose tissue in healthy adults.* N Engl J Med, 2009. **360**(15): p. 1518-25.
44. Cypess, A.M., et al., *Identification and importance of brown adipose tissue in adult humans.* N Engl J Med, 2009. **360**(15): p. 1509-17.
45. Cannon, B. and J. Nedergaard, *Nonshivering thermogenesis and its adequate measurement in metabolic studies.* J Exp Biol, 2011. **214**(Pt 2): p. 242-53.
46. Symonds, M.E., M. Pope, and H. Budge, *The Ontogeny of Brown Adipose Tissue.* Annu Rev Nutr, 2015. **35**: p. 295-320.
47. Van Obberghen, E., et al., *Surfing the insulin signaling web.* Eur J Clin Invest, 2001. **31**(11): p. 966-77.
48. Ramachandran, C. and B.P. Kennedy, *Protein tyrosine phosphatase 1B: a novel target for type 2 diabetes and obesity.* Curr Top Med Chem, 2003. **3**(7): p. 749-57.
49. Świderska, E., et al., *Role of PI3K/AKT Pathway in Insulin-Mediated Glucose Uptake*. 2018.

50. Lizunov, V.A., et al., *Insulin stimulates the halting, tethering, and fusion of mobile GLUT4 vesicles in rat adipose cells.* J Cell Biol, 2005. **169**(3): p. 481-9.
51. Bryant, N.J., R. Govers, and D.E. James, *Regulated transport of the glucose transporter GLUT4.* Nat Rev Mol Cell Biol, 2002. **3**(4): p. 267-77.
52. Valverde, A.M., et al., *Insulin and insulin-like growth factor I up-regulate GLUT4 gene expression in fetal brown adipocytes, in a phosphoinositide 3-kinase-dependent manner.* Biochem J, 1999. **337 (Pt 3)**: p. 397-405.
53. Leto, D. and A.R. Saltiel, *Regulation of glucose transport by insulin: traffic control of GLUT4.* Nat Rev Mol Cell Biol, 2012. **13**(6): p. 383-96.
54. Wang, S., et al., *From white to beige adipocytes: therapeutic potential of dietary molecules against obesity and their molecular mechanisms.* Food Funct, 2019. **10**(3): p. 1263-1279.
55. Handschin, C. and B.M. Spiegelman, *Peroxisome proliferator-activated receptor gamma coactivator 1 coactivators, energy homeostasis, and metabolism.* Endocr Rev, 2006. **27**(7): p. 728-35.
56. Puigserver, P., et al., *A cold-inducible coactivator of nuclear receptors linked to adaptive thermogenesis.* Cell, 1998. **92**(6): p. 829-39.
57. Wu, Z., et al., *Mechanisms controlling mitochondrial biogenesis and respiration through the thermogenic coactivator PGC-1.* Cell, 1999. **98**(1): p. 115-24.
58. Uldry, M., et al., *Complementary action of the PGC-1 coactivators in mitochondrial biogenesis and brown fat differentiation.* Cell Metab, 2006. **3**(5): p. 333-41.
59. Seale, P., et al., *Transcriptional control of brown fat determination by PRDM16.* Cell Metab, 2007. **6**(1): p. 38-54.
60. Ohno, H., et al., *PPARgamma agonists induce a white-to-brown fat conversion through stabilization of PRDM16 protein.* Cell Metab, 2012. **15**(3): p. 395-404.
61. Obregon, M.J., *Adipose tissues and thyroid hormones.* Front Physiol, 2014. **5**: p. 479.
62. Schroeder, A.C. and M.L. Privalsky, *Thyroid hormones, t3 and t4, in the brain.* Frontiers in endocrinology, 2014. **5**: p. 40-40.
63. Bianco, A.C. and B.W. Kim, *Deiodinases: implications of the local control of thyroid hormone action.* J Clin Invest, 2006. **116**(10): p. 2571-9.
64. Lavado-Autric, R., et al., *Deiodinase activities in thyroids and tissues of iodine-deficient female rats.* Endocrinology, 2013. **154**(1): p. 529-36.
65. Ribeiro, M.O., et al., *Expression of uncoupling protein 1 in mouse brown adipose tissue is thyroid hormone receptor-beta isoform specific and required for adaptive thermogenesis.* Endocrinology, 2010. **151**(1): p. 432-40.
66. Martinez de Mena, R., T.S. Scanlan, and M.J. Obregon, *The T3 receptor beta1 isoform regulates UCP1 and D2 deiodinase in rat brown adipocytes.* Endocrinology, 2010. **151**(10): p. 5074-83.
67. Lowell, B.B. and B.M. Spiegelman, *Towards a molecular understanding of adaptive thermogenesis.* Nature, 2000. **404**(6778): p. 652-60.
68. Lopez, M., et al., *Energy balance regulation by thyroid hormones at central level.* Trends Mol Med, 2013. **19**(7): p. 418-27.
69. de Jesus, L.A., et al., *The type 2 iodothyronine deiodinase is essential for adaptive thermogenesis in brown adipose tissue.* J Clin Invest, 2001. **108**(9): p. 1379-85.
70. Yau, W.W., et al., *Thyroid hormone (T3) stimulates brown adipose tissue activation via mitochondrial biogenesis and MTOR-mediated mitophagy.* Autophagy, 2019. **15**(1): p. 131-150.
71. Lin, J.Z., et al., *Pharmacological Activation of Thyroid Hormone Receptors Elicits a Functional Conversion of White to Brown Fat.* Cell Rep, 2015. **13**(8): p. 1528-37.
72. Holtorf, K., *Thyroid Hormone Transport into Cellular Tissue.* Journal of Restorative Medicine, 2014. **3**: p. 53-68.

73. Racataianu, N., et al., *Interplay between metabolic and thyroid parameters in obese pubertal children. Does visceral adipose tissue make the first move?* Acta Clin Belg, 2019: p. 1-9.
74. Kwakkel, J., et al., *Thyroid hormone receptor {alpha} modulates lipopolysaccharide-induced changes in peripheral thyroid hormone metabolism.* Endocrinology, 2010. **151**(4): p. 1959-69.
75. Feingold, K., et al., *Altered expression of nuclear hormone receptors and coactivators in mouse heart during the acute-phase response.* Am J Physiol Endocrinol Metab, 2004. **286**(2): p. E201-7.
76. Rodriguez-Perez, A., et al., *Identification of molecular mechanisms related to nonthyroidal illness syndrome in skeletal muscle and adipose tissue from patients with septic shock.* Clin Endocrinol (Oxf), 2008. **68**(5): p. 821-7.
77. Contreras-Jurado, C., et al., *The Thyroid Hormone Receptors Inhibit Hepatic Interleukin-6 Signaling During Endotoxemia.* Sci Rep, 2016. **6**: p. 30990.
78. Ferrannini, E., et al., *Insulin resistance and normal thyroid hormone levels: prospective study and metabolomic analysis.* Am J Physiol Endocrinol Metab, 2017. **312**(5): p. E429-e436.
79. Siddiqui, K., et al., *Variation in the level of thyroid markers in association with inflammation in patients with type 2 diabetes.* Endocr Metab Immune Disord Drug Targets, 2019.
80. Villarroya, F., et al., *Brown adipose tissue as a secretory organ.* Nat Rev Endocrinol, 2017. **13**(1): p. 26-35.
81. Lee, M.W., M. Lee, and K.J. Oh, *Adipose Tissue-Derived Signatures for Obesity and Type 2 Diabetes: Adipokines, Batokines and MicroRNAs.* J Clin Med, 2019. **8**(6).
82. Badman, M.K., et al., *Hepatic fibroblast growth factor 21 is regulated by PPARalpha and is a key mediator of hepatic lipid metabolism in ketotic states.* Cell Metab, 2007. **5**(6): p. 426-37.
83. Chartoumpekis, D.V., et al., *Brown adipose tissue responds to cold and adrenergic stimulation by induction of FGF21.* Mol Med, 2011. **17**(7-8): p. 736-40.
84. Fisher, F.M., et al., *FGF21 regulates PGC-1alpha and browning of white adipose tissues in adaptive thermogenesis.* Genes Dev, 2012. **26**(3): p. 271-81.
85. Giralt, M., A. Gavalda-Navarro, and F. Villarroya, *Fibroblast growth factor-21, energy balance and obesity.* Mol Cell Endocrinol, 2015. **418 Pt 1**: p. 66-73.
86. Itoh, N., *FGF21 as a Hepatokine, Adipokine, and Myokine in Metabolism and Diseases.* Front Endocrinol (Lausanne), 2014. **5**: p. 107.
87. Hondares, E., et al., *Thermogenic activation induces FGF21 expression and release in brown adipose tissue.* J Biol Chem, 2011. **286**(15): p. 12983-90.
88. Jimenez, V., et al., *FGF21 gene therapy as treatment for obesity and insulin resistance.* EMBO Mol Med, 2018. **10**(8).
89. Zorzano, A., M. Liesa, and M. Palacin, *Role of mitochondrial dynamics proteins in the pathophysiology of obesity and type 2 diabetes.* Int J Biochem Cell Biol, 2009. **41**(10): p. 1846-54.
90. Gomes, L.C., G. Di Benedetto, and L. Scorrano, *During autophagy mitochondria elongate, are spared from degradation and sustain cell viability.* Nat Cell Biol, 2011. **13**(5): p. 589-98.
91. Boutant, M., et al., *Mfn2 is critical for brown adipose tissue thermogenic function.* The EMBO journal, 2017. **36**(11): p. 1543-1558.
92. Mahdaviani, K., et al., *Mfn2 deletion in brown adipose tissue protects from insulin resistance and impairs thermogenesis.* EMBO Rep, 2017. **18**(7): p. 1123-1138.
93. Pisani, D.F., et al., *Mitochondrial fission is associated with UCP1 activity in human brite/beige adipocytes.* Molecular metabolism, 2018. **7**: p. 35-44.

94. Pickles, S., P. Vigie, and R.J. Youle, *Mitophagy and Quality Control Mechanisms in Mitochondrial Maintenance.* Curr Biol, 2018. **28**(4): p. R170-r185.
95. Cui, C., et al., *PINK1-Parkin alleviates metabolic stress induced by obesity in adipose tissue and in 3T3-L1 preadipocytes.* Biochem Biophys Res Commun, 2018. **498**(3): p. 445-452.
96. Yang, X., et al., *Mitophagy: A crucial modulator in the pathogenesis of chronic diseases.* Clin Chim Acta, 2019.
97. Kim, S.J., et al., *The essential role of mitochondrial dynamics in antiviral immunity.* Mitochondrion, 2018. **41**: p. 21-27.
98. Hahn, W.S., et al., *Proinflammatory cytokines differentially regulate adipocyte mitochondrial metabolism, oxidative stress, and dynamics.* Am J Physiol Endocrinol Metab, 2014. **306**(9): p. E1033-45.
99. Lim, S., et al., *Cold-induced activation of brown adipose tissue and adipose angiogenesis in mice.* Nat Protoc, 2012. **7**(3): p. 606-15.
100. Barbatelli, G., et al., *The emergence of cold-induced brown adipocytes in mouse white fat depots is determined predominantly by white to brown adipocyte transdifferentiation.* Am J Physiol Endocrinol Metab, 2010. **298**(6): p. E1244-53.
101. Collins, S., et al., *Strain-specific response to beta 3-adrenergic receptor agonist treatment of diet-induced obesity in mice.* Endocrinology, 1997. **138**(1): p. 405-13.
102. Klingenspor, M., *Cold-induced recruitment of brown adipose tissue thermogenesis.* Exp Physiol, 2003. **88**(1): p. 141-8.
103. Bastard, J.P., et al., *Recent advances in the relationship between obesity, inflammation, and insulin resistance.* Eur Cytokine Netw, 2006. **17**(1): p. 4-12.
104. Weisberg, S.P., et al., *Obesity is associated with macrophage accumulation in adipose tissue.* J Clin Invest, 2003. **112**(12): p. 1796-808.
105. Xu, H., et al., *Chronic inflammation in fat plays a crucial role in the development of obesity-related insulin resistance.* J Clin Invest, 2003. **112**(12): p. 1821-30.
106. Cancello, R., et al., *Reduction of macrophage infiltration and chemoattractant gene expression changes in white adipose tissue of morbidly obese subjects after surgery-induced weight loss.* Diabetes, 2005. **54**(8): p. 2277-86.
107. O'Rourke, R.W., et al., *Hypoxia-induced inflammatory cytokine secretion in human adipose tissue stromovascular cells.* Diabetologia, 2011. **54**(6): p. 1480-90.
108. Kosteli, A., et al., *Weight loss and lipolysis promote a dynamic immune response in murine adipose tissue.* J Clin Invest, 2010. **120**(10): p. 3466-79.
109. Boutens, L., et al., *Unique metabolic activation of adipose tissue macrophages in obesity promotes inflammatory responses.* Diabetologia, 2018. **61**(4): p. 942-953.
110. Chawla, A., K.D. Nguyen, and Y.P. Goh, *Macrophage-mediated inflammation in metabolic disease.* Nat Rev Immunol, 2011. **11**(11): p. 738-49.
111. Rath, M., et al., *Metabolism via Arginase or Nitric Oxide Synthase: Two Competing Arginine Pathways in Macrophages.* Frontiers in immunology, 2014. **5**: p. 532-532.
112. Famenini, S., et al., *Increased intermediate M1-M2 macrophage polarization and improved cognition in mild cognitive impairment patients on ω-3 supplementation.* FASEB journal : official publication of the Federation of American Societies for Experimental Biology, 2017. **31**(1): p. 148-160.
113. O'Neill, L.A., *A Metabolic Roadblock in Inflammatory Macrophages.* Cell Rep, 2016. **17**(3): p. 625-626.
114. Lumeng, C.N., J.L. Bodzin, and A.R. Saltiel, *Obesity induces a phenotypic switch in adipose tissue macrophage polarization.* J Clin Invest, 2007. **117**(1): p. 175-84.
115. Lumeng, C.N., et al., *Phenotypic switching of adipose tissue macrophages with obesity is generated by spatiotemporal differences in macrophage subtypes.* Diabetes, 2008. **57**(12): p. 3239-46.

116. Oh, D.Y., et al., *Increased macrophage migration into adipose tissue in obese mice.* Diabetes, 2012. **61**(2): p. 346-54.
117. Wentworth, J.M., et al., *Pro-inflammatory CD11c+CD206+ adipose tissue macrophages are associated with insulin resistance in human obesity.* Diabetes, 2010. **59**(7): p. 1648-56.
118. Shoelson, S.E., J. Lee, and A.B. Goldfine, *Inflammation and insulin resistance.* J Clin Invest, 2006. **116**(7): p. 1793-801.
119. Mancini, S.J., et al., *Activation of AMP-activated protein kinase rapidly suppresses multiple pro-inflammatory pathways in adipocytes including IL-1 receptor-associated kinase-4 phosphorylation.* Mol Cell Endocrinol, 2017. **440**: p. 44-56.
120. Ying, W., et al., *Adipose Tissue Macrophage-Derived Exosomal miRNAs Can Modulate In Vivo and In Vitro Insulin Sensitivity.* Cell, 2017. **171**(2): p. 372-384.e12.
121. Nisoli, E., et al., *Tumor necrosis factor alpha mediates apoptosis of brown adipocytes and defective brown adipocyte function in obesity.* Proc Natl Acad Sci U S A, 2000. **97**(14): p. 8033-8.
122. Roberts-Toler, C., B.T. O'Neill, and A.M. Cypess, *Diet-induced obesity causes insulin resistance in mouse brown adipose tissue.* Obesity (Silver Spring), 2015. **23**(9): p. 1765-70.
123. Sakamoto, T., et al., *Macrophage infiltration into obese adipose tissues suppresses the induction of UCP1 level in mice.* Am J Physiol Endocrinol Metab, 2016. **310**(8): p. E676-e687.
124. Martins, F.F., et al., *Thermogenesis, fatty acid synthesis with oxidation, and inflammation in the brown adipose tissue of ob/ob (-/-) mice.* Ann Anat, 2017. **210**: p. 44-51.
125. Bae, J., et al., *Activation of pattern recognition receptors in brown adipocytes induces inflammation and suppresses uncoupling protein 1 expression and mitochondrial respiration.* Am J Physiol Cell Physiol, 2014. **306**(10): p. C918-30.
126. Okla, M., et al., *Inhibitory Effects of Toll-Like Receptor 4, NLRP3 Inflammasome, and Interleukin-1beta on White Adipocyte Browning.* Inflammation, 2018. **41**(2): p. 626-642.
127. Nohr, M.K., et al., *Inflammation Downregulates UCP1 Expression in Brown Adipocytes Potentially via SIRT1 and DBC1 Interaction.* Int J Mol Sci, 2017. **18**(5).
128. Villarroya, J., et al., *New insights into the secretory functions of brown adipose tissue.* J Endocrinol, 2019.
129. Gunawardana, S.C. and D.W. Piston, *Insulin-independent reversal of type 1 diabetes in nonobese diabetic mice with brown adipose tissue transplant.* Am J Physiol Endocrinol Metab, 2015. **308**(12): p. E1043-55.
130. Stanford, K.I., et al., *Brown adipose tissue regulates glucose homeostasis and insulin sensitivity.* J Clin Invest, 2013. **123**(1): p. 215-23.
131. Liu, X., et al., *Brown Adipose Tissue Transplantation Reverses Obesity in Ob/Ob Mice.* Endocrinology, 2015. **156**(7): p. 2461-9.
132. Villarroya, J., R. Cereijo, and F. Villarroya, *An endocrine role for brown adipose tissue?* Am J Physiol Endocrinol Metab, 2013. **305**(5): p. E567-72.
133. Li, X., *SIRT1 and energy metabolism.* Acta Biochim Biophys Sin (Shanghai), 2013. **45**(1): p. 51-60.
134. Cao, Y., et al., *SIRT1 and insulin resistance.* J Diabetes Complications, 2016. **30**(1): p. 178-83.
135. Jokinen, R., et al., *Adipose tissue NAD(+)-homeostasis, sirtuins and poly(ADP-ribose) polymerases -important players in mitochondrial metabolism and metabolic health.* Redox biology, 2017. **12**: p. 246-263.
136. Vachharajani, V.T., et al., *Sirtuins Link Inflammation and Metabolism.* Journal of immunology research, 2016. **2016**: p. 8167273-8167273.

137. Kang, H., et al., *Sirt1 carboxyl-domain is an ATP-repressible domain that is transferrable to other proteins.* Nat Commun, 2017. **8**: p. 15560.
138. Yeung, F., et al., *Modulation of NF-kappaB-dependent transcription and cell survival by the SIRT1 deacetylase.* EMBO J, 2004. **23**(12): p. 2369-80.
139. Pfluger, P.T., et al., *Sirt1 protects against high-fat diet-induced metabolic damage.* Proc Natl Acad Sci U S A, 2008. **105**(28): p. 9793-8.
140. Yoshizaki, T., et al., *SIRT1 inhibits inflammatory pathways in macrophages and modulates insulin sensitivity.* Am J Physiol Endocrinol Metab, 2010. **298**(3): p. E419-28.
141. Purushotham, A., Q. Xu, and X. Li, *Systemic SIRT1 insufficiency results in disruption of energy homeostasis and steroid hormone metabolism upon high-fat-diet feeding.* Faseb j, 2012. **26**(2): p. 656-67.
142. Jin, Q., et al., *C/EBPalpha regulates SIRT1 expression during adipogenesis.* Cell Res, 2010. **20**(4): p. 470-9.
143. Chakrabarti, P., et al., *SIRT1 controls lipolysis in adipocytes via FOXO1-mediated expression of ATGL.* J Lipid Res, 2011. **52**(9): p. 1693-701.
144. Picard, F., et al., *Sirt1 promotes fat mobilization in white adipocytes by repressing PPAR-gamma.* Nature, 2004. **429**(6993): p. 771-776.
145. Li, F., et al., *Adipose-specific knockdown of Sirt1 results in obesity and insulin resistance by promoting exosomes release.* Cell Cycle, 2019. **18**(17): p. 2067-2082.
146. Qiang, L., et al., *Brown remodeling of white adipose tissue by SirT1-dependent deacetylation of Ppargamma.* Cell, 2012. **150**(3): p. 620-32.
147. Bordone, L., et al., *SIRT1 transgenic mice show phenotypes resembling calorie restriction.* Aging Cell, 2007. **6**(6): p. 759-67.
148. Feige, J.N., et al., *Specific SIRT1 activation mimics low energy levels and protects against diet-induced metabolic disorders by enhancing fat oxidation.* Cell Metab, 2008. **8**(5): p. 347-58.
149. Lagouge, M., et al., *Resveratrol improves mitochondrial function and protects against metabolic disease by activating SIRT1 and PGC-1alpha.* Cell, 2006. **127**(6): p. 1109-22.
150. Boutant, M., et al., *SIRT1 enhances glucose tolerance by potentiating brown adipose tissue function.* Mol Metab, 2015. **4**(2): p. 118-31.
151. Canto, C. and J. Auwerx, *PGC-1alpha, SIRT1 and AMPK, an energy sensing network that controls energy expenditure.* Curr Opin Lipidol, 2009. **20**(2): p. 98-105.
152. Canto, C., et al., *The NAD(+) precursor nicotinamide riboside enhances oxidative metabolism and protects against high-fat diet-induced obesity.* Cell Metab, 2012. **15**(6): p. 838-47.
153. Banks, A.S., et al., *SirT1 gain of function increases energy efficiency and prevents diabetes in mice.* Cell metabolism, 2008. **8**(4): p. 333-341.
154. Xu, F., et al., *Diet-induced obesity and insulin resistance are associated with brown fat degeneration in SIRT1-deficient mice.* Obesity (Silver Spring), 2016. **24**(3): p. 634-42.
155. Chalkiadaki, A. and L. Guarente, *High-fat diet triggers inflammation-induced cleavage of SIRT1 in adipose tissue to promote metabolic dysfunction.* Cell Metab, 2012. **16**(2): p. 180-8.
156. Sun, C., et al., *SIRT1 improves insulin sensitivity under insulin-resistant conditions by repressing PTP1B.* Cell Metab, 2007. **6**(4): p. 307-19.
157. Hubbard, B.P. and D.A. Sinclair, *Small molecule SIRT1 activators for the treatment of aging and age-related diseases.* Trends in pharmacological sciences, 2014. **35**(3): p. 146-154.
158. Milne, J.C., et al., *Small molecule activators of SIRT1 as therapeutics for the treatment of type 2 diabetes.* Nature, 2007. **450**(7170): p. 712-6.
159. Gonzalez-Rodriguez, A., et al., *Resveratrol treatment restores peripheral insulin sensitivity in diabetic mice in a sirt1-independent manner.* Mol Nutr Food Res, 2015. **59**(8): p. 1431-42.

160. Gonzalez-Rodriguez, A., et al., *Inhibition of PTP1B restores IRS1-mediated hepatic insulin signaling in IRS2-deficient mice.* Diabetes, 2010. **59**(3): p. 588-99.
161. Wang, S., M.J. Zhu, and M. Du, *Prevention of obesity by dietary resveratrol: how strong is the evidence?* Expert Rev Endocrinol Metab, 2015. **10**(6): p. 561-564.
162. Mendez-del Villar, M., et al., *Effect of resveratrol administration on metabolic syndrome, insulin sensitivity, and insulin secretion.* Metab Syndr Relat Disord, 2014. **12**(10): p. 497-501.
163. Mitterberger, M.C. and W. Zwerschke, *Mechanisms of resveratrol-induced inhibition of clonal expansion and terminal adipogenic differentiation in 3T3-L1 preadipocytes.* J Gerontol A Biol Sci Med Sci, 2013. **68**(11): p. 1356-76.
164. Lasa, A., et al., *Resveratrol regulates lipolysis via adipose triglyceride lipase.* J Nutr Biochem, 2012. **23**(4): p. 379-84.
165. Gomez-Zorita, S., et al., *Resveratrol directly affects in vitro lipolysis and glucose transport in human fat cells.* J Physiol Biochem, 2013. **69**(3): p. 585-93.
166. Wang, S., et al., *Resveratrol induces brown-like adipocyte formation in white fat through activation of AMP-activated protein kinase (AMPK) alpha1.* Int J Obes (Lond), 2015. **39**(6): p. 967-76.
167. Alberdi, G., et al., *Thermogenesis is involved in the body-fat lowering effects of resveratrol in rats.* Food Chem, 2013. **141**(2): p. 1530-5.
168. Andrade, J.M., et al., *Resveratrol increases brown adipose tissue thermogenesis markers by increasing SIRT1 and energy expenditure and decreasing fat accumulation in adipose tissue of mice fed a standard diet.* Eur J Nutr, 2014. **53**(7): p. 1503-10.
169. Wang, S., et al., *Resveratrol enhances brown adipocyte formation and function by activating AMP-activated protein kinase (AMPK) alpha1 in mice fed high-fat diet.* Mol Nutr Food Res, 2017. **61**(4).
170. Silvester, A.J., K.R. Aseer, and J.W. Yun, *Dietary polyphenols and their roles in fat browning.* J Nutr Biochem, 2019. **64**: p. 1-12.
171. Calderon-Dominguez, M., et al., *Brown Adipose Tissue Bioenergetics: A New Methodological Approach.* Adv Sci (Weinh), 2017. **4**(4): p. 1600274.
172. Morreale de Escobar, G., et al., *Effects of maternal hypothyroidism on the weight and thyroid hormone content of rat embryonic tissues, before and after onset of fetal thyroid function.* Endocrinology, 1985. **117**(5): p. 1890-900.
173. Weeke, J. and H. Orskov, *Synthesis of 125I monolabelled 3, 5, 3'-triiodothyronine and thyroxine of maximum specific activity for radioimmunoassay.* Scand J Clin Lab Invest, 1973. **32**(4): p. 357-60.
174. Obregon, M.J., G. Morreale de Escobar, and F. Escobar del Rey, *Concentrations of triiodo-L-thyronine in the plasma and tissues of normal rats, as determined by radioimmunoassay: comparison with results obtained by an isotopic equilibrium technique.* Endocrinology, 1978. **103**(6): p. 2145-53.
175. Garcia-Casarrubios, E., et al., *Rapamycin negatively impacts insulin signaling, glucose uptake and uncoupling protein-1 in brown adipocytes.* Biochim Biophys Acta, 2016. **1861**(12 Pt A): p. 1929-1941.
176. Herrero, L., et al., *Alteration of the malonyl-CoA/carnitine palmitoyltransferase I interaction in the beta-cell impairs glucose-induced insulin secretion.* Diabetes, 2005. **54**(2): p. 462-71.
177. Coleman, D.L., *Obese and diabetes: two mutant genes causing diabetes-obesity syndromes in mice.* Diabetologia, 1978. **14**(3): p. 141-8.
178. Susztak, K., et al., *Molecular profiling of diabetic mouse kidney reveals novel genes linked to glomerular disease.* Diabetes, 2004. **53**(3): p. 784-94.
179. Dalboge, L.S., et al., *Characterisation of age-dependent beta cell dynamics in the male db/db mice.* PLoS One, 2013. **8**(12): p. e82813.

180. Burke, S.J., et al., *db/db Mice Exhibit Features of Human Type 2 Diabetes That Are Not Present in Weight-Matched C57BL/6J Mice Fed a Western Diet.* J Diabetes Res, 2017. **2017**: p. 8503754.
181. Nyati, K.K., et al., *TLR4-induced NF-kappaB and MAPK signaling regulate the IL-6 mRNA stabilizing protein Arid5a.* Nucleic Acids Res, 2017. **45**(5): p. 2687-2703.
182. Belfiore, A., et al., *Insulin Receptor Isoforms in Physiology and Disease: An Updated View.* Endocr Rev, 2017. **38**(5): p. 379-431.
183. Festuccia, W.T., P.-G. Blanchard, and Y. Deshaies, *Control of Brown Adipose Tissue Glucose and Lipid Metabolism by PPARγ.* Frontiers in endocrinology, 2011. **2**: p. 84-84.
184. Quesada-Lopez, T., et al., *The lipid sensor GPR120 promotes brown fat activation and FGF21 release from adipocytes.* Nat Commun, 2016. **7**: p. 13479.
185. Saklayen, M.G., *The Global Epidemic of the Metabolic Syndrome.* Current hypertension reports, 2018. **20**(2): p. 12-12.
186. Reilly, S.M. and A.R. Saltiel, *Adapting to obesity with adipose tissue inflammation.* Nat Rev Endocrinol, 2017. **13**(11): p. 633-643.
187. Lumeng, C.N., et al., *Increased inflammatory properties of adipose tissue macrophages recruited during diet-induced obesity.* Diabetes, 2007. **56**(1): p. 16-23.
188. Furuhashi, M., et al., *Adipocyte/macrophage fatty acid-binding proteins contribute to metabolic deterioration through actions in both macrophages and adipocytes in mice.* J Clin Invest, 2008. **118**(7): p. 2640-50.
189. Hotamisligil, G.S., *Inflammation and metabolic disorders.* Nature, 2006. **444**(7121): p. 860-7.
190. Haase, J., et al., *Local proliferation of macrophages in adipose tissue during obesity-induced inflammation.* Diabetologia, 2014. **57**(3): p. 562-71.
191. Murano, I., et al., *Dead adipocytes, detected as crown-like structures, are prevalent in visceral fat depots of genetically obese mice.* J Lipid Res, 2008. **49**(7): p. 1562-8.
192. Cinti, S., et al., *Adipocyte death defines macrophage localization and function in adipose tissue of obese mice and humans.* J Lipid Res, 2005. **46**(11): p. 2347-55.
193. Sikaris, K.A., *The clinical biochemistry of obesity.* Clin Biochem Rev, 2004. **25**(3): p. 165-81.
194. Cani, P.D., et al., *Changes in gut microbiota control metabolic endotoxemia-induced inflammation in high-fat diet-induced obesity and diabetes in mice.* Diabetes, 2008. **57**(6): p. 1470-81.
195. Saad, M.J., A. Santos, and P.O. Prada, *Linking Gut Microbiota and Inflammation to Obesity and Insulin Resistance.* Physiology (Bethesda), 2016. **31**(4): p. 283-93.
196. Hersoug, L.G., P. Moller, and S. Loft, *Gut microbiota-derived lipopolysaccharide uptake and trafficking to adipose tissue: implications for inflammation and obesity.* Obes Rev, 2016. **17**(4): p. 297-312.
197. Robinson, L., et al., *Body mass index as a determinant of brown adipose tissue function in healthy children.* J Pediatr, 2014. **164**(2): p. 318-22.e1.
198. Arroba, A.I., et al., *Modulation of microglia polarization dynamics during diabetic retinopathy in db/db mice.* Biochim Biophys Acta, 2016. **1862**(9): p. 1663-74.
199. Jiang, C., et al., *Cyclocarya paliurus Triterpenoids Improve Diabetes-Induced Hepatic Inflammation via the Rho-Kinase-Dependent Pathway.* Front Pharmacol, 2019. **10**: p. 811.
200. Zhong, J., et al., *Micheliolide alleviates hepatic steatosis in db/db mice by inhibiting inflammation and promoting autophagy via PPAR-gamma-mediated NF-small ka, CyrillicB and AMPK/mTOR signaling.* Int Immunopharmacol, 2018. **59**: p. 197-208.
201. Song, W., et al., *Endothelial TFEB (Transcription Factor EB) Restrains IKK (IkappaB Kinase)-p65 Pathway to Attenuate Vascular Inflammation in Diabetic db/db Mice.* Arterioscler Thromb Vasc Biol, 2019. **39**(4): p. 719-730.

202. Park, C.H., T. Tanaka, and T. Yokozawa, *Anti-diabetic action of 7-O-galloyl-D-sedoheptulose, a polyphenol from Corni Fructus, through ameliorating inflammation and inflammation-related oxidative stress in the pancreas of type 2 diabetics.* Biol Pharm Bull, 2013. **36**(5): p. 723-32.
203. Liu, S., et al., *CXCL13/CXCR5 signaling contributes to diabetes-induced tactile allodynia via activating pERK, pSTAT3, pAKT pathways and pro-inflammatory cytokines production in the spinal cord of male mice.* Brain Behav Immun, 2019. **80**: p. 711-724.
204. Lim, A.K., et al., *Role of MKK3-p38 MAPK signalling in the development of type 2 diabetes and renal injury in obese db/db mice.* Diabetologia, 2009. **52**(2): p. 347-58.
205. Cheng, H.T., et al., *p38 mediates mechanical allodynia in a mouse model of type 2 diabetes.* Mol Pain, 2010. **6**: p. 28.
206. Todoric, J., et al., *Adipose tissue inflammation induced by high-fat diet in obese diabetic mice is prevented by n-3 polyunsaturated fatty acids.* Diabetologia, 2006. **49**(9): p. 2109-19.
207. Tamura, Y., et al., *Enzamin ameliorates adipose tissue inflammation with impaired adipocytokine expression and insulin resistance in db/db mice.* J Nutr Sci, 2013. **2**: p. e37.
208. Bouter, B., et al., *Diet-genotype interactions in the early development of obesity and insulin resistance in mice with a genetic deficiency in tumor necrosis factor-alpha.* Metabolism, 2010. **59**(7): p. 1065-73.
209. Tzanavari, T., P. Giannogonas, and K.P. Karalis, *TNF-alpha and obesity.* Curr Dir Autoimmun, 2010. **11**: p. 145-56.
210. Klover, P.J., A.H. Clementi, and R.A. Mooney, *Interleukin-6 depletion selectively improves hepatic insulin action in obesity.* Endocrinology, 2005. **146**(8): p. 3417-27.
211. Matsubara, T., et al., *PGRN is a key adipokine mediating high fat diet-induced insulin resistance and obesity through IL-6 in adipose tissue.* Cell Metab, 2012. **15**(1): p. 38-50.
212. Burke, S.J., et al., *db/db Mice Exhibit Features of Human Type 2 Diabetes That Are Not Present in Weight-Matched C57BL/6J Mice Fed a Western Diet.* Journal of diabetes research, 2017. **2017**: p. 8503754-8503754.
213. Hu, T., et al., *Myricetin-induced brown adipose tissue activation prevents obesity and insulin resistance in db/db mice.* Eur J Nutr, 2018. **57**(1): p. 391-403.
214. Shao, J., et al., *Decreased Akt kinase activity and insulin resistance in C57BL/KsJ-Leprdb/db mice.* J Endocrinol, 2000. **167**(1): p. 107-15.
215. Whittaker, J., et al., *Comparison of the functional insulin binding epitopes of the A and B isoforms of the insulin receptor.* J Biol Chem, 2002. **277**(49): p. 47380-4.
216. Menting, J.G., et al., *How insulin engages its primary binding site on the insulin receptor.* Nature, 2013. **493**(7431): p. 241-5.
217. Frasca, F., et al., *Insulin receptor isoform A, a newly recognized, high-affinity insulin-like growth factor II receptor in fetal and cancer cells.* Mol Cell Biol, 1999. **19**(5): p. 3278-88.
218. Escribano, O., et al., *The Role of Insulin Receptor Isoforms in Diabetes and Its Metabolic and Vascular Complications.* Journal of diabetes research, 2017. **2017**: p. 1403206-1403206.
219. Escribano, O., et al., *Beta-Cell hyperplasia induced by hepatic insulin resistance: role of a liver-pancreas endocrine axis through insulin receptor A isoform.* Diabetes, 2009. **58**(4): p. 820-8.
220. Huang, Z., et al., *Hyperinsulinemia is associated with altered insulin receptor mRNA splicing in muscle of the spontaneously obese diabetic rhesus monkey*. J Clin Invest, 1994. **94**(3): p. 1289-96.
221. Starr, M.E., B.M. Evers, and H. Saito, *Age-associated increase in cytokine production during systemic inflammation: adipose tissue as a major source of IL-6.* J Gerontol A Biol Sci Med Sci, 2009. **64**(7): p. 723-30.
222. Zick, Y., *Ser/Thr phosphorylation of IRS proteins: a molecular basis for insulin resistance.* Sci STKE, 2005. **2005**(268): p. pe4.

223. Sabio, G., et al., *A stress signaling pathway in adipose tissue regulates hepatic insulin resistance.* Science, 2008. **322**(5907): p. 1539-43.
224. Ota, T., *Obesity-induced inflammation and insulin resistance.* Frontiers in endocrinology, 2014. **5**: p. 204-204.
225. Zabolotny, J.M., et al., *Protein-tyrosine phosphatase 1B expression is induced by inflammation in vivo.* J Biol Chem, 2008. **283**(21): p. 14230-41.
226. Gillum, M.P., et al., *SirT1 regulates adipose tissue inflammation.* Diabetes, 2011. **60**(12): p. 3235-3245.
227. Fu, C., et al., *Activation of SIRT1 ameliorates LPS-induced lung injury in mice via decreasing endothelial tight junction permeability.* Acta Pharmacol Sin, 2019. **40**(5): p. 630-641.
228. Lee, J.H., et al., *SIRT1, a Class III Histone Deacetylase, Regulates LPS-Induced Inflammation in Human Keratinocytes and Mediates the Anti-Inflammatory Effects of Hinokitiol.* J Invest Dermatol, 2017. **137**(6): p. 1257-1266.
229. Zhang, W., et al., *Sirt1 Protects Endothelial Cells against LPS-Induced Barrier Dysfunction.* Oxidative medicine and cellular longevity, 2017. **2017**: p. 4082102-4082102.
230. Li, K., G. Lv, and L. Pan, *Sirt1 alleviates LPS induced inflammation of periodontal ligament fibroblasts via downregulation of TLR4.* Int J Biol Macromol, 2018. **119**: p. 249-254.
231. Gariani, K., et al., *Eliciting the mitochondrial unfolded protein response by nicotinamide adenine dinucleotide repletion reverses fatty liver disease in mice.* Hepatology, 2016. **63**(4): p. 1190-204.
232. Pardo, V., et al., *Opposite cross-talk by oleate and palmitate on insulin signaling in hepatocytes through macrophage activation.* J Biol Chem, 2015. **290**(18): p. 11663-77.
233. Lu, J., et al., *SIRT1 counteracted the activation of STAT3 and NF-kappaB to repress the gastric cancer growth.* Int J Clin Exp Med, 2014. **7**(12): p. 5050-8.
234. Rui, L., et al., *SOCS-1 and SOCS-3 block insulin signaling by ubiquitin-mediated degradation of IRS1 and IRS2.* J Biol Chem, 2002. **277**(44): p. 42394-8.
235. Emanuelli, B., et al., *SOCS-3 is an insulin-induced negative regulator of insulin signaling.* J Biol Chem, 2000. **275**(21): p. 15985-91.
236. Liu, Z., et al., *SOCS3 promotes inflammation and apoptosis via inhibiting JAK2/STAT3 signaling pathway in 3T3-L1 adipocyte.* Immunobiology, 2015. **220**(8): p. 947-53.
237. Shi, H., et al., *Suppressor of cytokine signaling 3 is a physiological regulator of adipocyte insulin signaling.* J Biol Chem, 2004. **279**(33): p. 34733-40.
238. Stouthard, J.M., R.P. Oude Elferink, and H.P. Sauerwein, *Interleukin-6 enhances glucose transport in 3T3-L1 adipocytes.* Biochem Biophys Res Commun, 1996. **220**(2): p. 241-5.
239. Carey, A.L., et al., *Interleukin-6 increases insulin-stimulated glucose disposal in humans and glucose uptake and fatty acid oxidation in vitro via AMP-activated protein kinase.* Diabetes, 2006. **55**(10): p. 2688-97.
240. Zambrano, A., et al., *Glut 1 in Cancer Cells and the Inhibitory Action of Resveratrol as A Potential Therapeutic Strategy.* International journal of molecular sciences, 2019. **20**(13): p. 3374.
241. Kim, H.J., et al., *Differential effects of interleukin-6 and -10 on skeletal muscle and liver insulin action in vivo.* Diabetes, 2004. **53**(4): p. 1060-7.
242. Docanto, M.M., et al., *Obesity-Associated Inflammatory Cytokines and Prostaglandin E2 Stimulate Glucose Transporter mRNA Expression and Glucose Uptake in Primary Human Adipose Stromal Cells.* J Interferon Cytokine Res, 2015. **35**(8): p. 600-5.
243. Rotter, V., I. Nagaev, and U. Smith, *Interleukin-6 (IL-6) induces insulin resistance in 3T3-L1 adipocytes and is, like IL-8 and tumor necrosis factor-alpha, overexpressed in human fat cells from insulin-resistant subjects.* J Biol Chem, 2003. **278**(46): p. 45777-84.
244. Albert, V., et al., *mTORC2 sustains thermogenesis via Akt-induced glucose uptake and glycolysis in brown adipose tissue.* EMBO Mol Med, 2016. **8**(3): p. 232-46.

245. Yoshizaki, T., et al., *SIRT1 exerts anti-inflammatory effects and improves insulin sensitivity in adipocytes.* Mol Cell Biol, 2009. **29**(5): p. 1363-74.
246. Chen, S., et al., *Resveratrol improves glucose uptake in insulin-resistant adipocytes via Sirt1.* J Nutr Biochem, 2018. **55**: p. 209-218.
247. Dawkins, M.J. and J.W. Scopes, *Non-shivering thermogenesis and brown adipose tissue in the human new-born infant.* Nature, 1965. **206**(980): p. 201-2.
248. Mowers, J., et al., *Inflammation produces catecholamine resistance in obesity via activation of PDE3B by the protein kinases IKKepsilon and TBK1.* Elife, 2013. **2**: p. e01119.
249. Reynisdottir, S., et al., *Catecholamine resistance in fat cells of women with upper-body obesity due to decreased expression of beta 2-adrenoceptors.* Diabetologia, 1994. **37**(4): p. 428-35.
250. Lee, Y.-E., et al., *Chronic resveratrol treatment protects pancreatic islets against oxidative stress in db/db mice.* PloS one, 2012. **7**(11): p. e50412-e50412.
251. Do, G.M., et al., *Resveratrol ameliorates diabetes-related metabolic changes via activation of AMP-activated protein kinase and its downstream targets in db/db mice.* Mol Nutr Food Res, 2012. **56**(8): p. 1282-91.
252. Masaki, T., et al., *Impaired response of UCP family to cold exposure in diabetic (db/db) mice.* Am J Physiol Regul Integr Comp Physiol, 2000. **279**(4): p. R1305-9.
253. Domouzoglou, E.M., et al., *Fibroblast growth factor 21 and thyroid hormone show mutual regulatory dependency but have independent actions in vivo.* Endocrinology, 2014. **155**(5): p. 2031-2040.
254. Gerhart-Hines, Z., et al., *The cAMP/PKA pathway rapidly activates SIRT1 to promote fatty acid oxidation independently of changes in NAD(+).* Mol Cell, 2011. **44**(6): p. 851-63.
255. Xu, C., et al., *Selective overexpression of human SIRT1 in adipose tissue enhances energy homeostasis and prevents the deterioration of insulin sensitivity with ageing in mice.* Am J Transl Res, 2013. **5**(4): p. 412-26.
256. Shin, S. and K.M. Ajuwon, *Lipopolysaccharide Alters Thermogenic and Inflammatory Genes in White Adipose Tissue in Mice Fed Diets with Distinct 18-Carbon Fatty-Acid Composition.* Lipids, 2018. **53**(9): p. 885-896.
257. Okla, M., et al., *Activation of Toll-like receptor 4 (TLR4) attenuates adaptive thermogenesis via endoplasmic reticulum stress.* J Biol Chem, 2015. **290**(44): p. 26476-90.
258. Goto, T., et al., *Proinflammatory cytokine interleukin-1beta suppresses cold-induced thermogenesis in adipocytes.* Cytokine, 2016. **77**: p. 107-14.
259. Fischer, K., et al., *Alternatively activated macrophages do not synthesize catecholamines or contribute to adipose tissue adaptive thermogenesis.* Nat Med, 2017. **23**(5): p. 623-630.
260. Shen, Z., et al., *Role of SIRT1 in regulation of LPS- or two ethanol metabolites-induced TNF-alpha production in cultured macrophage cell lines.* American journal of physiology. Gastrointestinal and liver physiology, 2009. **296**(5): p. G1047-G1053.
261. Wang, R., et al., *Sweroside Alleviated LPS-Induced Inflammation via SIRT1 Mediating NF-kappaB and FOXO1 Signaling Pathways in RAW264.7 Cells.* Molecules, 2019. **24**(5).
262. Zhang, H., et al., *Berberine suppresses LPS-induced inflammation through modulating Sirt1/NF-kappaB signaling pathway in RAW264.7 cells.* Int Immunopharmacol, 2017. **52**: p. 93-100.
263. Sarjeant, K. and J.M. Stephens, *Adipogenesis.* Cold Spring Harbor perspectives in biology, 2012. **4**(9): p. a008417-a008417.
264. Kajimura, S., P. Seale, and B.M. Spiegelman, *Transcriptional control of brown fat development.* Cell metabolism, 2010. **11**(4): p. 257-262.

265. Singh, B.K., et al., *Hepatic FOXO1 Target Genes Are Co-regulated by Thyroid Hormone via RICTOR Protein Deacetylation and MTORC2-AKT Protein Inhibition.* J Biol Chem, 2016. **291**(1): p. 198-214.
266. Yang, S.J., et al., *Sirt1 and Sirt6 mediate beneficial effects of rosiglitazone on hepatic lipid accumulation.* PLoS One, 2014. **9**(8): p. e105456.
267. Chuang, Y.C., et al., *Sirtuin 1 Regulates Mitochondrial Biogenesis and Provides an Endogenous Neuroprotective Mechanism Against Seizure-Induced Neuronal Cell Death in the Hippocampus Following Status Epilepticus.* Int J Mol Sci, 2019. **20**(14).
268. Houtkooper, R.H., E. Pirinen, and J. Auwerx, *Sirtuins as regulators of metabolism and healthspan.* Nat Rev Mol Cell Biol, 2012. **13**(4): p. 225-238.
269. Li, P., et al., *SIRT1 is required for mitochondrial biogenesis reprogramming in hypoxic human pulmonary arteriolar smooth muscle cells.* Int J Mol Med, 2017. **39**(5): p. 1127-1136.
270. Lee, J.H., et al., *The Role of Adipose Tissue Mitochondria: Regulation of Mitochondrial Function for the Treatment of Metabolic Diseases.* International journal of molecular sciences, 2019. **20**(19): p. 4924.
271. Lin, S., et al., *Sirtuins in mitochondrial stress: Indispensable helpers behind the scenes.* Ageing Res Rev, 2018. **44**: p. 22-32.
272. Mancini, G., et al., *Mitofusin 2 in Mature Adipocytes Controls Adiposity and Body Weight.* Cell Rep, 2019. **26**(11): p. 2849-2858.e4.
273. Wikstrom, J.D., et al., *Hormone-induced mitochondrial fission is utilized by brown adipocytes as an amplification pathway for energy expenditure.* The EMBO journal, 2014. **33**(5): p. 418-436.
274. Teruel, T., et al., *Rosiglitazone and retinoic acid induce uncoupling protein-1 (UCP-1) in a p38 mitogen-activated protein kinase-dependent manner in fetal primary brown adipocytes.* J Biol Chem, 2003. **278**(1): p. 263-9.
275. Petrovic, N., et al., *Chronic peroxisome proliferator-activated receptor gamma (PPARgamma) activation of epididymally derived white adipocyte cultures reveals a population of thermogenically competent, UCP1-containing adipocytes molecularly distinct from classic brown adipocytes.* J Biol Chem, 2010. **285**(10): p. 7153-64.
276. Seale, P., et al., *Transcriptional control of brown fat determination by PRDM16.* Cell metabolism, 2007. **6**(1): p. 38-54.
277. Koopmans, S.J., et al., *Antilipolytic action of insulin in adipocytes from starved and diabetic rats during adenosine-controlled incubations.* Endocrinology, 1989. **125**(6): p. 3044-50.
278. Nilsson, N.O., et al., *Regulation of adipose tissue lipolysis: effects of noradrenaline and insulin on phosphorylation of hormone-sensitive lipase and on lipolysis in intact rat adipocytes.* FEBS Lett, 1980. **111**(1): p. 125-30.
279. Stralfors, P., P. Bjorgell, and P. Belfrage, *Hormonal regulation of hormone-sensitive lipase in intact adipocytes: identification of phosphorylated sites and effects on the phosphorylation by lipolytic hormones and insulin.* Proc Natl Acad Sci U S A, 1984. **81**(11): p. 3317-21.
280. Lopez, M., et al., *Hypothalamic AMPK and fatty acid metabolism mediate thyroid regulation of energy balance.* Nat Med, 2010. **16**(9): p. 1001-8.
281. Bilezikian, J.P. and J.N. Loeb, *The influence of hyperthyroidism and hypothyroidism on alpha- and beta-adrenergic receptor systems and adrenergic responsiveness.* Endocr Rev, 1983. **4**(4): p. 378-88.
282. Iaglova, N.V. and T.T. Berezov, *[Regulation of thyroid and pituitary functions by lipopolysaccharide].* Biomed Khim, 2010. **56**(2): p. 179-86.
283. Beigneux, A.P., et al., *Sick euthyroid syndrome is associated with decreased TR expression and DNA binding in mouse liver.* Am J Physiol Endocrinol Metab, 2003. **284**(1): p. E228-36.

284. Boelen, A., et al., *Simultaneous changes in central and peripheral components of the hypothalamus-pituitary-thyroid axis in lipopolysaccharide-induced acute illness in mice.* J Endocrinol, 2004. **182**(2): p. 315-23.
285. Kondo, K., et al., *Inhibition of the Hypothalamic-Pituitary-Thyroid Axis in Response to Lipopolysaccharide Is Independent of Changes in Circulating Corticosteroids.* Neuroimmunomodulation, 1997. **4**(4): p. 188-194.
286. Suh, J.H., et al., *SIRT1 is a direct coactivator of thyroid hormone receptor β1 with gene-specific actions.* PloS one, 2013. **8**(7): p. e70097-e70097.
287. Akieda-Asai, S., et al., *SIRT1 Regulates Thyroid-Stimulating Hormone Release by Enhancing PIP5Kgamma Activity through Deacetylation of Specific Lysine Residues in Mammals.* PLoS One, 2010. **5**(7): p. e11755.
288. Broeders, E.P., et al., *Thyroid Hormone Activates Brown Adipose Tissue and Increases Non-Shivering Thermogenesis--A Cohort Study in a Group of Thyroid Carcinoma Patients.* PLoS One, 2016. **11**(1): p. e0145049.
289. Lin, J.Z., et al., *Pharmacological Activation of Thyroid Hormone Receptors Elicits a Functional Conversion of White to Brown Fat.* Cell reports, 2015. **13**(8): p. 1528-1537.

APPENDIX

Increased FGF21 in brown adipose tissue of tyrosine hydroxylase heterozygous mice: implications for cold adaptation[S]

Patricia Vázquez,[1,*,†,§] Catalina Hernández-Sánchez,[†,§] Carmen Escalona-Garrido,[*,§] Laura Pereira,[§,] Cristina Contreras,[††] Miguel López,[§§,***] Jesús Balsinde,[§,**] Flora de Pablo,[†,§] and Ángela M. Valverde[1,§,*]**

Alberto Sols Biomedical Research Institute (IIBm),* Consejo Superior de Investigaciones Científicas/Universidad Autónoma de Madrid (CSIC/UAM), Madrid, Spain; Centro de Investigaciones Biológicas,[†] Consejo Superior de Investigaciones Científicas, (CSIC) Madrid, Spain; Centro de Investigación Biomédica en Red de Diabetes y Enfermedades Metabólicas (CIBERdem),[§] Instituto de Salud Carlos III, Madrid, Spain; Instituto de Biología y Genética Molecular,** Consejo Superior de Investigaciones Científicas (CSIC), Universidad de Valladolid, Valladolid, Spain; Physiology Department,[††] Pharmacy School, Complutense University of Madrid, Madrid, Spain; NeurObesity Group,[§§] Department of Physiology, Centro Singular de Investigación en Medicine Molecular y Enfermedades Crónicas (CIMUS), University of Santiago de Compostela, Instituto de Investigación Sanitaria, Santiago de Compostela, Spain; and Centro de Investigación Biomédica en Red Fisiopatología de la Obesidad y Nutrición (CIBERobn),*** Santiago de Compostela, Spain

Abstract **Tyrosine hydroxylase (TH) catalyzes the first step in catecholamines synthesis. We studied the impact of reduced TH in brown adipose tissue (BAT) activation. In adult heterozygous ($Th^{+/-}$) mice, dopamine and noradrenaline (NA) content in BAT decreased after cold exposure. This reduced catecholaminergic response did not impair cold adaptation, because these mice induced uncoupling protein 1 (UCP-1) and maintained BAT temperature to a similar extent than controls ($Th^{+/+}$). Possible compensatory mechanisms implicated were studied. *Prdm16* and *Fgf21* expression, key genes in BAT activation, were elevated in $Th^{+/-}$ mice at thermoneutrality from day 18.5 of embryonic life. Likewise, plasma FGF21 and liver *Fgf21* mRNA were increased. Analysis of endoplasmic reticulum (ER) stress, a process that triggers elevations in FGF21, showed higher phospho-IRE1, phospho-JNK, and CHOP in BAT of $Th^{+/-}$ mice at thermoneutrality. Also, increased lipolysis in BAT of cold-exposure $Th^{+/-}$ mice was demonstrated by increased phosphorylation of hormone-sensitive lipase (HSL), as well as diacylglycerol (DAG) and FFA content.[F1r] Overall, these results indicate that the mild effects of *Th* haploinsufficiency on BAT function are likely due to compensatory mechanisms involving elevations in *Fgf21* and *Prdm16* and through adaptive changes in the lipid profile.**—Vázquez, P., C. Hernández-Sánchez, C. Escalona-Garrido, L. Pereira, C. Contreras, M. López, J. Balsinde, F. de Pablo, and Á. M. Valverde. **Increased FGF21 in brown adipose tissue of tyrosine hydroxylase heterozygous mice: implications for cold adaptation. *J. Lipid Res.* 2018.** 59: **2308–2320.**

Supplementary key words catecholamines • diabetes • fatty acids • metabolic disease • obesity • fibroblast growth factor 21

Obesity is an important global health problem that results from an imbalance between energy intake and expenditure (1). Three types of adipose cells (white, brown, and beige) have been described with different developmental origins, cell-specific gene expression, and distinct functions (2). Whereas white adipocytes accumulate energy in the form of triglyceride depots that are distributed in a large fat droplet and contain few mitochondria, brown

This work was supported by Ministry of Science, Technology and Innovation Grants BFU 2010-15868 (to F.d.P. and C.H-S.), SAF2015-73000-EXP and SAF2016-80883 (to J.B.), and SAF2015-65267-R (to A.M.V.). The authors also acknowledge Instituto de Salud Carlos III Grant INFLAMES PIE14/00045 (cofunded by European Regional Development Fund "Investing in your Future") (to A.M.V.) and Centro de Investigación Biomédica en Red de Diabetes y Enfermedades Metabólicas Asociadas. This is an initiative of the Instituto de Salud Carlos III. The authors acknowledge Ministerio de Ciencia e Innovación-Consejo Superior de Investigaciones Científicas and the European Social Fund for the JAE-DOC contract (2013 to P.V.) and a Centro de Investigación Biomédica en Red de Diabetes y Enfermedades Metabólicas Asociadas contract (2016 to P.V.).

Manuscript received 20 March 2018 and in revised form 10 October 2018.

Published, JLR Papers in Press, October 23, 2018
DOI https://doi.org/10.1194/jlr.M085209

Abbreviations: BAT, brown adipose tissue; CE, cholesteryl ester; DiO2, deiodinase 2; e18.5, embryonic day 18.5; ER, endoplasmic reticulum; FGF21, fibroblast growth factor 21; HSL, hormone-sensitive lipase; iWAT, inguinal white adipose tissue; NA, noradrenaline; TAG, triacylglycerol; TH, tyrosine hydroxylase; UCP-1, uncoupling protein 1; WAT, white adipose tissue.

[1]To whom correspondence should be addressed.
e-mail: patrivazquez@iib.uam.es (P.V.); avalverde@iib.uam.es (Á.M.V.)

[S] The online version of this article (available at http://www.jlr.org) contains a supplement.

adipocytes present multilocular fat droplets and contain a higher number of mitochondria (3). Brown adipocytes are responsible for nonshivering thermogenesis by uncoupling the proton gradient generated by oxidative phosphorylation and ATP synthesis, due to the specific expression of the uncoupling protein 1 (UCP-1) in the inner mitochondrial membrane. This brings out energy dissipation as heat (4). Recently, a third class of adipocytes has been identified and termed "beige" or "brite" adipose cells. They reside within white adipose tissue (WAT), but can acquire characteristics of brown adipocytes under different environmental or pharmacological stimuli (5, 6).

It is known that brown adipose tissue (BAT), which is maintained in adult humans (7), uses glucose and FAs as fuel (8), and its activity is reduced in obese and diabetic individuals (1). For this reason, understanding the mechanisms involved in the control of BAT activity could lead to improving the treatment of these patients. BAT is a highly vascularized and innervated tissue (9). Classical activation of thermogenesis occurs via noradrenaline (NA) released from the sympathetic nervous system, which binds to β3 adrenergic receptors (*Adrb3*) present in the brown adipocyte. Receptor activation increases intracellular cAMP, which induces lipolysis, leading to the release of FFAs that, in turn, activate UCP-1. In fact, the surgical denervation of interscapular BAT reduced the activation of brown adipocytes after cold exposure (10).

Tyrosine hydroxylase (TH) catalyzes the first and rate-limiting step in the synthesis of catecholamines. A null mutation in the mouse *Th* gene causes a depletion of catecholamines and lethality at prenatal stages because of cardiovascular failure (11–13). Additionally, this mutation has an impact on pancreatic β-cell development (14). Recently, it was reported that haploinsufficiency of *Th* increases mouse half-life by protecting against age-associated hypertension (15). In contrast, patients with pheochromocytomas that produce and secrete large amounts of catecholamines (NA or adrenaline) present body weight loss, among other abnormalities (16). The importance of the sympathetic stimulation in BAT for cold adaptation has also been shown because adrenal medullar TH is involved in the response to stress induced by cold (17). More recently, a role of TH on the antiinflammatory responses triggered by cold exposure has been reported (18).

BAT is also a secretory tissue that releases different molecules (batokines) with autocrine and paracrine roles (19). One of these batokines is the fibroblast growth factor 21 (FGF21), which was initially identified as a hepatokine and is considered, rather than a mitogenic factor, an atypical FGF due to its role in endocrine function over carbohydrates and FA metabolism (20). *Fgf21*-null mice have reduced hepatic FA oxidation and a concomitant increase in liver fat accumulation (21). More recently, it has been demonstrated that FGF21 is highly produced and released by BAT after cold exposure (19). FGF21 also impacts "browning" of WAT, and, as a consequence, it can improve lipid metabolic disorders and insulin resistance (22).

In this study, we examined how *Th*-haploinsufficiency in mice affects the response to the stress induced by cold exposure in BAT. Our data show that, despite reduced catecholamine levels, *Th*-haploinsufficiency does not impair cold adaptation in mice. We also demonstrate that this unaltered adaptive response is associated with increased FGF21 and increased lipolytic capacity in BAT. This evidence suggests a new mechanism for cold adaptation in a context of low adrenergic signaling.

MATERIALS AND METHODS

Animal procedures

All procedures involving animals were approved by the Ethics Committee of Consejo Superior de Investigaciones Científicas and Comunidad de Madrid in accordance with the European Union guidelines. The C57BL6/J *Th* heterozygote mouse strain was kindly provided by R. D. Palmiter (University of Washington, Seattle, WA) (12). All the studies were performed using littermates. We used three groups named adult mice (2–3 months), embryos at embryonic day (e) 18.5, and aged mice (15 months). The animals were maintained on 12 h:12 h light-dark cycles and at 22°C and allowed free access to standard rodent chow and water ad libitum. The adult mice were randomly divided into two experimental groups: One group was maintained at thermoneutral conditions (29°C), and the other one was subjected to cold challenge (4°C) for 6 h. Prior to the cold exposure, the two groups of mice were housed at 29°C for at least 1 week. Body weight and rectal temperature were measured in all mice before and after cold exposure.

Preparation of tissue extracts and Western blot

BAT samples were homogenized at 4°C in lysis buffer (in mmol/l: 50 Tris HCl, 2 EGTA, 10 EDTA, 2 orthovanadate, 50 NaF, and 1 sodium pyrophosphate) containing 1% (w/v) Triton X-100 and a mini EDTA-free protease inhibitor tablet. Samples were homogenized in lysis buffer using The Brinkmann Pt 10/35 Polytron. Tissue lysates were centrifuged at 20,000 *g* for 30 min at 4°C, and the supernatants were collected and stored at −80°C until further analysis. Total protein extracts (15–30 μg) were loaded into Any kD Criterion TGX Precast Gels (catalog no. 567-1124, Bio-Rad, CA) and transferred onto PVDF membranes (catalog no. 170-4157, Bio-Rad) for 14 min at 25 V using a Trans-Blot Turbo Transfer System (Bio-Rad). Membranes were activated with 100% methanol for 2 min and blocked for 1 h at room temperature with 5% (w/v) BSA or nonfat milk in TBS-Tween 20 (0.05% w/v) and incubated overnight at 4°C with primary Abs: anti-TH (1:500) (Millipore, AB 152), anti-β-III tubulin (1:500) (covance MRB 435P), anti-CHOP [1:4,000, GADD153(R-20) sc-793], anti-pJNK (1:4,000, Cell Signaling 9251S), anti-JNK (1:1,000, Santa Cruz, SC-571), anti-pIRE (1:1,000 NB100-2323), anti-pHSL-s660 (1:1,000, Cell Signaling 4126S), and anti-HSL (1:1,000, Cell Signaling 4107S). After washing, the membranes were reblotted with anti-β-actin (1:5,000) (Sigma, St. Louis, catalog no. A5316), anti-tubulin (1:2,000) (Sigma, T4026), or vinculin (7F9) (1:25,000) (Santa Cruz, 73614) Abs as loading controls. Additionally, we used Ponceau Red as a loading control (Sigma). Abs were detected with the corresponding HRP-labeled secondary Abs (Pierce, Rockford, IL) and visualized with the Super Signal West Pico chemiluminescent substrate (Pierce). Different experiments were quantified by scanning densitometry using ImageJ software.

RNA isolation and quantitative real-time PCR

Total RNA from BAT, inguinal WAT (iWAT), or liver was extracted using TRIzol reagent, and reverse transcription was

performed using the High-Capacity cDNA Reverse Transcription Kit (Applied Biosystems, Waltham, MA) using random primers and Superscript III enzyme according to the manufacturer's instructions. Quantitative real-time PCR was performed in a 7900 HT-Fast real-time PCR (Life Technologies) with SYBR or Taqman Universal PCR Master Mix. The following probes and primers are listed in **Table 1**. Results are expressed using the $2^{-\Delta\Delta Ct}$ (cycle threshold) quantification method. Results were normalized according to expression levels of *Tbp* or *Rlbp0* RNA.

Immunohistochemistry

For immunohistochemical analysis, a piece of BAT was fixed overnight at 4°C in 4% (w/v) paraformaldehyde, then rinsed with PBS and dehydrated through an ethanol gradient before embedding in paraffin for microtome sectioning. Paraffin sections (7–8 μm) were dewaxed in Histo-Clear-II (CONDA, Madrid, Spain) and rehydrated through a descending series of ethanol dilutions. Antigen retrieval was achieved by microwaving [twice for 5 min at 600 W in 0.01 mmol/l citrate buffer (pH 6) with 0.05% (w/v) Tween-20] followed by three washes in PBS. Tissue sections were permeabilized with PBS-Triton X-100 (2% w/v). Nonspecific binding was blocked with 3% (v/v) donkey immunoserum (Sigma, Diegen, Belgium) in PBS-Triton X-100 (1% w/v). Sections were incubated overnight at 4°C with primary Abs (1:100) in blocking buffer and then incubated with secondary Abs labeled with either Alexa 568 or Alexa 647 dyes (1:250) (Molecular Probes, Carlsbad, CA). Nuclei were labeled with 4',6-diamidino-2-phenylindole (DAPI) (Molecular Probes). Images were collected by confocal microscopy (Leica TCS-SP5; Leica Microsystems, Wetzlar, Germany). H&E staining was performed in paraffin sections of BAT of $Th^{+/+}$ and $Th^{+/-}$ mice for morphological analysis. Images were collected with an Axiophot light microscope (Zeiss) with a 40× objective. To estimate the size of the lipid droplets, we used ImageJ software (The National Institutes of Health; https://imagej.nih.gov/ij/). First, the color images were converted to black and white images and then inverted. The percentage of white area versus area total was calculated. To estimate the cell density, we counted the nuclei per section in at least 10 fields of different 5 μm BAT sections of each animal. Around 2,000 total nuclei per mouse were counted.

ELISA

Catecholamines were determined by ELISA (3-CAT research ELISA, BA E-5600 LDN, Nordhorn, Germany) following the manufacturer's instructions. One piece of BAT of each animal was homogenized in buffer (0.01 N HCl, 1 mM EDTA, and 4 mM $Na_2S_2O_5$), and following centrifugation at 17,949 *g* for 15 min at 4°C, the supernatants were collected and stored at −80°C. All measurements were normalized by protein concentration. FGF21 plasma levels were quantified by ELISA (catalog no. RD291108200R, BioVendor) following the manufacturer's instructions.

In vitro experiments

The immortalized brown preadipocyte cell line was generated from mouse interscapular BAT and fully differentiated to brown adipocytes following the protocol previously described (23). Cells (day 7 of differentiation) were incubated with or without 1 μg/ml recombinant FGF21 (catalog no. RD272108100-B, BioVendor) for 18 h. Then, cells were treated with 0.1 μM NA for a further 4 h. After washing with PBS, cells were lysed in lysis buffer (10 mM Tris-HCl, 5 mM EDTA, 50 mM NaCl, 1% Triton X-100, 30 mM sodium pyrophosphate, 50 mM fluoride, 1 mM phenylmethanelsulfonyl fluoride, and 10 μg/ml protease inhibitors, pH 7.4–7.6). After centrifugation at 12,000 *g* for 7 min at 4°C, the total protein in supernatants was quantified with the BCA Protein Assay Kit. The phosphorylation of HSL (Ser-660) and UCP-1 protein levels were analyzed by Western blot using vinculin (7F9) (1:25,000) (Santa Cruz, catalog no. 73614) as a loading control. The amount of glycerol released by the cells to the culture medium after the different treatments was analyzed using a commercial kit (F628, Sigma).

Analysis of FFAs and triacylglycerol levels

Plasma glycerol levels were quantified using a commercial kit (catalog no. F6428, Sigma) and plasma nonesterified ("free" or unsaturated) FAs (FFAs) were quantified using commercial kits (catalog nos. 919898, 91696, and 91096, WAKo Chemicals, Richmond, VA), according to the manufacturer´s instructions. Samples were normalized by protein concentration.

Lipidomic analysis

Total lipids from BAT were extracted according to Folch et al. (24). Lipid classes were separated by TLC. For neutral lipid separation, a solvent mixture consisting of *n*-hexane/diethyl ether/acetic acid (70:30:1, v/v/v) was used as the mobile phase (25). The various neutral lipid classes cholesteryl esters (CEs), triacylglycerol

TABLE 1. Primer sequences and Taqman probes used in real-time PCR

Gene	Forward	Reverse	Taqman Probe
Atf2	5′-CCGTTGCTATTCCTGCATCAA-3′	5′-TTGCTTCTGACTGGACTGGTT-3′	
Ppara	5′-AGAGCCCCATCTGTCCTCTC- 3′	5′-ACTGGTAGTCTGCAAAACCAAA-3′	
Rplp0(364B)	5′-ACTGGTCTAGGACCCGAGAAG-3′	5′-TCCCACCTTGTCTCCAGTCT-3′	
Adrb3			Mm02601819_g1
Adipoq			Mm00456425_m1
Agr1			Mm00475988_m1
β *klotho*			Mm00473122_m1
Bmp8b			Mm00432115_g1
Cebpa			Mm00514283_s1
Cidea			Mm00432554_m1
Cox8b			Mm00432648_m1
Cpt1a			Mm01231183_m1
Dio2			Mm00515664_m1
Fgf21			Mm00840165_g1
Fgfr1			Mm00438930_m1
Nos2			Mm00440502_m1
Pparg			Mm00440940_m1
Ppargc1a			Mm01208835_m1
Prdm16			Mm00712556_m1
Tbp			Mm00446971_m1
Ucp1			Mm01244861_m1

(TAG), diacylglycerol (DAG), and FFAs were scraped and extracted from the silica with 1 ml of chloroform/methanol (1:2, v/v) followed by 1 ml of chloroform/methanol (2:1, v/v). The CE, TAG, and DAG fractions were treated with 500 µl of 0.5 M KOH in methanol for 60 min at 37°C to obtain FA methyl esters. To neutralize, 500 µl of 0.5 M HCl was added. The FFA fraction was treated with 450 µl of MeOH in 0.5% HCl for 20 min at 45°C, and neutralized with one vol of 0.14 M KOH and 500 µl of deionized water was added. Extraction of the FA methyl esters was carried out with 2 ml of *n*-hexane, and 1 µl was subjected to GC/MS analysis as previously described (26, 27), using an Agilent 7890A gas chromatograph coupled to an Agilent 5975C mass-selective detector operated in electron impact mode (EI, 70 eV), equipped with an Agilent 7693 autosampler and an Agilent DB23 column (60 m length × 0.25 mm internal diameter × 0.15 µm film thickness). Data analysis was carried out with the Agilent G1701EA MSD Productivity Chemstation software, revision E.02.00.

Measurement of skin temperature surrounding BAT

The skin temperature surrounding BAT was recorded with an infrared camera (B335:Compact-Infrared-Thermal-Imaging-Camera; FLIR; West Malling, Kent, UK) and analyzed with a specific software package (FLIR-Tools-Software; FLIR), as previously shown (28, 29). Pictures were taken at both thermoneutral conditions or immediately after cold exposure (6 h).

Indirect calorimetry

$Th^{+/+}$ *and* $Th^{+/-}$ mice at 2–3 months of age were individually housed and maintained at thermoneutrality (28–29°C) under a 12:12 h light-dark cycle in a Phenomaster system (TSE Systems, Bad Homburg, Germany). Food and water were provided ad libitum in the appropriated devices. Mice were acclimated to the chambers for at least 24 h and then monitored for an additional 48 h period. After that, mice were placed into the cold room (4°C) for 6 h and then immediately moved to their original cages of the TSE system to continue the measurement for additional 24 h.

Statistical analysis

Statistical analyses were performed using a Student's *t*-test, a nonparametric test (Mann-Whitney *U* test), or two-way ANOVA with Bonferroni's post hoc test. All statistical analyses were performed with GraphPad Prism software version 5 (GraphPad Software, Inc., San Diego, CA). Statistical significance was set at * $P < 0.05$, ** $P < 0.01$, and *** $P < 0.001$, $Th^{+/-}$ versus $Th^{+/+}$ groups; and $^{\#}P < 0.05$, $^{\#\#}P < 0.01$, and $^{\#\#\#}P < 0.001$, 4°C versus 29°C groups.

RESULTS

Characterization of BAT in $Th^{+/+}$ and $Th^{+/-}$ mice at thermoneutrality

We first characterized adult (3 month old) $Th^{+/-}$ and $Th^{+/+}$ mice at thermoneutral conditions (29°C). As shown in **Fig. 1A**, no differences between the two genotypes of mice were found in body weight and rectal temperature. Likewise, temperature of skin surrounding BAT, energy expenditure, and respiratory exchange ratio were similar in the two genotypes (Fig. 1B and supplemental Fig. S1). As expected, Western blot analysis revealed a 50% decrease of TH protein content in the BAT of $Th^{+/-}$ mice compared with levels of their $Th^{+/+}$ littermates (Fig. 1C). The analysis of paraffin sections showed reduced TH-positive immunostaining

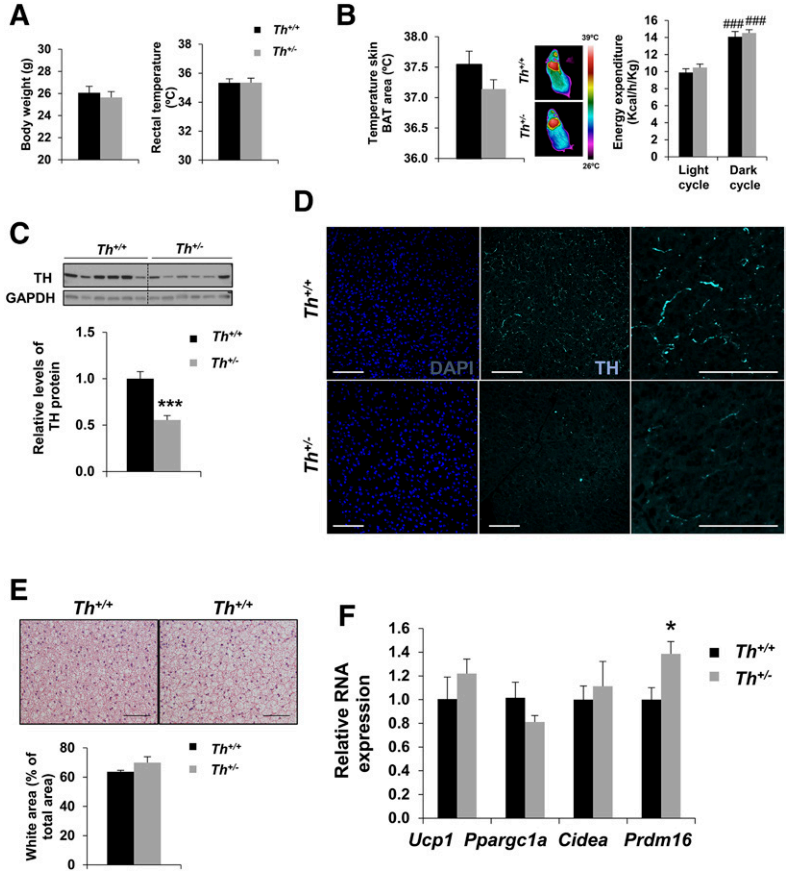

Fig. 1. Characteristics of $Th^{+/-}$ mice in thermoneutrality. Body weight and rectal temperature (A), skin temperature surrounding BAT, and energy expenditure (B) were measured in $Th^{+/+}$ and $Th^{+/-}$ mice housed 1 week at 29°C. C: Western blot analysis and quantification of lysates from BAT collected from $Th^{+/+}$ and $Th^{+/-}$ adult mice showing TH levels using GAPDH as a loading control. D: Representative immunohistochemistry of TH at paraffin sections. Nuclei were stained with DAPI (blue) and TH+ fibers were detected by immunostaining (cyan). E: Representative sections of BAT from $Th^{+/+}$and $Th^{+/-}$ mice stained with H&E and quantification of the percentage of white area versus total area. F: Quantitative RT-PCR of thermogenic gene expression in BAT. The graph represents the relative gene expression compared with $Th^{+/+}$ mice. The data were normalized by *Tbp* RNA expression. Data are mean ± SEM. n = 5–10/group in A–C, n = 5–7/group in E, and n = 4–10/group in F. Mann-Whitney *U* test was used. *$P < 0.05$; ***$P < 0.001$ (between $Th^{+/+}$ and $Th^{+/-}$ mice); ###$P < 0.001$ (between each genotypes in dark cycle versus light cycle). Scale bars: 75 µm.

in the BAT of $Th^{+/-}$ mice (Fig. 1D), although no major differences were observed in the amount of innervating fibers, as shown by Western blot and immunohistochemistry for β-III-tubulin (supplemental Fig. S2A, B). H&E staining revealed similar BAT histology in $Th^{+/-}$ and $Th^{+/+}$ mice (Fig. 1E), although a slight increase in white area (Fig. 1E) and decreased cell density (supplemental Fig. S2C) was found in $Th^{+/-}$ mice. We next analyzed the expression of some key genes for BAT identity. Whereas the expression of thermogenic-related genes such as *Ucp1*, *Ppargc1a* (which encodes PGC1α), and *Cidea* was similar between the two genotypes, the levels of *Prdm16*, a relevant gene in brown fat adipogenesis, were significantly higher in the $Th^{+/-}$ mice than in their WT littermates (Fig. 1F). Further characterization of BAT-related gene expression showed no differences between the two genotypes of mice at thermoneutral conditions (supplemental Fig. S2D).

$Th^{+/-}$ mice responded normally to cold exposure

Next, we addressed a possible impact of reduced TH expression in cold adaptation in young mice at 3 months of age. After 6 h of cold exposure (4°C), the BAT of $Th^{+/-}$ mice maintained lower TH protein levels than their WT littermates (supplemental Fig. S3A). Concordantly, dopamine and NA content, determined by ELISA, were diminished in BAT of $Th^{+/-}$ mice after 6 h of cold exposure (**Fig. 2A**). Similar to thermoneutrality, H&E-stained sections revealed more white area in $Th^{+/-}$ compared with $Th^{+/+}$ mice after cold exposure (supplemental Fig. S3B). Surprisingly, body weight (Fig. 2B), rectal temperature, and temperature of skin surrounding BAT (Fig. 2C, D), all indicators of cold adaptation, were similar in both genotypes of mice. Moreover, energy expenditure was elevated in $Th^{+/-}$ mice immediately after cold exposure and also during the following night period (Fig. 2E). Notably, despite the impaired catecholamine production, the expression of *Ucp1* and *Ppargc1a* was similarly increased in $Th^{+/-}$ and $Th^{+/+}$ mice upon cold challenge (Fig. 2F, G). It has been previously reported that cold exposure does not modify RNA expression levels of *Prdm16* and *Cidea* (30). In agreement with these results, no differences were found in either $Th^{+/+}$or $Th^{+/-}$ mice (Fig. 2H, I), although *Prdm16* levels, which were elevated at 29°C in the $Th^{+/-}$ mice, decreased to levels of the $Th^{+/+}$ mice after cold exposure (Fig. 2H). Body weight, rectal temperature, and the expression of *Ucp1* and *Ppargc1a* remained similar in both genotypes after more prolonged (16 h) cold exposure (supplemental Fig. S4). These results indicate that reduction of catecholamine levels does not alter the BAT acute response to cold. Notably, this effect was unrelated to compensatory changes in adrenergic signaling, because no differences between both genotypes were found in *Adrb3* RNA at basal conditions. Indeed, *Adrb3* RNA levels decreased similarly in both groups of mice after cold challenge (supplemental Fig. S5A), as reported (31–33).

Besides UCP-1, BAT thermogenesis relies on deiodinase 2 (DiO2) enzymatic activity (34). The conversion of T4 into

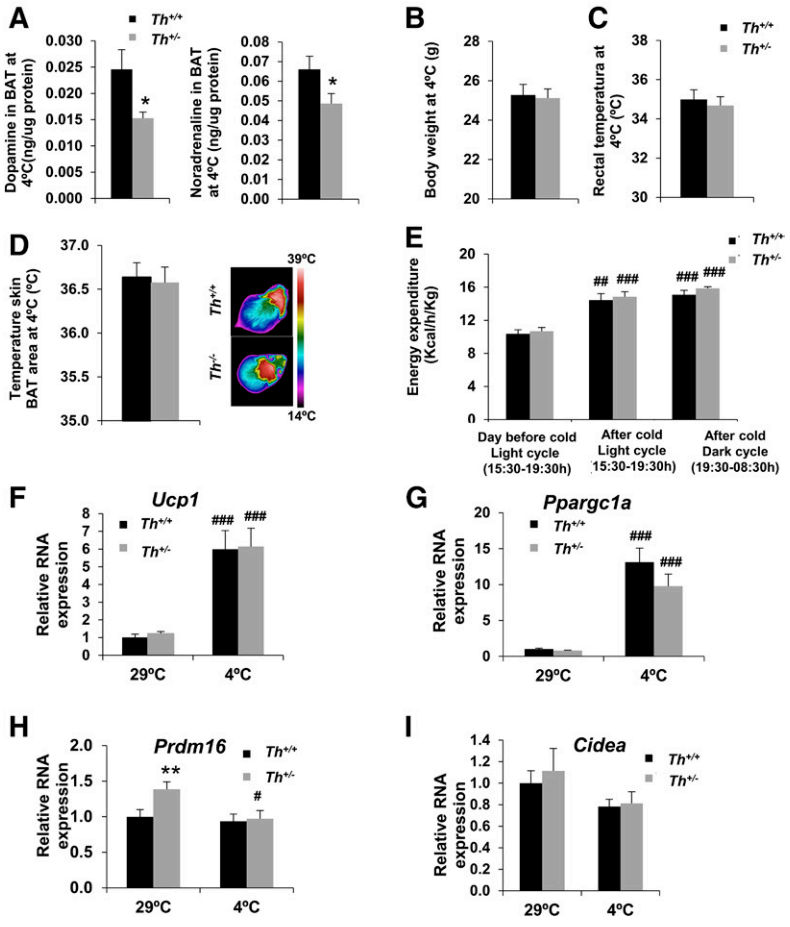

Fig. 2. $Th^{+/-}$ mice showed similar adaptation to cold exposure in BAT compared with $Th^{+/+}$ mice. A: The graphs represent the amount of dopamine or NA (ng/μg protein) after 6 h of cold exposure in BAT. B, C: Body weight and rectal temperature after cold exposure. D: Skin temperature surrounding BAT measured after 6 h of cold exposure. E: Energy expenditure was recorded during 4 h at both thermoneutrality and after 6 h of cold exposure (left and middle bars), as well as in the next night cycle as detailed in the graph (right bars). F–I: Quantitative RT-PCR of different thermogenic genes RNA expression in BAT. The data were normalized by *Tbp* RNA expression. All data were relative to $Th^{+/+}$ at 29°C. Data are mean ± SEM. n = 6/group in A, n = 10/group in B and C, n = 5–9/group in D and E, and n = 4–11/group in F–I. Unpaired *t*-test was used for catecholamine content analysis, and Mann-Whitney *U* test was used for gene expression analysis. A, F–I: $*P < 0.05$; $**P < 0.01$ (between $Th^{+/+}$ and $Th^{+/-}$ mice); $\#P < 0.05$; $\#\#P < 0.01$; $\#\#\#P < 0.001$ (between each genotype at 4°C and 29°C). E: $\#\#P < 0.01$; $\#\#\#P < 0.001$ [between light (15:30–19:30) or dark (19:30–08:30) periods after cold exposure (middle or right columns, respectively) versus light period (15:30–19:30) the day before cold exposure (left columns)].

T3 by DiO2 amplifies the cAMP response after adrenergic stimulation, thereby enhancing lipolysis and mitochondrial thermogenesis (35). In this context, we analyzed *Dio2* RNA levels and found similar basal levels at thermoneutrality in both genotypes, which increased to the same extent (about 100-fold) after cold exposure (supplemental Fig. S5B). Similarly, additional BAT-related gene expression analysis indicated no differences between the two genotypes after 6 h of cold exposure (supplemental Fig. S5C).

Th haploinsufficiency does not impact browning of iWAT

Prdm16 has been described to be essential in activating the thermogenic phenotype in inguinal subcutaneous depots (36). During cold acclimation, iWAT has been also reported to play a role in thermogenesis (37). The analysis of RNA levels of *Ucp1*, *Ppargc1a*, *Cidea*, and *Prdm16* in iWAT in 3 month old mice showed a similar expression pattern to that found in BAT at 29°C in the two genotypes (**Fig. 3A**; compare with Fig. 1F), a significant increase being detected exclusively in *Prdm16* in $Th^{+/-}$ mice (Fig. 3A). Moreover, upon cold exposure, the iWAT of *Th* heterozygous animals responded similarly to that of the controls, displaying comparable RNA levels of *Ucp1*, *Ppargc1a*, *Prdm16*, and *Cidea* genes (Fig. 3B–E), as well as levels of *Adrb3* and *Fgf21* (supplemental Fig. S6A, B).

Th haploinsufficiency increases FGF21 in BAT

After finding unaltered the key players in the thermogenic response in BAT and iWAT in $Th^{+/-}$ mice, we investigated possible factors that could compensate the catecholamine deficit. We hypothesized that unbalanced catecholamine levels may represent a stress with an impact on the expression of the batokine *Fgf21,* as occurred in the liver under lipotoxic conditions (38). As shown in **Fig. 4A**, significantly higher *Fgf21* RNA levels were found in BAT of $Th^{+/-}$ animals at 3 months of age at thermoneutral conditions. As occurred with other thermogenic genes, cold exposure increased BAT *Fgf21* expression to a similar extent in both genotypes of mice (Fig. 4A). Furthermore, plasma FGF21 levels were increased about 5-fold in $Th^{+/-}$ mice at thermoneutrality (Fig. 4B) in parallel to an elevated expression of *Fgf21* in the liver (Fig. 4C), the main source of circulating FGF21 (39). These results showed that, at thermoneutrality, $Th^{+/-}$ mice displayed an increase in both local BAT production and circulating levels of FGF21, suggesting a close relationship between the mild phenotype of *Th* haploinsufficency and the elevated *Fgf21* expression. Conversely, upon cold exposure plasma FGF21 and hepatic *Fgf21* RNA levels did not change in WT mice as described (40, 41), whereas both parameters decreased in $Th^{+/-}$ mice up to the levels of the WT. In BAT, FGF21 signals through heterocomplexes of the receptors bklotho (*Klb*) and FGFR1 (42). The analysis of the expression of both coreceptors at thermoneutrality and after cold exposure showed no differences in their RNA levels (Fig. 4D, E).

We next checked the timing of the onset of *Fgf21* upregulation. The analysis of BAT in e18.5 embryos showed

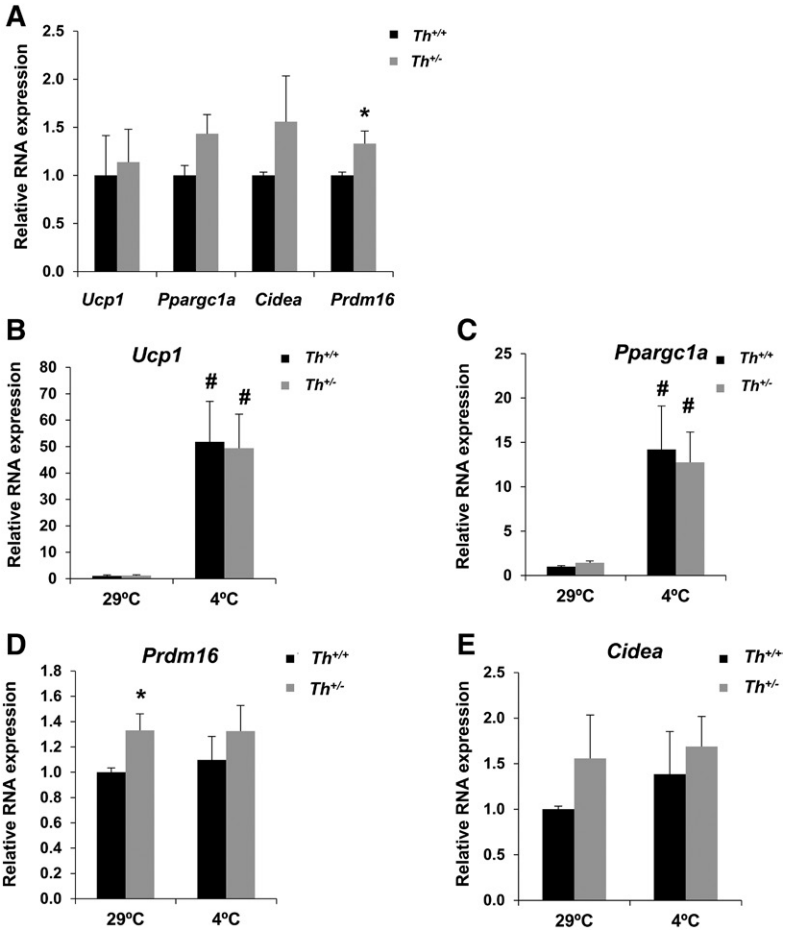

Fig. 3. $Th^{+/-}$ mice showed a similar adaptation to cold exposure in iWAT compared with $Th^{+/+}$ mice. A: Analysis by quantitative RT-PCR of different browning markers in iWAT at 29°C. All data were relative to RNA levels of $Th^{+/+}$. B–E: Quantitative RT-PCR of different thermogenic gene RNA expression in iWAT at 29°C and 4°C. All data were relative to $Th^{+/+}$ mice at 29°C. All expression data were normalized with *Tbp* RNA expression. Data are mean ± SEM. n = 4 or 5/group. Mann-Whitney *U* test was used. $*P < 0.05$ (between $Th^{+/+}$ and $Th^{+/-}$ mice); $\#P < 0.05$ (between each genotype at 4°C and 29°C).

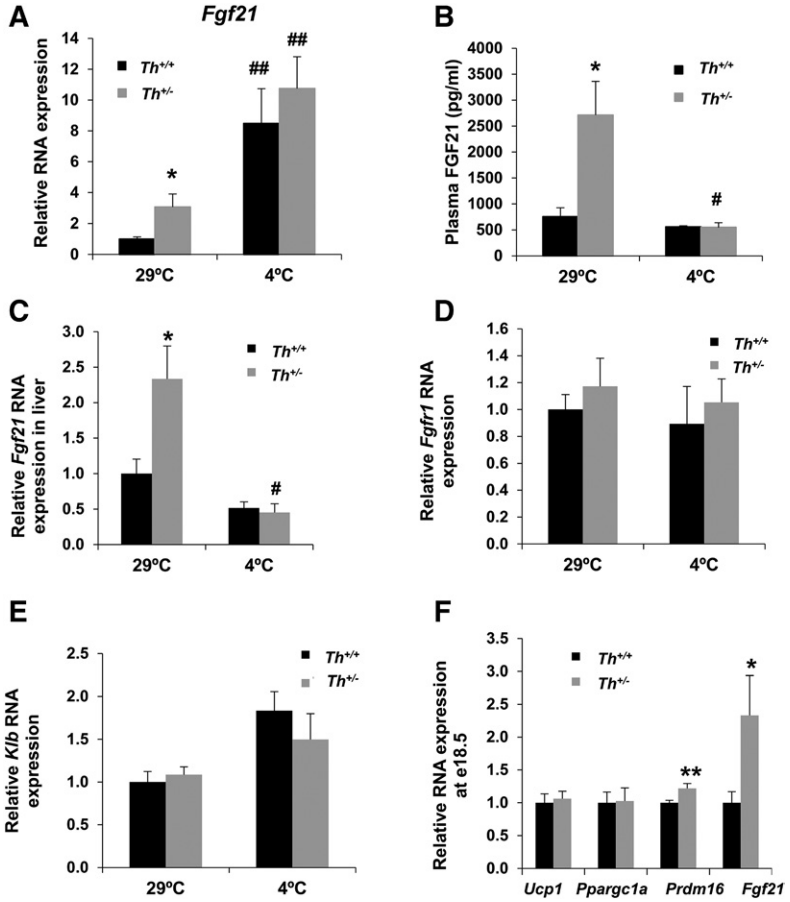

Fig. 4. *Th* haploinsufficiency increased *Fgf21* expression in BAT. A: Quantitative RT-PCR of *Fgf21* RNA expression in BAT at 29°C and 4°C. B: Content of FGF21 protein in plasma in thermoneutral and cold conditions measured by ELISA. C: Relative expression of *Fgf21* by quantitative RT-PCR analysis in livers at 29°C and 4°C. D, E: Relative expression of FGF21 coreceptors (*Fgfr1* and *Klb*) by quantitative RT-PCR analysis in BAT at 29°C and 4°C. All data were relative to RNA levels of $Th^{+/+}$ mice at 29°C. F: Quantitative RT-PCR of different browning markers RNA expression in BAT of e18.5 embryos. All data were relative to $Th^{+/+}$ animals. Data are mean ± SEM. n = 9 or 10/group in A, n = 9/group in B, n = 10/group in C, n = 4 or 5/group in D and E, and n = 12–20/group in F. All expression data were normalized with *Tbp* RNA expression. Mann-Whitney *U* test was used. *$P < 0.05$; **$P < 0.01$ (between $Th^{+/+}$ mice and $Th^{+/-}$ mice group); #$P < 0.05$; ##$P < 0.01$ (between each genotype at 4°C and 29°C).

higher levels of *Fgf21* RNA in the $Th^{+/-}$ embryos than in their WT littermates (Fig. 4F). Similarly, *Prdm16* RNA was increased at e18.5 in the $Th^{+/-}$ BAT, as described in adult mice. However, we did not observe differences in the RNA levels of the thermogenic-related genes *Ucp1* and *Ppargc1a*. Of note, a trend toward an increase in embryonic plasma and liver FGF21 content was detected in $Th^{+/-}$ embryos (supplemental Fig. S7A, B). In addition, the BAT of $Th^{+/-}$ old animals (15 months of age) showed a nearly significant increase in *Fgf21* RNA levels (supplemental Fig. S7C), reinforcing a possible role of this batokine in $Th^{+/-}$ mice.

$Th^{+/-}$ mice show increased BAT ER stress levels at thermoneutrality

To further explore a possible mechanism by which *Fgf21* expression was elevated in the BAT of $Th^{+/-}$ mice, we focused on endoplasmic reticulum (ER) stress, one of the well-known triggers of FGF21 expression (39, 43). The analysis of CHOP protein levels in BAT extracts showed a significant increase of this ER stress long-term marker in $Th^{+/-}$ mice at 3 months in thermoneutral conditions (**Fig. 5A**). However, in agreement with the absence of differences between both genotypes in *Fgf21* RNA levels in BAT after cold exposure, no differences in CHOP levels were found after cold challenge. Likewise, the relative phosphorylation of IRE1 and JNK, important signaling mediators in the unfolded protein response, was also increased in the BAT of $Th^{+/-}$ mice respect to the $Th^{+/-}$ control mice only at thermoneutrality (Fig. 5B, C).

Increased lipolytic capacity and TAG availability in the BAT of $Th^{+/-}$ mice

To get additional insight into the compensatory response of mice with reduced catecholamines during cold adaptation, we examined BAT lipolytic activity by the analysis of phosphorylation of the hormone-sensitive lipase (HSL) at the regulatory residue Ser-660. **Figure 6A** shows that although no differences were detected at thermoneutrality, HSL Ser-660 phosphorylation was significantly higher in the BAT of $Th^{+/-}$ mice at 3 months compared with that of the $Th^{+/+}$ controls after 6 h of cold exposure. This result indicated that a sustained lipolytic capacity of BAT in $Th^{+/-}$ mice was probably contributing to the activation of UCP-1. However, plasma glycerol and FFA levels were similar in both genotypes of mice (data not shown). To explain these results, we performed in vitro experiments using differentiated brown adipocytes previously characterized (23). As an experimental approach to mimic in vivo *Th* haploinsufficiency, brown adipocytes were stimulated with submaximal (0.1 μM) concentrations of NA for 4 h with or without a pretreatment with recombinant FGF21 (1 μg/ml) for 18 h. As shown in Fig. 6B, there was an increase in phospho-HSL in brown adipocytes pretreated with FGF21 prior to NA stimulation. Importantly, under these experimental conditions, a significant elevation was found in glycerol released to the culture medium (Fig. 6C) and, more importantly, in UCP-1 protein levels (Fig. 6D).

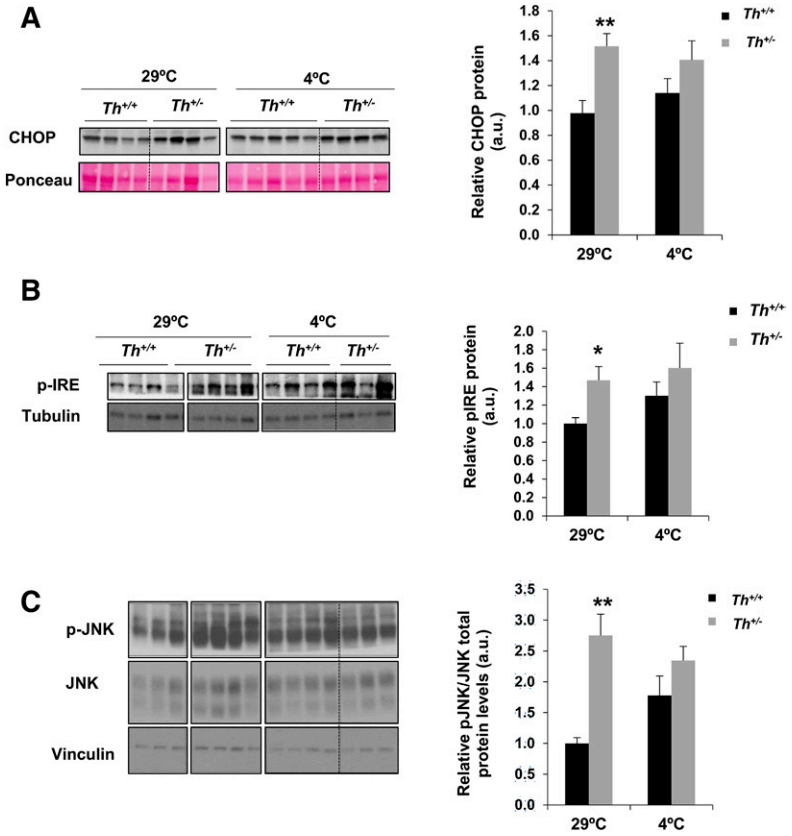

Fig. 5. The ER stress-mediated signaling was altered in BAT of $Th^{+/-}$ mice in thermoneutrality conditions. A: Western blot analysis and quantification of CHOP protein. Ponceau Red was used as a loading control. B, C: Western blot analysis and quantification of pIRE or pJNK, respectively. Tubulin, total JNK, and vinculin were used as loading controls. All data are relative to $Th^{+/+}$ mice densitometry at 29°C. Data are mean ± SEM. n = 4–10/group in A, and n = 3–10/group in B. Two-way ANOVA was used. $*P < 0.05$; $**P < 0.01$. a.u., arbitrary units.

To further investigate in detail the profile of different lipidic species in the two groups of mice, we performed a mass-spectrometry-based lipidomic study of total neutral lipid classes in BAT samples from mice at thermoneutral and cold conditions (**Tables 2** and **3** and **Fig. 7A**–D). Interestingly, at thermoneutrality, several FAs in TAG and DAG fractions were significantly elevated in $Th^{+/-}$ mice, suggesting that increased overall fat content, and likely lipotoxicity, which would lead to elevated ER stress in the BAT of $Th^{+/-}$ mice. Conversely, the levels of FFAs C16:0 (palmitic acid) and C18:0 (stearic acid) were reduced. The cholesteryl ester (CE) content showed no differences between the two genotypes (Fig. 7D). After cold exposure, the $Th^{+/-}$ animals maintained higher levels of TAG or DAG species compared with those of their WT littermates. In addition, the total amount of FFAs was higher in $Th^{+/-}$ BAT (Fig. 7C) compared with levels of the $Th^{+/+}$ BAT with significant increases in palmitic acid (Table 3).

DISCUSSION

Catecholamines are essential neurotransmitters for the maintenance of physiological homeostasis under basal and stress conditions. In BAT, catecholamines are responsible for the activation of nonshivering thermogenesis (5, 9). Also, dopamine has been shown to directly impact mitochondrial mass and thermogenesis in brown adipocytes (44). Whereas human pathologies with elevations of circulating catecholamines, such as pheochromocytoma, concur with excessive BAT activation (16, 45, 46), much less is known about the impact of reduced catecholamine biosynthesis in BAT functionality. The present work, using a murine preclinical model of global *Th* haploinsufficiency, has revealed an unexpectedly normal cold adaptation under reduced catecholamine availability. The early and life-long increase in FGF21 levels of $Th^{+/-}$ mice represents a potential new insight on the compensatory mechanisms that may operate in $Th^{+/-}$ BAT to ensure its full activation upon cold challenge.

The unique role of the sympathetic-mediated NA stimulation of BAT was highlighted by Lee et al. (10) showing that ablation of TH protein in BAT by denervation abolished UCP-1 induction during cold stress. More recently, a role of adipose tissue M2 macrophages or eosinophils as an additional catecholamine source in BAT or iWAT has been postulated (47–50), although controversies have also been raised regarding the contribution of these immune cells in secreting enough catecholamines to promote BAT activation or browning of iWAT (48). In our model, we found unexpected mild consequences of the global reduction of TH expression in BAT thermogenesis since $Th^{+/-}$ mice adapted normally to cold stress as manifested by the maintenance of rectal temperature, body weight, temperature of the skin surrounding BAT, and *Ucp1* induction. In particular, the significant increase in the expression of the thermogenic-related gene *Prdm16* that was detected in BAT of $Th^{+/-}$ mice suggests an early relationship between this master regulator of BAT development and TH. *Prdm16* has been previously described as a critical transcriptional

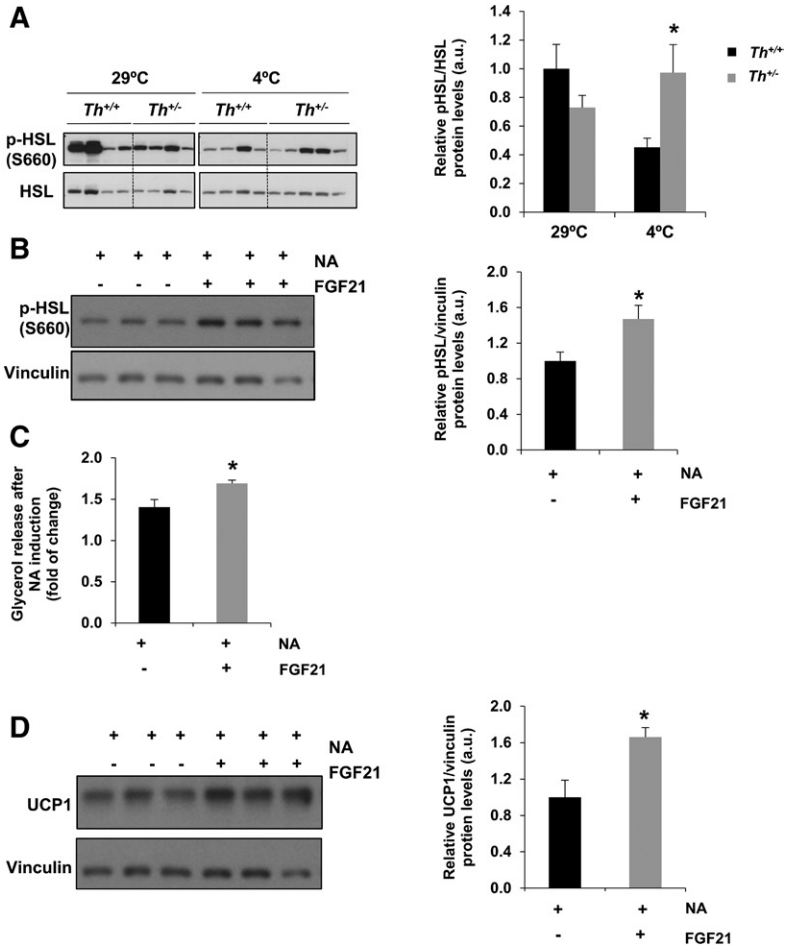

Fig. 6. Evaluation of phosphorylation of HSL in BAT of $Th^{+/+}$ and $Th^{+/-}$ mice and brown adipocytes stimulated with FGF21. A: Western blot analysis and quantification of phospho-HSL (S660) in BAT extracts. Total HSL was used as loading control. All data are relative to $Th^{+/+}$ mice densitometry at 29°C. B: Western blot analysis and quantification of phospho-HSL (S660) in differentiated brown adipocytes with or without FGF21 pretreatment (1 µg/ml for 18 h) before the addition of 0.1 µM NA for 4 h. Vinculin was used as a loading control. C: Quantification of glycerol release after NA stimulation under conditions described in B. D: UCP-1 protein levels under conditions described in B. Two-way ANOVA was used in Western blot analysis in A, and Mann-Whitney *U* test was used in B–D. $*P < 0.05$ (between $Th^{+/+}$ mice and $Th^{+/-}$ mice group or brown adipocytes pretreated or not with FGF21 and stimulated with NA between +FGF21 and –FGF21); $*P < 0.05$ (between each genotype). Data are mean ± SEM. n = 7–11/group in A, n = 5–7/group in B and D, and n = 3 independent experiments in C. a.u., arbitrary units.

regulator of thermogenesis that is essential for the differentiation of brown adipocytes, as well as for the browning process in beige fat cells (9, 51). A recent study has demonstrated that PRDM16 stabilizes the response to β3-adrenergic signaling to increase thermogenic gene expression and mitochondrial biogenesis in subcutaneous WAT by interacting with the transcription factor HLX (52). In agreement with these data, the iWAT of $Th^{+/-}$ mice showed an increase in *Prdm16* RNA levels, supporting the relevance of TH in the process of browning. These results were reinforced by the upregulation of *Prdm16* even in the embryonic BAT of $Th^{+/-}$ mice, indicating that during embryonic development, these mice have already activated compensatory mechanisms to overcome *Th* haploinsufficiency; *Prdm16* seems to be a relevant contributor to this phenotype. In fact, catecholamines are required to respond to stress during gestation. In this regard, it has been reported that *Th*-null mice die at midgestation due to cardiovascular failure (11, 12). This effect is likely a consequence of their inability to adapt to the gestational hypoxia (53). However, additional posttraslational modifications in PRDM16 such as sumoylation that primes its stabilization, as recently reported (54), cannot be excluded.

Beside changes in *Prdm16* gene expression, the largest changes found in BAT of $Th^{+/-}$ mice were detected in FGF21, which was significantly elevated under thermoneutral conditions compared with the $Th^{+/+}$ controls; this effect was maintained during aging. This batokine has been previously found to be increased under various situations including starvation, ketogenic diets, and overfeeding, as well as by deficiency or excess in dietary proteins and carbohydrates, respectively (43, 55). Although FGF21 is mainly synthetized and released by the liver (56), the BAT is another source of FGF21, where it has autocrine/paracrine functions related to upregulation of UCP-1 and thermogenesis (19, 57). We also found elevated FGF21 in the plasma from $Th^{+/-}$ mice, an effect that could be explained by the increased liver expression and secretion. Altogether, these results suggest that less TH availability induces regulatory mechanisms in BAT, likely mediated by *Prdm16* and/or *Fgf21,* which overall appear to compensate thermoregulatory changes and lead to normal adaptation to cold.

We next explored the possible molecular mechanisms that could explain the elevation of FGF21 in $Th^{+/-}$ mice. Several recent reports have demonstrated that the expression of *Fgf21* in the liver is induced by ER stress (58, 59). However, *Fgfr1* deficiency in WAT led to a sustained lipid droplet expansion and ER stress (42). In BAT, a direct relationship between ER stress and FGF21 levels has been well described under cold exposure or after birth during suckling (60). In agreement with the involvement of ER stress in the $Th^{+/-}$ phenotype, elevation of several ER stress markers was detected in the BAT of $Th^{+/-}$ mice at thermoneutrality, allowing us to speculate that ER stress in BAT,

TABLE 2. FA distribution profile of TAG, DAG, FFA, or CE in BAT from $Th^{+/+}$ and $Th^{+/-}$ mice

	Percent of $Th^{+/-}$ Content vs. $Th^{+/+}$ (29°C), %	Statistical Significance
TAG		
14:00	189.71	ns
16:0	175.58	***
16:1n-9	151.91	ns
16:1n-7	201.60	**
18:0	141.10	ns
18:1n-9	195.98	***
18:1n-7	22.24	ns
18:2n-6	164.42	**
18:3n-3	155.56	ns
20:0	187.69	ns
20:1n-9	230.35	ns
20:1n-7	70.53	ns
20:2n-6	319.92	ns
20:3n-6	281.93	ns
20:4n-6	153.95	ns
22:0	191.53	ns
22:1n-9	280.14	ns
CE		
16:0	99.99	ns
16:1n-9	87.56	ns
18:0	103.69	ns
18:1n-9	194.13	ns
DAG		
14:00	97.02	ns
16:0	144.27	***
16:1n-9	110.07	ns
16:1n-7	156.77	ns
18:0	132.05	ns
18:1n-9	137.05	*
18:2n-6	122.32	ns
FFA		
14:0	44.79	ns
16:0	56.52	***
16:1n-9	48.05	ns
16:1n-7	49.12	ns
18:0	64.87	***
18:1	73.91	ns
18:2	78.66	ns
20:0	36.71	ns
20:1n-9	66.85	ns
20:4n-6	57.76	ns
22:0	4.86	ns

Percentage of FAs in BAT of $Th^{+/-}$ versus $Th^{+/+}$ mice at 29°C. Data are mean ± SEM. n = 10 or 11/group. Two-way ANOVA was used. ns, not significant. *$P < 0.05$; **$P < 0.01$; ***$P < 0.001$.

TABLE 3. FA distribution profile of TAG, DAG, FFA, or CE in BAT from $Th^{+/+}$ and $Th^{+/-}$ mice

	Percent of $Th^{+/-}$ Content vs. $Th^{+/+}$ (4°C), %	Statistical Significance
TAG		
14:00	181.71	ns
16:0	173.28	***
16:1n-9	140.46	ns
16:1n-7	159.13	ns
18:0	188.45	ns
18:1n-9	175.79	***
18:1n-7	154.75	ns
18:2n-6	151.93	***
18:3n-3	136.76	ns
20:0	135.04	ns
20:1n-9	156.04	ns
20:1n-7	153.91	ns
20:3n-6	509.70	ns
20:4n-6	165.72	ns
22:0	71.27	ns
22:1n-9	618.31	ns
CE		
16:0	115.01	ns
16:1n-9	78.46	ns
18:0	103.95	ns
18:1n-9	100.63	ns
DAG		
14:0	105.54	ns
16:0	149.88	***
16:1n-9	45.13	ns
16:1n-7	143.62	ns
18:0	142.08	**
18:1n-9	141.47	***
18:2n-6	112.74	ns
20:0	110.29	ns
FFA		
14:0	121.51	ns
16:0	129.40	***
16:1n-9	142.10	ns
16:1n-7	148.56	ns
18:0	121.47	ns
18:1	166.77	ns
18:2	98.75	ns
20:0	73.58	ns
20:1n-9	99.28	ns
20:4n-6	58.98	ns
22:0	63.89	ns

Percentage of FAs in BAT of $Th^{+/-}$ versus $Th^{+/+}$ mice after 6 h exposure to cold at 4°C. Data are mean ± SEM. n = 10 or 11 per group. Two-way ANOVA was used. ns, not significant. *$P < 0.05$; * $P < 0.01$; ** $P < 0.001$.

probably due to reduced *Th* expression, may upregulate *Fgf*21.

Catecholamines are the inducers of lipolysis in adipose tissues. Zeng et al. (61) described that sympathetic denervation (or glucocorticoid administration) increased lipid accumulation in adipocytes due to defective lipolysis. In addition, lipolysis requires the activation of lipases such as adipose triglyceride lipase and HSL, as well as their stable association with the lipid droplets (62, 63). The analysis of phosphorylation of HSL at Ser-660, which is a direct indicator of its enzymatic activity, revealed elevations in the BAT of $Th^{+/-}$ mice after cold exposure, regardless of lower catecholamine levels. This response contrasted with decreased Ser-660 HSL phosphorylation in cold-exposed $Th^{+/+}$ mice, indicating that at least 6 h after cold exposure, the time at which the experiments were performed, the lipolytic activity due to HSL-mediated phosphorylation might be more sustained in the BAT of $Th^{+/-}$ mice, which would explain their maintained thermogenic capacity within a decreased catecholamine milieu. Interestingly, the stimulation of differentiated brown adipocytes with a submaximal dose of NA in the presence of FGF21 increased lipolysis and UCP-1 protein levels, reinforcing the in vivo data and indicating that the relationship between FGF21 and HSL might be important in this setting.

To find a possible explanation for such an effect, we analyzed TAG, DAG, and FFAs content in BAT from the two genotypes of mice. Again, substantial differences were found between genotypes. Decreased *Th* expression was accompanied by higher DAG and TAG content in BAT under basal conditions, and, importantly, TAG, DAG, and FFA content was increased after cold exposure compared with the levels of the $Th^{+/+}$ mice. This suggests an increased lipolysis rate, in accordance with the higher HSL phosphorylation. Interestingly, the differences observed in FFA levels

Supplemental Material can be found at:
http://www.jlr.org/content/suppl/2018/10/23/jlr.M085209.DC1.html

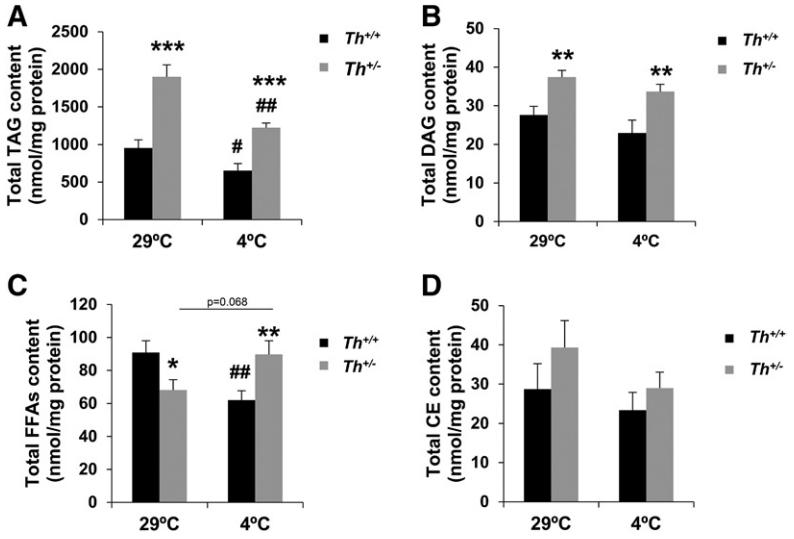

Fig. 7. TH heterozygous mice had different content of TAG, DAG, and FFAs at thermoneutrality or after cold exposure. The graph represents total content of TAG (A), DAG (B), FFAs (C), and CE (D) analyzed by lipidomics in BAT at 29°C or 4°C. The data were expressed by nmol/mg protein. Data are mean ± SEM. n = 10 or 11/group. Mann-Whitney *U* test was used in lipidomic analysis. *$P < 0.05$; **$P < 0.01$ (between $Th^{+/+}$ mice and $Th^{+/-}$ mice group); #$P < 0.05$; ##$P < 0.01$ (between each genotype at 4°C and 29°C).

upon cold exposure (i.e., significant increase in BAT from $Th^{+/-}$ mice was observed only for the saturated palmitic acid) suggest that BAT may adapt to temperature changes by modifying the ratio saturated versus unsaturated/polyunsaturated FFAs within neutral lipids via selective lipolysis. Thus, the loosening of acyl chain packing within TAG and DAG may provide BAT with a mechanism to finely adjust to temperature changes, as needed. These results suggest a more rapid replenishment and remodeling of fat stores in the lipid droplets in the BAT of $Th^{+/-}$ mice. In addition, the increased levels of highly lipotoxic species, such as DAG, might explain the existence of lipotoxicity and, subsequently, ER stress in *Th* haploinsufficiency. These complex mechanisms are likely to be necessary to respond to the stress of cold exposure in conditions of decreased *Th* expression because, as stated above, $Th^{+/-}$ mice adapted to cold with a similar pattern of thermogenic-related gene expression, body weight, and rectal and skin surrounding BAT temperature as the $Th^{+/+}$ mice. This adaptation may also be facilitated by elevated lipolytic substrates DAG and TAG under basal conditions, thereby yielding more availability of FFAs that ultimately are the fuels for UCP-1 activation in BAT (64). In fact, the histological analysis revealed an increase in fat (white) area in BAT from $Th^{+/-}$ mice at both thermoneutrality and cold conditions. Moreover, the lack of differences in plasma levels of FFAs and glycerol content between the two genotypes of mice (results not shown) could indicate that the FFAs resulting from lipolysis are being burned in the brown adipocytes as fuels generating the proton gradient in the mitochondria, rather than being exported to the circulation.

In summary, our results suggest the existence of an inverse relationship between *Th* expression and *Prdm16* and *Fgf21* in BAT under basal conditions that might operate under stress conditions in $Th^{+/-}$ mice to maintain BAT functionality/homeostasis. Thus, in a situation of *Th* haploinsufficiency, the elevation in FGF21, probably as a result of the subsequent lipotoxic-induced ER stress, together with the elevation in PRDM16 might ensure a normal response to cold exposure of BAT as well as iWAT. This compensation is likely facilitated by the higher content of DAG and TAG and increased activity of HSL in BAT from $Th^{+/-}$ mice, yielding more availability of FFAs that ultimately are the fuels for UCP-1 activation and thermogenesis. This evidence indicates a new mechanism for cold adaptation in a context of low adrenergic signaling, that may be therapeutically relevant. However, further research is needed to unravel whether additional intermediate factors are involved.

The authors thank personnel from the Centro de Investigaciones Biológicas (Madrid), A. Robles for technical assistance, and M. T. Seisdedos for assistance with confocal microscopy. The authors acknowledge the valuable input of F. Villarroya (University of Barcelona) in the discussion of the results.

REFERENCES

1. Lowell, B. B., and B. M. Spiegelman. 2000. Towards a molecular understanding of adaptive thermogenesis. *Nature.* **404:** 652–660.
2. Cinti, S. 2012. The adipose organ at a glance. *Dis. Models Mechanisms.* **5:** 588–594.
3. Carobbio, S., V. Pellegrinelli, and A. Vidal-Puig. 2017. Adipose tissue function and expandability as determinants of lipotoxicity and the metabolic syndrome. *In* Obesity and Lipotoxicity. A. B. Engin and A. Engin, editors. Springer International Publishing, Cham, Switzerland. **960:** 161–196.
4. Bhatt, P. S., W. S. Dhillo, and V. Salem. 2017. Human brown adipose tissue—function and therapeutic potential in metabolic disease. *Curr. Opin. Pharmacol.* **37:** 1–9.
5. Wankhade, U. D., M. Shen, H. Yadav, and K. M. Thakali. 2016. Novel browning agents, mechanisms, and therapeutic potentials of brown adipose tissue. *BioMed Res. Int.* **2016:** 2365609.
6. Chu, D-T., and B. Gawronska-Kozak. 2017. Brown and brite adipocytes: same function, but different origin and response. *Biochimie.* **138:** 102–105.
7. Lee, P., J. T. Zhao, M. M. Swarbrick, G. Gracie, R. Bova, J. R. Greenfield, J. Freund, and K. K. Y. Ho. 2011. High prevalence of brown adipose tissue in adult humans. *J. Clin. Endocrinol. Metab.* **96:** 2450–2455.
8. Bartelt, A., O. T. Bruns, R. Reimer, H. Hohenberg, H. Ittrich, K. Peldschus, M. G. Kaul, U. I. Tromsdorf, H. Weller, C. Waurisch, et al. 2011. Brown adipose tissue activity controls triglyceride clearance. *Nat. Med.* **17:** 200–205.
9. Bargut, T. C. L., M. B. Aguila, and C. A. Mandarim-de-Lacerda. 2016. Brown adipose tissue: updates in cellular and molecular biology. *Tissue Cell.* **48:** 452–460.

10. Lee, Y-H., A. P. Petkova, A. A. Konkar, and J. G. Granneman. 2015. Cellular origins of cold-induced brown adipocytes in adult mice. *FASEB J.* **29:** 286–299.
11. Kobayashi, K., S. Morita, H. Sawada, T. Mizuguchi, K. Yamada, I. Nagatsu, T. Hata, Y. Watanabe, K. Fujita, and T. Nagatsu. 1995. Targeted disruption of the tyrosine hydroxylase locus results in severe catecholamine depletion and perinatal lethality in mice. *J. Biol. Chem.* **270:** 27235–27243.
12. Zhou, Q-Y., C. J. Quaife, and R. D. Palmiter. 1995. Targeted disruption of the tyrosine hydroxylase gene reveals that catecholamines are required for mouse fetal development. *Nature.* **374:** 640–643.
13. Rios, M., B. Habecker, T. Sasaoka, G. Eisenhofer, H. Tian, S. Landis, D. Chikaraishi, and S. Roffler-Tarlov. 1999. Catecholamine synthesis is mediated by tyrosinase in the absence of tyrosine hydroxylase. *J. Neurosci.* **19:** 3519–3526.
14. Vázquez, P., A. M. Robles, F. de Pablo, and C. Hernández-Sánchez. 2014. Non-neural tyrosine hydroxylase, via modulation of endocrine pancreatic precursors, is required for normal development of beta cells in the mouse pancreas. *Diabetologia.* **57:** 2339–2347.
15. Gamella-Pozuelo, L., M. T. Grande, M. Clemente-Lorenzo, C. Murillo-Gómez, F. De Pablo, J. M. López-Novoa, and C. Hernández-Sánchez. 2017. Tyrosine hydroxylase haploinsufficiency prevents age-associated arterial pressure elevation and increases half-life in mice. *Biochim. Biophys. Acta Mol. Basis Dis.* **1863:** 113–120.
16. Nagano, G., H. Ohno, K. Oki, K. Kobuke, T. Shiwa, M. Yoneda, and N. Kohno. 2015. Activation of classical brown adipocytes in the adult human perirenal depot is highly correlated with PRDM16–EHMT1 complex expression. *PLoS One.* **10:** e0122584.
17. Tümer, N., and J. S. Larochelle. 1995. Tyrosine hydroxylase expression in rat adrenal medulla: Influence of age and cold. *Pharmacol. Biochem. Behav.* **51:** 775–780.
18. Vargovic, P., G. Manz, and R. Kvetnansky. 2016. Continuous cold exposure induces an anti-inflammatory response in mesenteric adipose tissue associated with catecholamine production and thermogenin expression in rats. *Endocr. Regul.* **50:** 137–144.
19. Villarroya, F., R. Cereijo, J. Villarroya, and M. Giralt. 2017. Brown adipose tissue as a secretory organ. *Nat. Rev. Endocrinol.* **13:** 26–35.
20. Xie, T., and P. S. Leung. 2017. Fibroblast growth factor 21: a regulator of metabolic disease and health span. *Am. J. Physiol. Endocrinol. Metab.* **313:** E292–E302.
21. Liu, L., C. Zhao, Y. Yang, X. Kong, T. Shao, L. Ren, X. Zhuang, B. Yin, G. Dryden, C. McClain, et al. 2017. Fibroblast growth factor 21 deficiency attenuates experimental colitis-induced adipose tissue lipolysis. *Gastroenterol. Res. Pract.* **2017:** 3089378.
22. Gimeno, R. E., and D. E. Moller. 2014. FGF21-based pharmacotherapy – potential utility for metabolic disorders. *Trends Endocrinol. Metab.* **25:** 303–311.
23. García-Casarrubios, E., C. de Moura, A. I. Arroba, N. Pescador, M. Calderon-Dominguez, L. Garcia, L. Herrero, D. Serra, S. Cadenas, F. Reis, et al. 2016. Rapamycin negatively impacts insulin signaling, glucose uptake and uncoupling protein-1 in brown adipocytes. *Biochim. Biophys. Acta.* **1861:** 1929–1941.
24. Folch, J., M. Lees, and G. H. S. Stanley. 1957. A simple method for the isolation and purification of total lipides from animal tissues. *J. Biol. Chem.* **226:** 497–509.
25. Diez, E., J. Balsinde, M. Aracil, and A. Schüller. 1987. Ethanol induces release of arachidonic acid but not synthesis of eicosanoids in mouse peritoneal macrophages. *Biochim. Biophys. Acta.* **921:** 82–89.
26. Guijas, C., G. Pérez-Chacón, A. M. Astudillo, J. M. Rubio, L. Gilde-Gómez, M. A. Balboa, and J. Balsinde. 2012. Simultaneous activation of p38 and JNK by arachidonic acid stimulates the cytosolic phospholipase A2-dependent synthesis of lipid droplets in human monocytes. *J. Lipid Res.* **53:** 2343–2354.
27. Guijas, C., C. Meana, A. M. Astudillo, M. A. Balboa, and J. Balsinde. 2016. Foamy monocytes Are enriched in cis-7-hexadecenoic fatty acid (16:1n-9), a possible biomarker for early detection of cardiovascular disease. *Cell Chem. Biol.* **23:** 689–699.
28. Martínez de Morentin, P. B., I. González-García, L. Martins, R. Lage, D. Fernández-Mallo, N. Martínez-Sánchez, F. Ruíz-Pino, J. Liu, D. A. Morgan, L. Pinilla, et al. 2014. Estradiol regulates brown adipose tissue thermogenesis via hypothalamic AMPK. *Cell Metab.* **20:** 41–53.
29. Martínez-Sánchez, N., P. Seoane-Collazo, C. Contreras, L. Varela, J. Villarroya, E. Rial-Pensado, X. Buqué, I. Aurrekoetxea, T. C. Delgado, R. Vázquez-Martínez, et al. 2017. Hypothalamic AMPK-ER stress-JNK1 axis mediates the central actions of thyroid hormones on energy balance. *Cell Metab.* **26:** 212–229.e12.
30. Festuccia, W. T., P-G. Blanchard, T. B. Oliveira, J. Magdalon, V. A. Paschoal, D. Richard, and Y. Deshaies. 2012. PPARγ activation attenuates cold-induced upregulation of thyroid status and brown adipose tissue PGC-1α and D2. *Am. J. Physiol. Regul. Integr. Comp. Physiol.* **303:** R1277.
31. Vatner, D. E., S. F. Vatner, J. Nejima, N. Uemura, E. E. Susanni, T. H. Hintze, and C. J. Homcy. 1989. Chronic norepinephrine elicits desensitization by uncoupling the beta-receptor. *J. Clin. Invest.* **84:** 1741–1748.
32. Granneman, J. G. 1992. Effects of agonist exposure on the coupling of beta 1 and beta 3 adrenergic receptors to adenylyl cyclase in isolated adipocytes. *J. Pharmacol. Exp. Ther.* **261:** 638.
33. Bengtsson, T., K. Redegren, A. D. Strosberg, J. Nedergaard, and B. Cannon. 1996. Down-regulation of β3 adrenoreceptor gene expression in brown fat cells is transient and recovery is dependent upon a short-lived protein factor. *J. Biol. Chem.* **271:** 33366–33375.
34. López, M., C. V. Alvarez, R. Nogueiras, and C. Diéguez. 2013. Energy balance regulation by thyroid hormones at central level. *Trends Mol. Med.* **19:** 418–427.
35. Obregon, M-J. 2014. Adipose tissues and thyroid hormones. *Front. Physiol.* **5:** 479.
36. Seale, P. 2015. Transcriptional regulatory circuits controlling brown fat development and activation. *Diabetes.* **64:** 2369–2375.
37. Keipert, S., M. Kutschke, M. Ost, T. Schwarzmayr, E. M. van Schothorst, D. Lamp, L. Brachthäuser, I. Hamp, S. E. Mazibuko, S. Hartwig, et al. 2017. Long-term cold adaptation does not require FGF21 or UCP1. *Cell Metab.* **26:** 437–446.e5.
38. Maratos-Flier, E. 2017. Fatty liver and FGF21 physiology. *Exp. Cell Res.* **360:** 2–5.
39. Gómez-Sámano, M. Á., M. Grajales-Gómez, J. M. Zuarth-Vázquez, M. F. Navarro-Flores, M. Martínez-Saavedra, Ó. A. Juárez-León, M. G. Morales-García, V. M. Enríquez-Estrada, F. J. Gómez-Pérez, and D. Cuevas-Ramos. 2017. Fibroblast growth factor 21 and its novel association with oxidative stress. *Redox Biol.* **11:** 335–341.
40. Hondares, E., R. Iglesias, A. Giralt, F. J. Gonzalez, M. Giralt, T. Mampel, and F. Villarroya. 2011. Thermogenic activation induces FGF21 expression and release in brown adipose tissue. *J. Biol. Chem.* **286:** 12983–12990.
41. Flachs, P., K. Adamcova, P. Zouhar, C. Marques, P. Janovska, I. Viegas, J. G. Jones, K. Bardova, M. Svobodova, J. Hansikova, et al. 2017. Induction of lipogenesis in white fat during cold exposure in mice: link to lean phenotype. *Int. J. Obes. (Lond.).* **41:** 372–380.
42. Ye, M., W. Lu, X. Wang, C. Wang, J. L. Abbruzzese, G. Liang, X. Li, and Y. Luo. 2016. FGF21-FGFR1 coordinates phospholipid homeostasis, lipid droplet function, and ER stress in obesity. *Endocrinology.* **157:** 4754–4769.
43. Jiang, S., C. Yan, Q-c. Fang, M-l. Shao, Y-l. Zhang, Y. Liu, Y-p. Deng, B. Shan, J-q. Liu, H-t. Li, et al. 2014. Fibroblast growth factor 21 is regulated by the IRE1Î±-XBP1 branch of the unfolded protein response and counteracts endoplasmic reticulum stress-induced hepatic steatosis. *J. Biol. Chem.* **289:** 29751–29765.
44. Kohlie, R., N. Perwitz, J. Resch, S. M. Schmid, H. Lehnert, J. Klein, and K. A. Iwen. 2017. Dopamine directly increases mitochondrial mass and thermogenesis in brown adipocytes. *J. Mol. Endocrino.* **58**: 57–66.
45. Wang, Q., M. Zhang, G. Ning, W. Gu, T. Su, M. Xu, B. Li, and W. Wang. 2011. Brown adipose tissue in humans is activated by elevated plasma catecholamines levels and is inversely related to central obesity. *PLoS One.* **6:** e21006.
46. Frontini, A., A. Vitali, J. Perugini, I. Murano, C. Romiti, D. Ricquier, M. Guerrieri, and S. Cinti. 2013. White-to-brown transdifferentiation of omental adipocytes in patients affected by pheochromocytoma. *Biochim. Biophys. Acta.* **1831:** 950–959.
47. Qiu, Y., K. D. Nguyen, J. I. Odegaard, X. Cui, X. Tian, R. M. Locksley, R. D. Palmiter, and A. Chawla. 2014. Eosinophils and type 2 cytokine signaling in macrophages orchestrate development of functional beige fat. *Cell.* **157:** 1292–1308.
48. Fischer, K., H. H. Ruiz, K. Jhun, B. Finan, D. J. Oberlin, V. van der Heide, A. V. Kalinovich, N. Petrovic, Y. Wolf, C. Clemmensen, et al. 2017. Alternatively activated macrophages do not synthesize catecholamines or contribute to adipose tissue adaptive thermogenesis. *Nat. Med.* **23:** 623–630.
49. Nguyen, K. D., Y. Qiu, X. Cui, Y. P. S. Goh, J. Mwangi, T. David, L. Mukundan, F. Brombacher, R. M. Locksley, and A. Chawla. 2011. Alternatively activated macrophages produce catecholamines to sustain adaptive thermogenesis. *Nature.* **480**: 104–108.
50. Qiu, Y., K. D. Nguyen, J. I. Odegaard, X. Cui, X. Tian, R. M. Locksley, R. D. Palmiter, and A. Chawla. 2014. Eosinophils and type

2 cytokine signaling in macrophages orchestrate development of functional beige fat. *Cell.* **157:** 1292–1308.
51. Seale, P., S. Kajimura, W. Yang, S. Chin, L. M. Rohas, M. Uldry, G. Tavernier, D. Langin, and B. M. Spiegelman. 2007. Transcriptional control of brown fat determination by PRDM16. *Cell Metab.* **6:** 38–54.
52. Huang, L., D. Pan, Q. Chen, L. J. Zhu, J. Ou, M. Wabitsch, and Y-X. Wang. 2017. Transcription factor Hlx controls a systematic switch from white to brown fat through Prdm16-mediated co-activation. *Nat. Commun.* **8:** 68.
53. Ream, M. A., R. Chandra, M. Peavey, A. M. Ray, S. Roffler-Tarlov, H-G. Kim, W. C. Wetsel, H. A. Rockman, and D. M. Chikaraishi. 2008. High oxygen prevents fetal lethality due to lack of catecholamines. *Am. J. Physiol. Regul. Integr. Comp. Physiol.* **295:** R942–R953.
54. Chen, Q., L. Huang, D. Pan, L. J. Zhu, and Y-X. Wang. 2018. Cbx4 sumoylates Prdm16 to regulate adipose tissue thermogenesis. *Cell Reports.* **22:** 2860–2872.
55. Staiger, H., M. Keuper, L. Berti, M. Hrabě de Angelis, and H-U. Häring. 2017. Fibroblast growth factor 21—Metabolic role in mice and men. *Endocr. Rev.* **38:** 468–488.
56. Liang, Q., L. Zhong, J. Zhang, Y. Wang, S. R. Bornstein, C. R. Triggle, H. Ding, K. S. L. Lam, and A. Xu. 2014. FGF21 maintains glucose homeostasis by mediating the cross talk between liver and brain during prolonged fasting. *Diabetes.* **63:** 4064.
57. Cereijo, R., J. Villarroya, and F. Villarroya. 2015. Non-sympathetic control of brown adipose tissue. *Int. J. Obes. Suppl.* **5:** S40–S44.
58. Schaap, F. G., A. E. Kremer, W. H. Lamers, P. L. M. Jansen, and I. C. Gaemers. 2013. Fibroblast growth factor 21 is induced by endoplasmic reticulum stress. *Biochimie.* **95:** 692–699.
59. Yang, C., W. Lu, T. Lin, P. You, M. Ye, Y. Huang, X. Jiang, C. Wang, F. Wang, M-H. Lee, et al. 2013. Activation of liver FGF21 in hepatocarcinogenesis and during hepatic stress. *BMC Gastroenterol.* **13:** 67.
60. Hondares, E., M. Rosell, F. J. Gonzalez, M. Giralt, R. Iglesias, and F. Villarroya. 2010. Hepatic FGF21 expression is induced at birth via PPARα in response to milk intake and contributes to thermogenic activation of neonatal brown fat. *Cell Metab.* **11:** 206–212.
61. Zeng, X., M. P. Jedrychowski, Y. Chen, S. Serag, G. G. Lavery, S. P. Gygi, and B. M. Spiegelman. 2016. Lysine-specific demethylase 1 promotes brown adipose tissue thermogenesis via repressing glucocorticoid activation. *Genes Dev.* **30:** 1822–1836.
62. Moore, H-P. H., R. B. Silver, E. P. Mottillo, D. A. Bernlohr, and J. G. Granneman. 2005. Perilipin targets a novel pool of lipid droplets for lipolytic attack by hormone-sensitive lipase. *J. Biol. Chem.* **280:** 43109–43120.
63. Holm, C. 2003. Molecular mechanisms regulating hormone-sensitive lipase and lipolysis. *Biochem. Soc. Trans.* **31:** 1120.
64. Townsend, K., and Y-H. Tseng. 2012. Brown adipose tissue: recent insights into development, metabolic function and therapeutic potential. *Adipocyte.* **1:** 13–24.